Novel therapeutic approaches for the cardiac dysfunction in sepsis

A thesis presented by

Caroline Elizabeth O'Riordan

Registered at

Bart's and the London School of Medicine and Dentistry

Queen Mary University of London

For the degree of

Doctor of Philosophy

Centre for Translational Medicine & Therapeutics

The William Harvey Research Institute

Charterhouse Square

London EC1M 6BQ

Declaration

I, Caroline Elizabeth O'Riordan, confirm that the research included within this thesis is my own work or that where it has been carried out in collaboration with, or supported by others, that this is duly acknowledged below, and my contribution indicated. Previously published material is also acknowledged below.

I attest that I have exercised reasonable care to ensure that the work is original and does not to the best of my knowledge break any UK law, infringe any third party's copyright or other Intellectual Property Right, or contain any confidential material.

I confirm that this thesis has not been previously submitted for the award of a degree by this or any other university.

The copyright of this thesis rests with the author and no quotation from it or information derived from it may be published without the prior written consent of the author.

Signature: Date: 26/08/2020

Details of collaboration and publications:

Collaboration with Professor Massimo Collino laboratory (Turin University) for allowing me to work in his laboratory and kindly assisting me in performing the western blots for samples I have generated. Collaboration with Dr. Sina Coldeway laboratory (Jena University) for kindly assisting me in performing cytokine analysis for the samples I have generated. Collaboration with Dr. Lukas Martin laboratory (Aarchen University) for kindly assisting me in performing TUNEL staining of the samples I have generated.

During my PhD I have published data from all 3 results chapters 2, 3 and 4, see list of publications.

In loving memory of my darling baby boy

04/05/09 – 10/06/20

Abstract

Sepsis is one of the most prevalent diseases in the world. The development of cardiac dysfunction in sepsis results in an increase of mortality from 20% to 70% and new treatments are urgently needed. In this thesis I have investigated novel therapeutic approaches to attenuate sepsis-induced cardiac dysfunction.

I have developed two models of cardiac dysfunction. Firstly, the endotoxemia model: co-administration of lipopolysaccharide (LPS)/peptidoglycan (PepG) and secondly the polymicrobial sepsis model: cecal ligation and puncture (CLP). It is known that Bruton's tyrosine kinase (BTK) plays a role in toll-like receptor signalling and NLRP3 inflammasome activation, two key components in the pathophysiology of sepsis and sepsis-associated cardiac dysfunction. Delayed treatment of BTK inhibitors (ibrutinib 30 mg/kg or acalabrutinib 3 mg/kg) attenuates sepsis associated cardiac dysfunction in mice by inhibiting BTK, reducing NF-κB activation and the activation of the NLRP3 inflammasome. Cytokines associated with sepsis were significantly reduced by both BTK inhibitors.

BTK-inhibitors have many off-target effects (which may account for their beneficial effects in sepsis), by conducting polymicrobial sepsis on X-linked immunodeficient (*Xid*) mice (which have a single point mutation in the BTK gene leading to inactivation of BTK), I have found that *Xid* mice are protected from sepsis induced cardiac dysfunction. In *Xid*-CLP mice, there was a reduction in the activation of BTK, NF-κB and NLRP3 inflammasome and a decrease in sepsis associated cytokines and chemokines. The peritoneal bacterial count was lower in *Xid*-CLP mice and this was associated with enhanced phagocytosis and reduced number of infiltrating macrophages and neutrophils.

Ribonuclease 1 belongs to a group of host-defence peptides that specifically cleave extracellular RNA. The activity of RNase 1 is inhibited by ribonuclease-inhibitor 1. The treatment of septic mice with RNase 1 resulted in a reduction in cardiac apoptosis, TNF expression, and septic cardiomyopathy.

In this thesis I have found that inhibition of BTK or RNase 1 attenuates sepsis-induced cardiac dysfunction and *Xid* mice are protected from developing sepsis-induced multiple organ failure.

Acknowledgements

I am forever grateful to my supervisor Professor Christoph Thiemermann, for the continuous support of my PhD study and related research, for your patience, motivation, and immense knowledge. Your positive guidance always made me feel confident in my abilities and has developed me into the scientist that I am today. Thank you for all the opportunity's you have given me and for allowing me to showcase our work at international and national conferences. I could not have imagined having a better supervisor and I will miss working for you.

Thank you to my unofficial second supervisor Dr. Gareth Purvis, not only are you a best friend and my go to drinking buddy, but your scientific advice throughout this PhD has been like none other and enabled me to widen my research from different perspectives. To Professor David Greaves and Professor Massimo Collino thank you so much for hosting me in your laboratory, I learnt a lot and enjoyed experiencing a different research group. It would not have been possible to conduct this research without your valuable collaborations and support. To Dr. Sina Coldewey and Dr. Lukas Martin thank you and your team for all the help in making this work possible.

My PhD family, where to begin with you beautiful people? Madeeha, Jack, Johannes, Dauda, Lauren, Liz, Sura, and Will; you have done nothing but supported me throughout the years, rain or shine, elation or desperation, tears or celebration. I know we will be friends forever. Not to single anyone out, but a special thanks to Madeeha and Jack for being there from day one till the bitter end. Madeeha, my partner in crime, the yin to my yang. Could you please just tell me what am I going to do now without you? One could not ask more from their best friend, from staying late to help me finish off experiments, to all the laughs and hot goss we've shared over the years. Jack, you're the brother I never had, always there to listen to my problems and help out. Us working late into the night at Christmas time, drinking mulled wine from mugs (because PhD is life) is something that I will cherish forever as one of my fondest memories. I know I have been very lucky to have some of the best people come into my life from this experience. Thank you all for making the hardest journey of my life so enjoyable.

No PhD is successful without the unconditional support and love from friends and family, for which I am forever indebted to you all. To my high school besties Michelle, Ruth and Millie

and my Cardiff girls Julia, Ely, Imogen, Chloe, Bex, Amy and Philly. Thank you for all being the most inspirational women, the kind which the world truly needs these days. And thank you for always being there for me with words of encouragement, regardless of how many miles there are between us. You've provided a shoulder to cry on when I needed it most and followed it up by reassuring me that things will get better.

To my London friends Tom, Louise, Charlotte, Callum and Mehow, I wouldn't have known any of you if it wasn't for Tom and I sharing the PhD course. Tom, thank you for letting me invite myself to infiltrate your friendship group, you all have made my London experience and provided the best distraction from work, often with great food and freely flowing drinks.

To Kalle, thank you for putting up with me constantly working in the lab and while at home, ensuring that I am kept well fed. You lifted my spirits up on a daily basis, comforted me when I got too stressed, gave sound advice when I needed it most and dragged me out for de-stressing swims. I look forward reclaiming my free time and to a more relaxing future together.

The most important thanks goes to my mother Tina, as if it wasn't for her being up at 23:50 helping me submit my application before the deadline of midnight, none of this would have happened. Your wisdom has guided me throughout life, taught me to smile in the face of adversity and to believe in myself no matter what anyone says. Throughout this PhD you have continuously kept me on track and been my number one personal cheerleader. You are my inspiration every day and I only hope to be half the woman you are. A simple thank you does not do justice for everything you have done for me. To my father Liam, thank you for all the sacrifices you made and the hard work you did to enable me to pursue my dreams. Your love and support mean the world to me. To my sister Joanna, you are a ray of sunshine who flutters into my life at the right moments to bring happiness and joy. And I've needed that a lot both in the past few years, thank you for being so wonderful. To my baby boy Bean, you were the love of my life and had the unrivalled, unique ability to turn any bad day into the best day. I am forever sorry I worked so much; I should have spent more time with you. I dedicate this thesis to you, my love. Rest in peace, we'll meet again one day.

Lastly, to me: Caroline, you did it! It's been an absolute roller-coaster ride, but if there's one clear takeaway from this, you can do anything you set your mind on. Don't you ever forget it!

List of published papers

1. **Caroline E. O'Riordan**, Gareth S.D. Purvis, Debora Collotta, Fausto Chiazza, Bianka Wissuwa, Sura Al Zoubi, Lara Stiehler, Lukas Martin, Sina M. Coldewey, Massimo Collino, Christoph Thiemermann. Bruton's Tyrosine Kinase Inhibition Attenuates the Cardiac Dysfunction Caused by Cecal Ligation and Puncture in Mice. Frontiers in Immunology (2019) 10:2129. doi:10.3389/fimmu.2019.02129

2. **Caroline E. O'Riordan**, Gareth S.D. Purvis, Debora Collotta, Bianka Wissuwa, Madeeha H. Shiekh, Gustavo Ferreira Alves, Nadine Krieg, Shireen Mohammad, Lauren A. Callender, Sina M. Coldewey, Massimo Collino, David R. Greaves*, and Christoph Thiemermann*. X-linked immunodeficient mice with no functional Bruton's Tyrosine Kinase are protected from sepsis-induced multiple organ failure. Frontiers in Immunology (2020) **11**:2354. doi:10.3389/fimmu.2020.581758

3. Elisabeth Zechendorf, **Caroline E. O'Riordan,** Lara Stiehler, Natalie Wischmeyer, Fausto Chiazza, Debora Collotta, Bernd Denecke, Sabrina Ernst, Gerhard Müller-Newen, Sina M. Coldewey, Bianka Wissuwa, Massimo Collino, Tobias Schuerholz, Christian Stoppe, Gernot Marx, Christoph Thiemermann and Lukas Martin. Ribonuclease 1 attenuates septic cardiomyopathy and cardiac apoptosis – a reverse-translational study. Journal of Clinical Investigation Insight (2020) 5: doi:10.1172/jci.insight.131571

4. Petros Andrikopoulos, Julius Kieswich, Sabrina Pacheco, Luxme Nadarajah, Steve M. Harwood, **Caroline E. O'Riordan**, Christoph Thiemermann, Magdi Yaqoob. The MEK Inhibitor Trametinib Ameliorates Kidney Fibrosis by Suppressing ERK1/2 and mTORC1 Signaling. J Am Soc Nephrol (2019) 30:33–49. doi:10.1681/ASN.2018020209

5. Gareth S. D. Purvis, Massimo Collino, Haidee M. A. Tavio, Fausto Chiazza, **Caroline E. O'Riordan**, Lynda Zeboudj, Nick Guisot, Peter Bunyard, David R. Greaves, Christoph Thiemermann. Inhibition of NF-κB and NLRP3 inflammasome by ibrutinib reduces high-fat-diet induced insulin resistance and microvascular disease. British Journal of Pharmacology (2020) bph.15182. doi:10.1111/bph.15182

List of published abstracts

1. **Caroline E. O'Riordan.** Role of Bruton's tyrosine kinase during systemic inflammation. Female role models in Truama science, 8-9th October 2020 Ulm, Germany (**Invited speaker**, oral presentation).

2. **Caroline E. O'Riordan** Gareth S.D. Purvis, Debora Collotta, Bianka Wissua, Madeeha Shiekh, Gustavo Ferreira Alves, Shireen Mohammad, Lauren Callender, Sina M. Coldewey, Massimo Collino, David R. Greaves, and Christoph Thiemermann. X-linked immunodeficient mice with no functional Bruton's Tyrosine Kinase are protected from sepsis-induced multiple organ failure. Shock conference Toronto, Canada, 2020. (Oral presentation)

3. **Caroline E. O'Riordan**, Gareth S.D. Purvis, Debora Collotta, Fausto Chiazza, Bianka Wissuwa, Sura Al Zoubi, Lara Stiehler, Lukas Martin, Sina M. Coldewey, Massimo Collino, Christoph Thiemermann. Bruton's Tyrosine Kinase Inhibition Attenuates the Cardiac Dysfunction Caused by Cecal Ligation and Puncture in Mice. William Harvery symposium Meeting, 15th January 2020, London, UK (Oral presentation).

4. **Caroline E. O'Riordan**, Gareth S.D. Purvis, Debora Collotta, Fausto Chiazza, Bianka Wissuwa, Sura Al Zoubi, Lara Stiehler, Lukas Martin, Sina M. Coldewey, Massimo Collino, Christoph Thiemermann. Bruton's Tyrosine Kinase Inhibition Attenuates the Cardiac Dysfunction Caused by Sepsis in Mice. UK Visual Sonics Cardio user Meeting, 25th October 2019, London, UK (Oral presentation, **invited speaker**).

5. **Caroline E. O'Riordan**, Gareth S.D. Purvis, Debora Collotta, Fausto Chiazza, Bianka Wissuwa, Sura Al Zoubi, Lara Stiehler, Lukas Martin, Sina M. Coldewey, Massimo Collino, Christoph Thiemermann. Bruton's Tyrosine Kinase Inhibition Attenuates the Cardiac Dysfunction Caused by Cecal Ligation and Puncture in Mice. 18th Congress of European Shock Society, 8th – 10th October 2019, Crete, Greece (Oral presentation). **Travel award winner.**

6. Lara Stiehler, **Caroline E. O'Riordan**, Elisabeth Zechendorf, Sina Coldewey, Bianka Wissuwa, Fiona Dohmen, Daniel Hinkelmann, Antje Ostareck-Lederer, Dirk Ostareck, Gernot Marx, Christoph Thiemermann, Lukas Martin. The role of ribonuclease a as potential new therapeutic in septic cardiomyopathy. 42nd Annual Conference on Shock from 8th to 11th of June 2019 in Coronado, CA (Poster presentation).

7. Gareth SD Purvis, **Caroline E. O'Riordan**, Haidee Aranda, David R Greaves and Christoph Thiemermann. Ibrutinib has both anti-inflammatory and anti-diabetic effects in a model of HFD induced insulin resistance and diabetic nephropathy. British Pharmacology Society, December 2018, London UK (Poster presentation)

8. Elisabeth Zechendorf, Sura Al Zoubi, **Caroline E. O'Riordan**, Martin Simons, Gernot Marx, Tobias Schuerholz, Christoph Thiemermann, Lukas Martin. The potential of Ribonuclease A as a new therapeutic strategy in trauma/sepsis-associated cardiomyopathy. 17th Congress of European Shock Society, 13th-15th September 2017, Paris, France (Poster presentation).

Abbreviations

ACCP	American College of Chest Physicians
AKI	acute kidney injury
ALT	alanine aminotransferase
ARDS	acute respiratory distress syndrome
ASC	apoptosis-associated speck-like protein containing a CARD
AST	aerum aspartate aminotransferase
ATS	American Thoracic Society
ATP	adenosine 5'-triphosphate
BAK	Bcl-2-antagonist killer
BAX	Bcl-2-associated x
BCL	B cell lymphoma
BCR	B-cell receptor
BTK	Bruton's tyrosine kinase
CARD	caspase recruitment domain
CCL	chemokine ligands
CLRs	C-type lectin receptors
CLP	caecal ligation and puncture
CO	cardiac output
DAG	diacylglycerol
DAMPs	damage-associated molecular patterns
DNA	deoxyribonucleic acid
EARs	eosinophil-associated ribonucleases
ECG	electrocardiography
EF	ejection fraction
EMA	European Medical Agency
eNOS	endothelial nitric oxide synthase
EPIC	European Prevalence of Infection in Intensive Care
ERK	extracellular single-regulated kinase
ESICM	European Society of Intensive Care Medicine
FAC	fractional area change
FIO_2	fraction of inspired oxygen

FS	fractional shortening
ICU	intensive care unit
IKK	Iκb kinase
IL	interleukin
IFN	interferon
iNOS	inducible nitric oxide synthase
IP3	inositol triphosphate
IRAK	IL-1 receptor-associated kinase
IRFs	interferon regulatory factors
IVS	interventricular septum
IκB	inhibitor of κb
JNK	C-Jun amino-terminal kinase
LDH	lactate dehydrogenase
LPS	lipopolysaccharide
LRR	leucine-rich repeats
LVID	left ventricular internal dimension
LVPW	left ventricular posterior wall
MAL	MyD88 adaptor-like
MAPK	mitogen-activated protein kinase
MINCLE	macrophage-inducible C-type lectin
MyD88	myeloid differentiation primary response gene 88
NF	nuclear factor
NLRP	NOD leucine-rich-repeat and pyrin domain-containing protein
NLRs	nucleotide-binding oligomerisation domain (NOD)-like receptors
nNOS	neuronal nitric oxide synthase
NO	nitric oxide
NOD	nucleotide-binding oligomerisation domain
PAMPs	pathogen-associated molecular patterns
PaO_2	partial pressure of oxygen
PepG	peptidoglycan
PI3K	phosphoinositide 3-kinase
PIP2	phosphatidylinositol-4,5-bisphosphate
PIP3	phosphatidylinositol-3,4,5-trisphosphate

PKC	protein kinase C
PLC	phospholipase C
PRRs	pattern recognition receptors
RLR	retinoic acid inducible gene I-like receptors
RNase	ribonuclease
SCCM	Society of Critical Care Medicine
SEM	standard error of the mean
SERCA	sacro/endoplasmic reticulum Ca^{2+}-ATPase
SIRS	systemic inflammatory response syndrome
SIS	Surgical Infection Society
SOFA	sequential organ failure assessment
SR	sarcoplasmic reticulum
SSC	Surviving Sepsis Campaign
SV	stroke volume
TAK	transforming growth factor-β-activated kinase
TBK	TRAF family member-associated NF-κb activator-binding kinase
TIR	Toll/IL-1 receptor
TLRs	Toll-like receptors
TNF	tumour necrosis factor
TRAF	TNF-α receptor associated factor
TRAM	TRIF-related adaptor molecule
TRIF	Toll/interleukin 1 receptor domain-containing adaptor inducing IFN-β
WT	wild type
Xid	X-linked immunodeficient

Units

%	percentage
bmp	beats per minute
dL	decilitre
g	gram
h	hour
mg/kg	milligram per kilogram
mg/ml	milligram per millilitre
min	minutes
mmHg	millimetres of mercury
mmol/L	millimole per litre
n	number
°C	degrees Celsius
µL	microlitres
µmol/L	micromole per litre
U/L	units per litre

Contents

Index of figures

Index of tables

Chapter 1 General Introduction

1.1 History of sepsis

The concept of sepsis has been around since 460-370 BC and is derived from the Greek word σήψις, meaning "decomposition of animal- or plant-derived organic materials by bacteria". In medical literature sepsis was first mentioned in poems of Homer as 'sepo' meaning 'I rotted'. The physician Hippocrates wrote about sepsis in the Hippocratic corpus using the term 'sepidon' to represent sepsis. Hippocrates viewed sepsis as a dangerous biological decay that could occur in the body releasing 'dangerous principles' leading to 'auto-intoxication' (1).

It wasn't until the 1800s that basic hygiene was introduced into the medical field and that germ theory was discovered. Ignaz Semmelweiss observed that medical students delivering babies caused more cases of puerperal sepsis (16%) than midwives (2%). He noticed that medical students would perform autopsies and deliver babies without washing their hands leading to increased infection rates. After introducing a policy to ensure hand washing between patients, the rates of puerperal sepsis dropped to 3% (2).

After Semmelweiss, Louis Pasteur formally proposed "Germ Theory", thus leading to Joseph Lister's theory that infectious agents entered the body through breaks in the skin. He developed the technique of dressing wounds with carbolic acid, which led to a decline in wound infections and sepsis (3).

Overall, the term sepsis has been in use for over 2700 years with little change in its meaning. It is the primary cause of death from infection and even today there are no specific and effective treatments for sepsis.

1.2 Evolution of the definitions/diagnosis of sepsis

1.2.1 Sepsis 1

In 1991, the American College of Chest Physicians (ACCP) and the Society of Critical Care Medicine (SCCM) held a consensus conference to internationally define sepsis, these included sepsis, severe sepsis, septic shock and multiple organ dysfunction syndrome (Table 1.1) (4). They proposed that sepsis was the result of a systemic inflammatory response syndrome

(SIRS). The definitions have contributed to an increase in the diagnosis of sepsis and, thus, resulted in an improvement of care.

Table 1.1 Definitions for SIRS, sepsis, severe sepsis, septic shock and multiple organ dysfunction syndrome based on 1991 ACCP/SCCM consensus conference. Adapted from (4).

ACCP/SCCM named conditions	Defining Criteria
SIRS	• Core body temperature >38°C or <36°C • Heart rate ≥ 90bpm • Respiration ≥20/min (or $PaCO_2$ <32 mmHg) • White blood cell ≥12000/μl or ≤4000/μl or 10% immature forms
Sepsis	At least two SIRS criteria caused by known or suspected infection
Severe sepsis	Sepsis with acute organ dysfunction (including hypoperfusion and hypotension) caused by sepsis
Septic shock	Sepsis with persistent or refractory hypotension or tissue hypoperfusion despite adequate fluid resuscitation
Multiple organ dysfunction	The presence of organ dysfunction in an acutely ill patient such that homeostasis cannot be maintained without intervention

1.2.2 Sepsis 2

In 2001, the Society of Critical Care Medicine, the American College of Chest Physicians, European Society of Intensive Care Medicine (ESICM), American Thoracic Society (ATS) and Surgical Infection Society (SIS) held a second consensus conference to redefine sepsis. They provided a more comprehensive list of diagnostic criteria (Table 1.2), yet due to a lack of evidence failed to offer any alternatives, resulting in definitions to remain approximately the same for 15 years (5). Additionally, the PIRO concept was also proposed, which is the predisposition, infection (or insult), response and organ dysfunction (PIRO). It is a staging system used to assess risk and predict prognosis of sepsis, by incorporating the patient's baseline assessment, factors that contribute to sepsis and their response to infection and therapy (Table 1.3) (6).

Table 1.2 Diagnostic criteria for sepsis based on 2001 ACCP/SCCM/ATS/ESICM/SIS conference. It serves as a supplement for diagnostic definitions of sepsis from 1991. Adapted from (5).

Diagnostic criteria for sepsis
General Parameter • Fever (core temperature >38.3°C) • Hypothermia (core temperature <36°C) • Heart rate >90 bpm or >2 SD above the normal value for age • Tachypnoea: >30 breaths per min • Altered mental status • Significant oedema or positive fluid balance (>20 ml/kg over 24 h) • Hyperglycaemia (plasma glucose >110 mg/dL or 7.7 mmol/L) in the absence of diabetes
Inflammatory parameter • Leukocytosis (white blood cell count >12,000/μL) • Leukopenia (white blood cell count <4,000/μL) • Normal white blood cell count with >10% immature forms • Plasma C reactive protein >2 SD above the normal value • Plasma procalcitonin >2 SD above the normal value
Haemodynamic parameters • Arterial blood pressure <90 mmHg, mean arterial pressure <70, or a systolic blood pressure decrease >40 mmHg in adults or <2 SD below normal for age) • Mixed venous oxygen saturation >70% • Cardiac index >3 • Organ dysfunction parameters • Arterial hypoxaemia (PaO_2/FIO_2 <300) • Acute oliguria (urine output <0.5 ml/kg/h or 45 mM/l for at least 2 h) • Creatinine increase ≥0.5 mg/dL • Coagulation abnormalities (international normalized ratio >1.5 or activated partial thromboplastin time >60 s) • Ileus (absent bowel sounds) • Thrombocytopenia (platelet count <100,000/μL) • Hyperbilirubinaemia (plasma total bilirubin >4 mg/dl or 70 mmol/L)
Tissue perfusion parameters • Hyperlactatemia (>3 mmol/L) • Decreased capillary refill or mottling

Table 1.3 PIRO concept from the 2001 SCCM/ACCP/ATS/ESCIM/SIS consensus conference

	Clinical aspects	Other tests
P (predisposing conditions)	Age, alcohol abuse, steroid or immunosuppressive therapy	Immunologic monitoring, genetic factors
I (insult)	Site specific e.g. pneumonia, peritonitis	X-rays, CT scan, bacteriology
R (response)	Malaise, temperature, heart rate, respiratory rate	White blood cell count, C-reactive protein, procalcitonin, modified activated partial thromboplastin time
O (organ dysfunction)	Arterial pressure, urine output, Glasgow coma score	PaO_2/FIO_2, creatinine, bilirubin, platelets

CT = computed tomography. Adapted from (6).

1.2.3 Sepsis 3

Advances have been made in our understanding of the pathophysiology, management and epidemiology of sepsis resulting in the definitions for sepsis to be re-examined in 2016 (Table 1.4) (7). As outlined by the 2016-consortium, sepsis is now defined as a "life-threatening organ dysfunction caused by a dysregulated host response to an infection" and septic shock is regarded as a "subset of sepsis in which underlying circulatory and cellular metabolic abnormalities are profound enough to substantially increase mortality". The concept of severe sepsis has been removed (8).

Table 1.4 New revised criteria for diagnosing sepsis based on the 2016 consensus conference. Table adapted from (8)**.**

Category	Definition
Sepsis	Suspected/documented infection + 2 or 3 on qSOFA (HAT): Hypotension (SBP < 100 mmHg) AMS (GCS < 13) Tachypnea (> 22/min) or Rise in SOFA score by 2 or more
Severe Sepsis	Category removed
Septic Shock	Sepsis + Vasopressors needed for MAP > 65 mmHg + Lactate > 2 mmol/L (after adequate fluid resuscitation

In addition to changing definitions, the scoring system has also been re-evaluated. The SIRS criteria have for many years been regarded as "overly sensitive" and "not specific" for sepsis, as SIRS is present in many hospitalised patients without infection (9,10). The revised criteria resulted in the introduction of a new scoring system, the Sequential [Sepsis-related] Organ Failure Assessment (SOFA) (Table 1.5) (11). An increase of SOFA score of ≥ 2 approximately represents a risk of 10 % mortality in hospitalised patients with suspected infection. In a general hospital setting, a quick SOFA is used as a mortality indicator at the bedside of patients with suspected infection to rapidly identify sepsis if the patient has two of the following signs: change in the level of consciousness, low blood pressure and/or a respiratory rate of greater than 22/min (Table 1.6) (8). This is a better mortality predictor than the previously used SIRS scoring system in patients with suspected infection who are not in the intensive care unit (ICU) (12).

Table 1.5 Sequential [Sepsis-related] Organ Failure Assessment Score based on 2016 consortium.
Table adapted from (8).

	Score				
System	**0**	**1**	**2**	**3**	**4**
Respiration					
PaO_2/FIO_2 mmHg (kPa)	≥400 (53.3)	<400 (53.3)	<300 (40)	<200 (26.7) with respiratory support	<100 (13.3) with respiratory support
Coagulation					
Platelets, $x10^3/\mu L$	≥150	<150	<100	<50	<20
Liver					
Bilirubin, mg/dL (μmol/L)	<1.2 (20)	1.2-1.9 (20-32)	2.0-5.9 (33-101)	6.0-11.9 (102-204)	>12.0 (204)
Cardiovascular	MAP ≥70 mmHg	MAP <70 mmHg	Dopamine <5 or dobutamine (any dose)	Dopamine 5.1-15 or epinephrine ≤0.1 or norepinephrine ≤0.1	Dopamine >15 or epinephrine >0.1 or norepinephrine >0.1
Central nervous system					
Glasgow Coma Scale score	15	13-14	10-12	6-9	<6
Renal					
Creatinine, mg/dL (μmol/L)	<1.2 (110)	1.2-1.9 (110-170)	2.0-3.4 (171-299)	3.5-4.9 (300-440)	>5.0 (440)
Urine output, mL/d				<500	<200

Table 1.6 qSOFA (Quick SOFA) criteria. A qSOFA score of ≥2 points indicate organ dysfunction. Table adapted from (8).

qSOFA (quick SOFA) criteria	Points
Respiratory rate ≥22/min	1
Change in mental status	1
Systolic blood pressure ≤ 100 mmHg	1

The revised scoring system still has limitations as our understanding of the pathology of sepsis is incomplete and remains a work in progress. The consensus also provides easily measurable, clinical criteria that can be translated and recorded objectively (Figure 1.1). It is essential to note that if a patient fails to meet the criteria, this should not automatically lead to dismissal of the diagnosis of sepsis and care should not be postponed if a clinician feels that it is required, as qSOFA and SOFA can miss occult organ dysfunction (8).

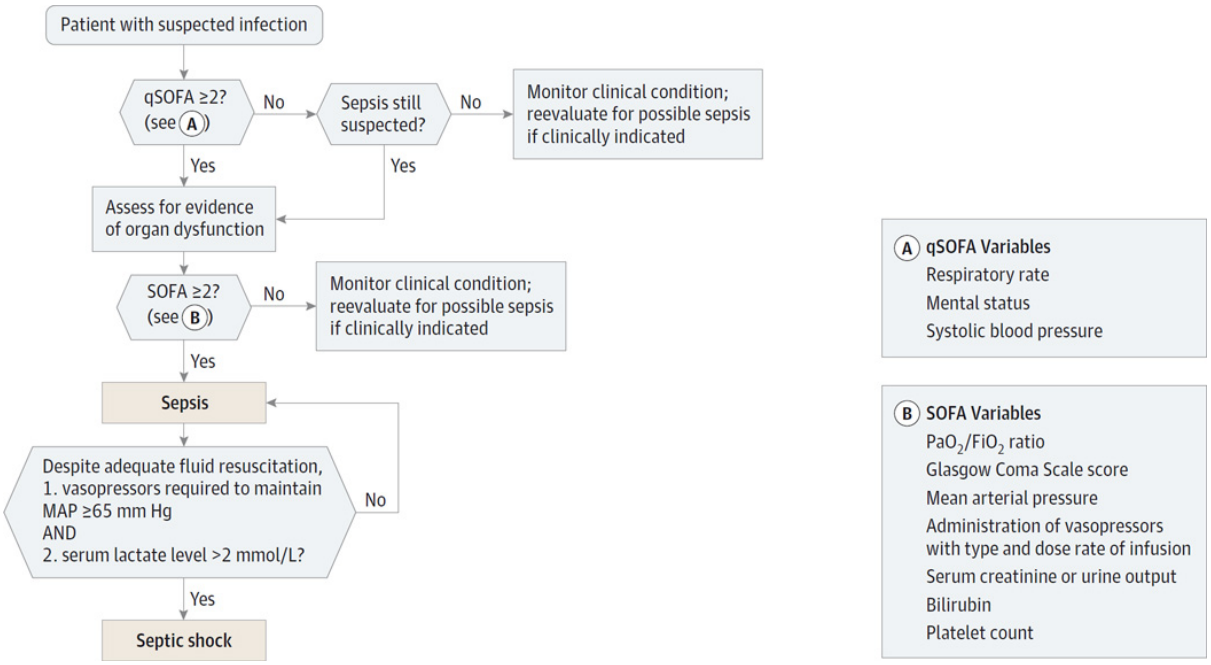

Figure 1.1 Workflow diagram for clinically identifying patients with sepsis and septic shock (8)**.**

1.3 Epidemiology

Sepsis has been recognised as one of the leading causes of morbidity and mortality. Globally there are 50 million cases of sepsis resulting in the death of 11 million people every year and representing 20% of all deaths worldwide (13). In the U.K., 48,000 lives are lost annually due to sepsis. A third of all admissions to the ICU are septic patients. Sepsis is an economic healthcare burden, costing the NHS approximately £2 billion every year. (14–16).

Over the past several decades multiple epidemiological studies have reported an increase in the incidence of sepsis, but a decrease in mortality (17–24). Even though mortality has decreased, these reports indicate that the annual number of sepsis-associated mortality has increased due to the rise in incidence. The increase in incidence could be due to advances in diagnosis/awareness, the development of antibiotic resistance and/or an increase in the number of patients with other diseases/conditions known to carry a higher risk of infection including type-II diabetes, the ageing population and cancer, to name but a few (25,26). Improvement in sepsis outcome is often attributed to an increase in sepsis awareness, faster treatment and improvement in care for the critically ill (27–29).

In general the incidence of sepsis reported worldwide is highly variable due to its complex condition, the changing definitions, difficulty in diagnosis and the majority of the studies identifying sepsis only in the ICU, for example in the US mortality rate ranged from 15% - 29% and 35% - 54% within Europe (30–33). Sepsis is often underreported as a cause of death due to the lack of a sepsis-specific International Classification of Diseases, 10th Revision (ICD-10) code and is, therefore, recorded as other infectious deaths such as pneumonia, kidney infection or influenza (34). Additionally, sepsis is not tracked in the Global Burden of Disease and taxonomy, but infections are reported separately, with only neonatal sepsis being reported (35). Historically, sepsis is often underreported in low and middle income countries, despite the fact that these countries have the highest incidence and mortality of sepsis, specifically the highest health-burden occurring in sub-Saharan Africa, Oceania, south Asia, east Asia, and southeast Asia (13,36). It is essential that global strategies are put in place in the future to measure the morbidity and mortality in these countries (37).

1.4 Therapy of sepsis and septic shock

1.4.1 Surviving sepsis campaign

In 2002, the European Society of Intensive Care Medicine, the Society of Critical Care Medicine and the International Sepsis Forum initiated and developed the Surviving Sepsis Campaign. The Surviving Sepsis Campaign brings together experts in the diagnosis and treatment of sepsis and infectious disease from 11 professional societies to produce internationally recognised guidelines. The evidence-based guidelines provide the best therapeutic approach in reducing mortality, with the first edition being published in 2004. The 7-point agenda proposed by the Society of Critical Care Medicine aims to reduce the relative mortality of sepsis by 25% over the next 5 years (Table 1.7) (38).

Table 1.7 7-point agenda proposed by SCC to reduce the relative mortality of sepsis by 25% over the next 5 years. Table adapted from (38).

7-point agenda plan proposed by SCC
1. Building awareness of sepsis
2. Improving diagnosis
3. Increasing the use of appropriate treatment
4. Educating healthcare professionals
5. Improving post-ICU care
6. Developing guidelines of care
7. Implementing a performance improvement program

The experts, with the addition of another 7 international organisations, updated the guidelines in 2008 by using a new grading system to determine the quality of the evidence and, thus, the strength of recommendations (39). A committee of 68 international experts from 30 professional organisations convened to update the guidelines in 2012 (published in 2013). It was recommended that care for patients with sepsis or septic shock become standardised including control of infection, initial resuscitation or other supportive therapy (40). In 2016, the guidelines were once again updated by a committee of 55 international experts from 25 professional societies, which recommend standardised care of a patient including procedures

of initial resuscitation, antimicrobial therapy and control of infection, to name but a few (Appendix 1). However, a significant proportion of aspects proposed on the early management and resuscitation of patients held weak support, with only 18/93 statements being regarded as "best practice". The surviving sepsis campaign have recently developed specific guidelines for neonates and children with sepsis and septic shock out of 77 statements only 9 were identified as best practice (41).

1.4.2 Care bundles

The committee proposed care bundles in 2008, which are known to provide greater benefit when implemented as a group rather than individually. They first introduced "the 6-h resuscitation bundle" and "the 24-h management bundle", which contain all therapeutic goals to be completed respectively within 6 and 24 h of the onset of sepsis (39). The bundles were updated in 2012, which resulted in the 24-h management bundle no longer being recommended and the resuscitation bundle to be split into two sections: "the severe sepsis 3 h resuscitation bundle" and "the 6 h septic shock bundle" (Table 1.8) (42). It has been shown that patients whose care consists of compliance with the 3 h bundle had a 40% reduction in mortality and a 36% reduction with the 6-h bundle. However, compliance was only reported at 19% for the 3 h bundle and in 36% for the 6 h bundle (43).

Table 1.8 2012 Surviving sepsis campaign care bundles. Table adapted from (44).

To be completed within 3 h of time of presentation*:
1. Measure lactate level 2. Obtain blood cultures prior to administration of antibiotics 3. Administer broad spectrum antibiotics 4. Administer 30 ml/kg crystalloid for hypotension or lactate ≥4 mmol/L * "Time of presentation" is defined as the time of triage in the emergency department or, if presenting from another care venue, from the earliest chart annotation consistent with all elements of severe sepsis or septic shock ascertained through chart review.
To be completed within 6 h of time of presentation:
5. Apply vasopressors (for hypotension that does not respond to initial fluid resuscitation) to maintain a mean arterial pressure (MAP) ≥ 65 mmHg 6. In the event of persistent hypotension after initial fluid administration (MAP < 65 mmHg) or if initial lactate was ≥ 4 mmol/L, re-assess volume status and tissue perfusion and document findings according to Table 1. **7.** Re-measure lactate if initial lactate elevated.

These sections were updated again in 2018, when the 3 and 6 h care bundles have been combined into a single 1 h bundle (Table 1.9) (45). In patients with septic shock, any delay in the initiation of antimicrobial therapy leads to a significant increase in the risk of dying, with the mortality risk increasing hourly by 10% (46).

Table 1.9 2018 Surviving sepsis campaign 1 h bundle. Table adapted from (45).

1-hour bundle: initial resuscitation for sepsis and septic shock
1. Measure lactate level 2. Obtain blood cultures prior to administration of antibiotics 3. Administer broad spectrum antibiotics 4. Administer 30 ml/kg crystalloid for hypotension or lactate ≥4 mmol/L 5. Apply vasopressors (for hypotension that does not respond to initial fluid resuscitation) to maintain a mean arterial pressure (MAP) ≥ 65 mmHg

1.4.3 Initial resuscitation

In sepsis, there is a release of vasodilatory mediators, resulting in increased membrane permeability and a dramatic decrease in intravascular fluids, leading to hypotension, low cardiac output and multiple organ injury. Therefore, early aggressive fluid resuscitation with crystalloids have been recommended to achieve a minimum of 30 mL/kg of fluids to counteract sepsis-induced hypotension and stabilise septic patients (45).

1.4.4 Vasopressors

If hypotension persists even after fluid resuscitation, vasopressors are the next line of treatment. The surviving sepsis campaign recommends norepinephrine as first choice in the treatment of septic shock patients and adding epinephrine or vasopressin in patients who respond poorly (44). Dopamine is recommended as an alternative to norepinephrine in patients with low risk of tachyarrhythmias and absolute or relative bradycardia. Studies have shown that dopamine is associated with increased cardiac arrhythmias (47) and De Backer *et al*. found that dopamine was associated with increased mortality in comparison to norepinephrine (48).

The recommendation to target the use of vasopressor to maintain a mean arterial pressure (MAP) value of 65 mmHg is based on studies by Asfar *et al*. and Lamontagne *et al*.. Asfar *et al*. found that there was no difference in mortality at 28 and 90 days when either maintaining a high MAP of 80-85 mmHg or a lower MAP of 65 -70 mmHg (49). Lamontagne *et al*. found that in patients 75 years or older a lower, MAP of 60-65 mmHg resulted in reduced mortality when compared to MAP of 75 – 80 mmHg (50).

1.4.5 Lactate clearance

Historically it is believed that elevated levels of lactate in the blood are due to an increase in anaerobic respiration as there is an inadequate supply of oxygen. Multiple studies have shown that serum lactate above 1 mmol/L is independently associated with mortality and as lactate increases further the risk of death also increases (51–54). The Surviving Sepsis Campaign confirmed that lactate guided resuscitation resulted in a decrease in mortality (than without lactate monitoring). However, recently Marick *et al*. proposed that raised lactate levels are due

to increased aerobic glycolysis as part of the stress response and that altering therapy in response to an increase in lactate may be detrimental (55).

1.5 Pathophysiology

Sepsis is a complex syndrome caused by an invading pathogen, which leads to activation/dysfunction of the innate immune response and suppression of the adaptive immune response. Early mortality is due to an overwhelming immune response e.g. the cytokine storm, while late mortality is due to persistent immunosuppression, leading to secondary opportunistic infections (Figure 1.2) (56).

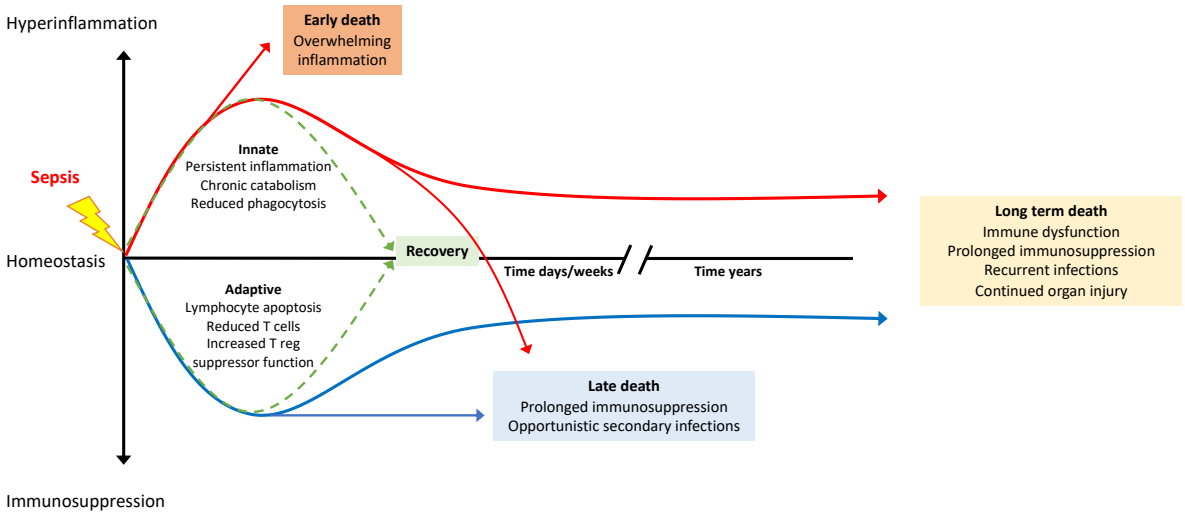

Figure 1.2 Immune responses in sepsis. Activation of both the adaptive and innate immune response is involved in the pathogenesis of sepsis. The peak of the red line represents early mortality due to excessive innate inflammation e.g. the cytokine storm, whereas late mortality results from prolonged immunosuppression and opportunistic secondary infections leading to organ injury/failure. Years after "surviving sepsis" patients can still present with prolonged immunosuppression, chronic catabolism and dysfunction of the immune system leading to late onset of mortality. Adapted from (56).

1.5.1 Pathogens

Shock and multiple organ failure can develop from inflammatory conditions, such as trauma, burns, drug reactions, pancreatitis, tissue ischaemia, thromboembolism etc. However, the three most common causes of infection are bacterial, viral and fungal (Table 1.10). They result in similar symptoms and as well as acting on similar mechanisms, but their differences lead to complications (Figure 1.3) (57).

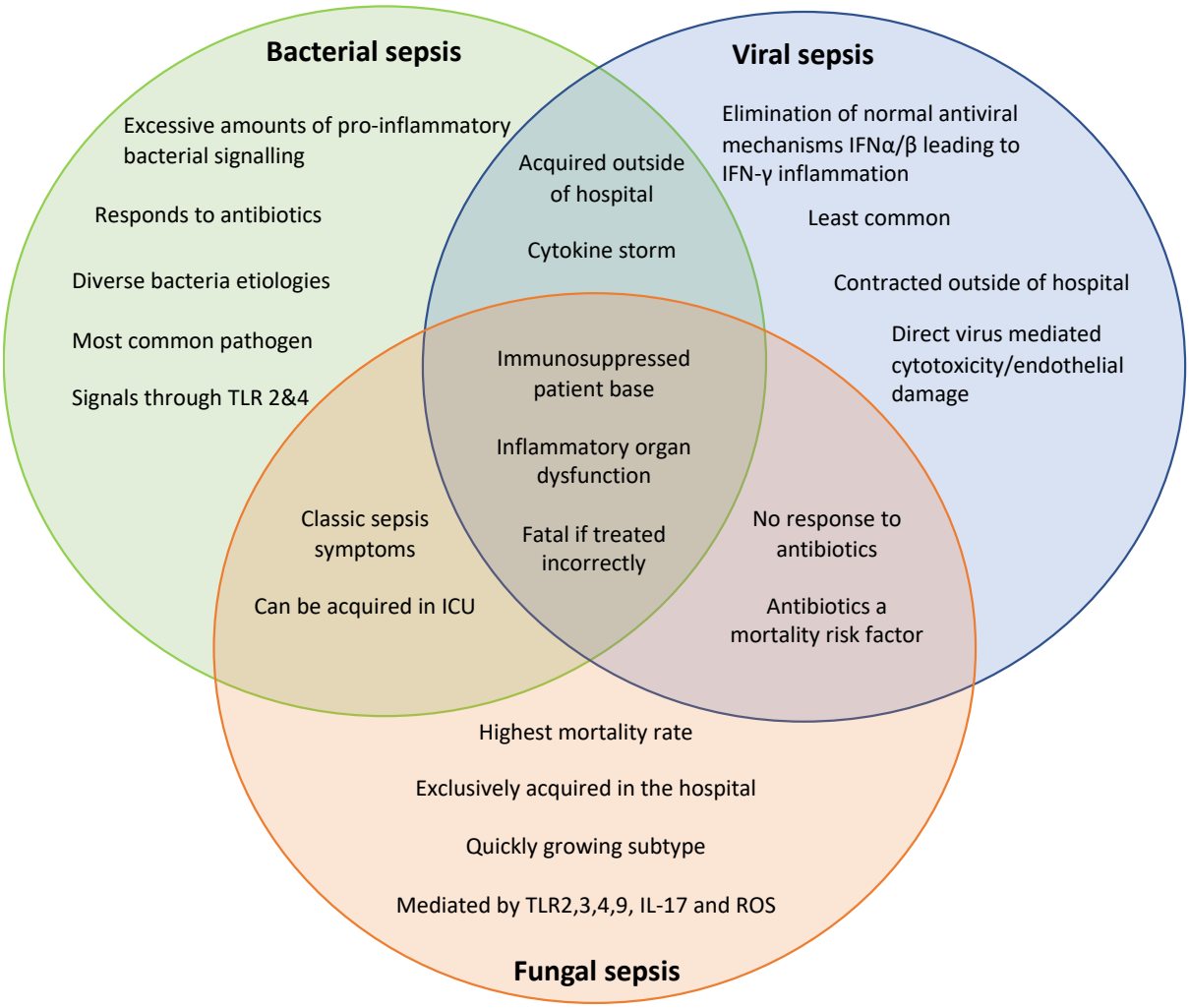

Figure 1.3 Representation of the differences and similarities between the three major types of infection: bacteria, fungal and viral. Adapted from (57).

Table 1.10 Major microbiologic isolates and types of organisms in septic patients from the Extended Prevalence of Infection in Intensive Care (EPIC II) study.

Microorganisms	Frequency (%)	Microorganisms	Frequency (%)	Microorganisms	Frequency (%)
Gram-positive	**46.8**	**Gram-negative**	**62.2**	**Fungi**	**19.4**
Staphylococcus aureus	20.5	*Eschericha coli*	16.0	*Candida*	17.0
MRSA	10.2	*Enterobacter*	7.0	*Aspergillus*	1.4
S. epidermidis	10.8	*Klebsiella species*	12.7	Others	1
Streptococcus pneumonia	4.1	*Pseudomonas species*	19.9	**Anaerobes**	**4.5**
Vancomycin sensitive *Enterococcus*	7.1	*Acinetobacter species*	8.8	**Other bacteria**	**1.5**
Vancomycin resistant *Enterococcus*	3.8	Others	17.0	**Parasite**	**0.7**
Others	6.4	ESBL-producing	1.9	**Other organisms**	**3.9**

Percentages may not add up to 100 due to patients having more than one type of infection. ESBL = extended spectrumβ-lactamases, MRSA = Methicillin-resistant *Staphylococcus aureus*. Table adapted from (36).

1.5.1.1 Bacteria

Bacteria are the most common cause of the infection that underlies sepsis and both Gram-positive and Gram-negative bacteria play a major role. The prevalence of Gram-negative bacteria remains at 62%, with the predominant species being *Pseudomonas aeruginosa* (20%) and *Escherichia coli* (16%) (57). However, the incidence of Gram-positive has increased to 47% worldwide according to the Extended Prevalence of Infection in Intensive Care (EPIC II) study (Table 1.3.1) (36) and was the most reported in North America at 55% (Gram-negative reported at 50%) (17). The rise of Gram-positive bacteria is attributed to the excessive use of antibiotics leading to methicillin-resistant *Staphylococcus aureus* (MRSA) (57). The diagnosis of Gram-negative sepsis carries an increased risk of mortality when compared to that of Gram-positive (58).

1.5.1.2 Fungi

Recently, the incidence of fungal sepsis has increased to 19% (25). This rise could represent effective treatment strategies for targeting bacteria, leading to fungi having a more influential role. Fungal sepsis differs drastically from bacterial in the fact that it is rarely found outside of the hospital, specifically 93% of bloodstream candidiasis is hospital-acquired, whereas bacterial sepsis is primarily found in patients being admitted to hospital (59,60). Additionally, there has been an increase in the number of nosocomial infections shifting away from *Candida albicans* to other fungi including, *Candida glabrata and Candida krusei* (61,62).

Therapy is primarily directed at treating bacterial sepsis (since it is most common) and often board spectrum antibiotics are administered before blood cultures are performed. Antibiotics have no effect on fungal or viral sepsis and are associated with increased mortality in fungal sepsis when high doses of antibiotics are administered (63).

1.5.1.3 Viruses

Viral sepsis is the most uncommon out of the three with cases occurring in 1% of documented patients (64). A normal antiviral immune response results in phagocytosis of the virus by macrophages, neutrophils or dendritic cells and the virus antigens are presented resulting in the production of IFN α/β, IFN-γ. T helper 1 cells and cytotoxic T cells are generated leading to apoptosis of virus cells. The virus is cleared, and memory T cells are produced to rapidly respond to any future infections. However, in viral sepsis there is downregulation of IFN's and increased production of TNF-α, IL-6, leading to the production of inappropriate T helper 2 and 17 which result in excessive inflammation and an inability to clear the virus. In the end, T cells become exhausted and the virus continues to replicate (65).

Viral sepsis can occur from almost any virus. Commonly viral sepsis is caused by dengue virus (in topical countries) (66), influenza (in young/old, pregnant women and immunocompromised) (67), herpes simplex virus and enterovirus (in neonatal) (68,69). Recently, the newly discovered coronavirus (identified as SARS-Cov-2) has been associated with clinical manifestations of septic shock and multiple organ failure in approximately 2-5% of COVID-19 patients (70). In the lung epithelial cells, the S protein on coronavirus binds to

ACE2, resulting in the release of viral RNA, which is detected by TLR 3, 7, 8 and 9 in the endosome (71). In severe cases the activation of the TLR signalling pathway leads to uncontrolled inflammation (cytokine storm), which in turn damages the endothelial cells leading to infiltration of fluid into the alveoli, resulting in acute respiratory distress syndrome and pneumonia (Figure 1.4) (72–74).

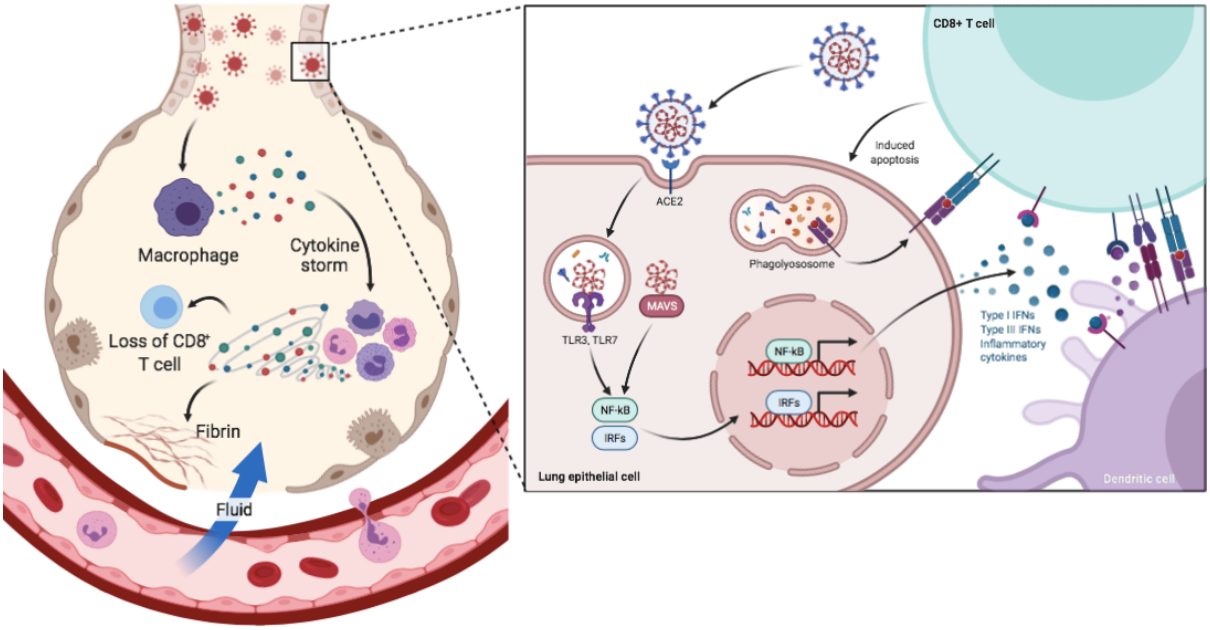

Figure 1.4 Schematic diagram of coronavirus infection in the lungs. In the lung epithelial cells, the S protein on coronavirus binds to angiotensin converting enzyme II (ACE2), releasing viral RNA. Viral RNA is detected by TLR3/7, leading to the downstream activation of NF-κB and interferon regulatory factors producing pro-inflammatory cytokines and type 1 interferons. Dendritic cells migrate to the lymph nodes and activate CD8 T cell (adaptive immunity) by presenting virus antigen to CD8 T cells. CD8 T cells then induces apoptosis. Excessive inflammation (from the cytokine storm) damages the lung epithelium through formation of fibrin and gap junctions appear in the blood vessels, allowing for fluid to infiltrate the alveoli space and result in acute respiratory distress.

1.5.1.4 Site of infection

The most common source of infection is the respiratory tract accounting for 64% of all sepsis cases (often community-acquired pneumonia). Other sources are the abdomen, genitourinary system, skin, catheter-related and the central nervous system (Table 1.11) (36).

Table 1.11 Site of infection for sepsis culture positive infected patients based on the Extended Prevalence of Infection in Intensive Care (EPIC II) study. Table adapted from (36).

Site of infection	Frequency (%)
Respiratory	63.5
Abdominal	19.3
Blood stream	15.1
Renal/urinary tract	14
Skin	6.6
Catheter-related	4.7
Central nervous system	3.2
Others	7.7

1.5.2 Pattern recognition receptors and signalling

The innate immune system has evolved to detect conserved molecular structures on bacteria known as pathogen-associated molecular patterns (PAMPs) and host-derived damage-associated molecular patterns (DAMPs) from injured cells such as ATP and mitochondrial DNA. PAMPs and DAMPs are not found in healthy vertebrate cells and activate the innate immune system, leading to the production of multiple pro-inflammatory and anti-inflammatory molecules secondary to the activation of NF-κB and interferon regulatory factors (IRFs) (75). PAMPs and DAMPs are recognised by highly conserved pattern recognition receptors (PRR), which are expressed on innate immune cells such as macrophages, NK cells, mast cells, dendritic cells, fibroblasts, neutrophils, monocytes and non-professional immune cells such as epithelia. There are four families of PRRs including, toll-like receptors (TLRs) and C-type lectin receptors (CLRs) that reside on the cell surface, as well as nucleotide-binding

oligomerisation domain (NOD)-like receptors (NLRs) and retinoic acid-inducible gene I-like receptors (RLRs), which are located inside the cytoplasm (76). PRR subfamilies differ in their structure and detect specific PAMPs (Table 1.12) leading to activation of distinct intracellular signalling cascades (77). PRRs activation is crucial in resolving the infection by eliminating invading pathogens, however, over-activation can cause a systemic inflammatory response damaging the host (78).

Table 1.12 Pattern recognition receptors and their corresponding pathogen-associated molecular pattern (PAMP) and origin of PAMP. Table adapted from (77).

Pattern recognition receptor		Microbial component	Origin
TLR	TLR1/2	Triacyl lipopeptides	Bacteria
	TLR2/6	Diacyl lipopeptides	*Mycoplasma*
		Lipoteichoic acid	Gram-positive bacteria
	TLR2	Lipoproteins	Various pathogens
		Peptidoglycan	Gram-positive and gram-negative bacteria
		Lipoarabinomannan	Mycobacteria
		Porins	*Neisseria*
		Envelope glycoproteins	Viruses (measles virus, HSV, cytomegalovirus)
		GPI-mucin	Protozoa
		Phospholipomann	*Candida*
		Zymosan	Fungi
		B-Glycan	Fungi
	TLR3	dsRNA	Viruses
	TLR4	LPS	Gram-negative bacteria
		Envelope glycoproteins	Viruses (RSV)
		Glycoinositolphospholipids	Protozoa
		Mannan	*Candida*
		HSP70	Host
	TLR5	Flagellin	Flagellated bacteria
	TLR7/8	ssRNA	RNA viruses
	TLR9	CpG DNA	Viruses, bacteria, protozoa
	TLR10	Unknown	Unknown
RLRs	RIG-I	Short dsRNA	Viruses (influenza A, HCV, RSV)
	MDA5	Long dsRNA	Viruses (picorna and noroviruses)
NLRs	NOD1	Diaminopimelic acid	Gram-negative bacteria
	NOD2	MDP	Gram-positive and gram-negative bacteria
	NALP1	MDP	Gram-positive and gram-negative bacteria
	NALP3	ATP, uric acid crystals, RNA, DNA, MDP	Viruses, bacteria and host
CLRs	Mannose receptor	Fungal mannans	Candida
	Dectin-1	Beta-1,3-glucans	Fungi
	Dectin-2-FcR γ	Mannans	Candida hyphae
	MINCLE – RcR γ	Mannans	Candida
		Mycobacterial cord factor	Mycobacteria
	Mannose binding lectin	Repetitive oligosaccharides	Bacteria and fungi

1.5.3 Toll-like receptors

TLRs are the most extensively researched family of PRR with 10 different TLRs being known in humans and 13 in mice. TLR1, TLR2, TLR4, TLR5, TLR6 and TLR10 reside on the cell surface and detect lipids primarily from bacteria and fungi, whereas TLR3, TLR7, TLR8 and TLR9 are located intracellularly in the membrane of the endosome, where they recognise nucleic acids from viruses and bacteria that have been taken into the cell by phagocytosis, receptor-mediated endocytosis or micropinocytosis (79). Structurally, TLRs are single-pass transmembrane proteins characterised by an extracellular domain consisting of 18-25 copies of leucine-rich repeat (LRR) motifs and a cytoplasmic Toll-IL-1 receptor (TIR) domain. LRRs create a horseshoe shape that adapts for ligand binding. When PAMPs bind, TLRs form dimers or oligomers subsequently triggering MyD88-dependent pathways and/or TRIF-dependent pathways. Heterodimers are also formed from TLR2 and TLR1, or TLR2 and TLR6 (80).

Cell walls and membranes of bacteria contain components not found in animal cells, which are detected by TLRs. Generally, TLR4 recognises a wall fragment located in the outer cell wall of Gram-negative bacteria called lipopolysaccharide (LPS) by binding to the lipid A domain of LPS (81). The structure of LPS consists of three regions: a hydrophobic lipid A domain, a core oligosaccharide and a highly variable O-antigen (82). In contrast, TLR2 detects components of the cell wall of Gram-positive bacteria including peptidoglycan (PepG) and lipoteichoic acid. PepG activates the innate immune system to a lesser extent than LPS (83,84). LPS and PepG can act synergistically to activate the inflammatory cascade, leading to cytokine production (85). Systemic injection of LPS leads to an overwhelming secretion of cytokines resulting in septic shock. During an infection, LPS is shed from the cell wall and binds to LPS-binding protein, this complex then binds to soluble CD14 or CD14 on the cell surface of macrophages, dendritic cells and neutrophils (86). The CD14/LPS complex binds to TLR4 with the help of another accessory protein called myeloid differentiation protein-2 (MD-2), leading to homodimerisation of TLR4 (87). The two TIR domains are now close enough to initiate signalling by interacting with their adaptor molecules. There are four adaptor molecules MyD88 (myeloid differentiation factor 88), MAL (MyD88 adaptor-like), TRIF (TIR domain-containing adaptor-inducing IFN-β) and TRAM (TRIF-related adaptor molecule). TLR4 signals using both MyD88/MAL and TRIF/TRAM (88).

1.5.3.1 MyD88 signalling

Activation of the MyD88-dependent pathway results in recruitment to MyD88 of the serine-threonine kinase interleukin-1 receptor-associated kinase (IRAK)4, which phosphorylates IRAK1 and IRAK2, allowing the complex to recruit TRAF6 (tumour-necrosis-factor-receptor-associated factor 6), an E3 ubiquitin ligase (89). TRAF6 ubiquitinates TAK1 (90). TAK1 activates the NF-κB pathway, which phosphorylates and activates the IκB kinase (IKK) complex. IKK complex consists of two catalytic subunits IKKα/IKK1 and IKKβ/IKK2 and a regulatory subunit IKKγ/NEMO (91). Normally, NF-κB is inactive within the cytoplasm by IκB (inhibitor of κB) molecules masking their nuclear localisation signals (92). Activated IKK phosphorylates IκB molecule on two serine residues leading to the dissociation of NF-κB (93). NF-κB then enters the nucleus and activates the transcription of genes for pro-inflammatory cytokines such as: tumour necrosis factor (TNF)-α, IL-1β and IL-6 (92). TAK1 also activates mitogen-activated protein kinases (MAPKs) such as c-Jun terminal kinase (JNK) and MAPK14 (p38 MAPK), which activate AP-1 transcription factors (94).

1.5.3.2 TRIF signalling

TLR4 signals via the TRIF-dependent pathway with additional adaptor molecule TRAM to recruit TRIF to TLR4 (95,96). Upon ligand binding, TRAF3 activates IKKs, TBK1 and IKKε, which leads to phosphorylation of transcription factor IRF3, which induces IFN-β expression, required for the production of type 1 interferon and inflammatory mediators (97,98). TRAF6 is also activated, leading to the activation of NF-κB through TAK1 ubiquitination (99). Overall, the two pathways allow TLRs to respond to both antiviral and antibacterial response by activating IRFs and NF-κB (Figure 1.5).

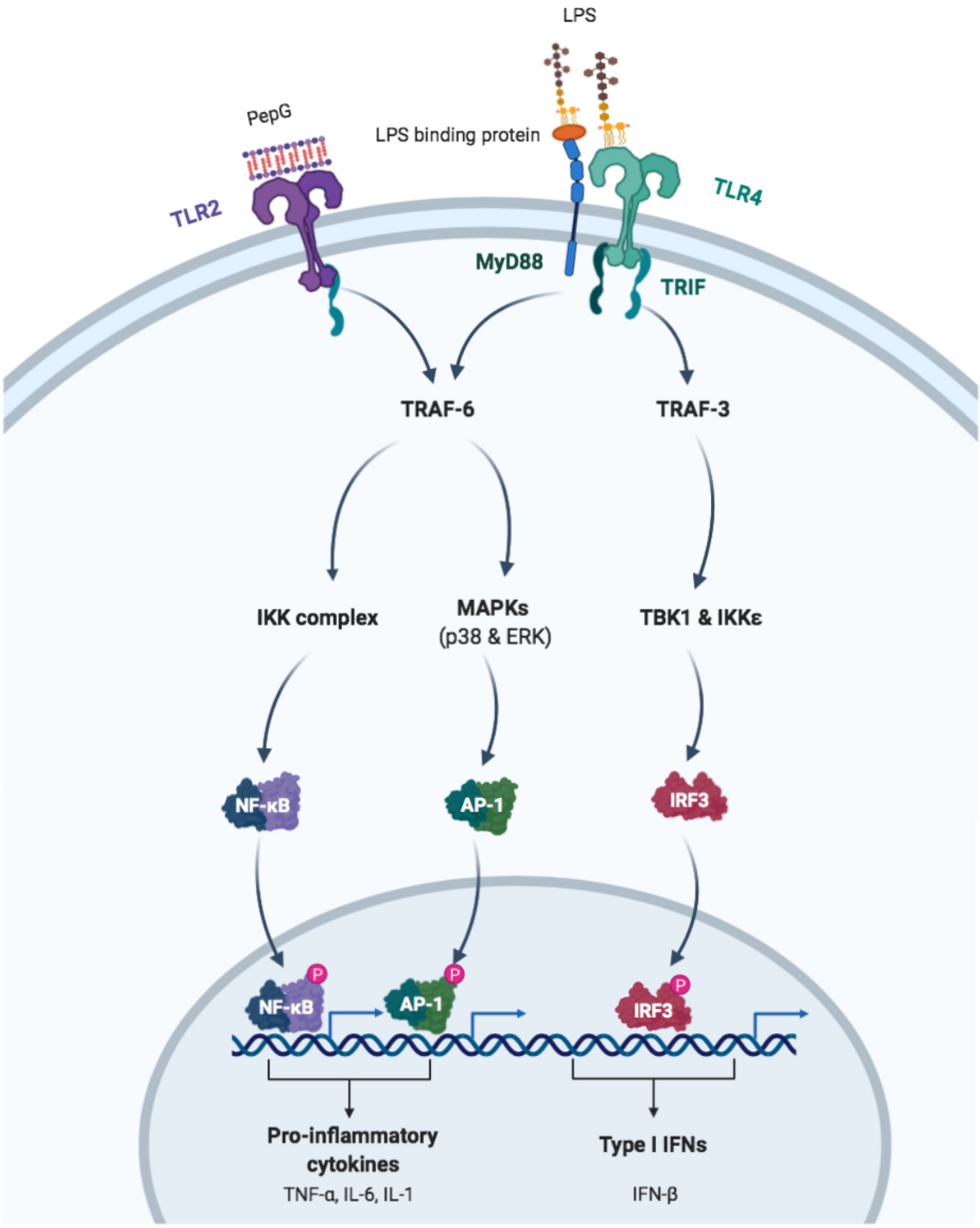

Figure 1.5 TLR4 and TLR2 signalling pathway.

1.5.4 NLR Proteins

NLRs are divided into 3 subfamilies based on their phylogenetic relationship: NODs, NLRPs and IPAF, which consists of 22 members. All members have a tripartite domain structure

consisting of centrally located conserved nucleotide-binding oligomerisation domain (NACHT), which facilitates self-oligomerisation by ATPase (100). A leucine rich repeat (LRR) domain to detect ligands and an N-terminal interaction domain consisting of either: caspase-recruitment domains (CARDs), pyrin domain, baculovirus inhibitor repeats, or acidic transactivating domain (101).

The subfamily NLRP is involved in the formation of the inflammasome in response to stress. NLRP3 senses PAMPs and DAMPs such as ATP derived from dead cells as well as potassium ions (K^+) which are released from stressed cells, resulting in activation of the NLRP3. The pyrin domain can interact with another pyrin domain on apoptosis-associated speck-like protein containing a CARD (ASC), which results in the ASC binding to pro-caspase-1 by CARD-CARD interactions and allowing the proteolytic cleavage to form active caspases (80,102). Active caspase-1 cleaves pro-IL-1β and pro-IL-18 to active IL-Iβ, IL-18 and also initiates programmed cell death, pyroptosis (Figure 1.6) (103). It has been found in endotoxemia models that the NLRP3 inflammasome is activated (104) and that a deficiency in NLRP3 protects mice against microbial sepsis (105).

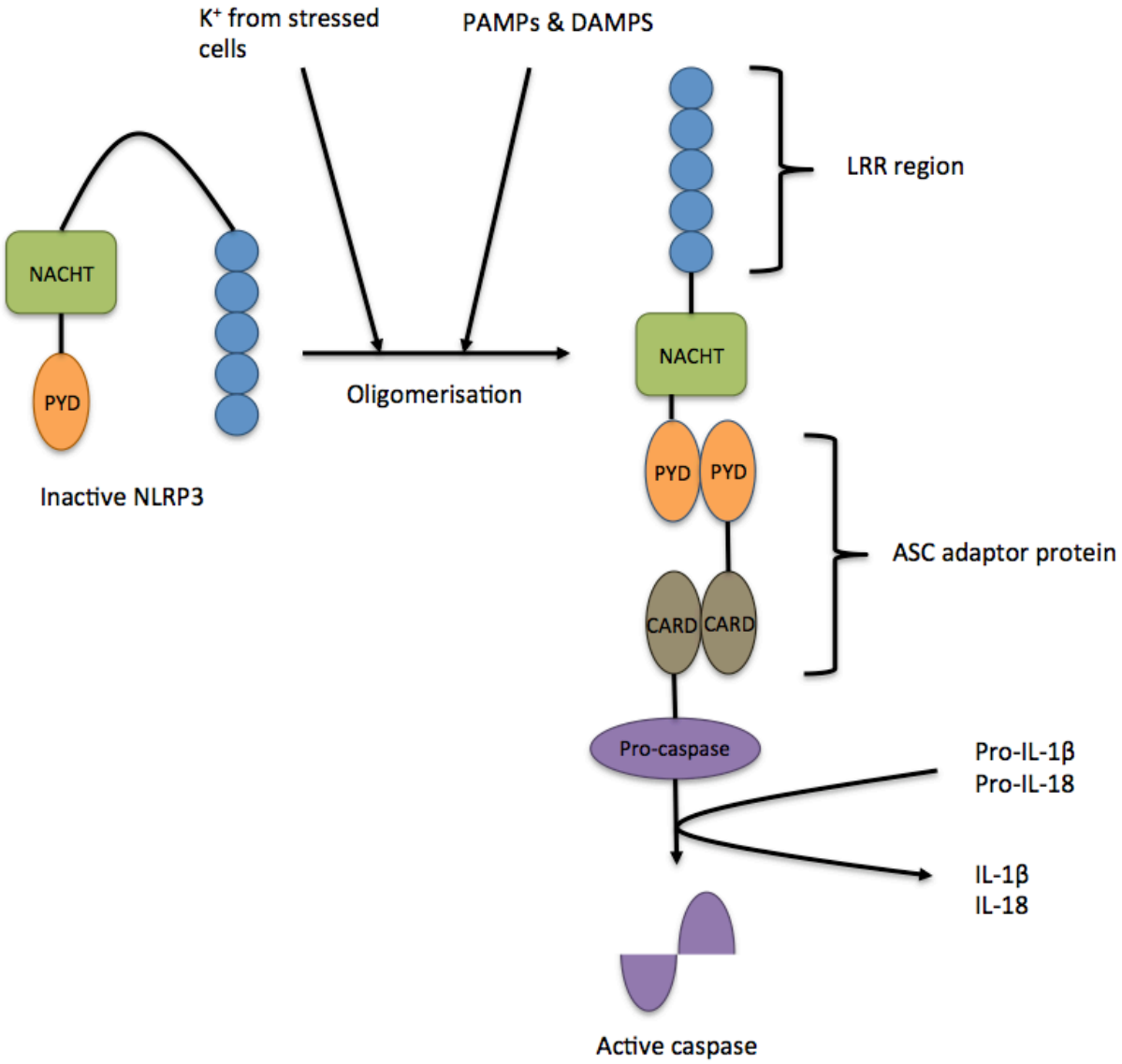

Figure 1.6 Formation and signalling pathway of the NLRP3 inflammasome. NACHT = nucleotide-binding oligomerisation domain, PYD = pyrin domain, CARD = caspase-recruitment domain, LRR = leucine rich region, PAMPs = pathogen associated molecular patterns, DAMPs = damage associated molecular patterns, ASC = apoptosis-associated speck-like protein containing a CARD.

1.6 Cardiac dysfunction in sepsis

Cardiovascular dysfunction is characterised as impaired biventricular myocardial contractility, reduced cardiac index, diastolic dysfunction and reduced left ventricular ejection fraction (EF) (106). The development of cardiovascular dysfunction in sepsis is associated with an increased mortality rate of 70-90% in comparison to 20% mortality in patients who do not present with cardiac dysfunction (107). However, the mechanisms that underlie cardiac dysfunction are not

well known. Evidence suggests that multiple factors contribute to the pathophysiology of the cardiac dysfunction associated with sepsis. These include the excessive formation of IL-1β, TNF-α (108) and nitric oxide (NO) (109), altered calcium homeostasis (110), myocardial ischaemia and mitochondrial dysfunction, to name but a few (111).

1.6.1 Myocardial depressing factors

Myocardial depressing factor(s) were first identified in 1947 in an animal model of haemorrhagic shock (112) and was later linked to sepsis in 1985, where Parrillo *et al*. exposed rat cardiomyocytes to the serum of septic shock patients resulting in a reduction in contractility; whereas the serum from healthy volunteers had no effect (113). Several factors, such as TNF-α and IL-1β, have been reported to reduce cardiac contractility (108). Both of these cytokines induce NO production secondary to the expression of inducible NO synthase (iNOS), and excessive formation of NO reduces myocardial contractility (114).

1.6.1.1 Cytokines

TNF-α is essential in controlling and removing an infection, however, in sepsis an excessive amount of TNF-α is released by activated macrophages from the spleen and liver. TNF-α causes expression of iNOS in blood vessels, resulting in excessive vasodilation and increased permeability. This leads to a loss of plasma volume. Both excessive vasodilation and plasma leakage contribute to the development of hypotension (115). TNF-α also leads to disseminated intravascular coagulation, a pathological condition in which the clotting cascade becomes activated resulting in blood clots being formed in small vessels. The tissue no longer receives adequate blood supply and together with an excessive local inflammation leads to the failure of multiple organs including the heart, liver, kidneys and lungs (116). Mice deficient in TNF-α receptors are resistant to septic shock but are unable to control a local infection (117). Also, other inflammatory cytokines such as IL-6, and IL-8 are amplified by TNF-α, as TNF-α activates macrophages in a paracrine and autocrine manner (118). IL-6 has a longer half-life than TNF-α and remains elevated in the blood of diseases, therefore excessive levels of IL-6 is a good marker of localised TNF-α activity (119).

1.6.1.2 Nitric oxide production

NO is produced from the oxidation of L-arginine to L-citrulline by a group of isoenzymes termed NO synthase (NOS) (120). Three isoforms of NOS have been identified so far: iNOS, endothelial NOS (eNOS) and neuronal NOS (nNOS). The production of NO from eNOS and nNOS is tightly regulated by intracellular calcium and small amounts of NO are continuously released, important in maintaining cardiovascular homoeostasis (121). In contrast, iNOS is independent of calcium and induced by pro-inflammatory stimuli, such as LPS, TNF-α, IL-1β and IFN-γ, resulting in the formation of excessive amounts of NO (122). Evidence shows that NO can have beneficial and detrimental effects, specifically when eNOS produces small amounts of NO it improves LV function. However, in sepsis, the hyperproduction of NO by iNOS contributes to cardiodepression, hypotension and vascular hyporeactivity (123,124). Non-specific NOS inhibition has been shown to attenuate LPS-induced left ventricular dysfunction, however, high doses of non-specific NOS inhibitors have been detrimental (125).

1.6.2 Mitochondrial dysfunction

Mitochondrial dysfunction is present in septic patients (126) and animal models of sepsis (127). The mitochondrial dysfunction seen in skeletal muscle biopsies obtained from septic patients is characterised by a reduced respiratory chain complex I activity and low ATP levels, resulting from an increase in NO production and a decrease in antioxidants e.g. glutathione. NO causes oedema of the mitochondria, thus suppressing its function. The severity of the disease and multiple organ failure correlated with the level of mitochondrial dysfunction (128). It has been proposed that the decrease of ATP supply is a *'last resort'* response to inflammation, similar to hibernation of the myocardium during ischaemia, where organ function is restored. Depression of the myocardium may, thus, be a protective response to conserve energy (129).

1.6.3 Calcium trafficking

Changes in calcium trafficking are often involved in cardiac dysfunction, for example, exposure to endotoxins and cytokines suppress the L-type calcium channels, decreasing intracellular calcium, as well as opening ATP-dependent potassium channels (130). This shortens the action potential and reduces calcium influx, thus suppressing cardiac contractility

(131). Calcium-calcium release from the sarcoplasmic reticulum (SR) in sepsis is thought to be decreased by a reduction of the density of ryanodine receptors (a sarcoplasmic reticulum-associated Ca^{2+}-sensitive release channel that together forms with LTCC structures called 'dyads' (132). The release of Ca^{2+} binds to troponin, resulting in the cross-linkage of actin/myosin. The entry of Ca^{2+} is determined by LTCC, but the amount of Ca^{2+} available for release is regulated by SR Ca^{2+}-ATP-ase (SERCA2) (133). The inhibition of SECRA2 leads to impaired diastolic relaxation due to the reuptake of Ca^{2+} into the SR being blocked (134).

1.6.4 Ischaemia and circulation

Sepsis is characterised by circulatory abnormalities due to vasodilation and intravascular volume depletion, potentially causing an imbalance in oxygen supply and demand. Originally it was thought that cardiac dysfunction in sepsis was the result of myocardial ischaemia (103). Cunnion *et al*. disproved this theory by using thermodilution catheters to measure coronary blood flow. They found that coronary blood flow was the same or greater in septic patients and healthy individuals, while the levels of lactate were not elevated in septic patients (100). This study was further supported by autopsies of septic patients showing no signs of cardiac necrosis (101). Even though coronary blood flow is increased in septic patients, the microcirculatory system undergoes major alterations, including endothelial disruption and maldistribution of blood flow secondary to the development of shunts (111). The disruption of the endothelium and vasodilation results in the accumulation of oedema fluid in body cavities and interstitial space.

1.6.5 Cardiac apoptosis

Apoptosis is a form of programmed cell death which plays a role in cardiac failure. In 1999 it was found that activation of the intrinsic apoptosis pathway occurred in the spleen of septic patients (135). The intrinsic apoptosis pathway is where a cell receives a signal to destroy itself from one of its own genes or proteins due to detection of DNA damage, whereas the extrinsic pathway is in response to an external stimuli by ligands binding to 'death' receptors (tumour necrosis factor receptor) on the cell surface (136). DNA damage activates BCL-2 homology 3 proteins which lead to activation of BCL-2-associated X (BAX) and BCL-2-antagonist killer (BAK). BAX and BAK form channels on the membrane of the mitochondria leading to the release of cytochrome C (proapoptotic factors) which then leads to the formation of the apoptosome by cytochrome C binding to the apoptotic protease activating factor 1 (APAF1) (137). The formation of the apoptosome activates caspase 9, which then activates caspase 3 and 7. Caspase 3 leads to the activation of caspase 6 and 2 and caspase 6 leads to the activation of caspase 8 and 10. Activation of the caspases leads to cell death (Figure 1.7) (136).

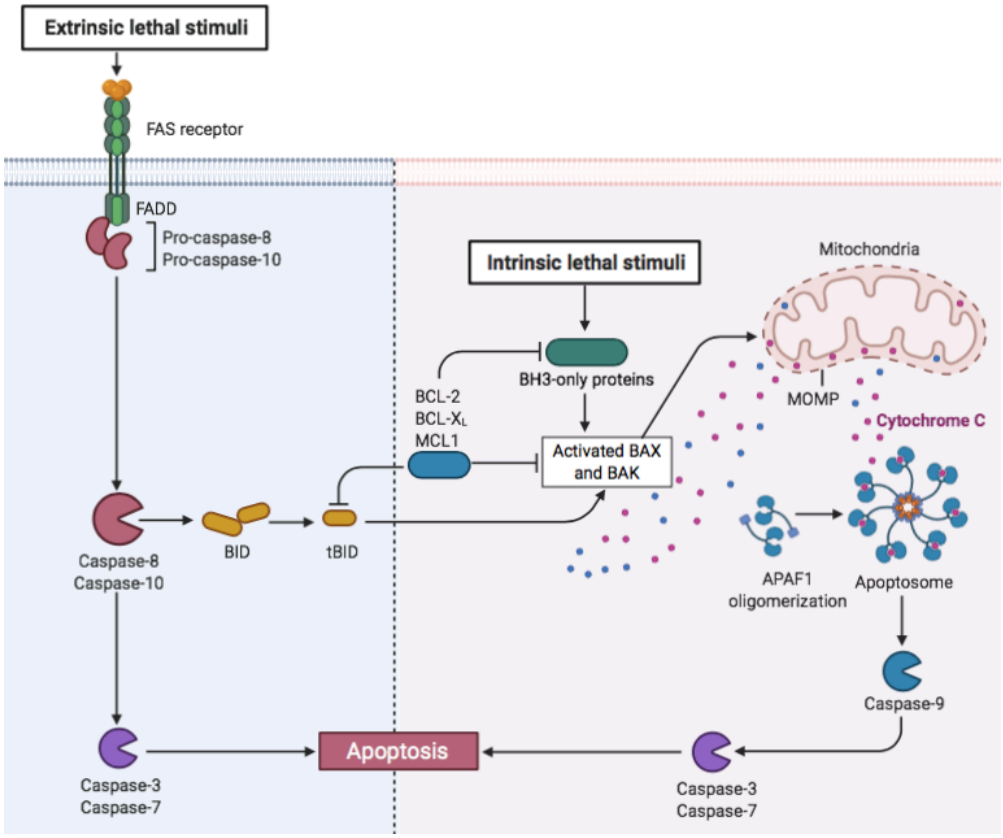

Figure 1.7 Extrinsic and intrinsic apoptosis signalling pathway.

1.7 Sepsis-induced lung injury

The most common cause of sepsis is respiratory infections such as community-acquired pneumonia, which in extreme cases can lead to acute respiratory distress syndrome (36). Pulmonary pathogens initiate the recruitment of innate immune cells, neutrophils and macrophages, leading to the production of pro-inflammatory cytokines: TNF-α, IL-6 and IL-1β. These cytokines lead to a disruption of the alveolar-endothelial barrier, resulting in the interstitial lung space and alveoli to be filled with fluid. Excessive fluid in the lungs is known as lung oedema and causes a decrease in respiration and oxygen intake, leading to hypoxia and a build-up of lactic acid due to anaerobic respiration (Figure 1.8) (138).

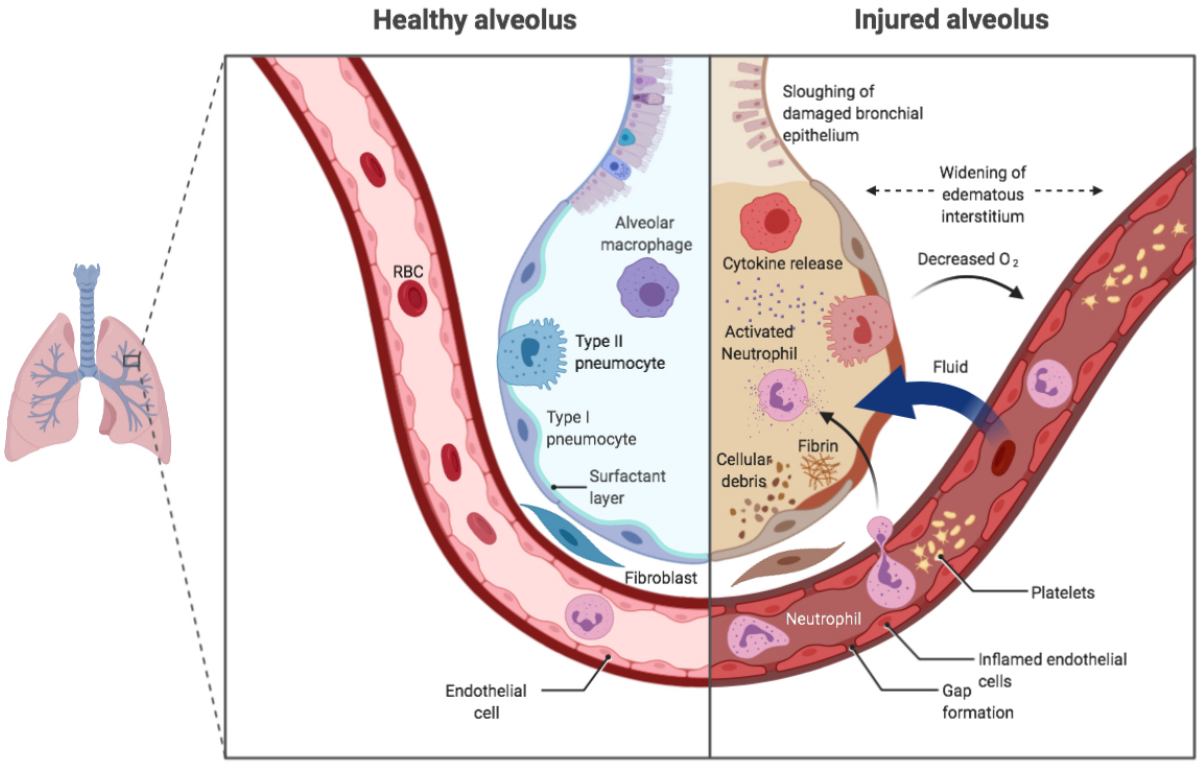

Figure 1.8 Schematic diagram of the pathophysiology of acute respiratory distress syndrome (ARDS).

1.8 Cognitive impairment in sepsis

An altered mental state is an underlying feature of sepsis, resulting from disruption of the blood-brain barrier, which is normally tightly regulated. Changes in the blood-brain barrier result in toxins, inflammatory cells and cytokines to cross into the brain, this causes oxidative stress, changes in cerebral oedema and disruption in neurotransmission, leading to septic encephalopathy (139). Septic encephalopathy can range from mild confusion to coma and is measured by the Glasgow coma scale, which assesses the patients: motor response, verbal response and eye-opening response (Table 1.13) (140).

Table 1.13 Glasgow coma scale.

Feature	Response	Score
Eye response	Open spontaneously	4
	Open to verbal command	3
	Open to pain	2
	No eye opening	1
Verbal response	Orientated	5
	Confused	4
	Inappropriate words	3
	Incomprehensible sounds	2
	No verbal response	1
Motor response	Obeys commands	6
	Localising pain	5
	Withdrawal from pain	4
	Flexion to pain	3
	Extension to pain	2
	No motor response	1

1.9 Sepsis-induced renal dysfunction

Acute kidney injury (AKI) is defined as "an abrupt and persistent decline in renal function" and clinical diagnosis is based on a rise in serum creatinine and decreased urinary output. AKI is a common result of sepsis occurring in 19% of patients with moderate sepsis, 23% with severe sepsis and 51% with septic shock (when blood cultures are positive) (141). AKI from sepsis independently increases mortality from 45.2% (patients with renal failure not from

sepsis) to 74.5% (patients with septic renal failure) (142). AKI is commonly thought to arise from impairment of renal blood flow; however, recent evidence suggests that septic AKI can result from preserved or increased renal blood flow. No single mechanism is responsible for septic AKI, but it arises from multiple mechanisms such as endothelial dysfunction, inflammation, changes intrarenal hemodynamic and tubular injury (143).

1.10 Sepsis-induced hepatocellular injury

The liver is the largest organ in the body and is responsible for maintaining normal systemic homeostasis. In sepsis, toxins and bacteria injure the liver within 1.5 h leading to hepatocellular injury/dysfunction, which increases mortality. Hepatocellular dysfunction is defined as subtle alterations in function such as decreased synthesis and clearance function (144). Ongoing inflammation and hypoperfusion result in irreversible injury of the hepatocytes, eventually leading to liver failure, which is defined as a loss of function in 80-90% of hepatocytes (145).

The liver has two main roles in sepsis: 1) it is responsible for clearing bacteria and toxins and 2) it also plays a role in inflammation, immunosuppression and organ damage. In patients with sepsis, bacterial clearance is essential for the survival with immune response and liver injury all correlate to bacterial levels. Within 10 minutes of intravenous bacterial injection, 60% of the bacteria from the bloodstream can be removed from and trapped in the liver, at 6 h this increases to 80% (146).

There are multiple types of cells in the liver that contribute to bacterial phagocytosis and clearance. The first line of defence involves Kupffer cells, liver sinusoidal endothelial cells and stellate cells (147). The Kupffer cells constitute 80-90% of the tissue macrophages in the body and reside in the lumen of the liver sinusoids, thus are constantly exposed to gut-derived bacteria and endotoxins (148). The pathogens are recognised by PRR, Deng *et al*. showed that TLR4 KO mice resulted in impaired phagocytosis and bacterial clearance by Kupffer cells post CLP (149). Chemokines are also secreted by the Kupffer cells during sepsis, resulting in neutrophils to migrate and accumulate in the liver sinusoids. This leads to the release of neutrophil extracellular traps to capture and remove the pathogen (150).

In the early phase of sepsis Kupffer cells are responsible for producing pro-inflammatory cytokines: TNF-α, IL-1, IL-6, IFN-γ, IL-8, MCP-1 as well as NO and ROS (secondary mediators of tissue injury) (151). An injured liver can induce detrimental inflammatory responses in other organs during sepsis e.g. the excessive production of cytokines and NO-induced acute lung injury, which leads to respiratory failure in patients with severe sepsis (152). Depleting Kupffer cells by administering gadolinium chloride before CLP results in a reduction of pro-inflammatory cytokines, prevents hepatocellular injury/dysfunction during early sepsis (5 h post CLP) as well as protecting distant organs from inflammation-induced injury. However, reduced numbers of Kupffer cells results in impaired bacterial clearance and therefore decreased survival (151).

1.11 Bruton's tyrosine kinase

Bruton's tyrosine kinase (BTK) was first identified in X-linked agammaglobulinemia as a non-receptor protein tyrosine kinase belonging to the Tec family of kinases (153). BTK is most well known as a critical component of the B-cell antigen receptor (BCR) signalling pathway and is involved in B-cell development in normal and malignant B cells (153,154). However, BTK expression is not just restricted to B cell it is also expressed in all cell lineages of the hematopoietic system except for T cells (155).

1.11.1 Structure

BTK is a member of the Tec family of protein tyrosine kinases. It compromises of five domains, N-terminal pleckstrin homology domain, responsible for membrane localisation and interaction of BTK with PIP3, a proline-rich Tec homology region, essential for autoregulation of Tec kinases and the binding site for protein kinase C (PKC)-B, Src-homology 3 domain (SH3), Scr-homology 2 domain (SH2) and tyrosine kinase or Src-homology 1 (Figure 1.9). Transphosphorylation takes place on tyrosine kinase resulting in autophosphorylation of SH2 and SH3 (156).

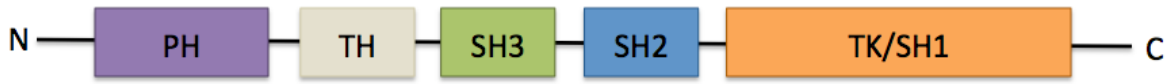

Figure 1.9 Schematic representation of the five BTK domains. PH = pleckstrin homology domain, TH = Tec homology region, SH3 = Src-homology 3 domain, SH2 = Scr-homology 2 domain, TK = tyrosine kinase, SH1 = Scr-homology 1. Adapted from (156).

1.11.2 Function

BTK is normally found in the cytosol, but upon stimulation of the BCR phosphatidylinositol 3-kinase (PI3K) is activated, resulting in phosphorylation of phatidylinositol-4,5-bisphosphate (PIP2) to phosphatidylinositol-3,4,5-triphosphate (PIP3) (157). PIP3 binds to the pleckstrin homology domain and recruits BTK to the plasma membrane, where upstream Src-family

kinases; Lyn and Syk, phosphorylate BTK at the Try^{551} residue (158). BTK becomes active by autophosphorylation at the Tyr^{223} residue (159). Once active, BLINK/SLP65 (an adaptor protein) binds at the SH2 domain, where the complex activates phospholipase C (PLC)-γ2 (160). BTK contains a PIP3 binding site, which signals through to PLC-γ2 resulting in the hydrolysis of PIP3 into inositol triphosphate (IP3) and diacylglycerol (DAG). IP3 induces the release of Ca^{2+} from intracellular stores and DAG leads to the activation of PKC isoenzymes including PKCβ. PKCβ activates the IKK complex, which phosphorylates IκBα at Ser^{32} and Ser^{36}, marking IκBα for ubiquitination and, hence, degradation to release NF-κB (161). NF-κB migrates to the nucleus initiating transcription factor that controls numerous fast-acting primary transcription factors utilised in cell survival, cytokine production and transcription of DNA e.g. TNF-α, IL-1β, IL-6 and iNOS (Figure 1.10) (162,163).

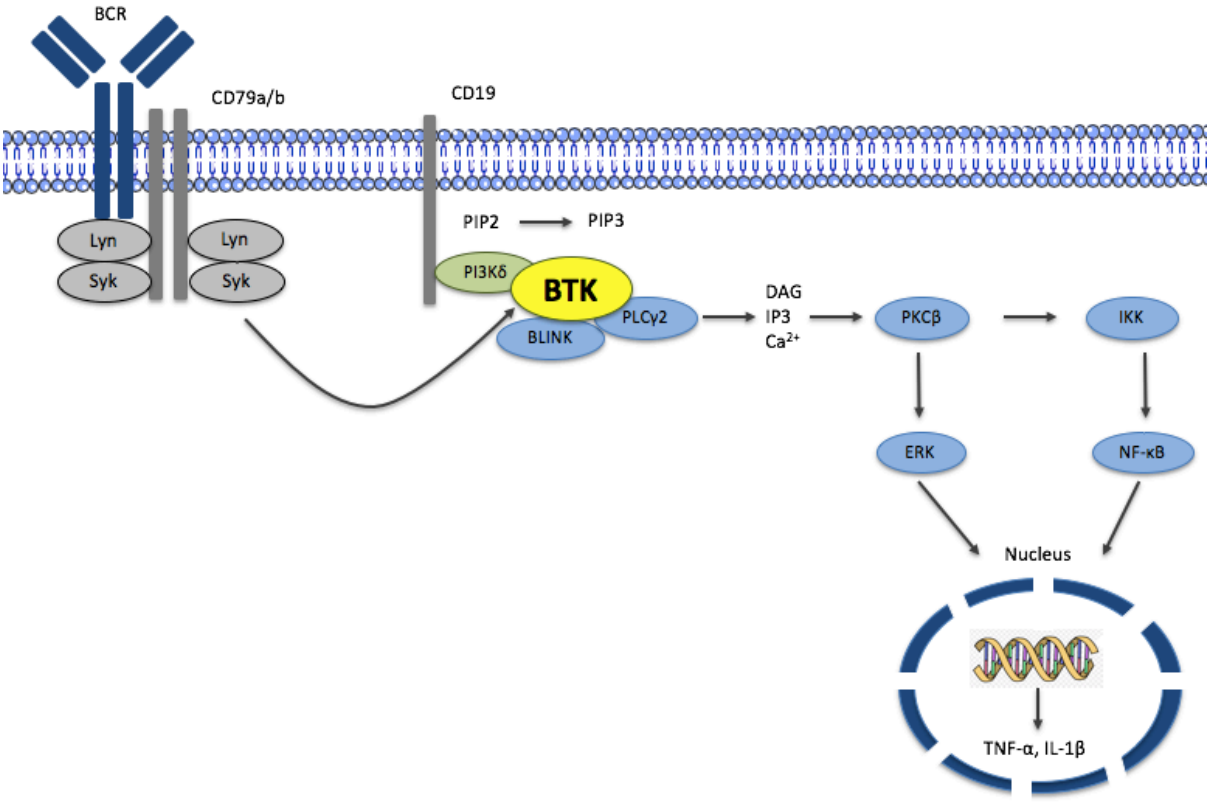

Figure 1.10 B-cell receptor signalling pathway.

BTK is also involved in TLR signalling pathways and regulates the activation of the NLRP3 inflammasome. BTK interacts with the TIR domain of TLR4 at MyD88, MAL, IRAK1 and TRIF, resulting in downstream activation of NF-κB and the generation of proinflammatory cytokines (Figure 1.11) (164,165). BTK is an essential component in specifically regulating the assembly and, hence, activation of the NLRP3 inflammasome. BTK directly phosphorylates ASC through its tyrosine kinase domain. In addition, overexpression of BTK induces oligomerisation of ASC, thus activating the inflammasome (Figure 1.11) (166,167).

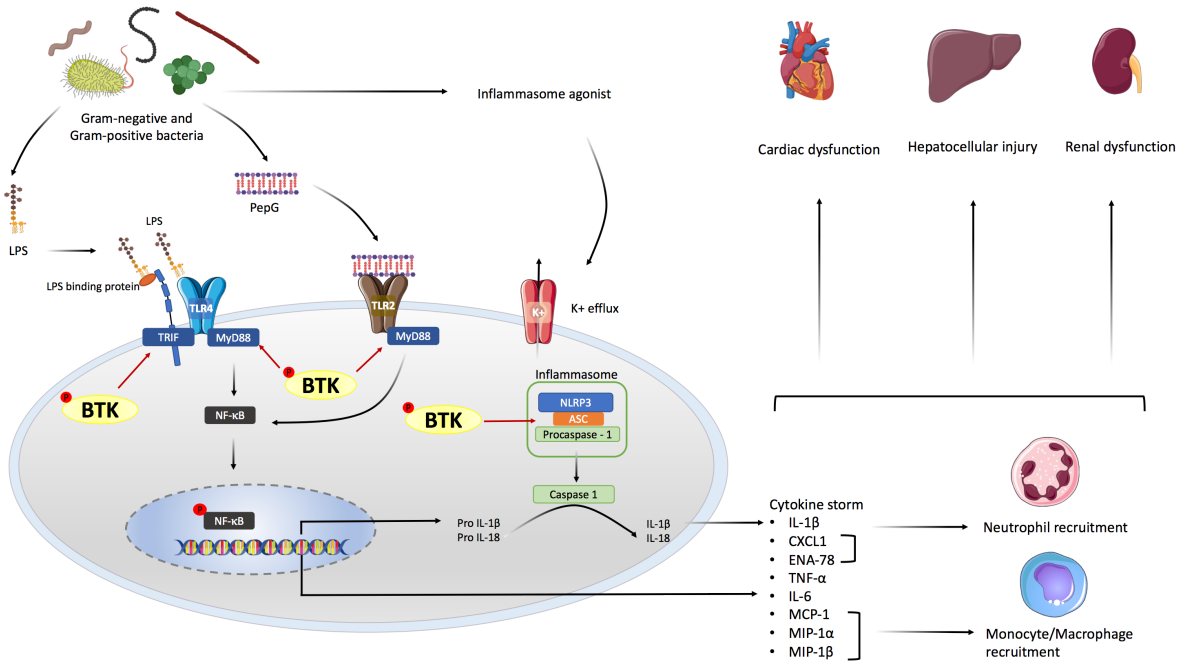

Figure 1.11 Schematic diagram of the role of BTK in the pathophysiology of sepsis. LPS is released from Gram-negative bacteria, which results in the activation of the TLR4 signalling pathway. The release of PepG from Gram-positive bacteria results in the activation the TLR2 signalling pathway. BTK is involved in the activation of TLR4 and TLR2 by binding to MyD88 and TRIF, thus activating their representative signalling cascades. The activation of the MyD88 signalling pathway, leads to the activation of NF-κB and the production of pro-inflammatory cytokines. Additionally, BTK activates the NLRP3 inflammasome by binding to the ASC component of the inflammasome. Once active the NLRP3 inflammasome cleaves pro-IL-1β to active IL-1β. The production of chemokines from NF-κB activation results in the recruitment of neutrophils and macrophages. Excessive inflammation from the cytokine storm and innate immune cells results in multiple organ failure/injury.

1.11.3 BTK inhibitors

Inhibition of BTK by BTK inhibitors reduces NF-κB activation and the formation of NF-κB-dependent cytokines in murine models of arthritis (168). Multiple irreversible and reversible BTK inhibitors have been developed, however, only two have been approved for use by the food and drug administration (FDA) and the European medicines agency (EMA). The FDA has approved the use of the irreversible BTK inhibitors ibrutinib (first generation) in chronic lymphatic leukaemia, mantle cell lymphoma, Waldenstrom macroglobulinemia and graft vs. host (169) and acalabrutinib (more selective, second-generation) in mantle cell lymphoma (170). Ibrutinib is also approved by the EMA for the treatment of chronic lymphatic leukaemia, mantle cell lymphoma and Waldenstrom macroglobulinemia (171), whereas acalabrutinib has an orphan status for chronic lymphatic leukaemia, mantle cell lymphoma and lymphoplasmacytic lymphoma (172–174).

1.11.3.1 BTK inhibitor – Ibrutinib

Ibrutinib is an irreversible, small-molecule inhibitor of BTK, approved for use as an anti-cancer drug in chronic lymphatic leukaemia, which targets B-cell malignancies (175). Ibrutinib forms a covalent bond with Cys^{481} of BTK resulting in inhibition of BTK tyrosine phosphorylation, thus, abrogating downstream BCR and TLR4 signalling pathways such as MAPK, AKT, NF-κB and the inflammasome. I propose here (hypothesis) that inhibition of these pathways by ibrutinib may reduce the cardiac dysfunction of septic patients. Mice deficient in BTK have a blunted response to LPS and produce significantly lower amounts of TNF-α, IL-1β and NO. In both animal models of sepsis and septic patients, activation of NF-κB is increased in every organ and the degree of activation of NF-κB correlates positively with mortality. Mice deficient in NF-κB dependent genes are resistant to developing sepsis (176). It has previously been reported that interventions that inhibit NF-κB and the inflammasome reduce sepsis-associated cardiac dysfunction, such as an IKK inhibitor (167,177,178). This beneficial effect of the IKK-inhibitor IKK-16 was still observed in models with both sepsis and chronic kidney disease, in which the cardiac dysfunction is more severe (179). Overall, NF-κB inhibition improves survival in septic murine models and prevents multiple organ injury.

1.11.3.2 BTK inhibitor – Acalabrutinib

Acalabrutinib is a second-generation BTK inhibitor, which is more selective than ibrutinib and does not inhibit other kinases including ITK, EGFR, ERBB2, JAK3, BLK, FGR, FYN, HCK LCK, LYN, SRC and YES1. Like ibrutinib, acalabrutinib forms a covalent bond with the Cys-481 residue in the ATP-binding pocket of BTK, but it does so with its butynamide group, whereas ibrutinib binds at the Cys-481 residue with an acrylamide group. In biochemical assays, ibrutinib is a more potent inhibitor of BTK (IC_{50} = 1.5 nM) than acalabrutinib (IC_{50} = 5.1 nM) (180). However, *in vivo* studies have shown that acalabrutinib is more effective than ibrutinib at a lower dose (acalabrutinib EC_{50} = 1.3 mg/kg and ibrutinib EC_{50} = 2.9 mg/kg) (181). In clinical studies, ibrutinib is associated with atrial fibrillation and bleeding, but these effects are not seen with acalabrutinib (182). Refer to Table 1.14 for a comparison of ibrutinib and acalabrutinib.

Table 1.14 A table comparing the differences between the two approved BTK inhibitors ibrutinib and acalabrutinib.

Ibrutinib	Acalabrutinib
1st generation BTK inhibitor.	2nd generation BTK inhibitor – more selective.
FDA approval for mantle cell lymphoma, chronic lymphocytic leukaemia, Waldenstrom macroglobulinemia, chronic graft vs host disease. EMA approval for chronic lymphatic leukaemia, mantle cell lymphoma and Waldenstrom macroglobulinemia.	FDA approval for mantle cell lymphoma, chronic lymphocytic leukaemia or small lymphocytic lymphoma. EMA approval for chronic lymphocytic leukaemia.
Irreversible inhibitor of BTK.	Irreversible inhibitor of BTK.
Forms covalent bond at the cys-481 with its acrylamide group.	Forms covalent bond at the cys-481 with its butynamide group
ED_{50} 2.9 mg/kg	ED_{50} = 1.3 mg/kg

1.11.3.3 X-linked immunodeficient mice

X-linked immunodeficient (*Xid*) mice have a missense mutation within the BTK gene (arginine to cysteine at position 28 (R28C)) in the N-terminally located pleckstrin homology domain, resulting in expression of a BTK protein that is functionally inactive (183,184). It is similar to the mutation found in human X-linked agammaglobulinemia, however, the murine mutation is milder form than the human mutation (185). *Xid* mice result in defective B cell differentiation, leading to reduced circulating numbers and are unresponsive to thymus-independent type 2 antigens. In response to some proteins they present with normal amounts of antibodies but have reduced IgM and IgG3 (186,187).

1.12 RNase background

Antimicrobial peptides have been found to play a role in the innate immune system by interacting with bacteria, viruses and fungi. All organisms express the antimicrobial peptide RNase (ribonuclease) a type of nuclease that catalyses the degradation of RNAs, which are classified either as endoribonuclease or exoribonuclease. RNase A is the most researched superfamily and is found in mammalian tissues and body fluids. RNase's are mainly expressed in innate immune cells, eosinophils (188), neutrophils (189), macrophages (190) and monocytes (191), contributing to host immune response due to their immune modulations and antimicrobial activity (192,193). The human RNase A family consists of eight canonical members: RNase 1 (pancreatic RNase), RNase 2 (eosinophil-derived cationic protein, EDN), RNase 3 (eosinophil cationic protein, ECP), RNase 4, RNase 5 (angiogenin), RNase 6, RNase 7 (skin-derived RNase) and RNase 8 (194). Below is a table of proposed functions of RNase in human host defence (Table 1.15).

Table 1.15 The proposed function of the eight human RNase on the host defence. Table adapted from (193).

Ribonuclease	Effect on host defence
RNase 1	• Degradation of vascular polyRNA • Anti-HIV-1 activity • Induces maturation and activation of dendritic cells
RNase 2/EDN	• Antiviral activity against HIV-1 and RSV-b • Secretion by eosinophil granulocytes and monocyte-derived macrophages • TLR2 binding and TH2 polarisation • Chemokine and cytokine induction for activation of maturation of dendritic cells
RNase 3/ECP	• Antiviral activity against RSV-B • Anti-bacterial activity against mycobacteria and gram-positive and Gram-negative bacteria • Induces degranulation of mast cells • Anthelmintic activity against *Schistosoma mansoni Brugia pahangi* and *Trichinella spiralis* • Cytotoxic activity against mammalian cells
RNase 4	• Expression in host-defence associated tissues • Coexpression with lactoferrin, lactoferricin and RNase 5 Enhances antimicrobial activity of lactoferrin and lactoferricin
RNase 5	• Increased serum levels during acute-phase response • Antiviral activity against HIV-1 • Activity against Candida • Activity against streptococcus • Synthesis and secretion by mast cells • Proinflammatory stimulation of leukocytes • Inhibition of degranulation of neutrophil granulocytes
RNase 6	• Infection-induced secretion in urinary tract • Antibacterial activity against Gram-positive and Gram-negative bacteria
RNase 7	• Synthesis upon microbial inflammatory and physiochemical challenge in epithelial tissues • Antibacterial activity against mycobacteria and gram-negative and gram-positive bacteria
RNase 8	• Antibacterial and antifungal activity against Gram-positive and Gram-negative bacteria and Candida

1.12.1 RNase structure

RNase's are small secretory proteins (13-15 kDa) with a short signal peptide (25-27 amino acid length). Even though there is low sequence identity between family members (approximately 30%) all RNase's share a common tertiary protein structure consisting of eight disulphide bridges, apart from RNase 5 which only contains six cysteine residues and a conserved motif signature (CKXXNTF). The catalytic activity of the protein is determined by a conserved trio of two histidine residues and one lysine residue of which the lysine residue is found in the CKXXNFT conserved motif (195). The N-terminal sequence on the initial RNase proteins directs the protein biosynthesis within the endoplasmic reticulum to finally become secretory, it has been found that the N-terminal of RNase is required for its antimicrobial activity, whereas the ribonucleolytic activity appears not to be crucial (196).

1.12.2 Human RNase 1

RNase 1 is expressed in almost all tissues, not just in the pancreas despite its name pancreatic RNase (197). It is highly expressed in endothelial cells (198,199) and in the blood, regulating vascular homeostasis (200). RNase 1 is a potent scavenger of pathogenic RNA and does not require any cofactor for its activation. RNase 1 targets single-stranded RNAs over double-stranded RNA cleaving the 3' end of unpaired C and U residues to produce a 3'-phosphorylated product. RNase 1 has been found to activate human dendritic cells leading to the production of pro-inflammatory cytokines, chemokines, growth factors and soluble receptors (201).

1.12.3 RNases role in health and disease

RNases are involved is a variety of tasks such as cellular housekeeping and sterility of body fluids ensuring the organism is kept healthy. However, tissue injury and necrotic cell death release DAMPS, such as extracellular RNA (eRNA). The eRNA act as proinflammatory mediators attracting innate immune cells e.g. macrophages and dendritic cells. The secretion of eRNA results in the expression of RNase 1 to contribute to tissue repair, removal of host damaged cells and directly killing the invading pathogen. Interestingly, prolonged periods of an infection result in downregulation of RNase expression, it is suggested that an adaptive

process by the pathogen to inhibit the host response, thus extending the survival life of the pathogen.

Genetic deficiencies in RNase leads to immune-related diseases, RNase 5 mutations are associated with amyotrophic lateral sclerosis (202,203) and RNaseT2 is associated with the neuronal disorder cystic leukoencephalopathy (204,205). In disease elevated levels of human RNase 1, 2, 3, 4, 6 and 7 are found in the blood of septic patients and have been proposed as a marker for organ failure (206,207). Additionally, RNase 1 is also proposed as a biomarker for cancer, specifically cholangiocarcinoma (208). The rise of RNase 3 levels is also used to monitor asthma processes (209).

1.12.4 Rodents and RNase

In the mouse and rat genome, RNase 1, 2, 3 and 5 lineages are found, but orthologs of RNase 6 and 7 are not. In 1996, two orthologs of the eosinophil RNase lineage were discovered and named eosinophil-associated ribonucleases (EARs), and since then 11 more have been identified (210). Phylogenetic analysis confirmed that the human and mouse loci once shared an ancestral gene, but rapid gene duplication has happened in primates and rodents independently, leading to high diversification (211). EARs are expressed in a multitude of cells/tissues such as lungs, cardiac, liver spleen, macrophages, to name but a few. Similar to the human counterpart EARs contribute to the host defence through their antimicrobial properties and tissue repair (207).

In animal models of disease, the removal of eRNA by administering RNase showed reduced inflammation (measured by TNF-α and IL-1β) after myocardial or hepatic ischaemia-reperfusion injury (212,213). The cognitive dysfunction induced by hepatic ischemia-reperfusion injury in aged mice (measured by the Morris water maze test) was also improved due to the administration of RNase (212). In a mouse model of atherosclerosis, treatment with RNase1 reduced inflammation and eRNA (214).

1.12.5 Ribonuclease inhibitor 1

The human ribonuclease inhibitor 1 (RNH1) is a 50 kDa cytosolic protein that is ubiquitously expressed in many tissues. It binds to and inactivates RNase 1, 2 and 4, thus eRNA is no longer degraded (215). RNH1 is induced by oxidative stress and limits the activity of RNase, thus negatively contributing to host defence functions (216).

1.13 Scientific aims and hypothesis

Sepsis is a major public health problem, and the development of sepsis and sepsis-induced cardiac dysfunction are associated with high mortality rates. Further research into new therapeutics for sepsis must be undertaken to tackle this global burden. The overall aims of this thesis are to investigate potential new therapeutics and determine their mechanisms of action. Specifically, I have investigated whether commercially available BTK inhibitors ibrutinib or acalabrutinib attenuate sepsis-induced multiple organ dysfunction and if the inhibition of BTK is solely responsible for any observed effects and not an off-target effect (by conducting CLP in *Xid* mice). Lastly, I have investigated the role of RNase 1 in the pathophysiology of sepsis and if its administration can protect mice from sepsis.

Chapter 2 Inhibition of Bruton's tyrosine kinase attenuates the cardiac dysfunction induced by sepsis in mice

2.1 Introduction

Sepsis is a life-threatening organ dysfunction caused by a dysregulated host response to an infection (8), which affects approximately 50 million people worldwide (13). In the UK, sepsis is the second leading cause of death with 48,000 patients dying each year (217) costing the NHS approximately £2 billion annually (218). The development of cardiac dysfunction affects 40% of septic patients (106) and is associated with an increased mortality rate of 70-90% in comparison to 20% mortality in patients who do not present with cardiac dysfunction (219). However, the mechanisms that underlie this cardiac dysfunction are not well known. Evidence suggests that multiple factors contribute to the pathophysiology of the cardiac dysfunction associated with sepsis. These include the activation of NF-κB and NLRP3 leading to excessive formation of e.g. TNF-α and IL-1, respectively (108,220). There are currently no drugs for the specific treatment of the cardiac dysfunction (or indeed the multiple organ dysfunction) associated with sepsis that specifically targets NF-κB and the NLRP3 inflammasome.

During sepsis, bacterial LPS stimulates TLR4, and PepG stimulates TLR2 (see section 1.5.3 for detail). BTK is involved in the activation of TLRs by specifically binding to the TIR domain of MyD88 and Mal, leading to the downstream activation of NF-κB (see section 1.11 for detail). BTK also regulates the assembly and, hence, activation of the NLRP3 inflammasome by binding to the ASC component (166,167). The activation of NF-κB and the NLRP3 inflammasome leads to the production of pro-inflammatory cytokines involved in the pathophysiology of sepsis. BTK inhibitors have been shown to inhibit the activation of NF-κB and its related cytokines/chemokines (168).

Given the importance of the activation of TLRs, NF-κB and NLRP3 in the pathophysiology of sepsis, I hypothesised that BTK inhibitors, such as ibrutinib (first-generation and non-specific) or acalabrutinib (second-generation and specific), may attenuate the cardiac dysfunction in murine models of sepsis.

Specifically, in this chapter I set out to:

1) Establish a model of endotoxemia – administration of LPS/PepG in order to investigate the effects
   a) of pre-treatment with oral ibrutinib (30 mg/kg, 1 h before LPS/PepG) on the cardiac dysfunction caused by LPS/PepG in mice.
   b) of intravenous administration of ibrutinib (3 or 30 mg/kg, 1 h after LPS/PepG) on the cardiac dysfunction caused by LPS/PepG in mice.

2) Establish a surgical model of sepsis - caecal ligation and puncture (CLP) in order to investigate
   a) whether administration of ibrutinib (3 mg/kg & 30 mg/kg) or acalabrutinib attenuates sepsis-induced multiple organ failure (cardiac dysfunction, renal dysfunction and liver injury).
   b) whether the activation of BTK, NF- κB and NLRP3 inflammasome are involved in the pathophysiology of sepsis-induced cardiac dysfunction.
   c) whether delayed administration of BTK inhibitors reduce the activation of BTK, NF-κB and NLRP3 inflammasome in septic cardiac tissue.
   d) the effects of BTK inhibitors on the production of sepsis-associated cytokines and chemokines.

2.2 Methods and materials

2.2.1 Ethical statement

The Animal Welfare Ethics Review Board of Queen Mary University of London approved all experiments in accordance with the Home Office guidance on the operation of Animals (Scientific Procedures Act 1986) published by Her Majesty's Stationery Office and the Guide for the Care and Use of Laboratory Animals of the National Research Council. Work was conducted under U.K. home office project licence number PCF29685.

2.2.2 Animals

This study was carried out on 10-week old male C57BL/6 mice (Charles River Laboratories UK Ltd., Kent, UK) weighing 20-30 g and kept under standard laboratory conditions. The animals were allowed to acclimatise to laboratory conditions for at least one week before undergoing experiments. Six mice were housed together in ventilated cages lined with absorbent bedding material. Tubes and chewing blocks were placed in the cage for environmental enrichment. They were subjected to 12-h light and dark cycle with the temperature maintained at 19-23^{o}C. All animals had free access to a chow diet and water *ad libitum*. The cages were cleaned regularly approximately every three days, with water being changed daily. Research staff inspected the animals each day for any signs of illness or abnormal behaviour.

2.2.3 Establishing a model of LPS/PepG-induced cardiac dysfunction

Ten-week-old, male C57BL/6 mice received LPS (derived from *Escherichia coli* 0111:B4) and PepG at either: 6 mg/kg/0.1 mg/kg, 6 mg/kg/1 mg/kg or 7 mg/kg/1 mg/kg in PBS via intraperitoneal (i.p.) administration (Table 2.1). Sham-operated mice were injected with PBS only (i.p.) but were otherwise treated identical to LPS/PepG-mice. Cardiac dysfunction was examined *in vivo* by echocardiography at 18 h after LPS/PepG co-administration under anaesthesia as described below (Figure 2.1).

Table 2.1 Experimental groups used in establishing a model of LPS/PepG-induced cardiac dysfunction.

Strain	Group	Total number
C57BL/6	Sham	6
10 weeks	LPS (6 mg/kg) + PepG (0.1 mg/kg)	3
	LPS (6 mg/kg) + PepG (1 mg/kg)	3
	LPS (7 mg/kg) + PepG (1mg/kg)	5

Figure 2.1 Schematic representation of LPS/PepG model. At 0 h, 10-week-old C57BL/6 male mice were administered with LPS/PepG i.p. to induce cardiac function. At 18 h cardiac function was assessed by echocardiography *in vivo*.

2.2.4 Pre-treatment with ibrutinib via oral gavage

One hour before LPS (7 mg/kg)/PepG (1 mg/kg) i.p. administration, animals were randomised to receive either ibrutinib (30 mg/kg p.o.) or vehicle (5% DMSO + 30% cyclodextrin p.o.). Sham-operated mice received PBS (5 ml/kg i.p.) (Table 2.2). Cardiac dysfunction was examined *in vivo* by echocardiography at 18 h after LPS/PepG co-administration under anaesthesia (see below). At the end of the experiment, all mice were deeply sedated by inhalation of 3% isoflurane and delivered in 0.4 L/min oxygen. Approximately 0.7 ml of blood was obtained via cardiac puncture; the mice were then killed by removal of the heart, lungs, liver, kidney and spleen were all collected and stored at -80°C for further analyses (see below). The blood samples were centrifuged for 3 min at 9000 RPM and serum was collected and frozen at -80°C (Figure 2.2).

Table 2.2 Experimental groups used to investigate whether pre-treatment with oral ibrutinib (30 mg/kg p.o.) attenautes LPS/PepG-induced cardiac dysfunction.

Strain	Group	Procedure	Total number
C57BL/6 10 weeks	Sham	PBS (5 ml/kg i.p.)	5
	Control + vehicle	5% DMSO + 30% cyclodextrin p.o. 1 h before LPS (7 mg/kg) + PepG (1 mg/kg) i.p.	5
	LPS/PepG + ibrutinib (30 mg/kg p.o.)	Ibrutinib (30 mg/kg) p.o. 1 h before LPS (7 mg/kg) + PepG (1 mg/kg)	5

Figure 2.2 Schematic representation of LPS/PepG model to investigate whether pre-treatment with ibrutinib attenuates LPS/PepG-induced cardiac dysfunction. At -1 h, 10-week-old C57BL/6 mice were administered ibrutinib (30 mg/kg p.o.). One hour later mice were injected with LPS (7 mg/kg) and PepG (1 mg/kg) i.p. to induce cardiac function. At 18 h cardiac function was assessed by echocardiography *in vivo*. At the end of the experiment blood samples and organs were collected to quantify organ dysfunction.

2.2.5 Post-treatment with intravenous Ibrutinib

One hour after i.p. injection of LPS (7 mg/kg)/ PepG (1 mg/kg) animals were randomised to receive either ibrutinib (3 mg/kg), ibrutinib (30 mg/kg) or vehicle (5% DMSO + 30% cyclodextrin) intravenously. Sham-operated mice only received PBS (5 ml/kg i.p.) (Table 2.3). Cardiac dysfunction was examined *in vivo* by echocardiography at 18 h after LPS/PepG co-administration under anaesthesia (see below). At the end of the experiment, all mice were deeply sedated by inhalation of 3% isoflurane delivered in 0.4 L/min oxygen and approximately 0.7 ml of blood were obtained via cardiac puncture; the mice were then killed by removal of the heart. Heart, lungs, liver, kidney and spleen were all collected and stored at -80°C for further analyses (see below). The blood samples were centrifuged for 3 min at 9000 RPM and the plasma was collected and also frozen at -80°C (Figure 2.3).

Table 2.3 Experimental groups used to investigate whether post-treatment of ibrutinib (3 mg/kg or 30 mg/kg) attenuates LPS/PepG-induced cardiac dysfunction.

Strain	Group	Procedure	Total number
C57BL/6 10 weeks	Sham + vehicle	0 h PBS (5 ml/kg i.v.)	10
	Control + vehicle	0 h - LPS (7 mg/kg) + PepG (1 mg/kg) i.p. 1 h - 5% DMSO + 30% cyclodextrin i.v.	10
	LPS/PepG + ibrutinib (3 mg/kg i.v.)	0 h - LPS (7 mg/kg) + PepG (1 mg/kg) i.p. 1 h – (ibrutinib 3 mg/kg i.v.)	10
	LPS/PepG + Ibrutinib (30 mg/kg i.v.)	0 h - LPS (7 mg/kg) + PepG (1 mg/kg) i.p. 1 h - ibrutinib (30 mg/kg i.v.)	10

Figure 2.3 Schematic representation of LPS/PepG model to investigate whether delayed intravenous administration of ibrutinib (3 mg/kg or 30 mg/kg) attenuates LPS/PepG-induced cardiac dysfunction. At 0 h, 10-week-old C57BL/6 mice were injected with LPS (7 mg/kg) and PepG (1 mg/kg) via i.p. to induce cardiac dysfunction. At 1 h ibrutinib 3 mg/kg or 30 mg/kg was administered via i.v. At 18 h cardiac function was assessed by echocardiography *in vivo*. At the end of the experiment blood samples and organs were collected to quantify organ dysfunction.

2.2.6 Caecal ligation and puncture (CLP) surgery

Ten-week-old C57BL/6 mice were randomly selected to undergo CLP or sham-operated surgery. Buprenorphine (0.05 mg/kg i.p.) was administered as an analgesic at the start of the experiment. Mice were initially anaesthetised with 3% isoflurane and delivered with 1 L/min oxygen in an anaesthetic chamber, after which maintenance was kept at isoflurane 2% and delivered with 1 L/min oxygen via a facemask throughout the surgery. The temperature of the mice was monitored throughout the experiment by a rectal thermometer and maintained at 37°C via a homoeothermic blanket. The fur is removed from the abdominal area by Veet hair removal cream and the area is cleaned with 70% ethanol. The abdomen of the animals was then opened up by a 1.5 cm midline incision, where the caecum is exposed. The caecum was fully ligated below the ileocaecal valve and a G-18 needle was used to puncture both ends of the ligated caecum, where a small amount of faeces was then squeezed out (Figure 2.4). The caecum was returned to the abdomen in its anatomical position and 5 ml/kg of normal saline (0.9 % NaCl) was administered into the abdomen before its closure. Saline (10 ml/kg) is also administered s.c. directly after surgery for fluid resuscitation. Antibiotics (Imipenem/Cilastatin; 20 mg/kg dissolved in the resuscitation fluid s.c.) and an analgesic (buprenorphine; 0.05 mg/kg i.p.) were administered at 6 h and 18 h after surgery. After 24 h, cardiac function was assessed by echocardiography *in vivo*. Mice were anaesthetised with isoflurane and cardiac puncture took place to obtain blood samples. Mice were then killed by removal of the lungs and heart. The organs and blood collected were used to quantify injury. Mice that underwent sham-operated surgery were not subjected to ligation or perforation of the caecum but were otherwise treated the same way.

A reduction in temperature to <30°C or a change of 5°C over time in each animal has been reported to predict death in mice with CLP (221). As mortality of animals is not an acceptable routine endpoint in the UK, I used the reduction in rectal temperature <30°C as a surrogate marker for mortality.

A clinical score for monitoring the health of experimental mice was used to evaluate the symptoms consistent with murine sepsis. The maximum score of 6 comprised the presence of the following signs: lethargy, piloerection, tremors, periorbital exudates, respiratory distress,

and diarrhoea. Mice with a clinical score >3 were defined as exhibiting severe sepsis, against a moderate sepsis for a score ≤3.

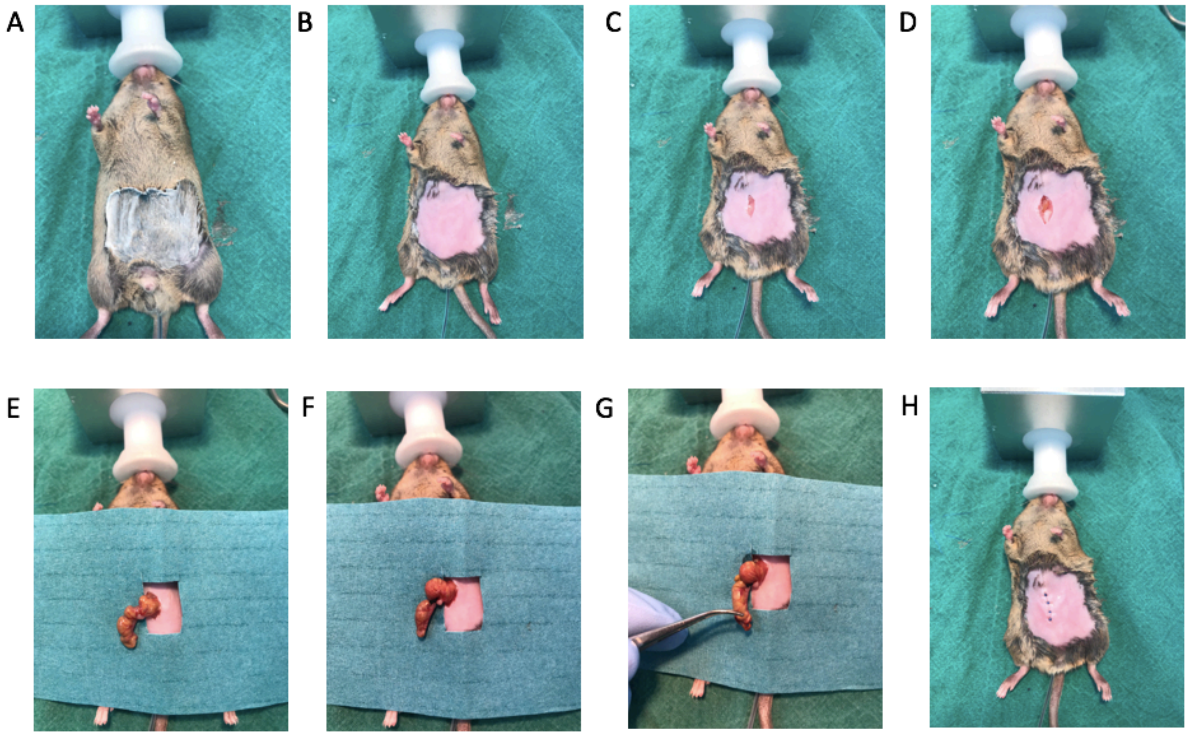

Figure 2.4 Schematic representation of the caecal ligation and puncture model. Mice were initially anaesthetised with 3% isoflurane, delivered in 1 L/min oxygen and maintained at 2% isoflurane and 1 L/min oxygen through nosecone. **(A)** Veet is applied to abdomen. **(B)** Veet cream is removed and skin is cleaned with ethanol. **(C)** A small incision in the midline of the abdomen. **(D)** Second incision on epithelia layer. **(E)** The caecum is taken out of the abdomen. **(F)** The caecum is completely ligated below the ileocaecal valve (roughly 1.5 cm from end of cecum). **(G)** A G-18 needle is used to puncture the top and end of the caecum and a small amount of faeces is squeezed out (roughly 3-4mm). **(H)** The caecum is then placed back into cavity and sutured up with proline 5mm needles.

2.2.7 The development of CLP-induced cardiac dysfunction over 24 h

10-week-old C57Bl/6 male mice underwent CLP surgery, or sham-operated surgery. At 0, 1, 3, 6, 12 and 24 h the development of cardiac dysfunction was assessed *in vivo* by echocardiography (Table 2.4).

Table 2.4 Experimental groups used to investigate CLP-induced cardiac dysfunction over 24 h

Group	Time (h)	Number
Sham	0	3
	1	3
	3	3
	6	3
	12	3
	24	5
CLP	0	4
	1	4
	3	4
	6	4
	12	4
	24	5

2.2.8 BTK inhibitors

Ibrutinib and acalabrutinib were purchased from Selleck Chemicals. Stock solutions were made in DMSO 5% and cyclodextrin 30% (vehicle).

2.2.9 Post-treatment with ibrutinib or acalabrutinib after CLP surgery

One hour after CLP surgery, animals were randomised to receive either ibrutinib (3 mg/kg i.v.), ibrutinib (30 mg/kg i.v.), acalabrutinib (3 mg/kg i.v.), or vehicle (5% DMSO + 30% cyclodextrin 3 ml/kg i.v.). Sham-operated mice were not subjected to ligation or perforation of the caecum but were otherwise treated the same way and received the vehicle 1 h after surgery (Table 2.5). Cardiac dysfunction was examined *in vivo* by echocardiography at 24 h after CLP surgery under anaesthesia (as described below) (Figure 2.5). At the end of the experiment, all mice were deeply sedated by inhalation of 3% isoflurane delivered in 0.4 L/min oxygen and approximately 0.7 ml of blood was obtained via cardiac puncture; the mice were then killed by removal of the heart. Heart, lungs, liver, kidney and spleen were all collected and stored at -80^{o}C for further analyses. The blood samples were centrifuged for 3 min at 9000 RPM and the serum was collected and frozen at -80^{o}C for further analysis (as described below).

Table 2.5 Experimental groups used to investigate the post-treatment with ibrutinib (3 mg/kg or 30 mg/kg) or acalabrutinib in CLP-induced cardiac dysfunction.

Strain	Group	Procedure	Total number
C57BL/6 10 weeks	Sham + vehicle	Sham surgery, then 5% DMSO + 30% cyclodextrin (3 ml/kg) i.v. at 1 h	10
	Control + vehicle	CLP surgery at 0 h, then 5% DMSO + 30% cyclodextrin (3 ml/kg) i.v. at 1 h	10
	CLP + ibrutinib (3 mg/kg i.v.)	CLP surgery at 0 h, then ibrutinib (3 mg/kg i.v.) at 1 h	10
	CLP + ibrutinib (30 mg/kg i.v.)	CLP surgery at 0 h, then ibrutinib (30 mg/kg i.v.) at 1 h	10
	CLP + acalabrutinib (3 mg/kg i.v.)	CLP surgery at 0 h, then acalabrutinib (3 mg/kg i.v.) at 1 h	10

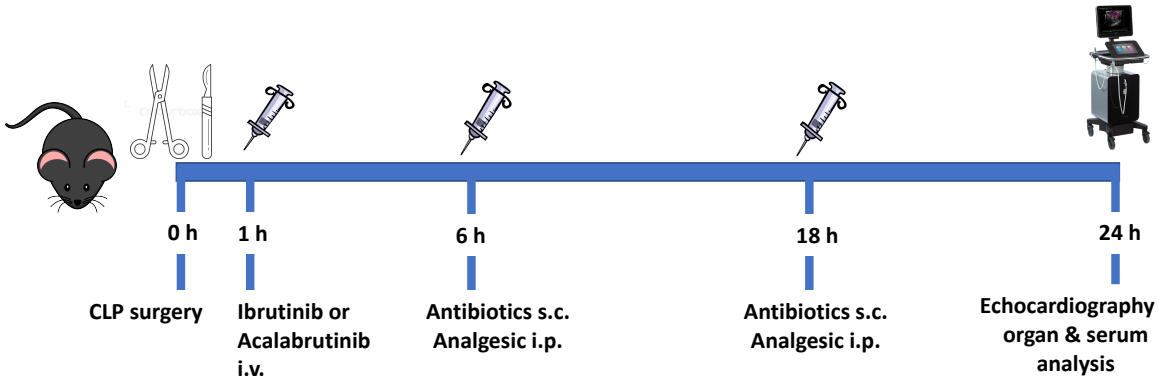

Figure 2.5 Schematic representation of caecal ligation and puncture model to investigate whether delayed intravenous administration of ibrutinib (3 mg/kg or 30 mg/kg) or acalabrutinib (3 mg/kg) attenuates CLP-induced cardiac dysfunction. At 0 h, 10-week-old, C57BL/6 mice underwent caecal ligation and puncture surgery to induce cardiac dysfunction. At 1 h, ibrutinib (3 mg/kg or 30 mg/kg), acalabrutinib (3 mg/kg), or vehicle (5% DMSO + 30% cyclodextrin) was administered intravenously. At 6 and 18 h antibiotics and analgesic were administration. At 24 h, cardiac function was assessed by echocardiography *in vivo*. At the end of the experiment blood samples and organs were collected to quantify organ dysfunction.

2.2.10 Assessment of cardiac function *in vivo* (echocardiography)

Cardiac function in mice was assessed by echocardiography *in vivo* by the Vevo 3100 imaging system (VisualSonics, Toronto, Ontario, Canada) (Figure 2.6). Mice were initially anaesthetised with 3% isoflurane (and received 1 - 0.4 L/min oxygen), and then anaesthesia was maintained between 2 - 1% isoflurane (and 1 - 0.4 L/min oxygen). Mice were left to stabilise for 10 min before assessment began. During echocardiography, the heart rate was maintained between 400 – 500 bpm. Mice were placed on a thermoregulatory platform (set at 42^{o}C) and a rectal thermometer was used to measure core body temperature, which maintained the body temperature at 37^{o}C. Electro-conducting gel was applied to the metal ECG pads and the paws of the animal were taped onto the ECG leads. Veet hair removal cream was applied to remove the fur from the chest and the chest was cleaned with 70% ethanol. Warmed ultrasound transmission gel was placed onto the shaven chest and the heart was imaged with the MX550D probe, whilst the platform was positioned pointing downwards slightly to the left (Figure 2.6). All images were downloaded and analysed offline using the Vevo Lab software.

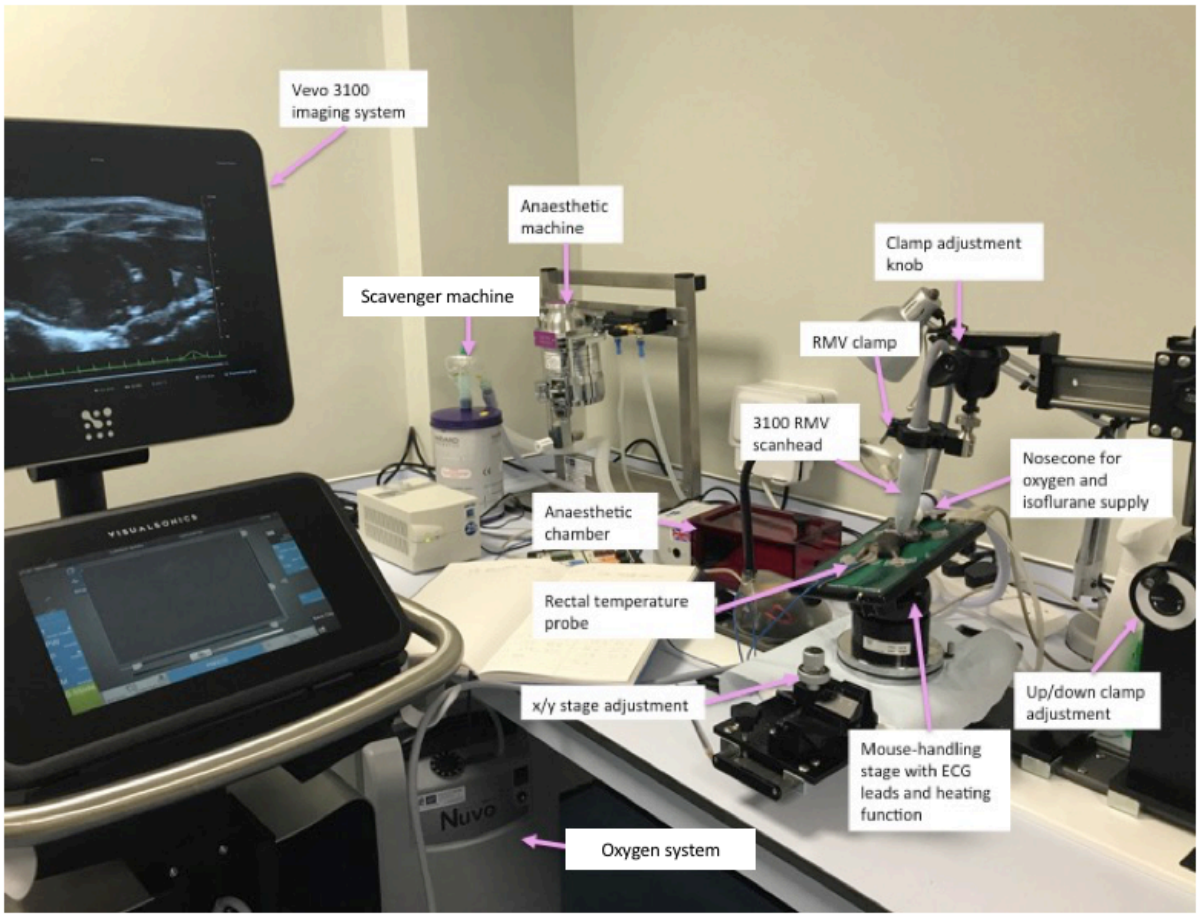

Figure 2.6 Vevo 3100 imaging system. Echocardiography was carried out on mice anesthetised with isoflurane. Mice were anesthetised in an aesthetic chamber. Once fully unconscious the mouse was moved onto the mouse handling platform where anaesthesia and oxygen were continuously supplied to the mouse through a nosecone. The platform could be adjusted by x/y stage adjustment. The paws were sellotaped to the ECG leads on the platform, where the heart rate was obtained from the ECG trace. The temperature was monitored throughout the experiment by a rectal probe. MX550D probe was connected to the RMV clamp. The clamp adjustment handle and the up/down adjustment scroll could be used to change the orientation of the RMV clamp and therefore the probe. All images were recorded on the Vevo 3100 imagining system.

To obtain the two-dimensional B-mode trace of the left ventricle (LV), the transducer was placed along the long axis of LV and directed towards the right of the mouse. The probe was then rotated clockwise by 90° to visualise the short axis (Figure 2.7). Percentage fraction area change (FAC) was calculated from two-dimensional B-mode LV image 100 x ([LV end-diastolic area – LV end-systolic area)/ LV end-diastolic area]. This was done by tracing the endocardial surface of the LV in the parasternal short-axis view at the papillary muscles (Figure 2.8).

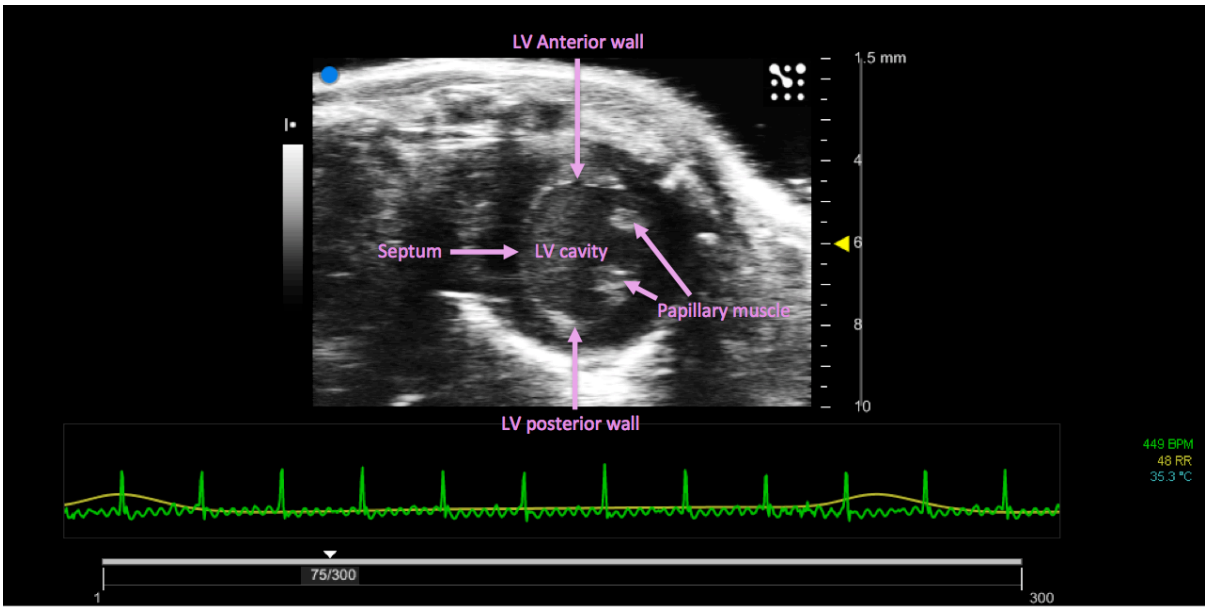

Figure 2.7 Representative B-mode echocardiography image of the mouse heart. The image was taken in the parasternal short-axis view showing the left ventricle (LV) in the centre and the papillary muscles to the right.

Systole

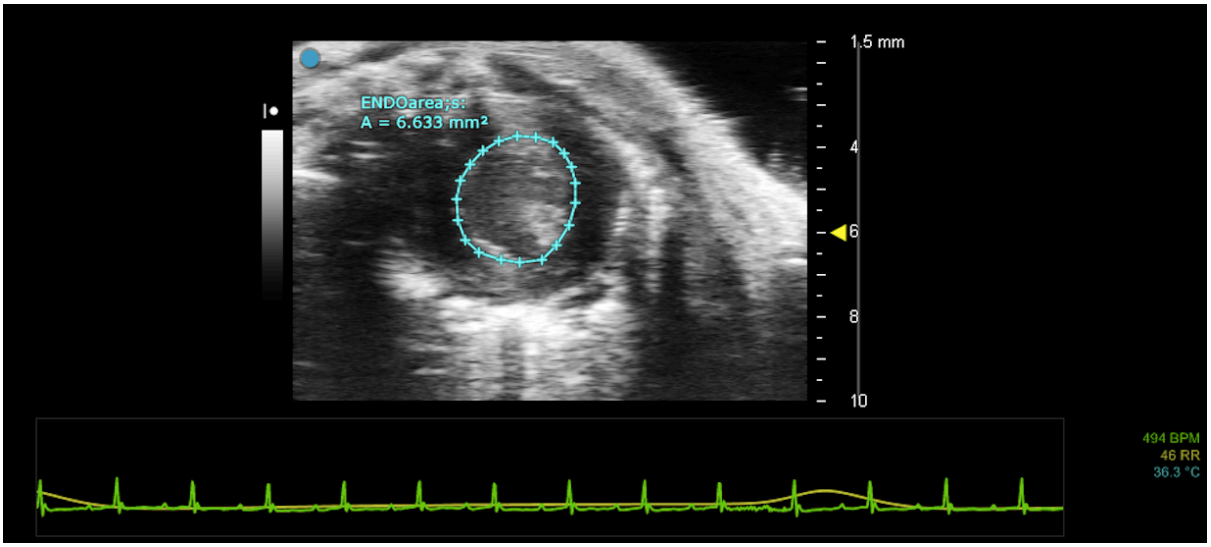

Diastole

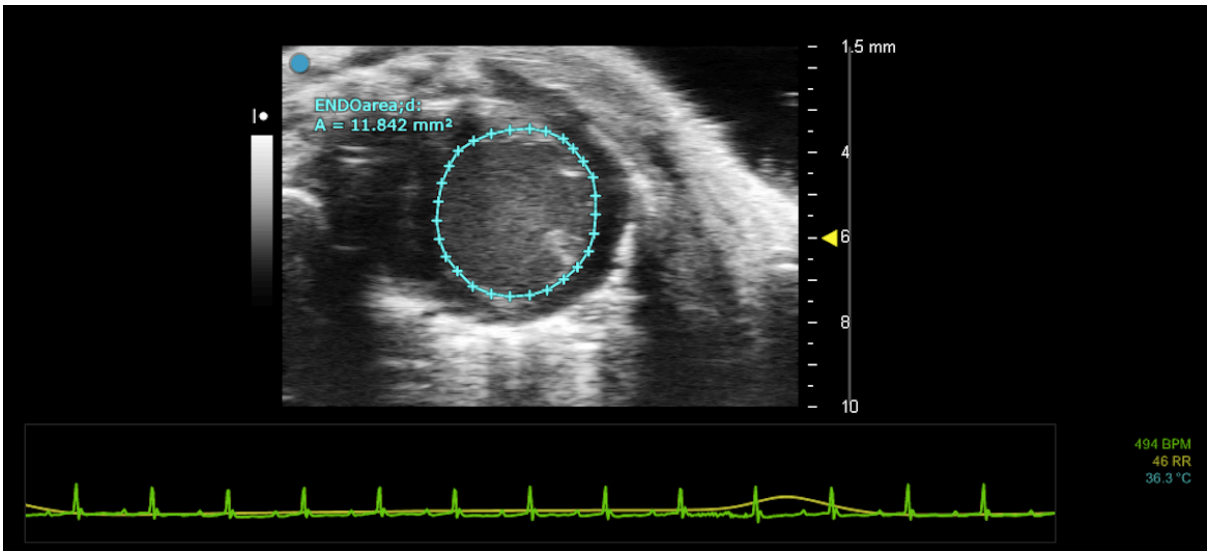

Figure 2.8 Endocardial tracing. In the parasternal short-axis B-mode view, measurements were taken by tracing the endocardial surface of the LV at the LV end-diastolic area and LV end-systolic area to calculate the percentage fractional area change (FAC).

One-dimensional M-mode images were obtained in the parasternal short-axis view of the papillary muscles (Figure 2.9) where the following was measured by LV trace (Figure 2.10):

- Ejection fraction (EF %) = 100 x [(LVIDd^3 – LVIDs)^3) / LVIDd^3]
- Fractional shortening (FS %) = 100 x [(LVIDd – LVIDs) / LVIDd]
- End diastole volume (EDV μL) = $\frac{7.0}{2.4+LVID;d} \times (LVID;d)^3$ x 1000
- End systole volume (ESV μL) = $\frac{7.0}{2.4+LVID;s} \times (LVID;s)^3$ x 1000
- Stroke volume (SV μL) = EDV - ESV
- Cardiac output (ml/min) = (SV x heart rate)/1000

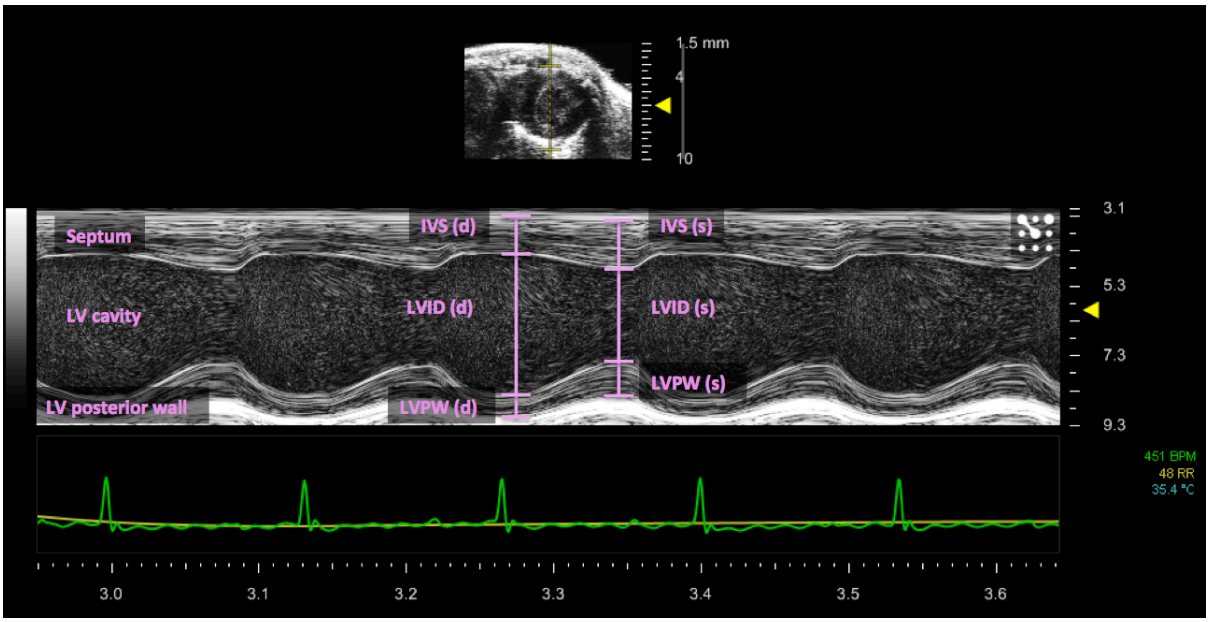

Figure 2.9 Representative M-mode echocardiography image of the mouses heart. The M-mode is a representative line of motion over time of the cardiac cycle, which is detected from the B-mode imaging in the parasternal short axis view at the level of the papillary muscles. IVS = Interventricular septum thickness, LVID = left ventricular internal diameter, LVPW = left ventricular posterior wall.

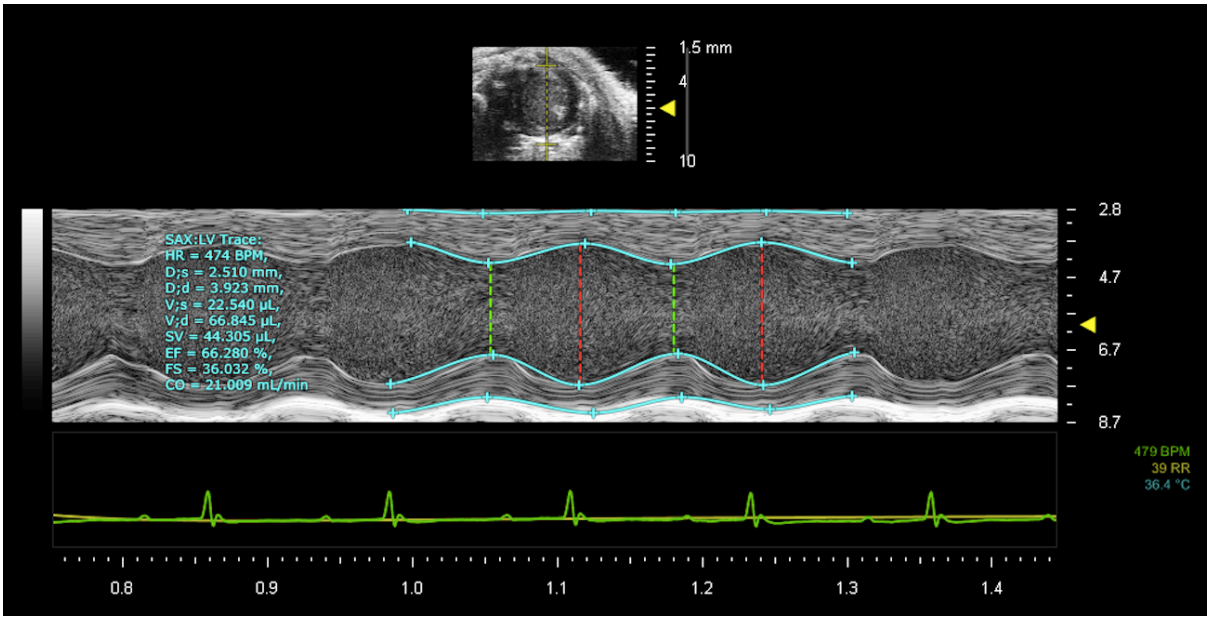

Figure 2.10 Left Ventricle (LV) trace. From this image ejection fraction (EF), fractional shortening (FS), cardiac output (CO), stroke volume (SV), end-diastolic volume and end-systolic volume, can be calculated, by measuring left ventricle internal dimension (LVID) in the diastolic and systolic phase. The measurements were taken from the inner surface of the interventricular septum (IVS) to the inner surface of the LV posterior wall (LVPW), whilst avoiding any interference from papillary muscles.

The four-chamber view was used to assess the diastolic dysfunction of the left side of the heart by measuring the blood flow in the mitral valve via pulsed wave Doppler (Figure 2.11). The following calculations were carried out:

- E/A ratio
- Myocardial performance index = (IVCT + IVRT)/ET or (NFT – AET)/ ET

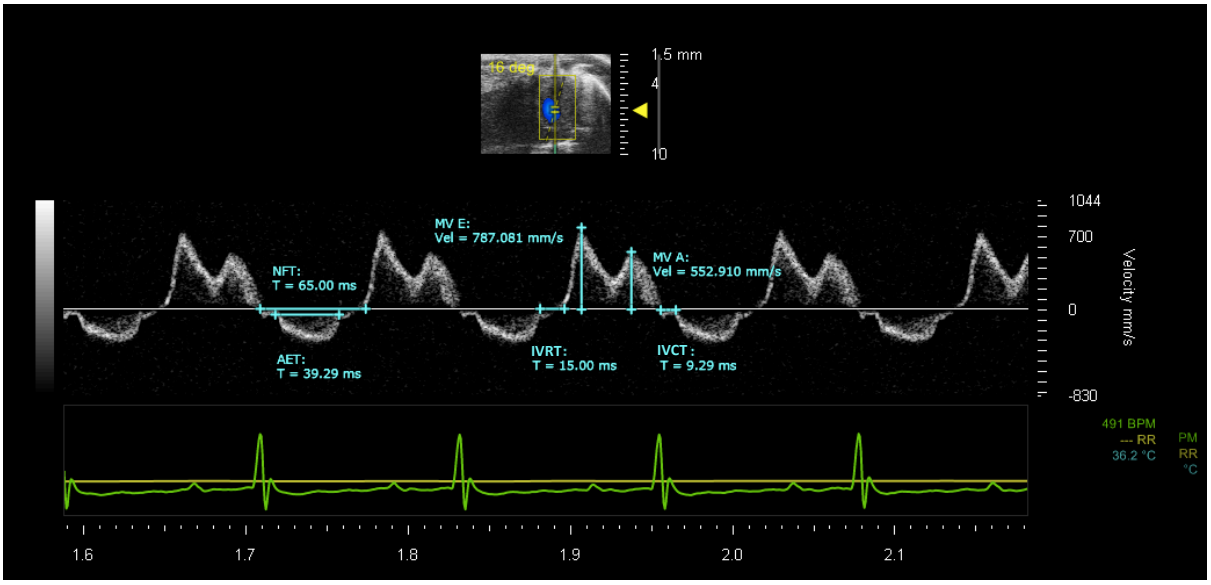

Figure 2.11 Representative four chamber view of the mitral valve blood flow in the mouse heart. The pulsed wave Doppler is used to measure the diastolic function of the left side of the heart through the mitral valve. The following measurements can be taken: the peak velocity of the early (E) and atrial (A) peak, isovolumic relaxation times (IVRT), isovolumic contraction times (IVCT), the no-flow time (NFT) and the aortic ejection time (AET).

Blood flow in the pulmonary artery was measured by pulsed wave Doppler (Figure 2.12). The following measurements are taken:

- Pulmonary valve peak velocity, which is an indicator of contractility.
- Pulmonary valve velocity-time integral (VTI), which indicates how far blood travels during the flow period.

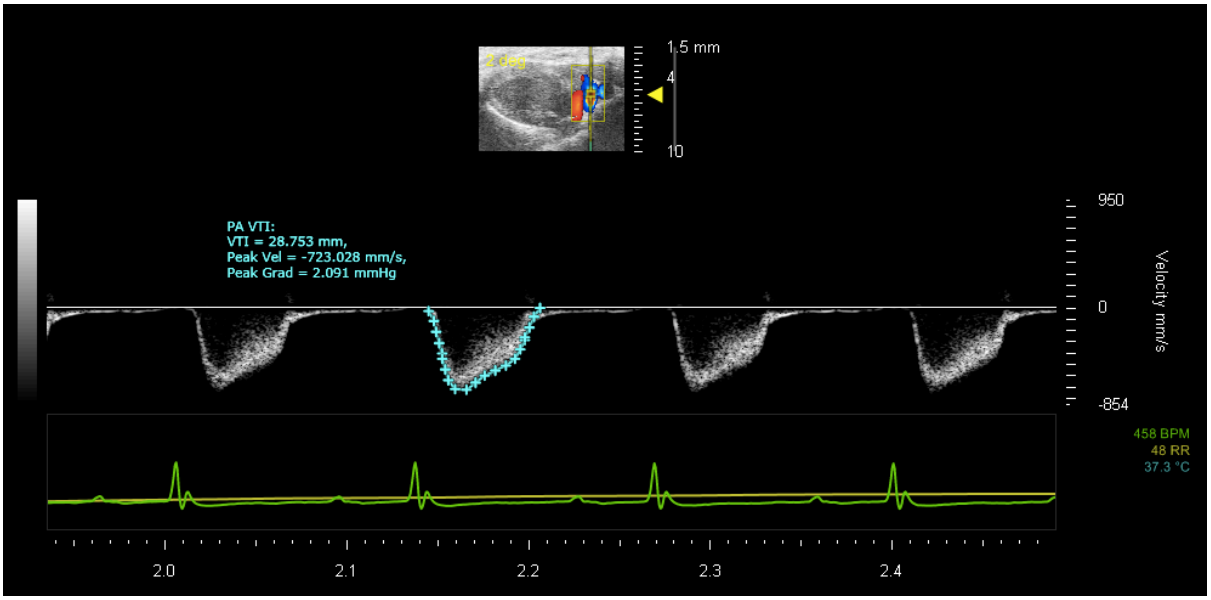

Figure 2.12 Representative blood flow in the pulmonary artery. The pulsed wave Doppler was used to measure the velocity and gradient of the blood flow through the pulmonary valve. The PA peak measures the peak velocity of blood flow and PA VTI measures the velocity-time integral.

2.2.11 Quantification of renal dysfunction and hepatocellular injury

Renal dysfunction and hepatocellular injury were analysed in all mice. The mice were anaesthetised with 3% isoflurane and delivered in 0.4 L/min. Full sedation was confirmed by no withdrawal response upon pain stimulation to the paws. The cardiac puncture was carried out with a G-26 needle and non-heparinized syringes to obtain approximately 0.7 ml of blood. The blood was immediately decanted into 1.3 ml serum gel tubes (Sarstedt, Nürnbrecht, Germany). The heart and lungs were then removed. Blood samples were left to coagulate for at least 10 min at room temperature, then samples were centrifuged at 9000 rpm for 3 min to separate the serum. Then 100 µL of serum was pipetted into a 1.5 ml Eppendorf and snap-frozen in liquid nitrogen. Serum and organs were stored at -80^{o}C for further analysis. The serum was then sent to an independent veterinary testing laboratory (MRC, Harwell) to blindly quantify serum urea, creatinine (markers of renal dysfunction), alanine aminotransferase (ALT) and aspartate aminotransferase (AST) (markers of hepatocellular injury).

2.2.12 Western blot

Immunoblot analyses of cardiac tissue samples were carried out using a semi-quantitative western blotting analysis.

2.2.12.1 Solutions and reagents

Solutions	Components	Solutions	Components
Homogenization buffer	20 mM Hepes-KOH pH 7.9 1 mM $MgCl_2$ 0.5 mM EDTA 1 mM EGTA 1% NP-40 100 ml dH_2O Protease inhibitors (add just before use) 1 µl/ml protease inhibitor cocktail (PIC) 0.5 mM PMSF 0.1 mM DL-Dithiethrectol (DTT)	**Extraction buffer**	20 mM Hepes-KOH pH 7.9 1.5 mM $MgCl_2$ 0.2 mM EDTA 1 mM EGTA 20 % glycerol 420 mM NaCl 50 ml dH_2O Protease inhibitors (add just before use) 1 µl/ml (PIC) 0.5 mM PMSF 0.1 mM (DTT)
Loading buffer	4% SDS 20% glycerol 0.004% Bromophenol blue 0.125 MTris-HCl	**Running buffer**	25 mM TRIS 190 mM glycine 0.1% SDS dH_2O
Transfer buffer	48 mM TRIS 39 mM glycine 15% methanol 0.04% SDS dH_2O	**Blocking buffer**	0.1% tween 10% milk TBS
Primary antibody solution	0.1% Tween 5% milk 1:1000 rabbit anti-$Ser^{176/180}$-IKKα/β 1:1000 rabbit anti-total IKKα/β 1:1000 mouse anti-$Ser^{32/36}$-IκB□□ 1:1000 mouse anti-total IκB□□, 1:1000 rabbit anti-NF-κB, 1:1000 rabbit anti-total BTK, 1:1000 rabbit anti-Tyr^{1217} PLCγ, 1:1000 rabbit anti-total PLCγ (from Cell Signaling), 1:1000 rabbit anti-Tyr^{223}-BTK, 1:5000 rabbit anti NLRP3 inflammasome (from Abcam), 1:1000 mouse anti-caspase 1 (p20) (from Adipogen) TBS	**Secondary antibody solution**	25 ml TBS 5% milk Dilution 1:50000 secondary antibody conjugated with horseradish peroxidase (HRP) 0.005% StrephTactin-HRP
Washing buffer	0.1% Tween TBS		

2.2.12.2 Tissue homogenization and cytosolic and nuclear protein collection

1. The apex of the heart was taken and homogenized with homogenization buffer in ice at a concentration of 1:10 (e.g. 30 g of tissue in 300 µl of homogenization buffer).
2. Centrifuge at 4000 RPM (1320 G) for 5 min at 4°C.
3. Separate the supernatant (supernatant 1) from the pellet (pellet 1).
4. Centrifuge the supernatant 1 at 14000 RPM (16215 G) for 40 min at 4°C. The obtained supernatant (supernatant 2) contains the cytosolic proteins.
5. Resuspend the Pellet 1 in extraction buffer at a concentration of 1/3 compared to the homogenization buffer (e.g. 100 µl).
6. Incubate for 30 min in ice vortexing occasionally.
7. Centrifuge at 14000 RPM (16215 G) for 20 min at 4°C. The obtained supernatant (supernatant 3) contains the nuclear proteins.
8. Freeze the supernatant 2 (cytosolic proteins) and supernatant 3 (nuclear proteins) at -80°C for future use. Refer to Figure 2.13 for schematic diagram.

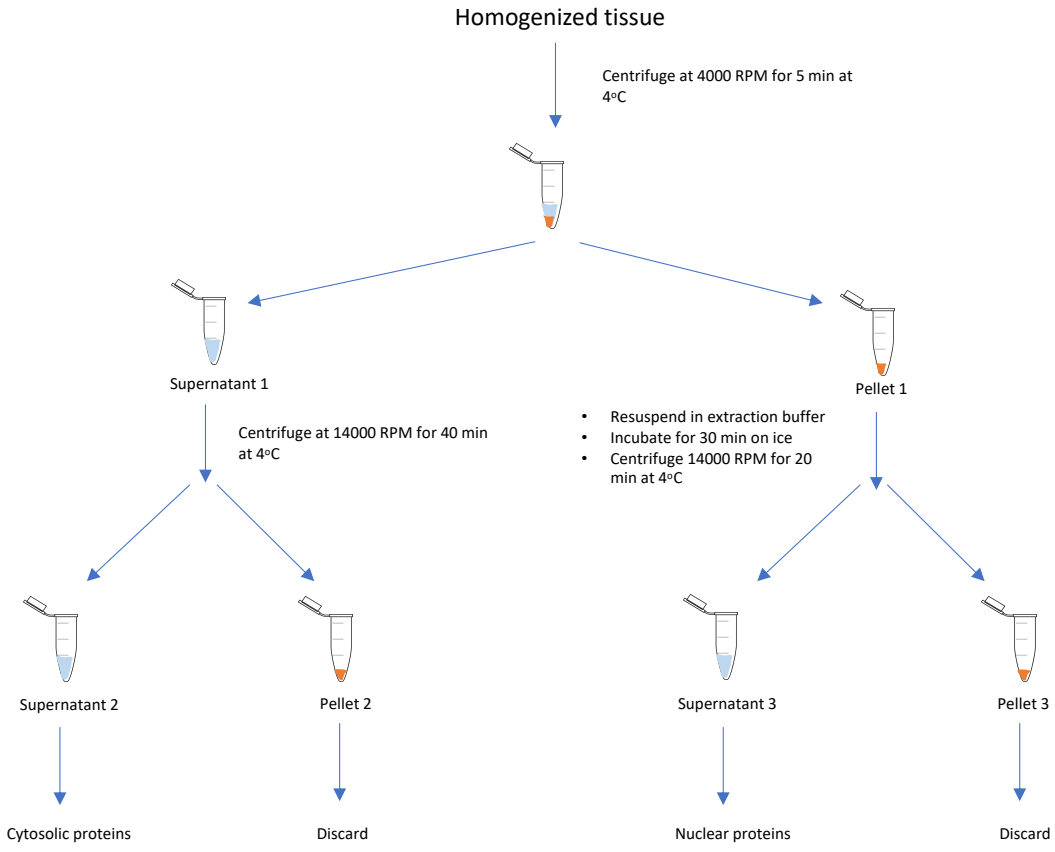

Figure 2.13 Diagram of extracting cytosolic and nuclear proteins from homogenised tissue.

2.2.12.3 Bicinchoninic acid (BCA) protein assay

Protein concentrations were quantified by bicinchoninic acid (BCA) protein assay (Thermo Fisher Scientific Rockford, IL) refer to Figure 2.14 for mechanism of the assay.

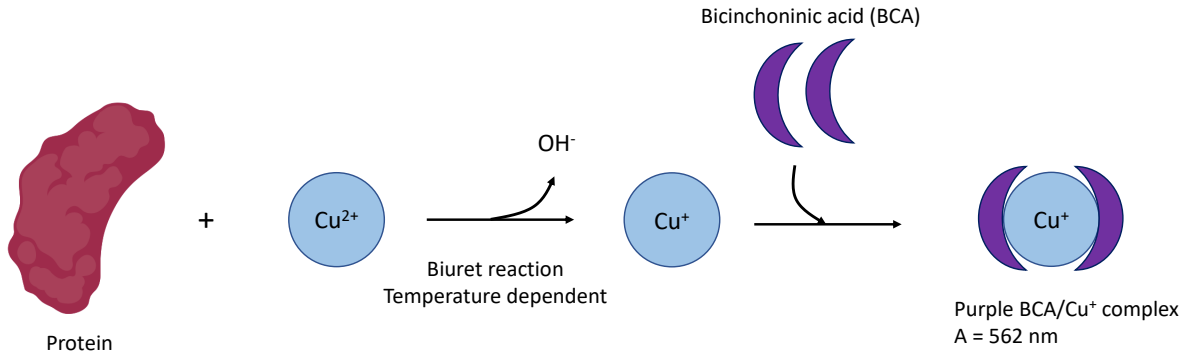

Figure 2.14 Schematic diagram of the mechanism of action of the Bicinchoninic acid (BCA) protein assay. First step - the biuret reaction: proteins reduce Cu^{+2} to Cu^{+} in an alkaline solution. Second step: Cu^{+} bind with bicinchoninic acid forming a Cu^{+}/BCA complex which results in an intense purple colour.

Make up BCA standard curve albumin.

1. Make up BCA buffer by adding buffer A to buffer B at 50:1.
2. Add 3 µl of cytosolic or nuclear protein sample, 27 µl of distilled water and 570 µl BCA solution to each well (in duplicates).
3. Negative control – add 30 µl of distilled water and 570 µl of BCA solution into one well.
4. Incubate at 37°C for 30 min in the dark for the reaction to take place (Figure 2.15).
5. Read plate (program, 560 nm).
6. Calculate protein concentrations.

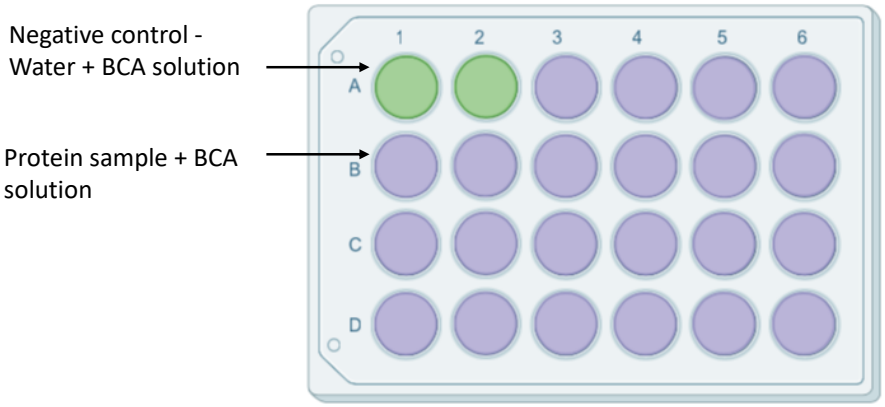

Figure 2.15 Plate after incubation of BCA. The purple BCA/copper complex results in strong linear absorbance at 562 nm with increasing protein concentration. Negative control does not react and stays light green.

2.2.12.4 Loading and running the gel

1. Load 60 µg total cytosol protein samples or 30 µg of nuclear protein samples into the wells of 8% sodium dodecyl sulphate polyacrylamide gel electrophoresis (SDS-PAGE), along with 5 µl molecular weight markers. Empty wells were loaded with 5 µl sample buffer.
2. Total loading volume for protein sample loaded well was 15 µl (e.g. 4.96 µl protein sample + 7.04 µl distilled water (12 µl total) + 3 µl sample buffer).
3. Before loading boil the sample at 60^{o}C for 10 min to accelerate the effect of SDS in breaking 3rd protein structures.
4. Vortex samples for 30 sec.
5. Load samples into the wells – load molecular weight sample first (5 µl of precision plus protein western standard). Slowly pipette and avoid bubbles.
6. Run the gel for 35 min at 200 V (the smaller the protein the faster it runs).

2.2.12.5 Transferring protein from the gel to polyvinyldenedifluroide (PVDF) paper membrane

1. Cut filter 8.5 cm by 5.5 cm.
2. Place filter in methanol for 10 sec.
3. Place membrane into transfer buffer for 5 min.
4. Make transfer sandwich (Figure 2.16).
5. Place into machine and put a magnet at the bottom and a block of ice fill with transfer buffer. Place on a magnetic stirrer and running for 70 min at 100 V, 180 mA.

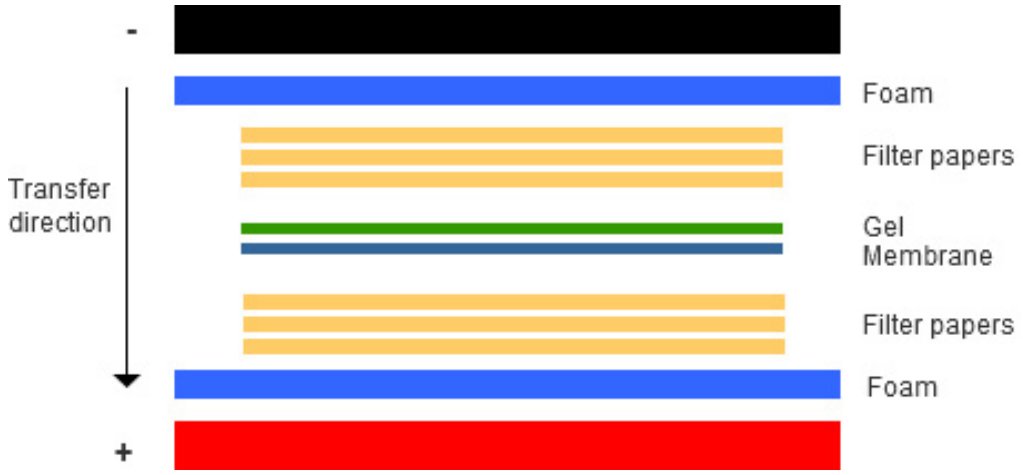

Figure 2.16 Transfer sandwich.

2.2.12.6 Antibody incubation

1. Remove PVDF membrane and wash in washing buffer for 10 min.
2. Block membrane for 30 min at 4°C.
3. Wash membrane with washing buffer for 10 sec.
4. Incubate membrane with appropriate dilutions of primary antibody in 5% blocking solution overnight at 4°C.
5. Wash membrane with washing buffer 3 x 5 min.
6. Incubate membrane with secondary antibody solution for 30 min at room temperature.
7. Wash membrane with washing buffer 3 x 5 min.

2.2.12.7 Visualisation

1. ECL: add buffer 1 to buffer 2 (2 ml in total for 1 filter 1:1 concentration) stand 1 min then pour the solution onto membrane.
2. Leave in the dark for 10 min then discard.
3. Cover the membrane in transparent plastic wrap, place it into film cassette in dark room, and place a film on it.
4. Place film into developing solution for 10 sec, then stop the reaction by placing it into water, fix film in fixing solution.
5. Ensure all light sensitive products have been put away before turning on the light.
6. Strip membrane (add Invitrogen Western stripping solution. Incubate 10 min/ RT/ shaking).

7. Wash membrane in washing buffer 3 x 5 min.
8. Incubate in blocking buffer for 30 min shaking at room temperature.
9. Store in fridge, or reprobe with another primary antibody.
10. The immunoreactive bands were analysed by the Bio-Rad Image Lab Software™ 6.0.1 and results were normalized to the sham bands.

2.2.13 Multiplex flow immunoassay

The principle of multiplex flow immunoassay technology has been reviewed previously (222,223). Cytokines, chemokines and a growth factor were determined in serum by Bio-Plex Pro Mouse Chemokine 33-plex panel assay (Bio-Rad, Kabelsketal, Germany). The cytokines IL-1ß, -2, -4, -6, -10, -16, CCL1, -2, -3, -4, -5, -7, -11, -12, -17, -19, -20, -22, -24, -25, -27, IFN-γ, TNF-α and the chemokines CX3CL1, CXCL1, -2, -5, -10, -11, -12, -13, -16 and the growth factor GM-CSF were measured according to the manufacturer's instructions. The assays were performed in one batch, with samples randomly distributed (Figure 2.17). The lower detection limit was 3.2 pg/ml for all the analytes. Data were collected and analysed using a Bio-Plex® 200 instrument equipped with Bio-Plex Manager software (Bio-Rad).

1. Add 50 µl of 1 x beads to each well.
2. Wash the plate twice with 100 µl of Bio-plex wash buffer per well.
3. Add 50 µl standards, samples, controls and incubate on shaker at 850 RPM for 30 min at room temperature.
4. Wash the plate three times with 100 µl of Bio-plex wash buffer per well.
5. Add 25 µl 1 x detection antibody and incubate on shaker at 850 RPM for 30 min at room temperature.
6. Wash three times.
7. Add 50 µl 1 x streptavidin-PE and incubate on shaker at 850 RPM for 10 min at room temperature.
8. Wash three times.
9. Resuspend in 125 µl assay buffer and shake at 850 RPM for 30 sec.
10. Acquire data on Bio-Plex system.

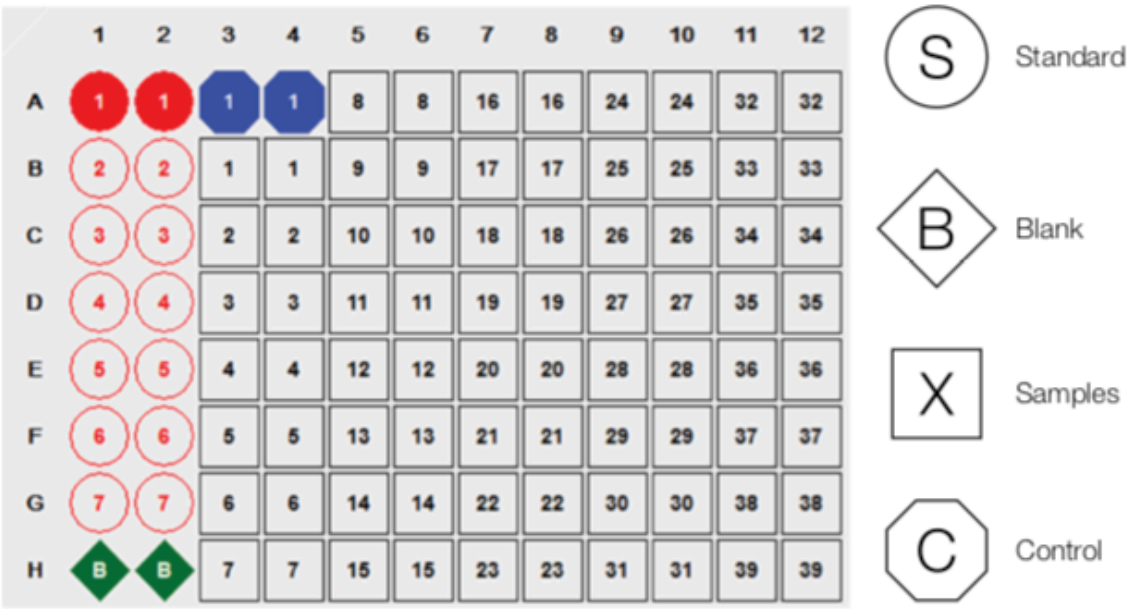

Figure 2.17 Diagram of multiplex layout

2.2.14 Peritoneal lavage

Mice were anaesthetised by overdose of isoflurane. Once confirmed dead, peritoneal cells were obtained by injecting 5 ml of 2mM EDTA + PBS -/- using a 25-G needle. Cells attached were dislodged by gentle massage of the peritoneum and collected by using an 18-G needle. Approximately 4 ml of the peritoneal fluid was obtained and decanted into 15 ml falcon tubes on ice.

2.2.15 Quantification of immune cells in the peritoneum

One ml of peritoneal exudate was added to FACS tubes and immediately washed in 1 ml FACS buffer (0.05 % BSA, 2 mM EDTA in PBS pH 7.4). Tubes were then centrifuged at 300 G for 5 min. After centrifugation, the supernatant was discarded. Before staining for cell surface markers Fc receptors were blocked using anti-CD16/32 (Biolegend) for 10 min at 4°C. The cells were then washed with FACS buffer, centrifuged and the supernatant was discarded. Peritoneal cells were incubated for 30 min at 4°C in the dark with anti-CD45 (clone 30-F11; BioLegend), anti-CD11b (clone M1/70; BioLegend), anti-F4/80 (clone BM8; BioLegend), anti-Ly6G (clone 1A8; BioLegend), anti-CD3 (clone 145–2C11; BioLegend) and anti-B220 (clone. RA-3–6B2; BioLegend) antibodies, all at 1:200 concentration. After 30 min the cells were washed with FACS buffer, centrifuged and the supernatant was discarded. The cells were then fixed in 200 µl of 2% PFA ready for FACS analysis and stored in the dark at 4°C to be analysed within 48 hours. On the day of analysis, 10 µl of counting beads (Biolegend) was added. Data were acquired using BD LSR II Fortessa (Becton Dickinson) and analysed using FlowJo analysis software (version 10.6, Treestar Inc.). Gating strategy is seen below in Figure 2.18.

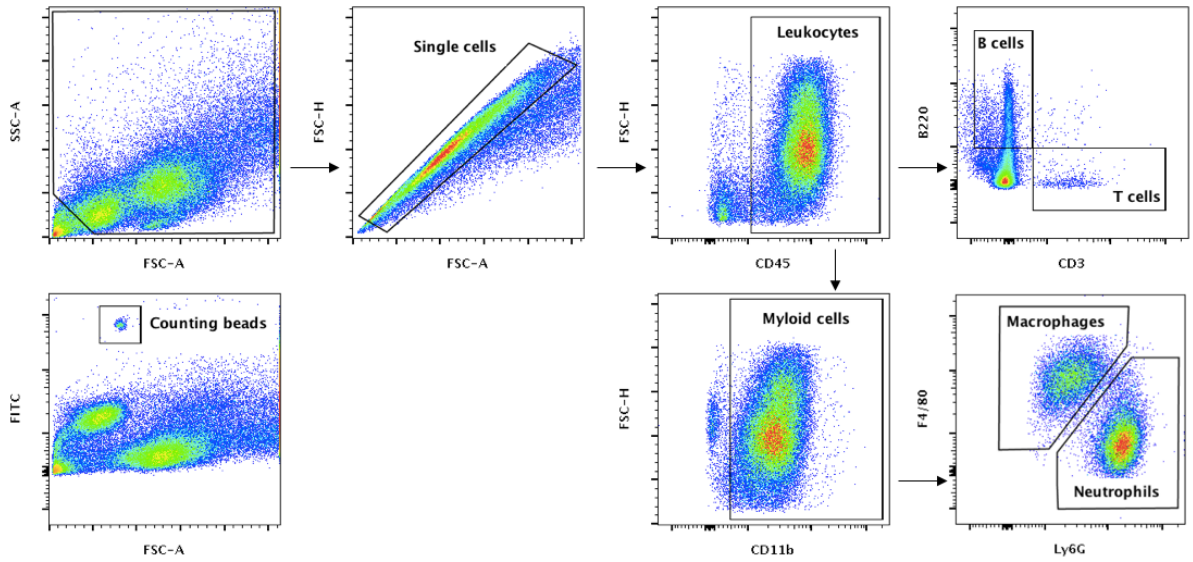

Figure 2.18 Flow cytometry gating strategy for infiltrating immune cells in sham-operated and CLP mice over 24 h.

2.2.16 Bacteria quantification

Accurate evaluation of the number of bacteria in peritoneal lavage fluid was performed by flow cytometry using the SYTO BC bacteria counting kit (Thermo Fischer Scientific). One ml of peritoneal exudate was centrifuged at 300 G for 5 min at 4°C. The supernatant was discarded, and the cells were stained with SYTO® BC bacteria stain (1:1000) at room temperature for 15 min. Cells were then washed in PBS, centrifuged at 300 G for 5 min at 4°C and the supernatant was discarded afterwards. Cells were then resuspended in 990 µl PBS and 10 µl of Microspheres (counting beads) were added ready for analysis.

2.2.17 Statistical analysis

All data are expressed as mean ± standard error mean (SEM) where *n* represents the number of animals studied. Statistical differences were determined using a one-way ANOVA, followed by Bonferroni post hoc test. Correlations coefficients were determined by Pearson's correlation with *P*-values based on two-tailed tests. All statistical tests were carried out on GraphPad Prism 8.0 (GraphPad Software, Inc., La Jolla, CA, USA) and differences were considered to be statistically significant when $P < 0.05$.

2.3 Results – LPS/PepG model

2.3.1 LPS (7 mg/kg) and PepG (1 mg/kg) caused sufficient cardiac dysfunction in 10-week-old C57BL/6 mice

Left ventricular function was assessed by echocardiography 18 h after i.p. administration of LPS/PepG or vehicle (PBS). When compared to sham-operated mice, co-administration of LPS (6 mg/kg) and PepG (0.1 mg/kg) had no significant effect on any of the parameters of cardiac dysfunction (EF, FS and FAC). The dose of PepG was then increased from 0.1 mg/kg to 1 mg/kg. When compared to sham-operated mice, the co-administration of LPS (6 mg/kg) and PepG (1 mg/kg) resulted in a significant reduction of EF and FS (Figure 2.19 A-C), but only a small (nonsignificant) decrease was observed for FAC (Figure 2.19 D). The dose of LPS was then increased from 6 mg/kg to 7 mg/kg. When compared to sham-operated, co-administration of LPS (7 mg/kg) and PepG (1 mg/kg) resulted in significant reductions for all parameters of cardiac function (Figure 2.19 A-D). Thus, I selected the following dose of LPS (7 mg/kg) and PepG (1 mg/kg) for all further studies of the LPS/PepG model.

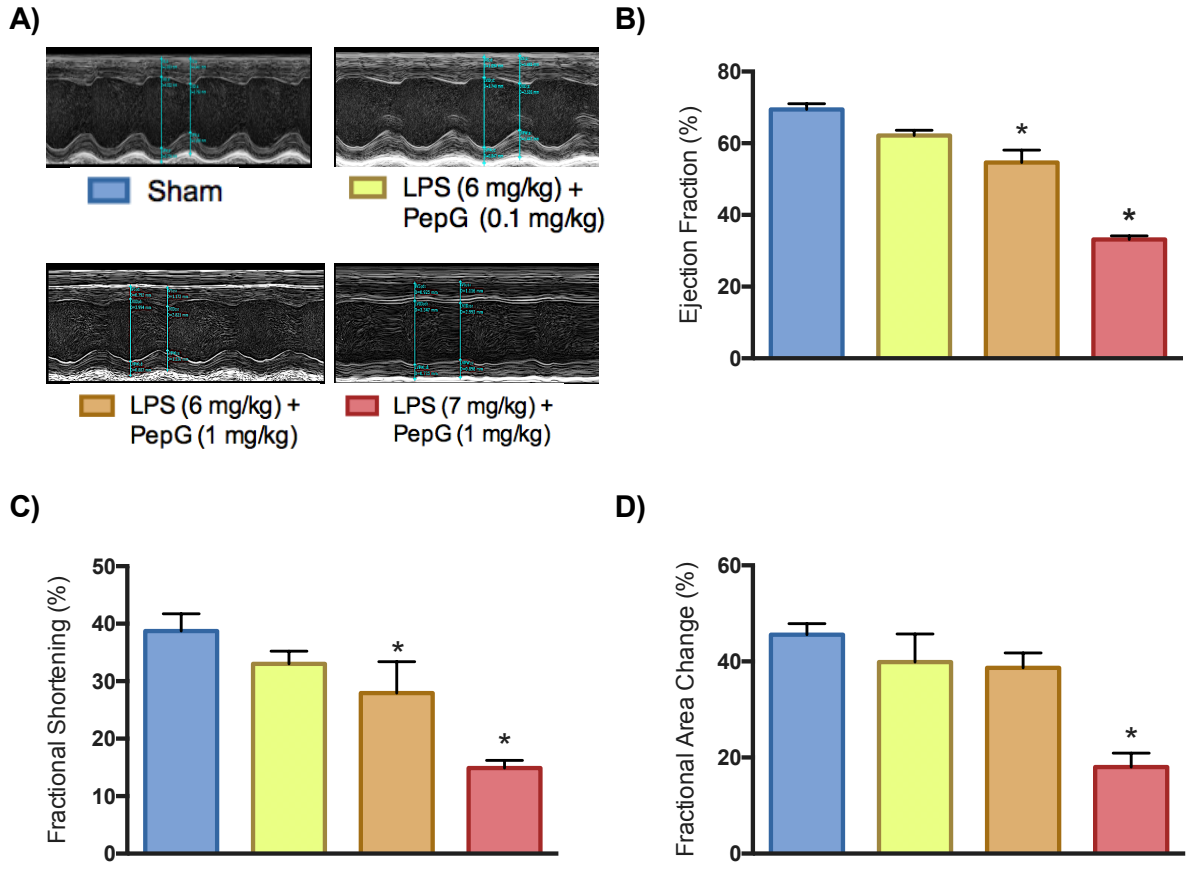

Figure 2.19 LPS (7 mg/kg) and PepG (1 mg/kg) caused sufficient cardiac dysfunction in 10-week-old C57BL/6 mice. Mice were randomly selected to be injected with either LPS/PepG or PBS i.p. 18 h later cardiac function was assessed via echocardiography. **(A)** Representative M-mode echocardiograms. **(B)** Ejection fraction (%). **(C)** Fractional shortening (%). **(D)** Fractional area change (%). The following groups were studied, sham (n = 6), LPS (6 mg/kg) + PepG (0.1 mg/kg) (n = 3), LPS (6 mg/kg) + PepG (1 mg/kg) (n = 3), LPS (7 mg/kg) + PepG (1 mg/kg) (n = 5). All data are expressed as mean ± SEM for n number of observations. A value of $^*P < 0.05$ was considered to be statistically significant when compared to sham by one-way ANOVA followed by a Bonferroni's post hoc test.

2.3.2 The effects of oral ibrutinib pre-treatment on heart rate and temperature in mice subjected to LPS/PepG

When compared to sham-operated animals, mice subjected to LPS/PepG and treated with vehicle resulted in a significant decrease in temperature. When compared to LPS/PepG mice treated with vehicle, the administration of ibrutinib 1 h before LPS/PepG attenuated LPS/PepG-induced hypothermia (demonstrated as a significant rise in temperature). No significant differences were observed for the changes in mean heart rates for all groups (Table 2.6).

Table 2.6 The effects of oral ibrutinib pre-treatment on heart rate and temperature in mice subjected to LPS/PepG

	Sham	**LPS/PepG + vehicle**	**LPS/PepG + ibrutinib (30 mg/kg p.o.)**
Number	5	5	5
Temperature (°C)	36.24 ± 0.103*	28.74 ± 1.422	32.02 ± 1.317*
Heart rate (bpm)	456.8 ± 21.15	392.8 ± 32.01	440.4 ± 12.31

Mice received LPS/PepG or vehicle (PBS) (i.p.). One hour later, mice were treated with either ibrutinib (30 mg/kg p.o.) or vehicle (5% DMSO + 30% cyclodextrin p.o.). Heart rate and temperature were recorded 18 h after LPS/PepG administration. All data are expressed as mean ± SEM for *n* number of observations. A value of $*P < 0.05$ was considered to be statistically significant when compared to control by one-way ANOVA followed by a Bonferroni's post hoc test.

2.3.3 Pre-treatment of oral ibrutinib attenuates LPS/PepG-induced cardiac dysfunction.

When compared to sham-operated animals, mice subjected for 18 h to LPS/PepG and treated with vehicle demonstrated a significant reduction in left ventricular EF, FS and FAC indicating the development of systolic cardiac dysfunction (Figure 2.20 A-D). In contrast, pre-treatment of ibrutinib (30 mg/kg p.o.) 1 h before LPS/PepG significantly prevented the decline in percentage EF, FS and FAC (Figure 2.20A-D).

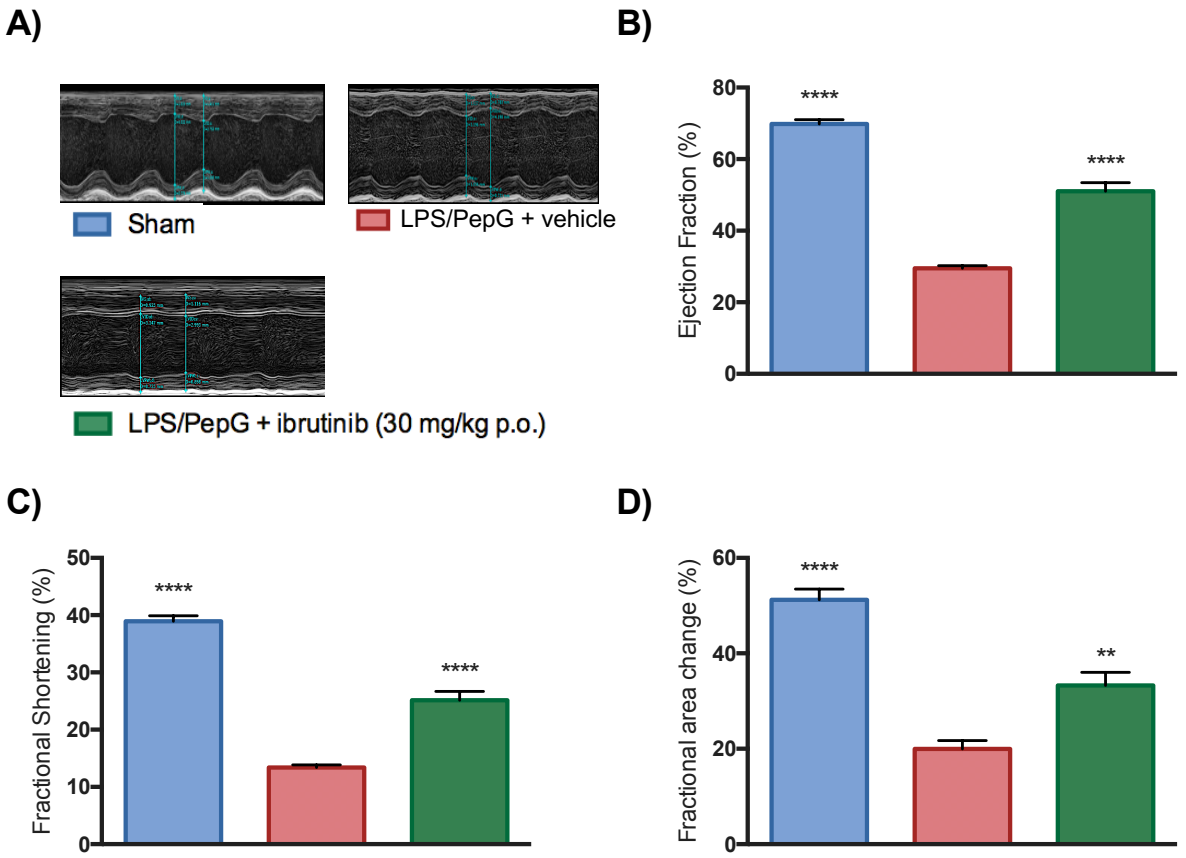

Figure 2.20 Pre-treatment of oral ibrutinib (30 mg/kg) attenautes LPS/PepG-induced cardiac dysfunction. Mice were pre-treated with ibrutinib (30 mg/kg p.o.) or vehicle (5% DMSO + 30% cyclodextrin p.o.) 1 h before administration of LPS/PepG (i.p.). Cardiac function was assessed 18 h after LPS/PepG administration. **(A)** Representative M-mode echocardiograms. **(B)** Ejection fraction (%). **(C)** Fractional shortening (%). **(D)** Fractional area change (%). The following groups were studied sham, LPS/PepG + vehicle, LPS/PepG + ibrutinib (30 mg/kg p.o.). All data are expressed as mean ± SEM for $n = 5$ per group. A value of $^{**}P < 0.01$, $^{****}P < 0.0001$ was considered to be statistically significant when compared to LPS/PepG + vehicle by one-way ANOVA followed by a Bonferroni's post hoc test.

2.3.4 The effects of oral ibrutinib pre-treatment on LPS/PepG-induced renal dysfunction and hepatocellular injury

When compared to sham-operated mice, mice subjected to LPS/PepG and treated with vehicle resulted in a significant increase in serum urea and ALT (Figure 2.21 A&B). However, the increase in AST caused by LPS/PepG was not significant (Figure 2.21 C). In comparison to LPS/PepG mice pre-treated with vehicle, mice pre-treated with ibrutinib 1 h before LPS/PepG had lower serum levels of urea, ALT and AST, but these effects were not significant (Figure 2.21 A-C).

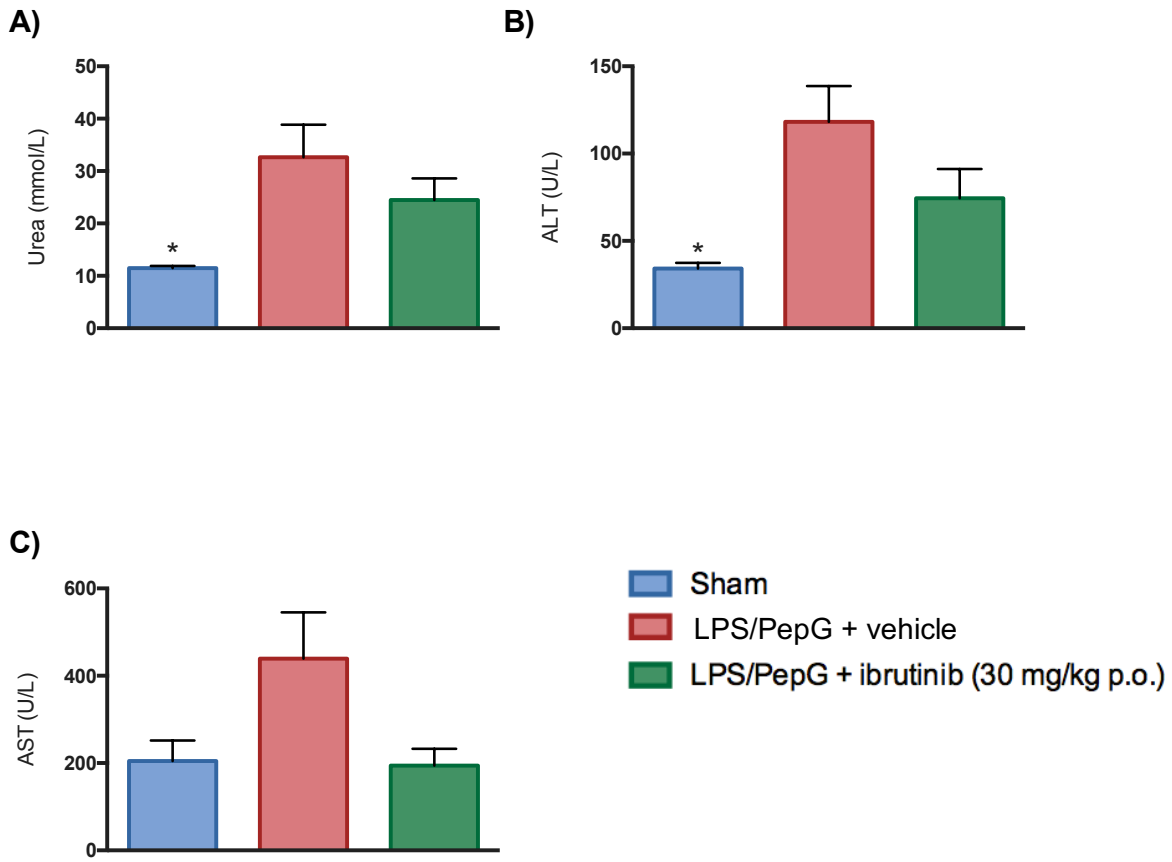

Figure 2.21 The effects of oral ibrutinib pre-treatment on LPS/PepG-induced renal dysfunction and hepatocellular injury. Mice were pre-treated with ibrutinib (30 mg/kg p.o.) or vehicle (5% DMSO + 30% cyclodextrin p.o.) 1 h before administration of LPS/PepG (i.p.). 18 h after LPS/PepG administration blood samples were collected for analyses. **(A)** Serum urea (mmol/L). **(B)** Alanine aminotransferase (ALT) (U/L). **(C)** Aspartate transaminase (AST) (U/L). The following groups were studied sham, LPS/PepG + vehicle and LPS/PepG + ibrutinib (30 mg/kg p.o.). All data are expressed as mean ± SEM for $n = 5$ per group. A value of $^*P < 0.05$ was considered to be statistically significant when compared to LPS/PepG + vehicle by one-way ANOVA followed by a Bonferroni's post hoc test.

2.3.5 The effects of delayed administration of ibrutinib (3 mg/kg or 30 mg/kg) in a model of endotoxemia

When compared to sham-operated mice, mice subjected to LPS/PepG and treated with vehicle, resulted in a decrease in mean heart rate. When compared to LPS/PepG mice treated with vehicle, the administration of ibrutinib (3 mg/kg or 30 mg/kg i.v.) resulted in no significant difference of mean heart rate (Table 2.7).

When compared to sham-operated mice, mice subjected to LPS/PepG and treated with vehicle resulted in a decrease in temperature. When compared to LPS/PepG mice treated with vehicle, the administration of ibrutinib (3 mg/kg or 30 mg/kg i.v.) resulted in no significant differences in temperature (Table 2.7).

When compared to sham-operated mice, mice subjected to LPS/PepG and treated with vehicle developed, at 18 h, significant increases in urea and AST (Table 2.7), while the increase in ALT was not significant (Table 2.7). In contrast, mice treated with (3 mg/kg or 30 mg/kg i.v.) 1 h after LPS/PepG showed no significant differences in serum urea, ALT and AST when compared to LPS/PepG mice (Table 2.7).

Table 2.7 Heart rate, temperature, renal dysfunction and hepatocellular injury responses to intravenous administrated ibrutinib at low (3 mg/kg) and high concentrations (30 mg/kg) in LSP/PepG mice.

	Sham	LPS+PepG + vehicle	LPS/PepG + ibrutinib (3 mg/kg i.v.)	LPS/PepG + ibrutinib (30 mg/kg i.v.)
Number	10	10	10	10
Temperature (°C)	36.1 ± 0.1*	28 ± 0.9	30.3 ± 1.1	31.7 ± 1.2
Heart rate (bpm)	444 ± 7*	372 ± 26	422 ± 20	414 ± 22
Urea (mmol/L)	9.060 ± 0.337*	38.01 ± 2.728	32.64 ± 2.886	34.77 ± 3.816
ALT (U/L)	36.6 ± 5.81	98.1 ± 19.04	124.5 ± 32.16	100.2 ± 16.24
AST (U/L)	109.2 ± 14.2*	303.6 ± 57.12	280.2 ± 42.07	322.1 ± 41.35

Mice received LPS (7 mg/kg) and PepG (1 mg/kg), or vehicle (i.p.). One hour later, mice were treated with ibrutinib (3 mg/kg i.v.), ibrutinib (30 mg/kg i.v.) or vehicle (5% DMSO + 30% cyclodextrin i.v.). The heart rate, temperature, serum urea, ALT and AST were measured in mice 18 h after co-administration of LPS/PepG. All data are expressed as mean ± SEM for *n* number of observations. A value of $*P < 0.05$ was considered to be statistically significant when compared to LPS/PepG + vehicle by one-way ANOVA followed by a Bonferroni's post hoc test.

2.3.6 Delayed administration of ibrutinib (3 mg/kg or 30 mg/kg) attenuates LPS/PepG-induced cardiac dysfunction

When compared to sham-operated mice, mice subjected for 18 h to LPS/PepG and treated with vehicle demonstrated a significant reduction in percentage EF, FS and FAC (Figure 2.22 A-D). When compared to LPS/PepG mice treated with vehicle, the administration of ibrutinib (3 mg/kg or 30 mg/kg i.v.) 1 h after LPS/PepG significantly attenuated the decline in EF, FS and FAC caused by LPS/PepG (Figure 2.22 A-D). No significant difference in effect size was observed for any of the cardiac parameters between the two doses of ibrutinib used (3 mg/kg and 30 mg/kg) (Figure 2.22 A-D).

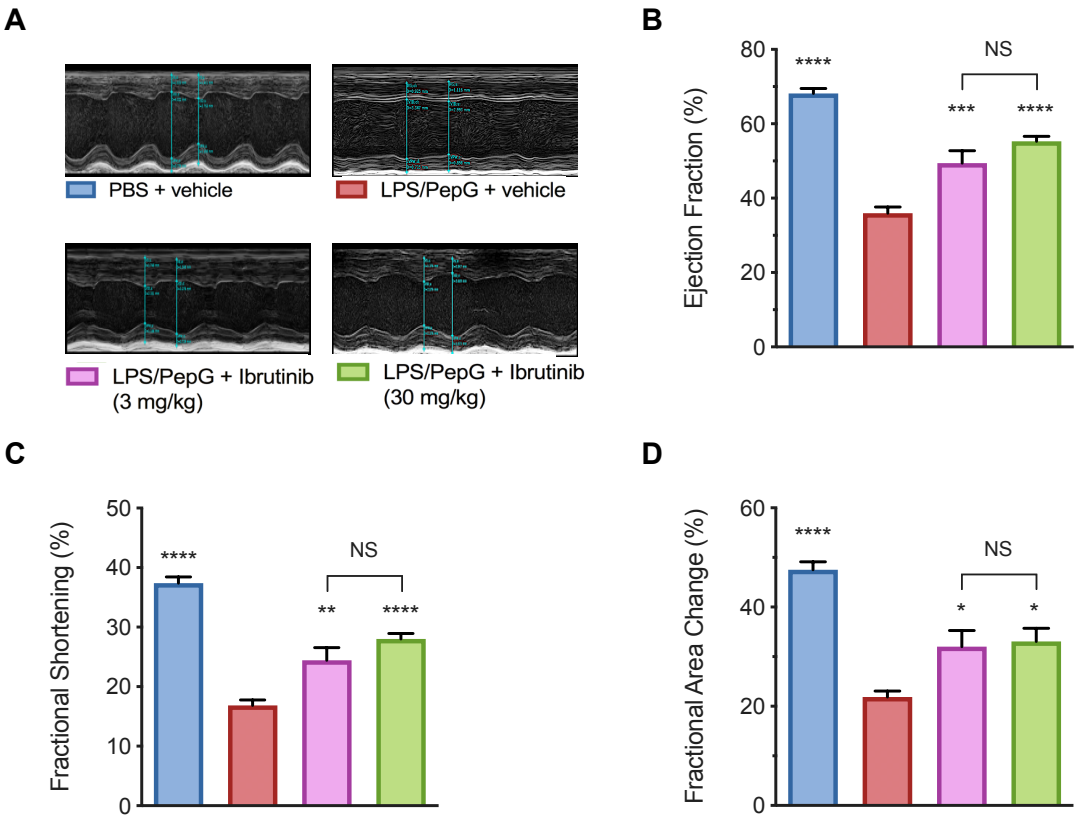

Figure 2.22 Intravenous ibrutinib (3 mg/kg or 30 mg/kg) attenuates LPS/PepG induced cardiac dysfunction. Mice received LPS (7 mg/kg) and PepG (1 mg/kg), or vehicle (i.p.). One hour later, mice were treated with ibrutinib (3 mg/kg i.v.), ibrutinib (30 mg/kg i.v.) or vehicle (5% DMSO + 30% cyclodextrin i.v.). Cardiac function was assessed 18 h after LPS/PepG administration. **(A)** Representative M-mode echocardiograms. **(B)** Ejection fraction (%). **(C)** Fractional shortening (%). **(D)** Fractional area change (%). The following groups were studied sham, LPS/PepG + vehicle, LPS/PepG + ibrutinib (3 mg/kg i.v.) and LPS/PepG + ibrutinib (30 mg/kg i.v.). All data are expressed as mean ± SEM for n =10 per group. A value of $^{*}P < 0.05$, $^{**}P < 0.01$, $^{***}P < 0.001$ and $^{****}P < 0.0001$ was considered to be statistically significant when compared to LPS/PepG + vehicle by one-way ANOVA followed by a Bonferroni's post hoc test.

2.4 Results – CLP model

2.4.1 Physiological parameters of mice subjected to CLP for 24 h

When compared to sham-operated mice, mice subjected to CLP for 24 h showed an increase in severity score. At 12 h, the severity score in CLP mice was >3 indicating severe sepsis, whereas sham-operated mice remained at 0, showing no physical indication of disease. Before 12 h, the severity score in CLP mice remained ≤3 indicating moderate sepsis (Figure 2.23 A). When compared to sham-operated mice, the heart rate of CLP-mice dropped below 400 bpm at 24 h, whereas in sham-operated mice, the heart rate remained between 400-500 bpm (Figure 2.23 B). Over 24 h the temperature of sham-operated mice remained at physiological temperature, 36°C. In contrast, CLP mice experienced a significant drop in temperature 1 h after the surgery, and the temperature slowly decreased to < 30°C over the remainder of the experiment (Figure 2.23 C). A drop of temperature below 30°C has been reported to be a reliable marker of mortality. Sham-operated mice resulted in predicted mortality of 0% for all time points. At 1 and 3 h after CLP mice had predicted mortality of 0%, however, 6 h after CLP resulted in predicted mortality of 25%, decreasing to 80% at 24 h after CLP (Figure 2.23 D).

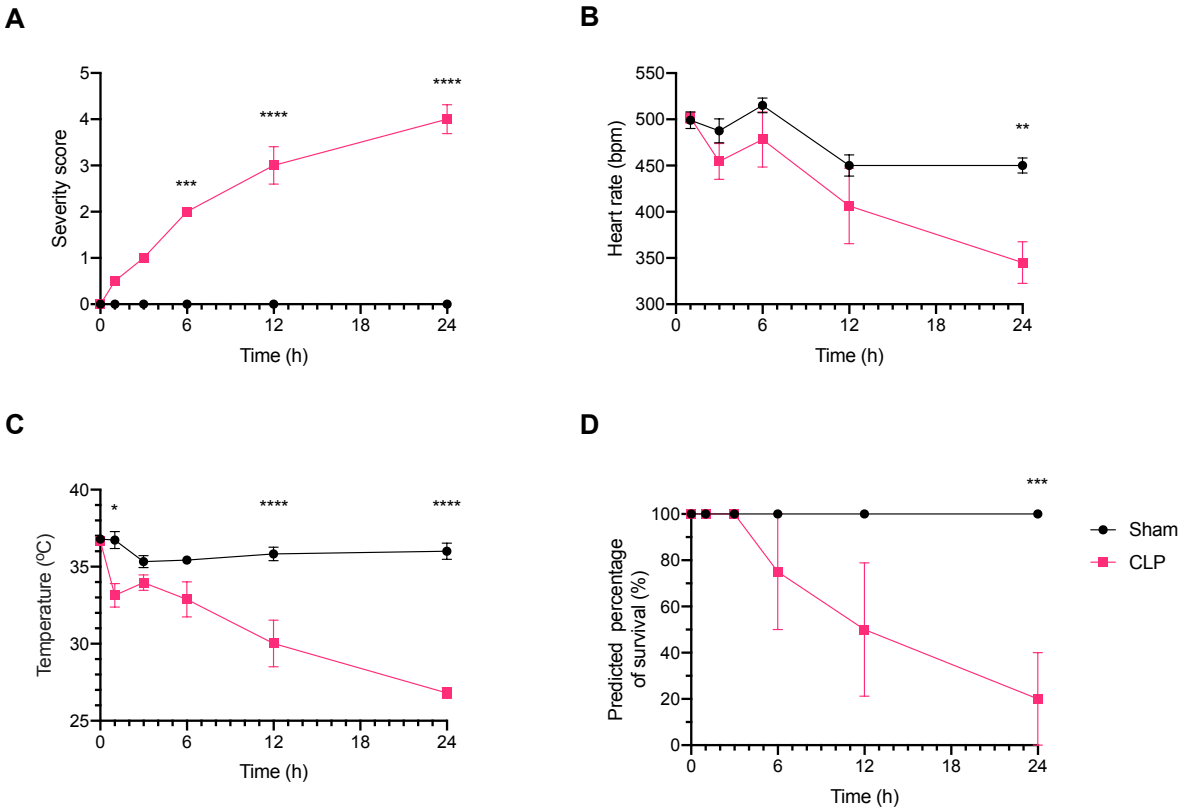

Figure 2.23 Physiological parameters of mice subjected to CLP for 24 h. Mice were randomly assigned to undergo sham-operated or CLP surgery. At 1 h, 3 h, 6 h, 12 h, 24 h after surgery mice were assessed on **(A)** Severity score. **(B)** Heart rate (bpm). **(C)** Temperature °C. **(D)** Predicted percentage of survival (%). Sham-operated mice ($n = 3$) and CLP ($n = 4$). All data are expressed as mean ± SEM for n number of observations. A value of ****$P < 0.0001$, *** $P < 0.001$, **$P < 0.01$, *$P < 0.05$ was considered to be statistically significant when compared to CLP by two-way ANOVA followed by a Bonferroni's post hoc test.

2.4.2 Changes in left ventricular cardiac systolic parameters of septic mice over 24 h

Sham-operated mice exhibited no significant alterations in any of the cardiac parameters measured over the 24 h experimental period. When compared to sham-operated mice, mice subjected to CLP exhibited a gradual and continuous decline in EF, FS, FAC, CO, SV, over 24 h (Figure 2.24 A-F). Most notably, I observed a significant decrease in CO and SV in CLP mice as early as 1 h after CLP, which remained decreased throughout the experimental period (Figure 2.24 E&F). The end systolic volume measured in CLP-mice was not different from the end-systolic volume measured in sham-operated mice. However, in CLP-mice, I found a decrease in the end-diastolic volume as early as 1 h after CLP when compared to sham-operated mice. End-diastolic volume remained decreased throughout the experimental period (Figure 2.24 G-H).

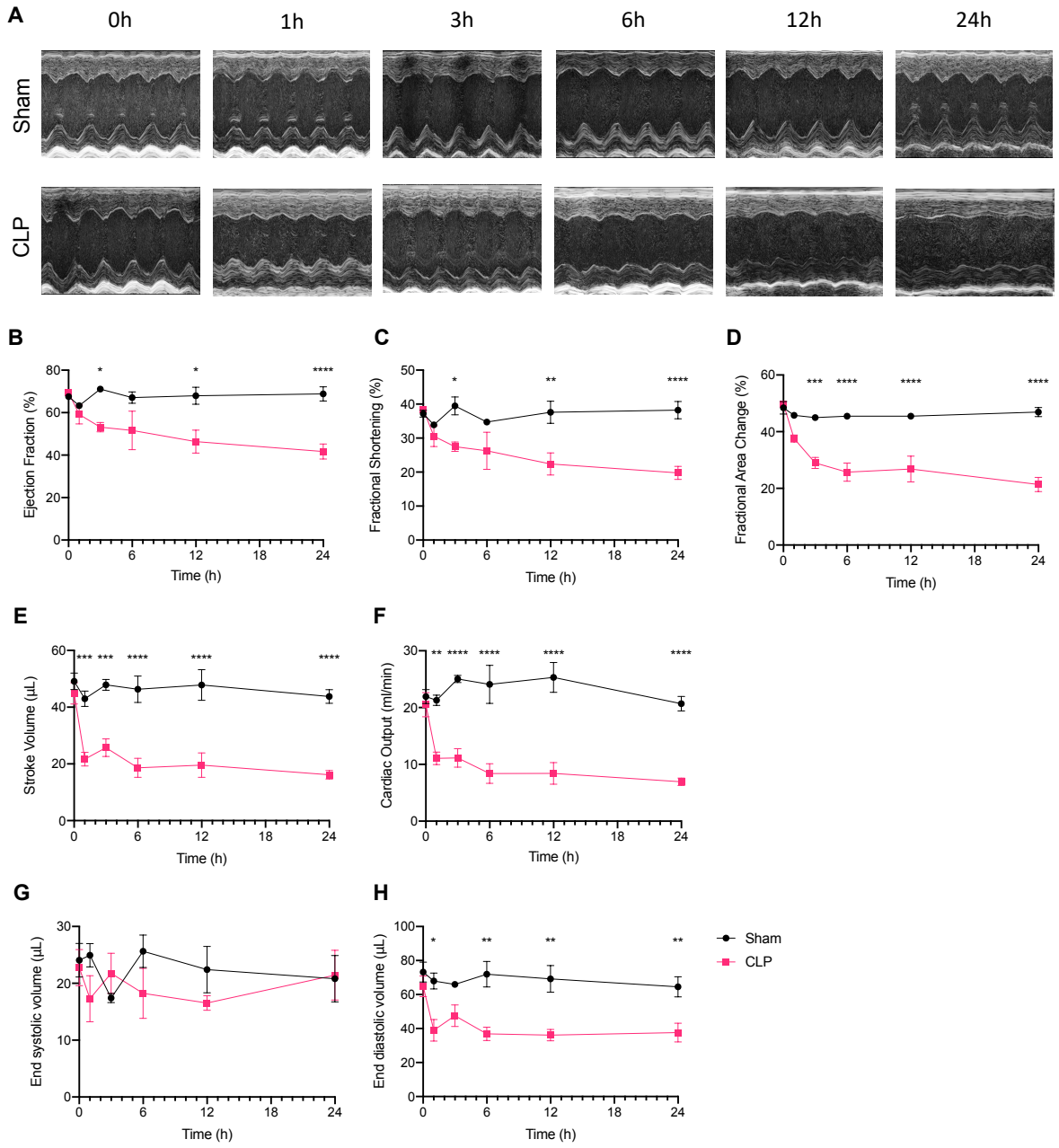

Figure 2.24 Changes in cardiac parameters of septic mice over 24 h. Mice were randomly assigned to undergo sham or CLP surgery. Cardiac function was assessed at 1 h, 3 h, 6 h, 12 h, 24 h after surgery via echocardiography **(A)** M-mode echocardiograms representatives. **(B)** Ejection Fraction (%). **(C)** Fractional shortening (%). **(D)** Fractional area change (%). **(E)** Stroke volume (µL). **(F)** Cardiac output (mL/min). **(G)** End systolic volume (µL). **(H)** End diastolic volume (µL)**.** Sham-operated (n = 3) and CLP (n = 4). All data are expressed as mean ± SEM for n number of observations. A value of ****P < 0.0001, *** P < 0.001, **P < 0.01, *P < 0.05 was considered to be statistically significant when compared to CLP by a two-way ANOVA followed by a Bonferroni's post hoc test.

2.4.3 Changes in left ventricular diastolic function in septic mice over 24 h

Sham-operated mice exhibited no significant alterations in any of the cardiac parameters measured over the 24 h experimental period. When compared to sham-operated mice, mice subjected to CLP resulted in a significant decline of E/A ratio and an increase in the myocardial performance index at 24 h after surgery, indicating diastolic dysfunction (Figure 2.25 A&B).

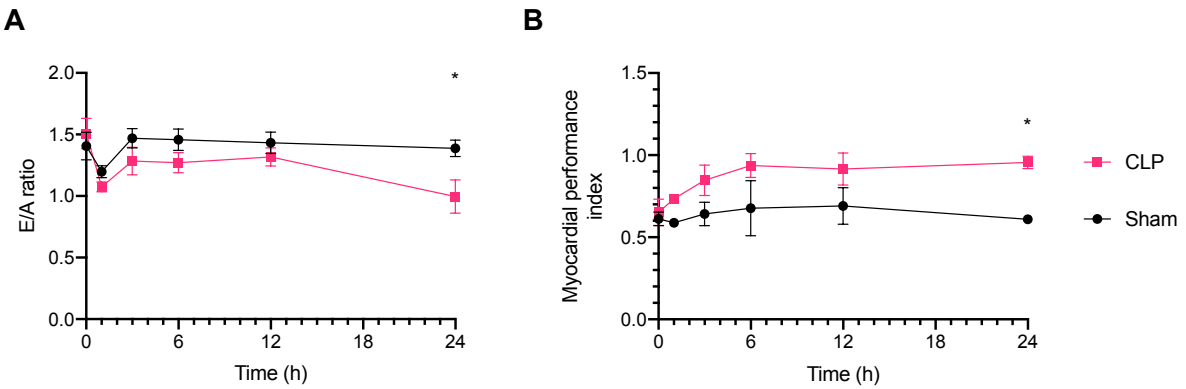

Figure 2.25 Changes in left ventricular diastolic function in septic mice over 24 h. Mice were randomly assigned to undergo sham-operated or CLP surgery. Cardiac function was assessed at 1 h, 3 h, 6 h, 12 h, 24 h after surgery via echocardiography. **(A)** E/A ratio. **(B)** Myocardial performance index. Sham-operated (n = 3) and CLP (n = 4). All data are expressed as mean ± SEM for n number of observations. A value of $^*P < 0.05$ was considered to be statistically significant when compared to CLP by two-way ANOVA followed by a Bonferroni's post hoc test.

2.4.4 Changes in pulmonary artery flow in septic mice over 24 h

Sham-operated mice exhibited no significant alterations in any of the cardiac parameters measured over the 24 h experimental period. When compared to sham-operated mice, mice subjected to CLP resulted in a significant decline of pulmonary artery VTI and peak velocity 1 h after surgery and remained decreased for the duration of the 24 h (Figure 2.26 A&B).

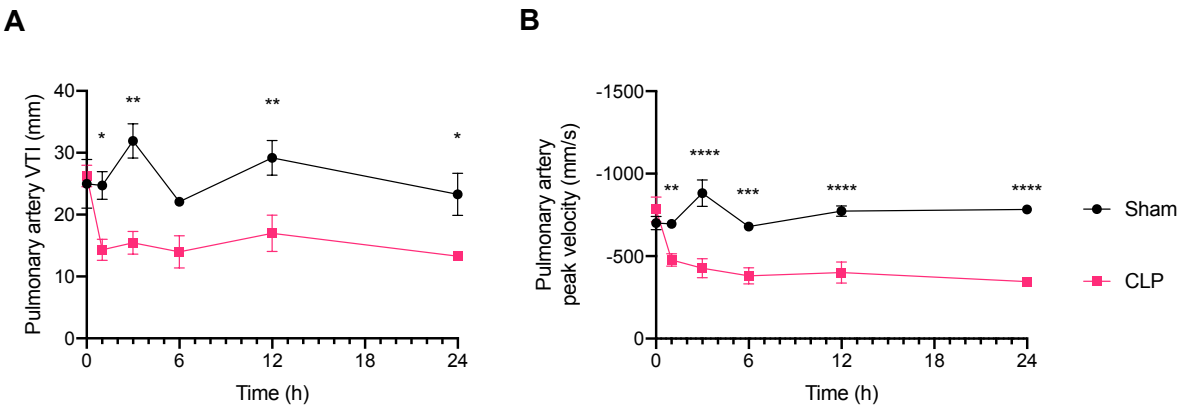

Figure 2.26 Changes in pulmonary artery flow in septic mice over 24 h. Mice were randomly assigned to undergo sham-operated or CLP surgery. Cardiac function was assessed at 1 h, 3 h, 6 h, 12 h, 24 h after surgery via echocardiography. **(A)** Pulmonary artery flow VTI (mm). **(B)** Pulmonary artery peak velocity (mm/s). Sham-operated (n = 3) and CLP (n = 4). All data are expressed as mean ± SEM for n number of observations. A value of ****$P < 0.0001$, *** $P < 0.001$, **$P < 0.01$, *$P < 0.05$ was considered to be statistically significant when compared to CLP by two-way ANOVA followed by a Bonferroni's post hoc test.

2.4.5 Changes in bacteria and infiltrating immune cells in the peritoneal cavity of septic mice over 24 h

When compared to sham-operated mice, mice subjected to CLP resulted in no significant differences in the number of bacteria in the peritoneal cavity between 1 - 12 h. However, 24 h after CLP the number of bacteria in the peritoneal cavity is significantly higher than sham-operated mice (Figure 2.27 A).

When compared to sham-operated mice, mice subjected to CLP resulted in a significant increase in the number of macrophages and neutrophils in the peritoneal cavity at 12 h and 24 h after surgery (Figure 2.27 B&C). A significant increase of T cells and B cells in the peritoneal cavity of CLP-mice was only observed at 24 h after surgery when compared to sham-operated mice (Figure 2.27 D&E).

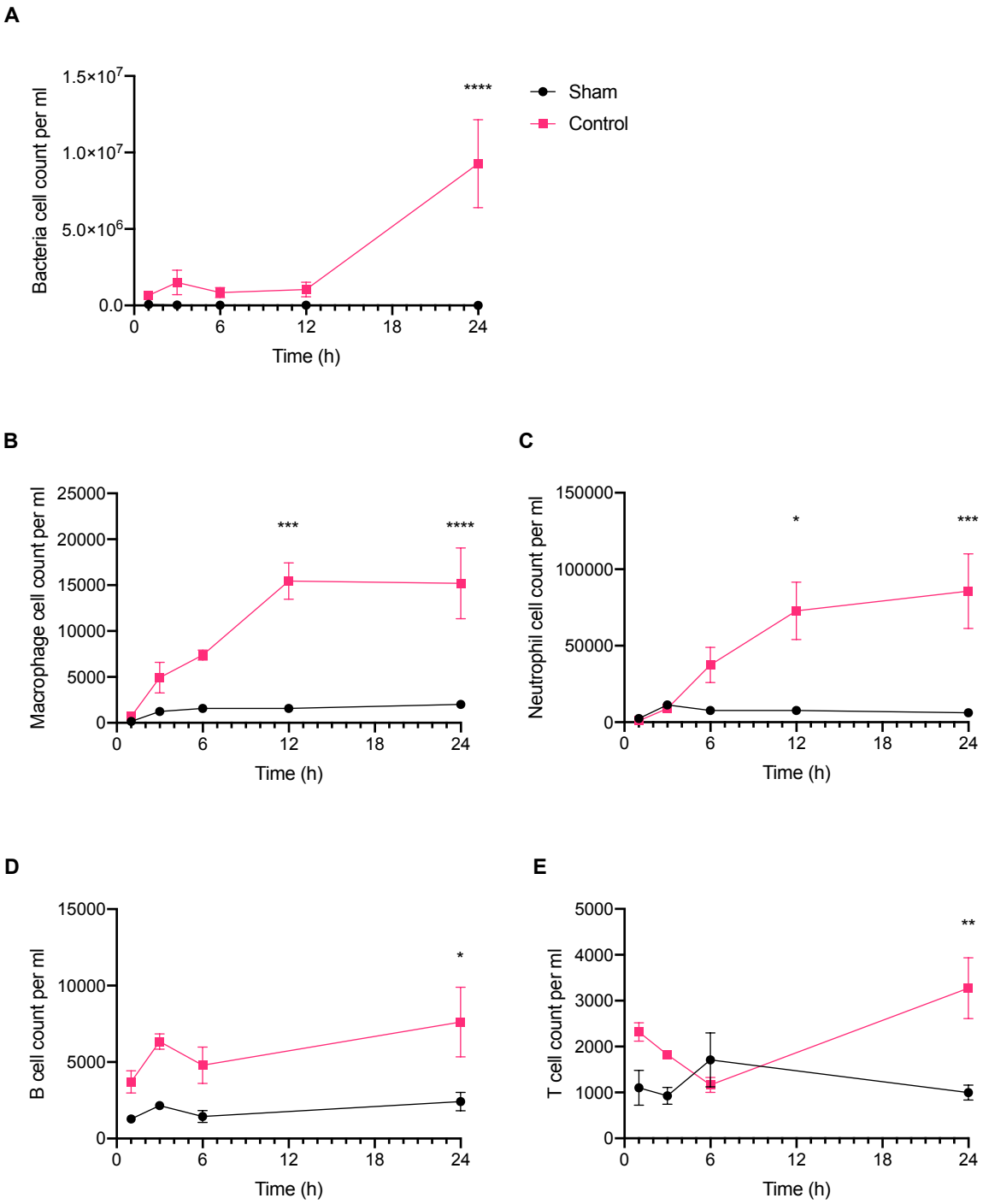

Figure 2.27 Changes in bacteria and immune cell in the peritoneal cavity of septic mice over 24 h. Mice were randomly assigned to undergo sham-operated or CLP surgery. At 1 h, 3 h, 6 h, 12 h, 24 h after surgery peritoneal lavage fluid from mice were assessed. **(A)** Bacteria cell count (ml). **(B)** Macrophage cell count (ml). **(C)** Neutrophil cell count (ml). **(D)** B cell count (ml). **(E)** T cell count (ml). Sham-operated (n = 3) and CLP (n = 4). All data are expressed as mean ± SEM for n number of observations. A value of ****$P < 0.0001$, *** $P < 0.001$, **$P < 0.01$, *$P < 0.05$ was considered to be statistically significant when compared to CLP by two-way ANOVA followed by a Bonferroni's post hoc test.

2.4.6 Changes in physiological parameters in responses to post-treatment of ibrutinib (3 mg/kg or 30 mg/kg), or acalabrutinib (3 mg/kg) 1 h after CLP surgery

Sham-surgery resulted in a severity score of 0 at 24 h, demonstrating that sham-operated mice experienced no clinical symptoms of sepsis and had recovered well from the surgical procedure. When compared to sham-operated mice, CLP-mice showed severe clinical signs of sepsis, with 80% having a score of >3. In contrast, CLP-mice treated with ibrutinib (3 mg/kg) resulted in 80% with a score of ≤3. All CLP-mice which received ibrutinib (30 mg/kg) and acalabrutinib (3 mg/kg) had a score of ≤3 indicating moderate sepsis (Figure 2.28 A).

When compared to sham-operated animals, the mean values for the heart rate of the CLP-animals were significantly reduced. When compared to CLP-mice treated with vehicle, the initial heart rate was significantly increased in ibrutinib (30 mg/kg) and acalabrutinib (3 mg/kg), while no significant increase in heart rate was observed for ibrutinib (3 mg/kg) (Figure 2.28 B).

When compared to sham-operated mice, mice subjected to CLP and treated with vehicle for 24 h resulted in hypothermia (temperature < 30°C) this equated to a predicted mortality of 90% in CLP-mice. When compared to CLP + vehicle mice, mice subjected to CLP and treated with ibrutinib (3 mg/kg or 30 mg/kg) or acalabrutinib (3 mg/kg) 1 h after surgery prevented hypothermia, this equated to a predicted mortality of 30% for low dose ibrutinib (3 mg/kg) and 20% predicted mortality for high dose ibrutinib (30 mg/kg) and acalabrutinib (3 mg/kg) (Figure 2.28 C&D).

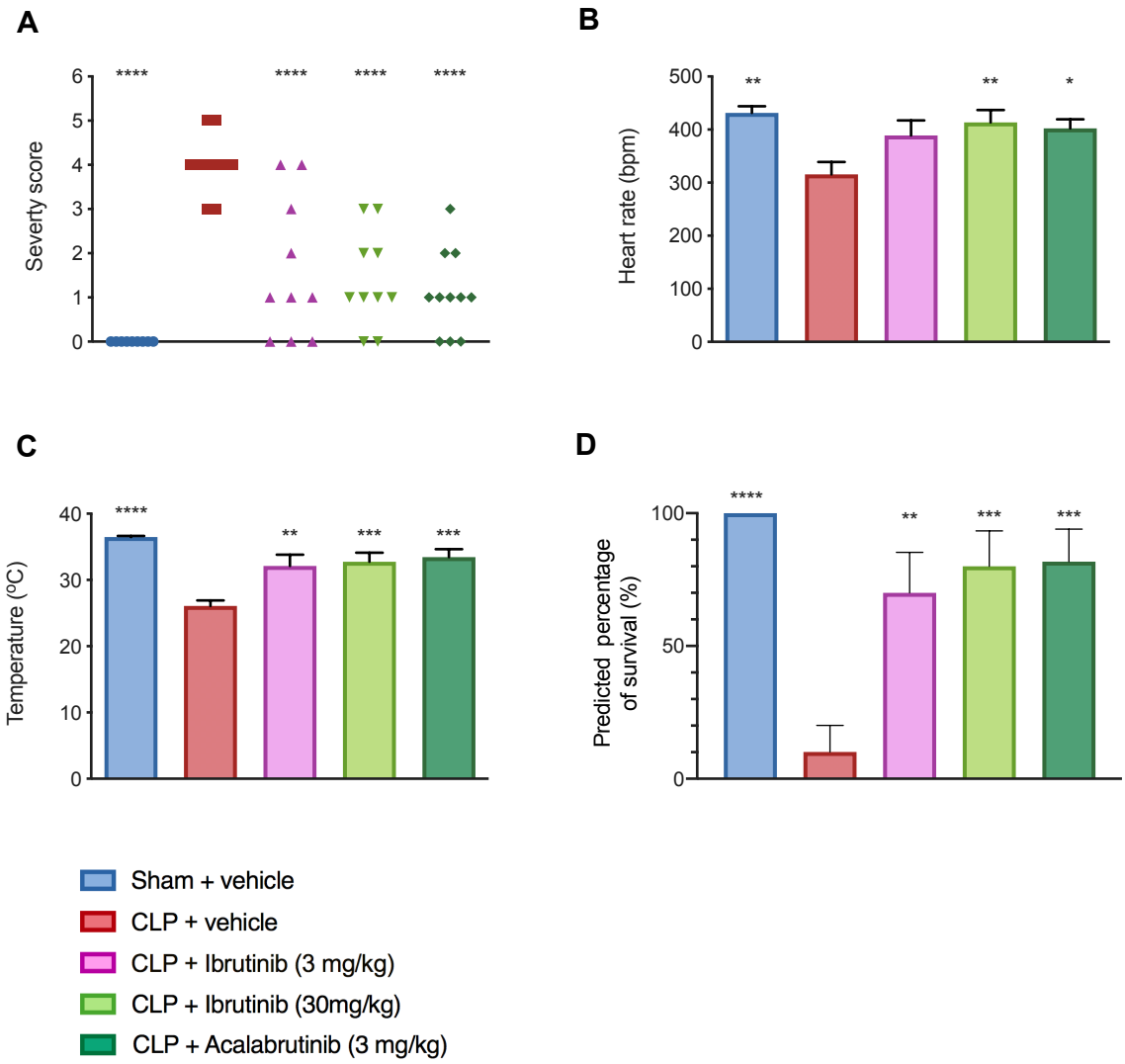

Figure 2.28 Physiological changes to post-treatment of ibrutinib (3 mg/kg or 30 mg/kg) or acalabrutinib (3 mg/kg) 1 h after CLP surgery. Mice underwent CLP surgery or sham operated surgery. One hour later, mice were treated with ibrutinib (3 mg/kg i.v.), ibrutinib (30 mg/kg i.v.), acalabrutinib (3 mg/kg i.v.), or vehicle (5% DMSO + 30% cyclodextrin i.v.). At 24 h after surgery mice were assessed on the following **(A)** Severity score. **(B)** Heart rate (bpm). **(C)** Temperature °C. **(D)** Predicted percentage of survival (%). All data are expressed as mean ± SEM for $n = 10$ per group. A value of ****$P < 0.0001$, *** $P < 0.001$, **$P < 0.01$, *$P < 0.05$ was considered to be statistically significant when compared to CLP + vehicle by two-way ANOVA followed by a Bonferroni's post hoc test.

2.4.7 Intravenous ibrutinib or acalabrutinib attenuates sepsis-induced cardiac dysfunction

When compared to sham-operated animals, mice subjected for 24 h to CLP demonstrated a significant reduction in percentage EF, FS, FAC, SV, CO and EDV (Figure 2.29 A-H) indicating the development of systolic, cardiac dysfunction. When compared to CLP-mice treated with vehicle, the delayed administration of ibrutinib (3 mg/kg), ibrutinib (30 mg/kg), or acalabrutinib (3 mg/kg) at 1 h after CLP significantly attenuated the decline in EF, FS, FAC, SV and CO caused by CLP (Figure 2.29 A-F). Only acalabrutinib significantly attenuated the decline of EDV, while no significant differences were observed for ibrutinib (3 mg/kg and 30 mg/kg). No change in ESV was observed between any of the groups studied. No significant differences were observed in any of the cardiac parameters measured when comparing the data obtained with any of the BTK inhibitors (Figure 2.29 A-H).

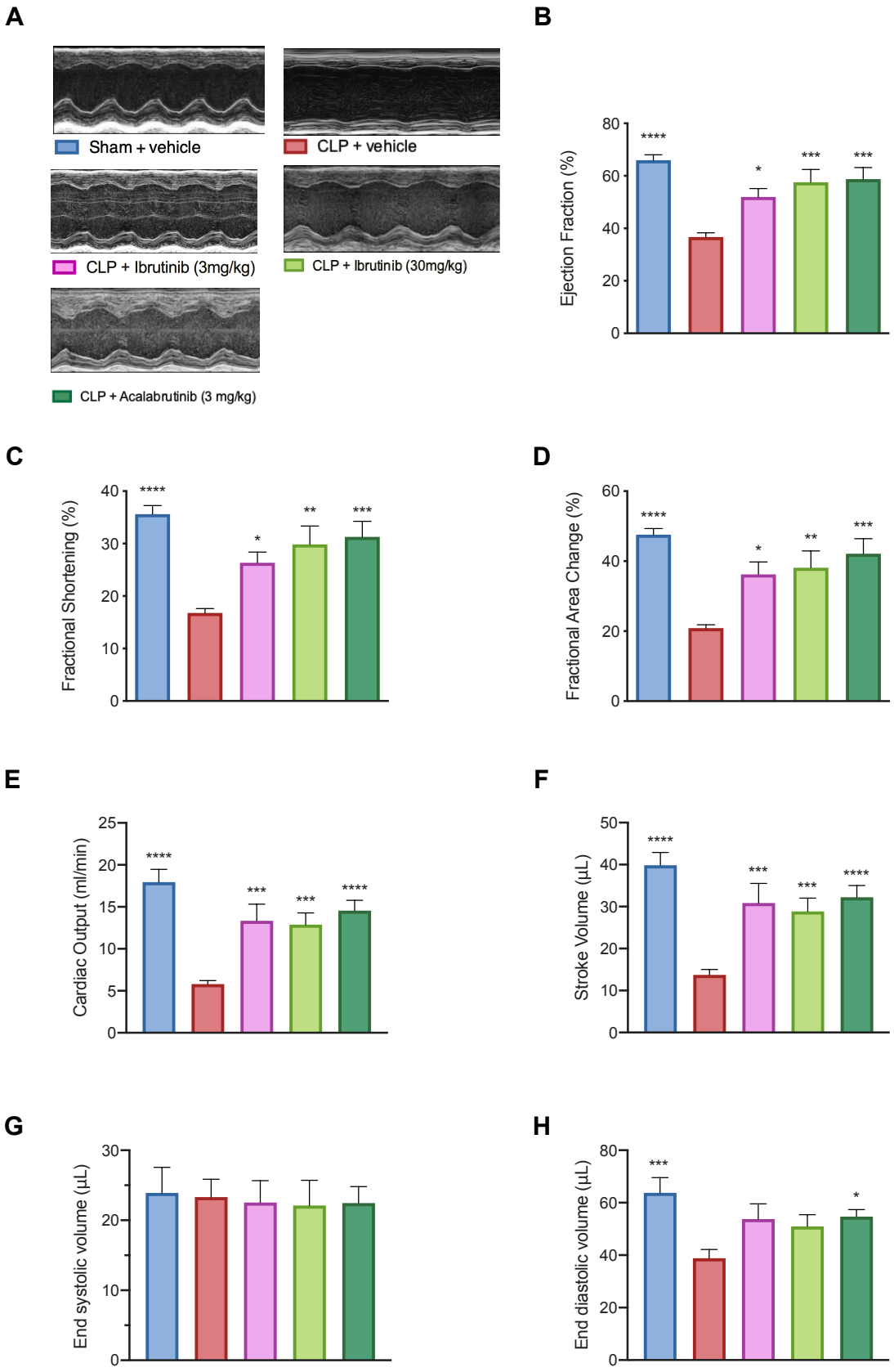

Figure 2.29 Intravenous ibrutinib (3 mg/kg or 30 mg/kg) or acalabrutinib (3 mg/kg) attenuates sepsis-induced cardiac dysfunction.

Mice were randomly assigned to undergo CLP surgery or sham-operated surgery. One hour later, mice were treated with ibrutinib (3 mg/kg i.v.), ibrutinib (30 mg/kg i.v.), acalabrutinib (3 mg/kg i.v.), or vehicle (5% DMSO + 30% cyclodextrin i.v.). Cardiac function was assessed 24 h after CLP surgery via echocardiography. **(A)** Representative M-mode echocardiograms. **(B)** Ejection fraction (%). **(C)** Fractional shortening (%). **(D)** Fractional area change (%). **(E)** Cardiac output (ml/min). **(F)** Stroke volume (μL). **(G)** End systolic volume (μL). **(H)** End diastolic volume (μL). The following groups were studied sham + vehicle, control + vehicle, CLP + ibrutinib (3 mg/kg i.v.), CLP + ibrutinib (30 mg/kg i.v.) and CLP + acalabrutinib (3 mg/kg i.v.). All data are expressed as mean ± SEM for $n = 10$ per group. A value of $^{****}P < 0.0001$, $^{***}P < 0.001$, $^{**}P < 0.01$, $^{*}P < 0.05$ was considered to be statistically significant when compared to CLP + vehicle by one-way ANOVA followed by a Bonferroni's post hoc test.

2.4.8 Post-treatment of ibrutinib or acalabrutinib on sepsis-induced renal dysfunction and hepatocellular injury

When compared to sham-operated mice, mice subjected to CLP for 24 h and treated with vehicle developed both kidney dysfunction (rise in urea and creatinine) and hepatocellular injury (rise in ALT) (Figure 2.30 A-C). When compared to CLP-animals treated with vehicle, CLP-animals treated with ibrutinib (3 mg/kg or 30 mg/kg i.v.) or acalabrutinib (3 mg/kg i.v.) at 1 h after CLP showed significant decreases in serum urea (Figure 2.30 A), but only the high dose of ibrutinib (30 mg/kg) and acalabrutinib (3 mg/kg) significantly prevented the rise in serum creatinine caused by sepsis. In contrast, the BTK-inhibitors did not affect the rise in serum ALT caused by CLP (Figure 2.30 B&C).

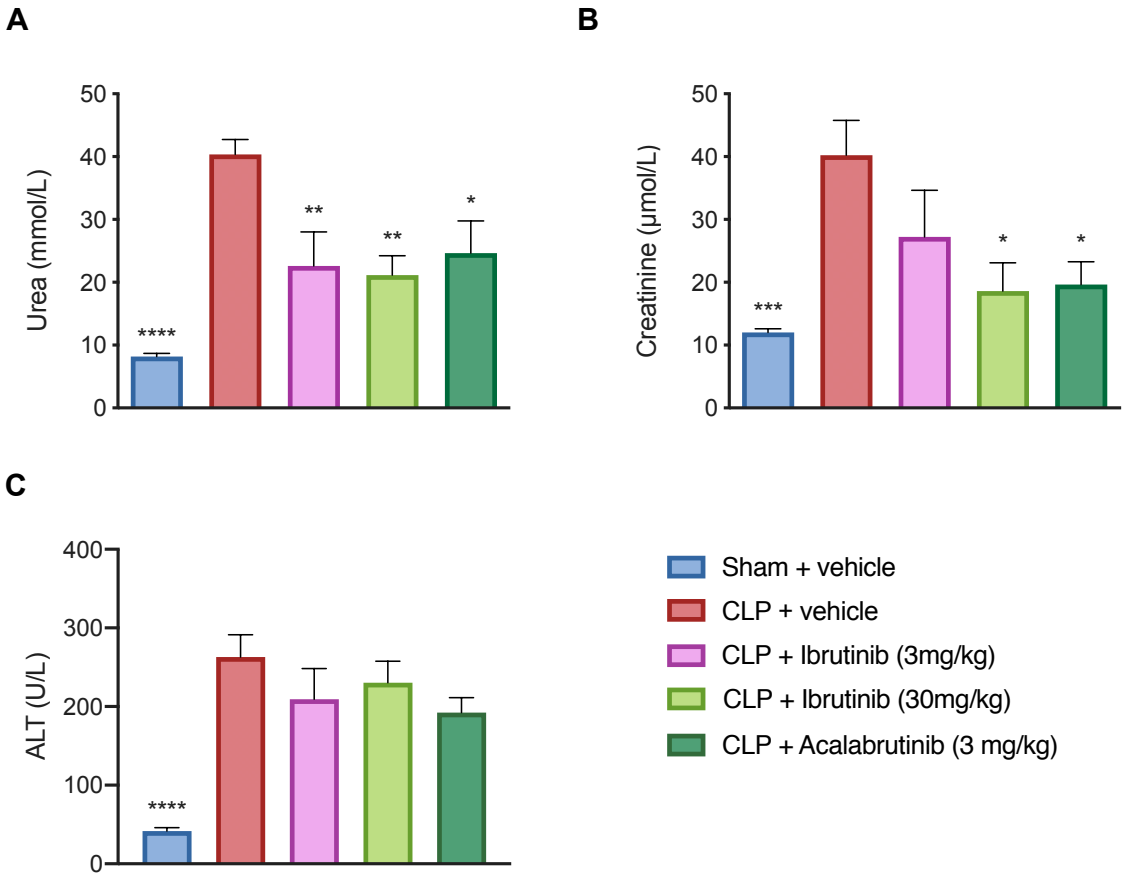

Figure 2.30 Post-treatment of ibrutinib or acalabrutinib on sepsis-induced renal dysfunction or hepatocellular injury. Mice were randomly assigned to undergo CLP surgery or sham-operated surgery. One hour later, mice were treated with ibrutinib (3 mg/kg i.v.), ibrutinib (30 mg/kg i.v.), acalabrutinib (3 mg/kg i.v.), or vehicle (5% DMSO + 30% cyclodextrin i.v.). 24 h after CLP surgery blood samples were collected for analyses. **(A)** Serum urea (mmol/L). **(B)** Creatinine (µmol/L). **(C)** Alanine aminotransferase (U/L). The following groups were studied sham + vehicle, control + vehicle, CLP + ibrutinib (3 mg/kg i.v.), CLP + ibrutinib (30 mg/kg i.v.) and CLP + acalabrutinib (3 mg/kg i.v.). All data are expressed as mean ± SEM for $n = 10$ per group. A value of $^{****}P < 0.0001$, $^{***}P < 0.001$, $^{**}P < 0.01$, $^{*}P < 0.05$ was considered to be statistically significant when compared to CLP + vehicle by one-way ANOVA followed by a Bonferroni's post hoc test.

2.4.9 Ibrutinib or acalabrutinib attenuate the formation of chemokine biomarkers of left ventricular dysfunction caused by CLP-sepsis

When compared to sham-operated animals, mice subjected for 24 h to CLP demonstrated a significant rise in the serum levels of known biomarkers of left ventricular dysfunction, the chemokines CXCL10 and CXCL11 (Figure 2.31 A-B). The rise of the chemokines CXCL10 and CXCL11 also negatively correlated to the reduction in EF (Figure 2.31 C-D). The rise in the serum levels of the chemokines CXCL10 and CXCL11 caused by CLP were also significantly reduced by either ibrutinib or acalabrutinib (Figure 2.31 A-B). No significant differences were observed in any of the cardiac parameters or cytokines measured in CLP animals treated with either ibrutinib or acalabrutinib (Figure 2.31 C-D).

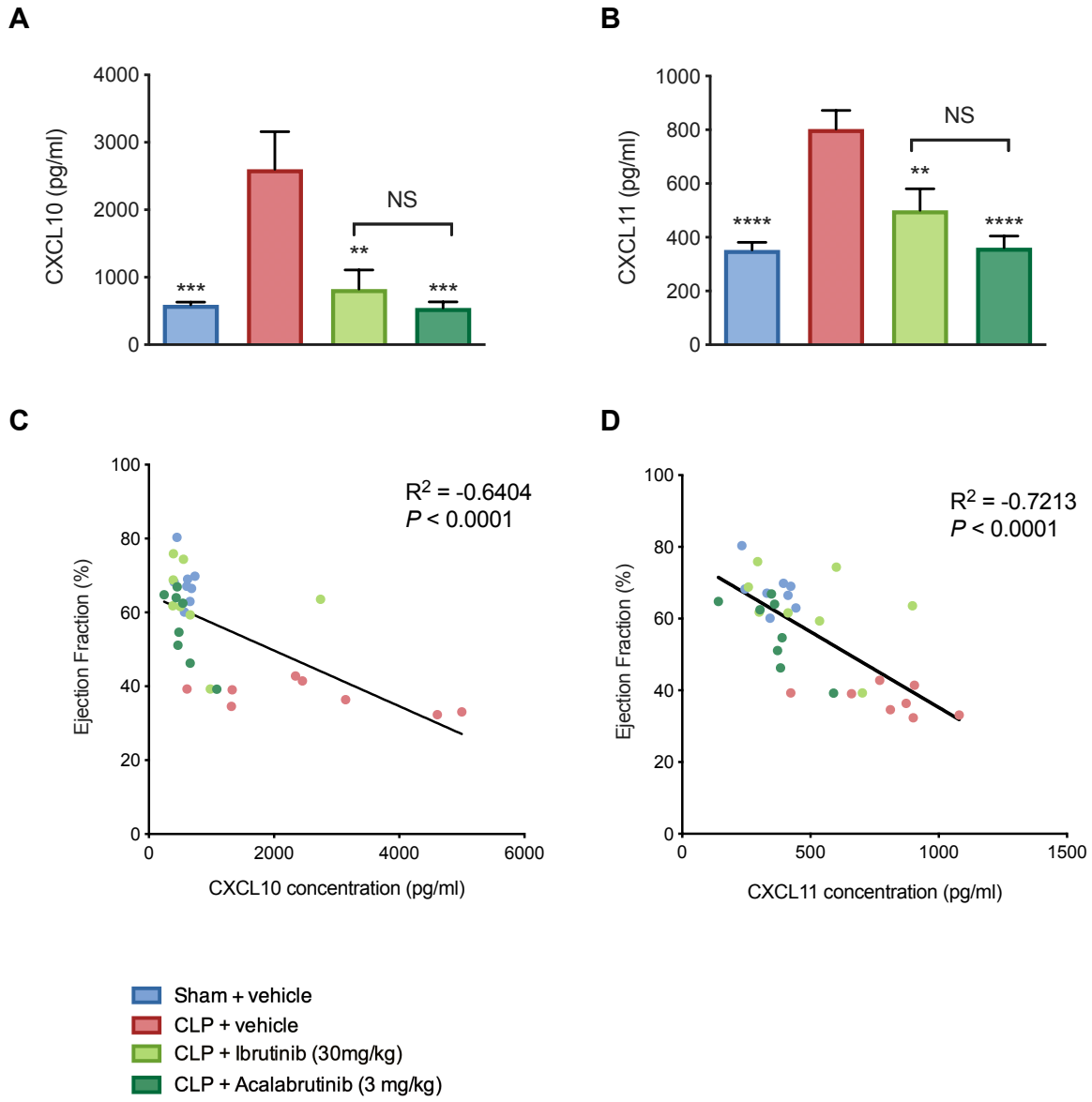

Figure 2.31 Ibrutinib or acalabrutinib attenuate the formation of chemokine biomarkers of left ventricular dysfunction caused by CLP-sepsis. Mice were randomly assigned to undergo CLP or sham-operated surgery. One hour later, mice were treated with ibrutinib (30 mg/kg i.v.), acalabrutinib (3 mg/kg i.v.), or vehicle (5% DMSO + 30% cyclodextrin i.v.). Cardiac function was assessed 24 h after CLP surgery. **(A)** CXCL10 serum concentration (pg/ml). **(B)** CXCL11 serum concentration (pg/ml). **(C)** Correlation of ejection fraction and CXCL10 serum concentration. **(D)** Correlation of ejection fraction and CXCL11 serum concentration. All data are expressed as mean ± SEM for $n = 8$ per group. A value of $^{****}P < 0.0001$, $^{***}P < 0.001$ and $^{**}P < 0.01$, was considered to be statistically significant when compared to CLP + vehicle by one-way ANOVA followed by a Bonferroni's *post hoc* test. Correlations coefficients were determined by Pearson's correlation with P values based on two-tailed tests.

2.4.10 Cardiac BTK is activated in CLP mice and reduced by ibrutinib or acalabrutinib

Using Western blot analysis, I investigated whether CLP-sepsis leads to an activation of BTK in the heart. The activation of BTK and the subsequent activation of BTK-signalling involves the phosphorylation of BTK at Tyr^{223} and the phosphorylation of PLCγ at Tyr^{1217} by phosphorylated (activated) BTK as the first step in the BTK-signalling cascade.

When compared to sham-operated mice, CLP mice treated with vehicle demonstrated significant increases in the phosphorylation of cardiac BTK at Tyr^{223} and the phosphorylation of PLCγ at Tyr^{1217}, indicating that BTK is activated in septic hearts (Figure 2.32 A&B). When compared to CLP mice treated with vehicle, delayed administration of ibrutinib (30 mg/kg), or acalabrutinib (3 mg/kg) in CLP mice resulted in a significant decrease in the phosphorylation of cardiac BTK at Tyr^{223} and the phosphorylation of PLCγ at Tyr^{1217} (Figure 2.32 A&B) demonstrating that both BTK inhibitors caused significant inhibition of BTK-signalling in the heart. No significant differences were observed in the degree of phosphorylation of cardiac BTK at Tyr^{223} and the phosphorylation of PLCγ at Tyr^{1217} in CLP-animals treated with either ibrutinib or acalabrutinib (Figure 2.32 A&B).

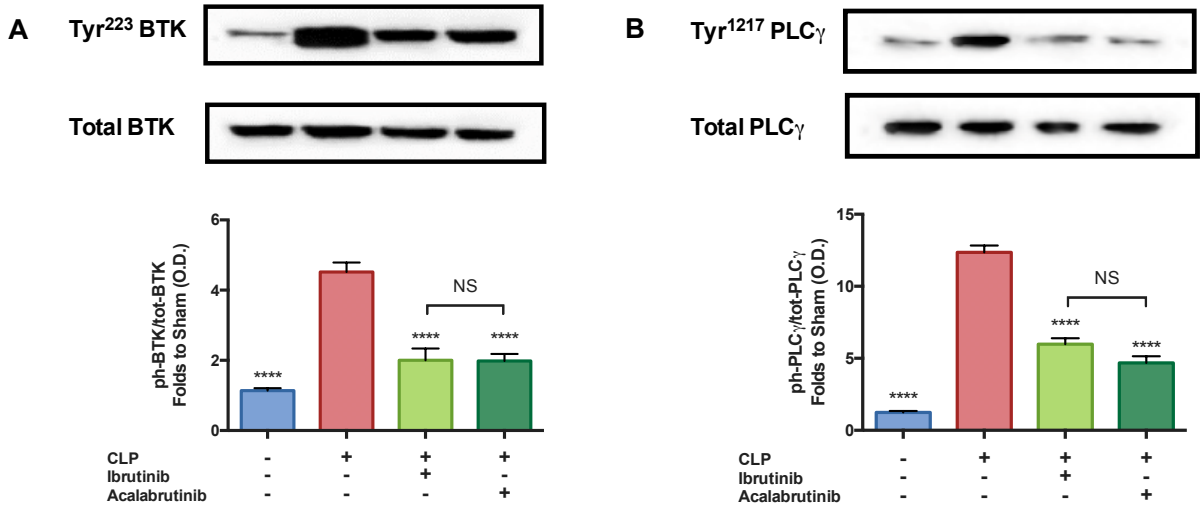

Figure 2.32 Cardiac BTK is activated in CLP mice and reduced by delayed administration of ibrutinib or acalabrutinib. Mice were randomly assigned to undergo CLP or sham-operated surgery. One hour later, mice were treated with ibrutinib (30 mg/kg i.v.), acalabrutinib (3 mg/kg i.v.), or vehicle (5% DMSO + 30% cyclodextrin i.v.). At 24 h after CLP surgery, the activation of BTK in the heart was analysed by western blot analysis. Specifically, densitometric analysis of the bands is expressed as relative OD of **(A)** phosphorylation of BTK at Tyr^{223} corrected for the corresponding total BTK and normalised using the related sham band. **(B)** Phosphorylation of PLCγ at Tyr^{1217} corrected for the corresponding total PLCγ. All data are expressed as mean ± SEM for $n = 5$ per group. A value of $^{****}P < 0.0001$ was considered to be statistically significant when compared to CLP + vehicle by one-way ANOVA followed by a Bonferroni's *post hoc* test.

2.4.11 Cardiac activation of NF-κB in septic mice is reduced by ibrutinib or acalabrutinib

To understand the signalling mechanism(s) associated with the observed cardiac dysfunction, I investigated the effect of BTK inhibition on the activation of key signalling pathways of inflammation including pathways leading to the activation of NF-κB. When compared to sham-operated mice, CLP mice treated with vehicle had significant increases in the phosphorylation of IKKα/β at $Ser^{176/180}$, the phosphorylation of IκBα at $Ser^{32/36}$ and the translocation of p65 to the nucleus (Figure 2.33 A-C). When compared with CLP mice treated with vehicle, treatment of CLP mice with ibrutinib (30 mg/kg) or acalabrutinib (3 mg/kg) significantly attenuated the increases in cardiac phosphorylation of IKKα/β at $Ser^{176/180}$ and IκBα at $Ser^{32/36}$ and the nuclear translocation of p65 (Figure 2.33 A-C). No significant differences were observed in the degree of phosphorylation of IKKα/β at $Ser^{176/180}$, the phosphorylation of IκBα at $Ser^{32/36}$ and the translocation of p65 to the nucleus in CLP animals treated with either ibrutinib or acalabrutinib (Figure 2.33 A-C).

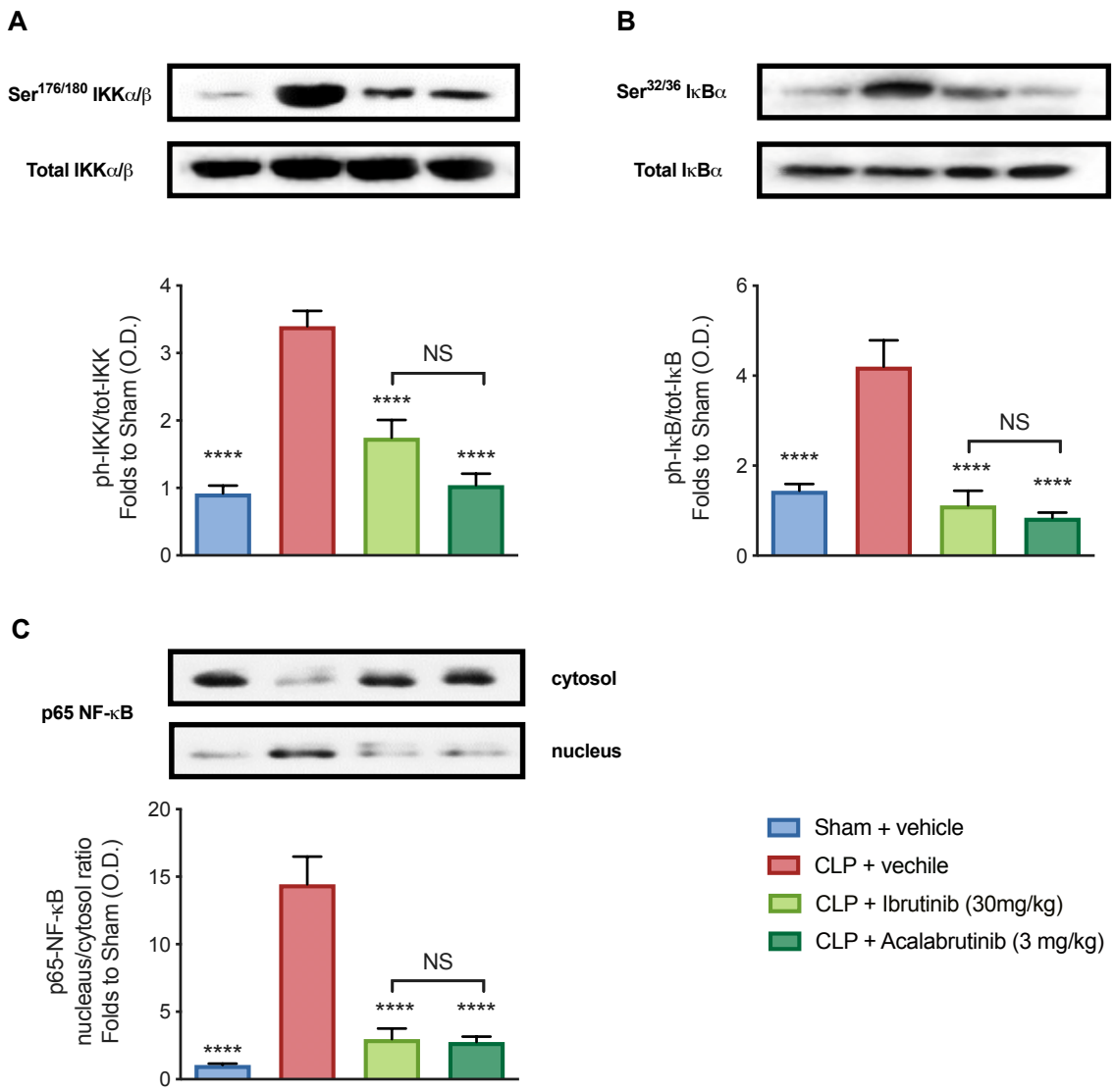

Figure 2.33 BTK inhibitors reduce cardiac NF-κB activation in septic mice. Mice were randomly assigned to undergo CLP or sham-operated surgery. One hour later, mice were treated with ibrutinib (30 mg/kg i.v.), acalabrutinib (3 mg/kg i.v.), or vehicle (5% DMSO + 30% cyclodextrin i.v.). At 24 h cardiac tissue was collected, and signalling was assessed. Densitometric analysis of the bands is expressed as relative OD of **(A)** phosphorylation of IKKα/β at $Ser^{176/180}$ corrected for the corresponding total IKKα/β and normalised using the related sham band. **(B)** Phosphorylation of IκBα at $Ser^{32/36}$ corrected for the corresponding total IκBα and normalised using the related sham band. **(C)** NF-κB p65 in both nucleus and cytosol and expressed as a ratio, normalised using the sham related bands. All data are expressed as mean ± SEM for $n = 5$ per group. A value of $^{****}P < 0.0001$ was considered to be statistically significant when compared to CLP + vehicle by one-way ANOVA followed by a Bonferroni's *post hoc* test.

2.4.12 Cardiac NLRP3 activation in septic mice is reduced by ibrutinib or acalabrutinib

I next assessed the potential involvement of the activation of the NLRP3 inflammasome in the cardiac dysfunction of CLP mice. When compared to sham-operated mice, CLP-sepsis (vehicle-treatment) exhibited an increased expression of the NLRP3 inflammasome and an increase in the cleavage of pro-caspase-1 to caspase-1 in the heart, which was associated with a rise in serum IL-1β (Figure 2.34 A-C). When compared to CLP mice treated with vehicle, treatment of CLP mice with ibrutinib or acalabrutinib significantly inhibited the expression of the NLRP3 inflammasome, cleavage of pro-caspase-1 to caspase-1 and this was associated with lower levels of serum IL-1β (Figure 2.34 A-C). There were no significant differences between the two BTK inhibitors.

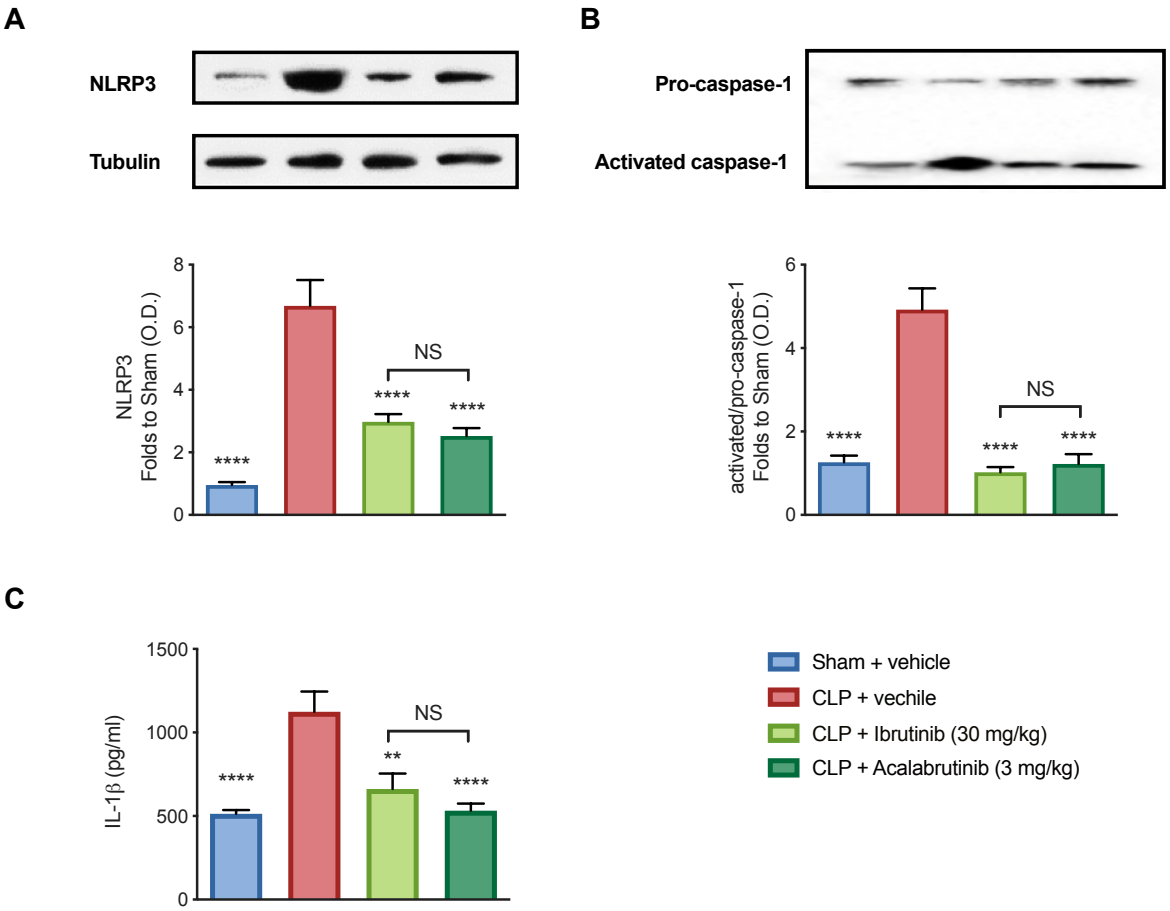

Figure 2.34 Cardiac NLRP3 activation in septic mice is reduced by ibrutinib or acalabrutinib. Mice were randomly assigned to undergo CLP or sham surgery. One hour later, mice were treated with ibrutinib (30 mg/kg i.v.), acalabrutinib (3 mg/kg i.v.), or vehicle (5% DMSO + 30% cyclodextrin i.v.). At 24 h after CLP surgery, the assembly and activation of NLRP3 in the heart was analysed by western blot analysis. Specifically, densitometric analysis of the bands is expressed as relative OD of **(A)** NLRP3 activation, corrected against tubulin and normalised using the sham related bands (n = 5 per group). **(B)** Pro-caspase-1 against activated caspase-1 and normalised using the sham related bands (n = 5 per group). **(C)** IL-1β serum concentration analysed by multiplex assay (n = 8 per group). All data are expressed as mean ± SEM for n number of observations. A value of $^{****}P < 0.0001$ and $^{**}P < 0.01$, were considered to be statistically significant when compared to CLP + vehicle by one-way ANOVA followed by a Bonferroni's *post hoc* test.

2.4.13 Relationship between BTK activation and cardiac dysfunction in CLP-sepsis

To address the question whether the degree of activation of BTK correlates with the observed alterations in cardiac function, I correlated the degree of phosphorylation of BTK at Tyr^{223} (Figure 2.35 A) and the phosphorylation of PLCγ at Tyr^{1217} (Figure 2.35 B) with EF. I found a highly significant negative correlation between the degree of BTK and PLCγ activation and the decline in EF, strongly suggesting that BTK activation drives or precedes the cardiac dysfunction associated with sepsis. To address the question whether the degree of activation of BTK also correlates with alterations in the activation of NF-κB, I correlated the degree of phosphorylation of BTK at Tyr^{223} with the translocation of p65 (Figure 2.35 C) and the phosphorylation of IKKα/β at $Ser^{176/180}$ (Figure 2.35 D). I found a highly significant positive correlation between the degree of BTK activation and the activation of NF-κB when measured as either the translocation of p65 (Figure 2.35 C) and the phosphorylation of IKKα/β at $Ser^{176/180}$ (Figure 2.35 D). To address the question whether the degree of activation of BTK also correlates with alterations in the assembly and activation of the inflammasome, I correlated the degree of phosphorylation of BTK at Tyr^{223} with either NLRP3 assembly (Figure 2.35 E) or the activation of caspase-1 (Figure 2.35 F). I found a highly significant positive correlation between the degree of BTK activation and the NLRP3 (Figure 2.35 E) increased expression and the activation of caspase-1 (Figure 2.35 F).

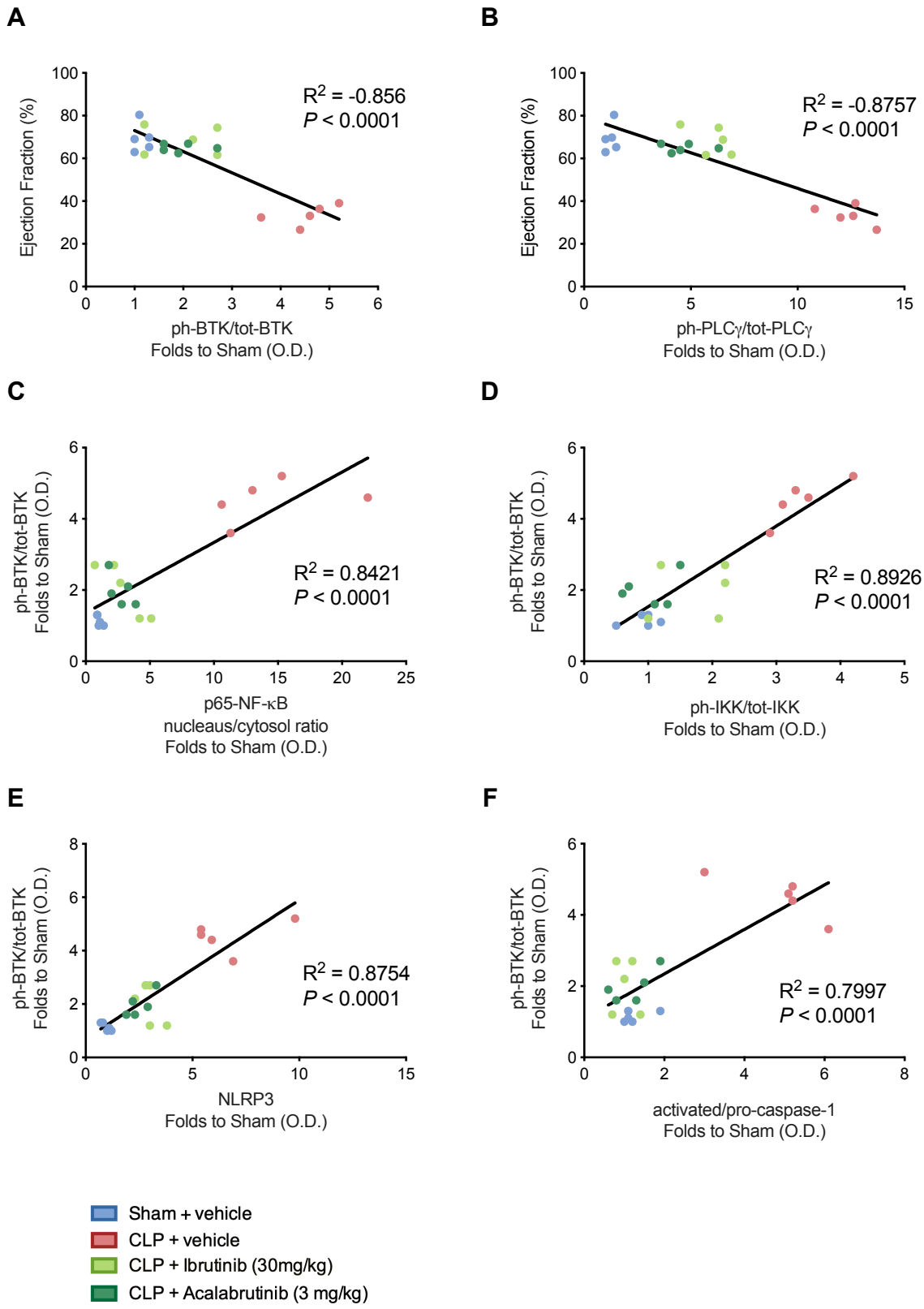

Figure 2.35 Relationship between BTK activation and cardiac dysfunction in CLP-sepsis. Correlation data to show **(A)** ejection fraction (%) vs. phosphorylation of BTK at Tyr^{223}. **(B)** Ejection fraction (%) vs. of PLCγ at Tyr^{1217}. **(C)** Phosphorylation of BTK at Tyr^{223} vs. NF-κB p65. **(D)**

Phosphorylation of BTK at Tyr^{223} vs. phosphorylation of IKKα/β at$Ser^{176/180}$. **(E)** Phosphorylation of BTK at Tyr^{223} vs. NLRP3. **(F)** Phosphorylation of BTK at Tyr^{223} vs. activated/pro-caspase-1. Data were analysed by the Pearson correlation coefficient test to calculate the R value and a two-tailed T-test for significance, a value of $P < 0.0001$, was considered to be statistically significant.

2.4.14 Systemic inflammation in septic mice is reduced by ibrutinib or acalabrutinib

I also studied the effect of CLP (in the absence and presence of BTK inhibitors) on the synthesis of pro-inflammatory cytokines, anti-inflammatory cytokines and pro-inflammatory chemokines in the serum. When compared to sham-operated mice, CLP mice treated with vehicle showed a significant rise in the serum levels of a) the pro-inflammatory cytokines TNF-α, IFN-γ, IL-6; b) the anti-inflammatory cytokines IL-4 and IL-10, and c) the pro-inflammatory chemokines KC/CXCL1, eotaxin-1/CCL11, eotaxin-2/CCL24 (Figure 2.36 A-H). The sepsis-induced increase in these cytokines and chemokines was significantly attenuated by the delayed administration of both BTK inhibitors, the only exception being IL-6, which was not significantly reduced by ibrutinib. No significant differences were observed in the levels of cytokines or chemokines in CLP animals treated with either ibrutinib or acalabrutinib (Figure 2.36 A-H).

The data of all other cytokines/chemokines/growth factors that I measured in all groups are provided in Figure 2.37.

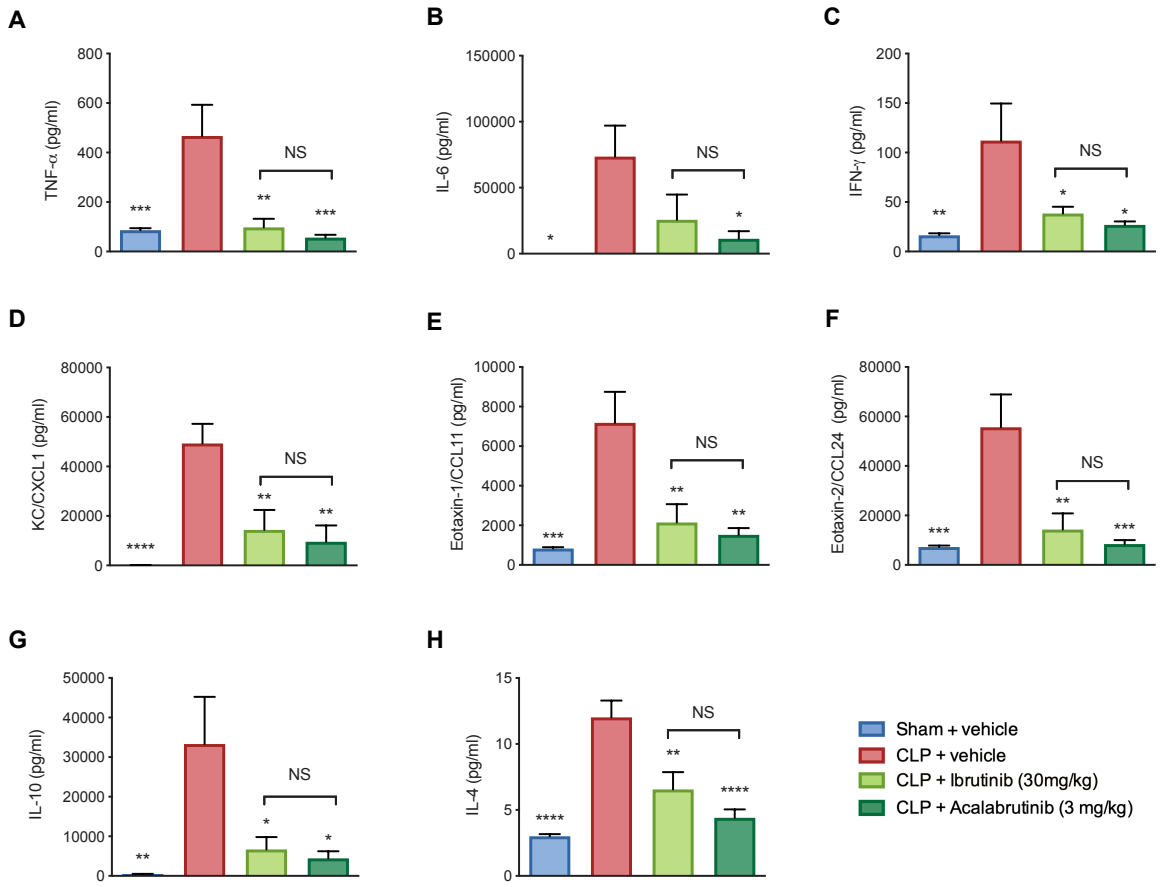

Figure 2.36 Systemic inflammation in septic mice is reduced by ibrutinib or acalabrutinib. Mice were randomly assigned to undergo CLP or sham-operated surgery. One hour later, mice were treated with ibrutinib (30 mg/kg i.v.), acalabrutinib (3 mg/kg i.v.), or vehicle (5% DMSO + 30% cyclodextrin i.v.). At 24 h after CLP, blood samples were collected, and the serum concentration of cytokines and chemokines were measured by a multiplex assay. **(A)** TNF-α serum concentration (pg/ml). **(B)** IL-6 serum concentration (pg/ml). **(C)** IFN-γ serum concentration (pg/ml). **(D)** KC/CXCL1 serum concentration (pg/ml). **(E)** Eotaxin-1/CCL11 serum concentration (pg/ml). **(F)** Eotaxin-2/CCL24 serum concentration (pg/ml). **(G)** IL-10 serum concentration (pg/ml). **(H)** IL-4 serum concentration (pg/ml). All data are expressed as mean ± SEM for $n = 8$ per group. A value of $^{****}P < 0.0001$, $^{***}P < 0.001$, $^{**}P < 0.01$ and $^{*}P < 0.05$, were considered to be statistically significant when compared to CLP + vehicle by one-way ANOVA followed by a Bonferroni's *post hoc* test.

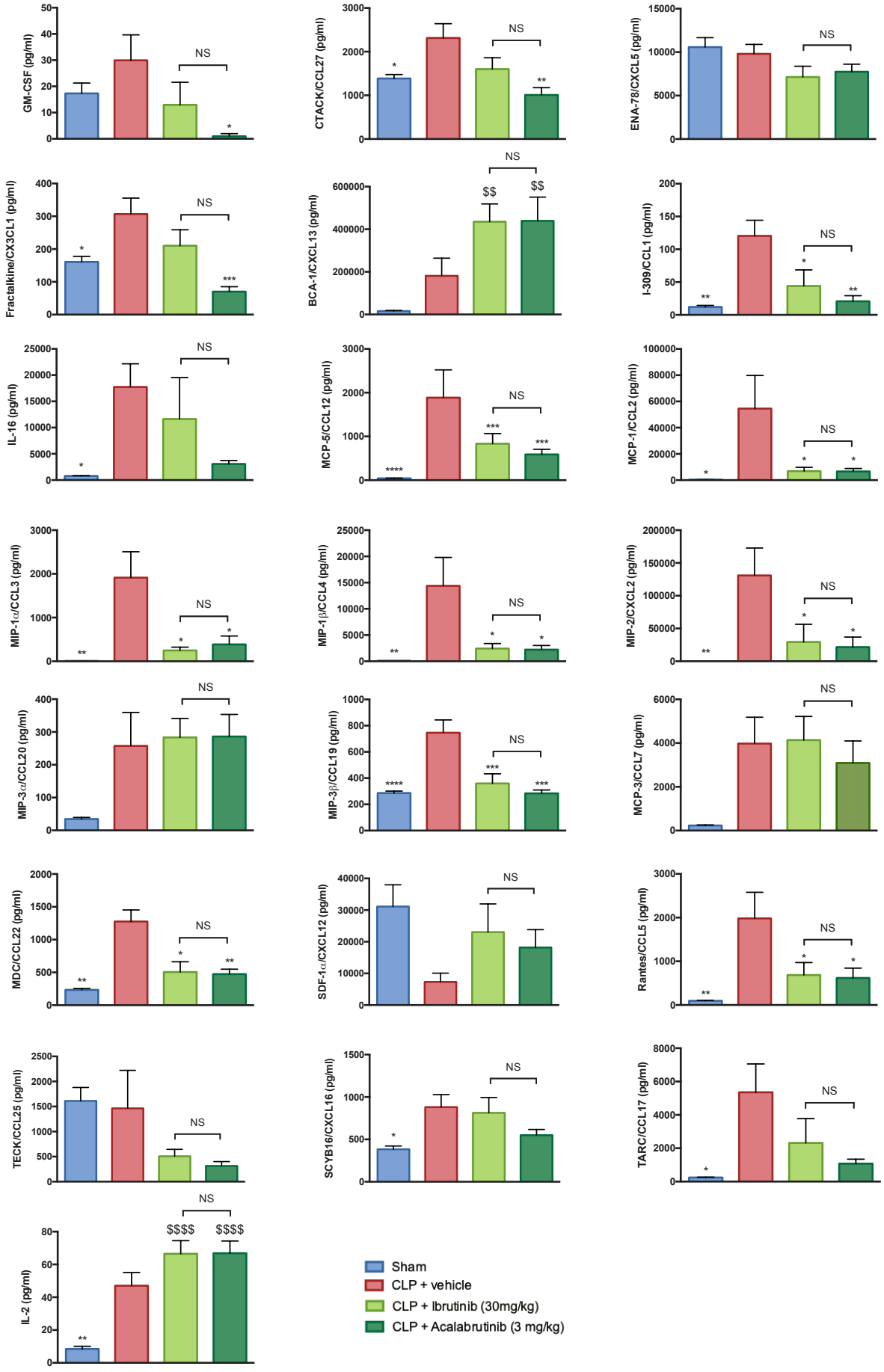
GM-CSF (pg/ml)
CTACK/CCL27 (pg/ml)
ENA-78/CXCL5 (pg/ml)
Fractalkine/CX3CL1 (pg/ml)
BCA-1/CXCL13 (pg/ml)
I-309/CCL1 (pg/ml)
IL-16 (pg/ml)
MCP-5/CCL12 (pg/ml)
MCP-1/CCL2 (pg/ml)
MIP-1α/CCL3 (pg/ml)
MIP-1β/CCL4 (pg/ml)
MIP-2/CXCL2 (pg/ml)
MIP-3α/CCL20 (pg/ml)
MIP-3β/CCL19 (pg/ml)
MCP-3/CCL7 (pg/ml)
MDC/CCL22 (pg/ml)
SDF-1α/CXCL12 (pg/ml)
Rantes/CCL5 (pg/ml)
TECK/CCL25 (pg/ml)
SCYB16/CXCL16 (pg/ml)
TARC/CCL17 (pg/ml)
IL-2 (pg/ml)
NS
$$
$$$$
Sham
CLP + vehicle
CLP + Ibrutinib (30mg/kg)
CLP + Acalabrutinib (3 mg/kg)

Figure 2.37 Serum cytokines measured in septic mice treated with or without BTK inhibitors. Mice were randomly assigned to undergo CLP or sham-operated surgery. One hour later, mice were treated with ibrutinib (30 mg/kg i.v.), acalabrutinib (3 mg/kg i.v.), or vehicle (5% DMSO + 30% cyclodextrin i.v.). At 24 h after CLP, blood samples were collected, and the serum concentration of cytokines and chemokines were measured by a multiplex assay. All data are expressed as mean ± SEM for $n = 8$ per group. A value of $^{****}P < 0.0001$, $^{***}P < 0.001$, $^{**}P < 0.01$ and $^{*}P < 0.05$, were considered to be statistically significant when compared to CLP + vehicle by one-way ANOVA followed by a Bonferroni's *post hoc* test. $^{\$\$\$\$}P < 0.0001$ and $^{\$\$}P < 0.01$ *versus* sham + vehicle.

2.5 Discussion

In this study, I developed a model of endotoxaemia where LPS (7 mg/kg) and PepG (1 mg/kg) were administered systemically to activate TLR4 and TLR2 leading to systemic inflammation and the induction of cardiac dysfunction. I report in this chapter that the pre- and post-treatment with ibrutinib (3 or 30 mg/kg) attenuates the cardiac dysfunction caused by LPS/PepG, indicating that BTK inhibitors suppress the LPS/PepG-induced systemic inflammation. The LPS/PepG model is useful to evaluate the efficacy of potential therapeutic interventions, however, it is not the "gold standard model" for sepsis research. The LPS/PepG model does not reflect the development of sepsis as seen in humans, since it is not an infection of bacteria (224). Thus, I developed the caecal ligation and puncture model which is a model of polymicrobial sepsis in 10-week-old male C57BL/6 mice to further assess the role of BTK inhibitors in sepsis.

Death is a frequently used endpoint in animal studies, but with rising ethical standards over animal research a new humane endpoint is required to allow early termination of the experiments, thus reducing suffering while still reliably predicting mortality/survival. Body temperature is an essential parameter in evaluating the animal's wellbeing and it has been reported that a reduction in temperature to <30°C or a change in temperature of 5°C (or more) over 24 h in mice with CLP is a reliable marker to predict death (221). Specifically, Mai *et al*. investigated whether temperature could be used as a predictor of death in the CLP model of sepsis by subjecting mice to sham, moderate or severe CLP and measuring the change in body temperature via rectal probe and survival of the mouse over 24 h. They conducted ROC analyses using the last recorded body temperature and using change from baseline to final temperature of survivors and non-survivors. They found that the area under the curve (AUC) of 0.88 (95% confidence interval 0.77–0.99) for last recorded temperature indicates that body temperature < 30 °C is an independent predictor of outcome for animals that reached endpoint in the study, as well as the reduction in body temperature (> 5 °C) over time (AUC 0.89, 95% confidence interval 0.78–0.99) in each animal. In a cecal slurry procedure surface temperature was measured by non-invasive infrared thermometry on the xiphoid surface, to predict mortality. It was found that surface temperature < 30.5°C at 24 h was 90% specific and 84% sensitive in predicting mortality of mice. By using temperature reduction as a surrogate endpoint, it reduced the animals suffering by 41% and provided an accurate survival rate

estimate, as a result only 13 out of 154 mice would have died, 67 would have been euthanized at 24 h and only 7 would have been euthanized unnecessarily (225). Mei *et al*. also assessed temperature change as a predictor for mortality in the LPS-endotoxin model via two different methods: method 1 core body temperature by implanted radio frequency identification (RFID) temperature transponders and method 2 surface temperature by non-contact infrared thermometry (226). They found that both methods predicted death with high accuracy resulting in a temperature threshold of 28.1°C for core body (96.3% accuracy) and 24.3°C for surface temperature (95.3% accuracy). Further studies have also confirmed hypothermia as a reliable marker for determining whether mice would survive during infectious disease research (227–229). These studies highlight the reliability of change in temperature to predict morality and encourage researchers to apply a more humane endpoint to their research. The development and accuracy of non-contact infrared thermometry reduces the stress of the animals further and allows easy monitoring of disease progression.

As mortality of animals is not an acceptable routine endpoint in the UK, I used the reduction in rectal temperature <30°C as a surrogate marker for mortality. Over the course of 24 h, the temperature of CLP mice gradually decreased reaching a predicted mortality of 80% at 24 h, indicating that this is a severe model of sepsis that I have developed. Here I measured a clinical score and also the decrease in temperature. Over the course of 24 h in CLP mice, I observed the development of physiological symptoms of sepsis: lethargy, piloerection, tremors, periorbital exudates, respiratory distress, and diarrhoea, with severe sepsis being defined as a score of > 3 only observed at 24 h, the clinical score increased with the severity of sepsis cardiac dysfunction. However, a clinical score is subjective, an objective measurement is change in temperature.

Cardiac dysfunction is commonly reported by measuring the percentage of EF or FS, but it is not clear whether these are the most sensitive parameters for determining systolic dysfunction in CLP mice? Over 24 h, I measured a multitude of cardiac parameters at varying time intervals. Interestingly, I found a significant reduction in SV and CO 1 h after CLP, whereas EF and FS were only significantly reduced at 12 h and 24 h after CLP-sepsis. This demonstrates that SV and CO are early and sensitive biomarkers of dysfunction and warrant reporting in future studies, alongside EF & FS. However, the reduction of CO and SV may be secondary to the reduction in preload e.g. vascular leak. Hoffman *et al*. reported that 2 h after CLP, the CO is

significantly decreased and that it is a highly sensitive and specific marker for predicting mortality in mice at 48 h (224). It has also been reported in septic patients that reduced CO is associated with higher rates of mortality (230). With respect to diastolic dysfunction, significant differences in E/A ratio and myocardial performance index are only observed at 24 h, suggesting that diastolic dysfunction appears at a later onset.

The change in body temperature from normothermia to either hypothermia or hyperthermia effects cardiac function. During a septic insult, mice exhibit a decrease in temperature called inflammation associated hypothermia, which is a CNS-mediated response, impacting the autonomic nervous system and, thus, impairing the sympathetic cardiovascular system leading to systolic cardiac dysfunction. In contrast, humans with sepsis develop an increase in temperature (fever). This raises the question as to what degree does increasing or decreasing core body temperature effect the cardiac function? *In vivo,* acute cold exposure (reducing the core body temperature of rats to 15^{o}C) resulted in severe, systolic cardiac dysfunction (231). In another study, the decrease in body temperature to 25^{o}C resulted in 20% of rats having hypotension, 30% having a low cardiac output and 50% having bradycardia (232). Human subjects were exposed to a warm or cool environment via a water-perfused garment (fitted suit that covers the body except the hands, feet, neck and head) to measure the effect of heat and cold stress on their cardiac function. Heat resulted in a decrease in preload and afterload and systolic function increased to maintain or increase stroke volume. In addition, heart rate increased and the increase in stroke volume resulted in an increase in cardiac output. During exposure to a cold environment, preload and afterload increased and hypothermia results in decreased depolarisation of cardiac pacemaker cells, causing bradycardia (233). To what extent does treating CLP-induced hypothermia affect the outcome in murine sepsis? Mice which underwent CLP and have their hypothermia corrected (by being placed into a heat box (maintained at 35^{o}C) resulted in an improvement in survival from 42% to 60% and also reduced the levels of IL-6 (234). Most animal studies of sepsis do not maintain physiological temperature throughout the study. In my study, cardiac parameters were only measured in all groups when temperature returned to normothermia and heart rate was approximately 450bpm to mitigate the cofounding variable effects that change in temperature and heart rate have upon the cardiac parameters.

I investigated the increases of bacteria and infiltrating immune cells throughout 24 h in my CLP model. I observed that bacteria levels in the peritoneum remain low till 12 h and this corresponds in a gradual increase in phagocytosing immune cells macrophages and neutrophils, which plateau out (reach their maximum) at 12 h. At 24 h the bacterial count is significantly increased and there is little increase in the numbers of macrophages and neutrophils, this demonstrates that at 24 h the immune system has been overwhelmed and is no longer able to control the source of infection. Additionally, I find that there is a small number of infiltrating B and T cells in my CLP model, with significant increases only being observed at 24 h in CLP mice for B cells when compared to sham-operated mice. The data suggests that up to 12 h, the body can control the levels of bacteria, indicating a therapeutic window of 12 h to provide an intervention to aid the body in clearing a microorganism. I have, however, chosen to provide delayed interventions 1 h after CLP, for the reason that 1 h after CLP physical symptoms of the mice are observed e.g. a significant decrease in temperature and a drastic decrease in cardiac output (which is a sensitive marker for mortality), suggesting that onset of sepsis can be documented within 1 h of CLP.

I show here, for the first time, that administration of two structurally different irreversible BTK inhibitors (ibrutinib and acalabrutinib) both ameliorate the cardiac dysfunction (measured as the decline in EF, FS, FAC, CO and SV by echocardiography) caused by CLP-sepsis. The observed decline in EF also was associated with a significant increase in the serum levels of two, well-known biomarkers of left ventricular dysfunction, namely CXCL10 and CXCL11 (235–237). Most notably, ibrutinib or acalabrutinib also attenuated the rises in CXCL10 and CXCL11 caused by CLP-sepsis. In addition, ibrutinib or acalabrutinib also reduced renal dysfunction (measured as an increase in serum urea or creatinine) caused by CLP-sepsis. Thus, both BTK inhibitors reduced the cardiac and renal dysfunction caused by sepsis.

What, then, is the mechanism by which ibrutinib or acalabrutinib reduce the cardiac (renal) dysfunction caused by sepsis? Ibrutinib is a potent BTK inhibitor, but not very specific (as it also inhibits a multitude of other kinases), which is approved by the FDA and the EMA for the use in chronic lymphatic leukaemia, mantle cell lymphoma and Waldenstrom macroglobulinemia. Acalabrutinib is a potent, but highly specific BTK inhibitor: at a (relatively high) concentration of 1 μM, acalabrutinib strongly inhibited only the following 5 kinases: BTK, Bmx, ErbB4, RIPK2 and TEC, while the same concentration of ibrutinib inhibited 35

kinases. The activation of BTK and the subsequent activation of BTK signalling involves a) phosphorylation of BTK at Tyr^{223} and b) the phosphorylation of PLCγ at Tyr^{1217} by phosphorylated (activated) BTK as the first step in the BTK signalling cascade (238). I report here that sepsis results in significant increases in the phosphorylation of cardiac BTK at Tyr^{223} and the phosphorylation of PLCγ at Tyr^{1217}, indicating that BTK is activated in septic hearts. Most notably, the activation of BTK negatively correlated with EF, indicating that activation of BTK is associated with the cardiac dysfunction in sepsis. Indeed, inhibition of BTK activity with ibrutinib or acalabrutinib in the heart of septic animals reduces the cardiac dysfunction in sepsis suggesting that activation of BTK plays a pivotal role in the pathophysiology of the cardiac dysfunction in sepsis. It should be noted that the doses of acalabrutinib and ibrutinib that I used in our study in the mouse resulted in a similar, approximately 70%, inhibition of BTK activity in septic hearts. I, therefore, propose that inhibition of BTK activity explains the observed beneficial effects of ibrutinib or acalabrutinib in sepsis.

What are the mechanisms by which the activation of BTK (in the heart) leads to cardiac dysfunction in sepsis? There is good evidence that a) the activation of BTK precedes the activation of NF-κB (239), and b) the activation of NF-κB plays an important role in the cardiac dysfunction in sepsis (240,241). Specifically, inhibition of the activity of NF-κB attenuates the cardiac dysfunction in sepsis and the production of pro-inflammatory cytokines/chemokines (179,242). I report here, for the first time, that a) activation of BTK is associated activation of NF-κB in septic hearts, and b) inhibition of BTK activity with ibrutinib or acalabrutinib reduces both the activation of NF-κB in septic hearts and the cardiac dysfunction caused by sepsis. Thus, I propose that inhibition of the activation of NF-κB contributes to the observed beneficial effects of the BTK inhibitors ibrutinib and acalabrutinib in sepsis. When challenging BTK KO-mice with LPS, Gabhann and colleagues observed reduced i) activation of NF-κB p65, ii) Akt phosphorylation and iii) M2 polarisation of macrophages (243).

Activation of NF-κB drives the formation of a number of pro- and anti-inflammatory cytokines and chemokines. I report here that CLP-sepsis leads to a significant increase in the serum levels of the pro-inflammatory cytokines TNF-α, IL-6, IFN-γ, anti-inflammatory cytokines IL-10, IL-4 and the chemokines KC/CXCL1, eotaxin-1/CCL11, eotaxin-2/CCL24, all of which importantly contribute to the local and systemic inflammation and organ injury associated with sepsis (244). Most notably, the powerful pro-inflammatory cytokine TNF-α is ameliorated by

both BTK inhibitors. TNF-α has been implicated in murine models of sepsis and humans with sepsis. TNF-α acts in an autocrine and paracrine manner leading to macrophage production and activation, resulting in the release of other proinflammatory cytokines such as IL-6 and IL-8 (245,246).

Similarly, there is also good evidence that activation of BTK plays a crucial role in the assembly and activation of the NLRP3 inflammasome (166,167). The activation of the NLRP3 inflammasome has been suggested to play a role in cardiac dysfunction (247) and the pathophysiology of sepsis (105). Others have reported that inhibition of the assembly and activation of NLRP3 inflammasome protects against microbial sepsis (105). I report here for the first time that a) activation of BTK is associated with the activation of the NLRP3 inflammasome in septic hearts, and b) inhibition of BTK activity with ibrutinib and acalabrutinib reduces both the assembly and subsequent activation of the NLRP3 inflammasome in septic hearts (and the cardiac dysfunction caused by sepsis). Thus, I propose that inhibition of the activation of the NLRP3 inflammasome may also contribute to the observed beneficial effects of the BTK inhibitors ibrutinib and acalabrutinib in sepsis.

Activation of the NLRP3 inflammasome drives the formation of IL-1β and IL-18, both of which play an important role in the systemic inflammation and/or organ dysfunction in sepsis (248). Specifically, inhibition of caspase-1 results in an inhibition of IL-18 and IL-1β secretion, which, in turn, attenuated the cardiac dysfunction caused by myocardial ischemia (249). The role of the inflammasome in the pathophysiology of sepsis, however, is still controversial: For example, survival was similar in wild-type and caspase-1/11 knockout mice with sepsis, while the neutralization of IL-1 and IL-18 reduced mortality in endotoxemia (248). Furthermore, inhibition of NLRP3 inflammasome with NLRP3 inhibitor MCC950 results in attenuation of sepsis-associated encephalopathy (250). Here I show that BTK inhibition results in reduced serum levels of IL-1β, and this was associated with an improvement of cardiac function.

The evaluation of the efficacy of the BTK inhibitors used in our study depends on the assumption that the development of organ dysfunction (and specifically cardiac and renal dysfunction) correlates with outcome. There is good evidence that the occurrence of cardiac and/or renal dysfunction correlates positively with an increase in mortality in patients with sepsis (219).

2.5.1 Conclusions

There are currently no specific treatments, which reduce cardiac dysfunction or, indeed, mortality in sepsis. My data shows for the first time that two commercially available BTK inhibitors, ibrutinib or acalabrutinib, attenuate the CLP-induced cardiac dysfunction through inhibition of the activation of BTK/NF-κB and/or the NLRP3 inflammasome, which in turn reduces the formation of many chemokines and cytokines including TNF-α. Notably, no significant qualitative or quantitative differences were found with two, chemically distinct BTK-inhibitors suggesting that the observed beneficial effects of both compounds in experimental sepsis are likely to be a drug class-related effect. Thus, BTK inhibitors are FDA-approved drugs that may be repurposed for the use in sepsis, but also other diseases associated with either local or systemic inflammation.

Chapter 3 *Xid* mice are protected against sepsis-induced multiple organ failure

3.1 Introduction

In the previous chapter, I have shown that inhibition of BTK by BTK inhibitors attenuated the systemic inflammation and cardiac dysfunction induced by a model of polymicrobial sepsis (CLP model). However, the two BTK inhibitors have off-target effects: As seen in the kinome array below (Figure 3.1), both BTK inhibitors strongly inhibit four other kinases: RIPK2, ErbB4, Tec and BMX. This triggered two important questions: (1) Does inhibition of BTK activity alone account for the observed beneficial effects? And (2) Does inhibition of systemic inflammation reduce the host response to infection and ultimately cause increased harm? Interestingly, of the kinases which are strongly inhibited by ibrutinib and acalabrutinib, expression of ErbB4 (rather than its activation) may play a role in the cardiac dysfunction and cognitive impairment associated with sepsis (251). In contrast, RIPK2 kinase is unlikely to play a significant role in sepsis, as the CLP-induced septic peritonitis was similar in RIPK2 knockout mice and their wild-type littermates (252).

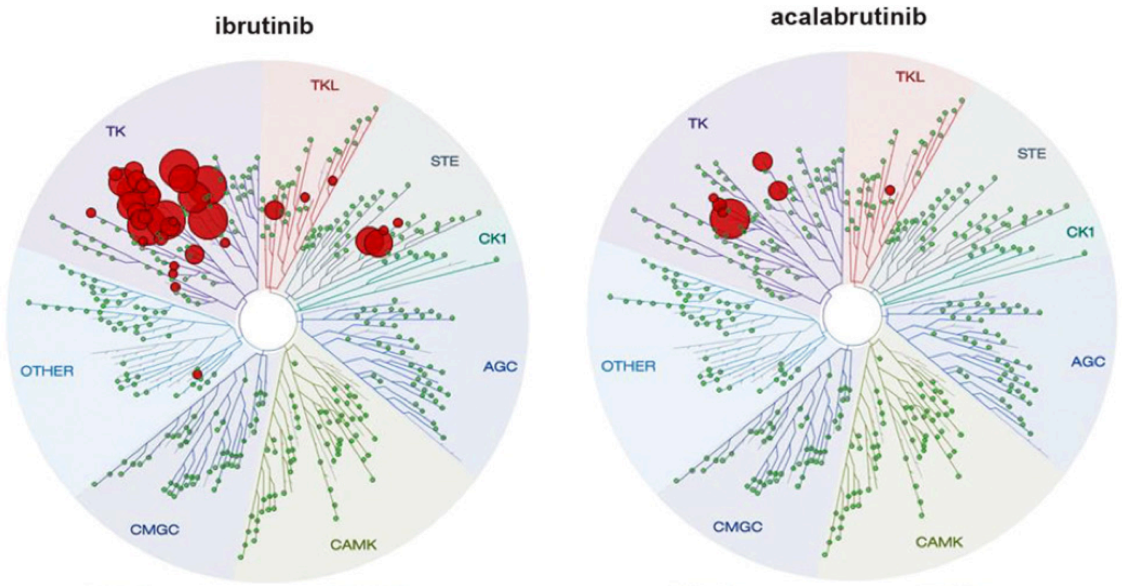

Figure 3.1 Kinome array of ibrutinib and acalabrutinib. Ibrutinib and acalabrutinib were profiled for 395 human kinases at 1 μM via DiscoverRx kinase assay. The size of the red circles represents the extent of inhibition with larger circles meaning stronger inhibition. Image is taken from (181).

To investigate whether inhibition of BTK, indeed, accounts for the inhibition of NF-κB and the NLRP3 inflammasome and ultimately the observed beneficial effects in sepsis, I repeated the sepsis model in X-linked immunodeficient (*Xid*) mice, which have a deficiency in the activation of BTK due to a single point mutation in the BTK gene. Specifically, *Xid*-mice have

a C to T transition point mutation at position 219, which changes amino acid 28 from arginine to cysteine (183,184). The *Xid* mice are a model of the human X-linked agammaglobulinemia and are in the background of CBA mice, in contrast to my previous work, which was done in C57BL/6 mice. Both mice and humans with BTK deficiency experience reduced numbers of B cells, however, this B cell depletion is more severe in humans than mice. The expression of BTK is not restricted to B cells, as BTK is also expressed in cells of the myeloid lineage, including macrophages and neutrophils (253), activation of which contributes to the pathophysiology of sepsis.

Having developed a model of sepsis in *Xid* mice (and wild-type mice, CBA background), in this chapter I have investigated the following:

1) Whether *Xid* mice are protected from sepsis-induced multiple organ failure (cardiac, renal and liver dysfunction).
2) Whether *Xid* mice result in reduced activation of BTK, NF-κB and NLRP3 inflammasome in cardiac tissue when under septic insult.
3) The production of sepsis-associated cytokines and chemokines in *Xid* mice.
4) Determine the ability of *Xid* mice to remove bacteria by measuring:
    a) Bacteria in the peritoneal cavity and blood.
    b) The number of infiltrating immune cells in the peritoneal cavity.
    c) The phagocytic ability of neutrophils and macrophages.

3.2 Methods

3.2.1 Animals

This study was carried out on twenty-three 10-week-old, male CBA mice (Charles River Laboratories UK Ltd., Kent, UK) and twenty-one 10-week-old, male CBA/CaHN-*Btk*^{xid}/J (*Xid)* mice (from Jackson laboratory), weighing 25–30 g and kept under standard laboratory conditions. The animals were allowed to acclimatise to laboratory conditions for at least one week before undergoing experiments. Six mice were housed together (in each cage) with access to a chow diet and water *ad libitum*. They were subjected to a 12-h light and dark cycle with a temperature maintained at 19–23°C. The cages were cleaned regularly approximately every three days, with water being changed daily. Research staff inspected the animals each day for any signs of illness or abnormal behaviour.

3.2.2 Caecal ligation and puncture (CLP) surgery

Caecal ligation and puncture (CLP) surgery was performed in 10-week-old male CBA (wild type) or *Xid* mice as previously described in chapter 2 (Table 3.1). Mice were randomly assigned to undergo CLP or sham-operated surgery, the surgeon was blinded to the genotype of the mouse. Briefly, mice were anaesthetised with isoflurane (2% delivered in O_2) and the caecum was fully ligated below the ileocaecal valve. A double puncture was made with an 18-G needle into the caecum and a small amount of faeces was squeezed out after which the caecum was returned to its anatomical position, then the laparotomy was closed. All animals received fluids (5 ml/kg saline into the abdomen before closure and 10 ml/kg saline s.c., immediately after surgery), antibiotics (Imipenem/Cilastatin; 20 mg/kg dissolved in 7.5 ml/kg of saline s.c.), and analgesics (buprenorphine; 0.05 mg/kg i.p.) at 6 h and 18 h after surgery. Sham-operated mice underwent the same procedure, but without CLP. At 1 h after CLP, WT or *Xid* mice received 30 mg/kg ibrutinib (Selleck Chemicals) intravenously. At the end of the study, mice were sacrificed, peritoneal lavage fluid and organs were collected under sterile conditions, and blood was withdrawn by cardiac puncture.

A clinical score for monitoring the health of experimental mice was used to evaluate the symptoms consistent with murine sepsis. The maximum score of 6 comprised the presence of the following signs: lethargy, piloerection, tremors, periorbital exudates, respiratory distress,

and diarrhoea. Mice with a clinical score >3 were defined as exhibiting severe sepsis, against moderate sepsis for a score ≤3. Animals were culled at 24 h after the onset of sepsis (CLP).

Table 3.1 Groups used in the study to evaluate the effects of CLP-induced cardiac dysfunction.

Strain	Group	Procedure	Total number
WT CBA 10 weeks	Sham + vehicle	Sham surgery at 0 h	5
	CLP + vehicle	CLP surgery at 0 h	10
	CLP + ibrutinib	CLP surgery at 0 h, then ibrutinib (30 mg/kg i.v.) at 1 h	8
***Xid* mice CBA background**	Sham + vehicle	Sham surgery at 0 h	5
	CLP + vehicle	CLP surgery at 0 h	10
	CLP + ibrutinib	CLP surgery at 0 h, then ibrutinib (30 mg/kg i.v.) at 1 h	6

3.2.3 Assessment of cardiac function *in vivo*

At 24 h post CLP, mice were anaesthetised (0.5 - 2% isoflurane in O_2); body temperature was maintained at 37°C and heart rate was maintained at 450 bpm. Then, cardiac function was assessed by M-mode and B-mode echocardiography using the VisualSonics Vevo 3100 echocardiographic system and an MX550D transducer as previously described in chapter 2. The following parameters were measured: left ventricular EF, FS, FAC, CO, SV, MPI, global longitudinal strain and global circumferential strain.

3.2.4 Quantification of renal dysfunction, hepatocellular injury and cell injury

After 24 h, mice were sacrificed by terminal cardiac puncture, where terminal blood samples were immediately decanted into 1.3 ml serum gel tubes (Sarstedt, Nürnbrecht, Germany). Blood was left to coagulate for at least 10 min at room temperature, then samples were centrifuged at 9000 rpm for 3 min to separate the serum. Then 100 µl of serum was snap-frozen in liquid nitrogen and sent to an independent veterinary testing laboratory (MRC Harwell Institute, Oxford, UK) to evaluate the following biomarkers in a blinded fashion: Urea and creatinine (as markers of renal dysfunction), ALT, AST (markers of hepatocellular injury) and lactate dehydrogenase (LDH) (a marker of cell injury).

3.2.5 Cytokine analysis

Cytokines, chemokines and a growth factor were determined in serum by Bio-Plex Pro Mouse Chemokine 31-Plex panel assay (Bio-Rad, Kabelsketal, Germany) as previously described in chapter 2. The cytokines IL-1ß, –2, –4, –6, –10, –16, CCL1, –2, –3, –4, –5, –7, –11, –12, –17, –19, –20, –22, –24, –27, IFN-γ, TNF-α and the chemokines CX3CL1, CXCL1, –2, –5, –10, –11, –12, –13, –16 and the growth factor GM-CSF were measured according to the manufacturer's instructions.

3.2.6 Quantification of immune cells in the peritoneum

As previously described in chapter 2, the peritoneal lavage exudate was collected by injecting 5 ml of 2 mM of EDTA in PBS into the peritoneal cavity. After gentle massaging, approximately 4 ml of exudate was removed with an 18-G needle**.** Cells were washed in FACS buffer (0.05 % BSA, 2 mM EDTA in PBS pH 7.4) and then blocked using anti-CD16/32 (Biolegend) for 10 min at 4°C. Peritoneal cells were analysed using anti-CD45 (clone 30-F11; BioLegend), anti-CD11b (clone M1/70; BioLegend), anti-F4/80 (clone BM8; BioLegend), anti-Ly6G (clone 1A8; BioLegend), anti-CD206 (clone C068C2; BioLegend), anti-MHCII (clone. M5/114.15.2; BioLegend), anti-CD3 (clone 145–2C11; BioLegend), and anti-B220 (clone. RA-3–6B2; BioLegend) antibodies. Absolute cell count was calculated by the addition of counting beads (BioLegend). Data were acquired using BD LSR II Fortessa (Becton Dickinson) and analysed using FlowJo analysis software (version 10.6, Treestar Inc.). Gating strategy as seen below in Figure 3.2.

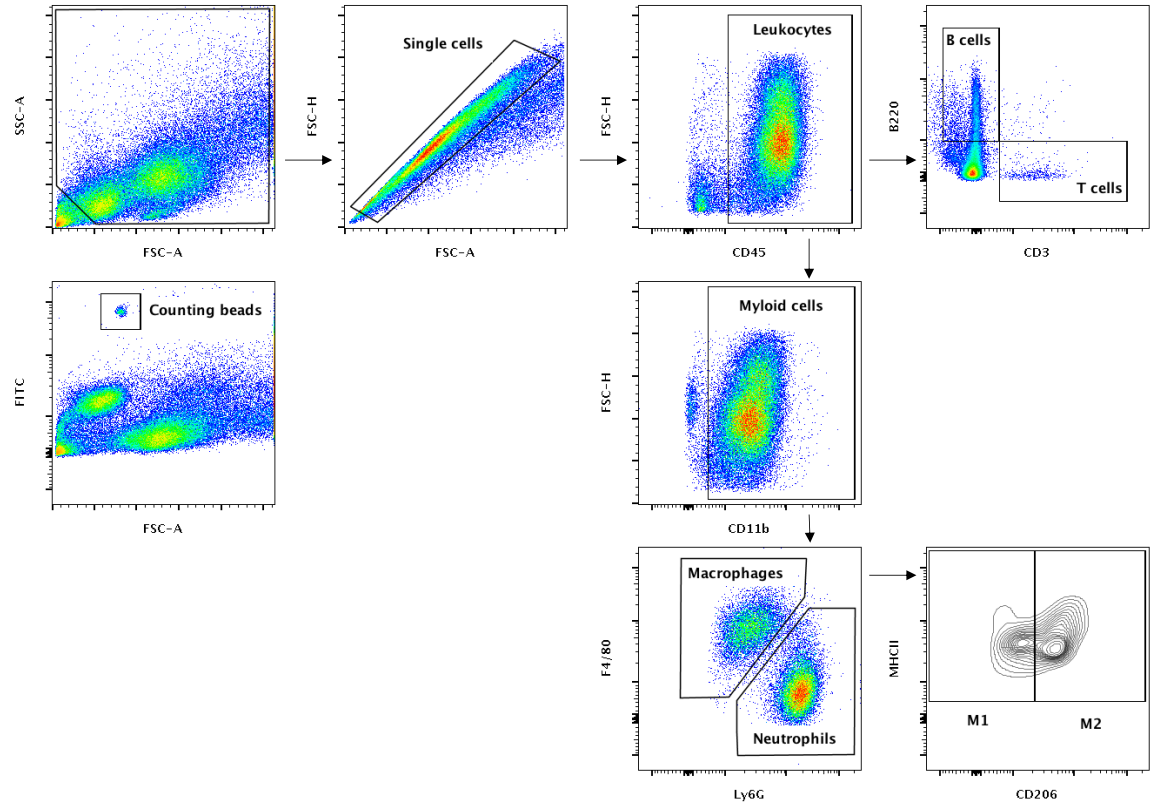

Figure 3.2 Representative flowcytometry gating strategy. Illustrating peritoneal lavage fluid being subgated to the level of B cells, T cells, neutrophils, macrophages: M1 phenotype and M2 phenotype.

3.2.7 Quantification of bacteria

Accurate evaluation of the number of bacteria in peritoneal lavage fluid and blood samples was performed by flow cytometry using the SYTO BC bacteria counting kit (Thermo Fischer Scientific) as previously described in chapter 2.

3.2.8 Phagocytic ability

Peritoneal lavage exudate containing neutrophils and macrophages were obtained 24 h after CLP as described above. pHrodo™ red *E.Coli* bioparticles™ (Thermo Fischer Scientific) were resuspended in live-cell imagining solution (BioLegend) at 10 mg/ml and 10 µL of bioparticles were opsonised with 20 µL of fresh serum for 1 h at 37°C under gentle agitation, after which they were washed and resuspended in 10 µL of live cell imagining solution. 1×10^6 cells of peritoneal exudate were collected by centrifugation (300 g x 5 min) and resuspended in 890

µL of live cell imaging solution, after which 100 µl of fresh serum and 10 µL of optimised bioparticles were added and incubated for 45 min at 37°C under gentle agitation. Cells were washed and then blocked using anti-CD16/32 (Biolegend) for 10 min at 4°C followed by staining with surface markers anti-CD11b (clone M1/70; BioLegend), anti-Ly6G (clone 1A8; BioLegend) and anti-F4/80 (clone BM8; BioLegend) for 30 min at 4°C. Neutrophils were identified as ($CD11b^+$, $Ly6G^+$, $F4/80^-$) and macrophages were identified as ($CD11b^+$, $Ly6G^-$, $F4/80^+$). 10,000 $CD11b^+$ cells were collected by Amnis® ImageStream®^{X} Mk II Imaging Flow Cytometer (Luminex) at a magnification of x40 and analysed by IDEAS software for each experimental sample.

3.2.8.1 Imagestream acquisition

The flow rate was set to slow speed for high-resolution imaging at magnification x40. Firstly, multi-fluorophore labelled samples to determine optimal laser power settings based on Raw Max Pixel (RMP) intensity values of the channel corresponding to each fluorophore used to prevent saturated events. Lasers and power settings were set according to Table 3.2.

Table 3.2 Laser wavelengths and power settings for phagocytosis analysis.

Excitation Laser (nm)	Power Setting (mW)	Fluorophore Ab	Emission Channel
		Bright Field	1 & 9
488	150	CD11b	2
488	150	pHrodo Red Bioparticles	3
488	2	SSC (Side scatter)	6
405	80	Ly6G	8
633	100	F4/80	11

3.2.8.2 Data acquisition

1,000 events were collected for each single fluorophore labelled sample with the brightfield and SSC turned off during acquisition to create the compensation matrix. For each experimental sample 10,000 events in the CD11b acquisition gate were collected.

3.2.8.3 Data analysis with IDEAS software

The compensation matrix file was created and applied to the raw dataset for each experimental sample.

Gating strategy (Figure 3.3):

1. Gate single cells (Aspect ratio M01 vs. Area M01).
2. Gate cells in focus (Normalized frequency vs. Gradient RMS).
3. Gate CD11b positive cells (normalized frequency vs. intensity channel 2).
4. Gate macrophages (F4/80+/Ly6G-) and neutrophils (Ly6G+/F4/80-) (intensity channel 11 (F4/80) vs. intensity channel 8 (Ly6G)).
5. Gate macrophages and neutrophils positive with bacteria. (normalized frequency vs. intensity of channel 3 (pHrodo red *E. coli*)). Events with a value greater than 1e3 were gated as positive signal ($pHrodo^{+}$). The percent of phagocytosis was calculated based on the percentage of events in the $pHrodo^{+}$ events and were analysed further to determine the spot count of pHrodo *E. coli* bioparticles.
6. To quantify the phagocytic ability of macrophages and neutrophils in *Xid* mice I utilized the capabilities of the imaging flow analysis software to count the spots of intensity emitted by the pHrodo-E. coli bioparticles.

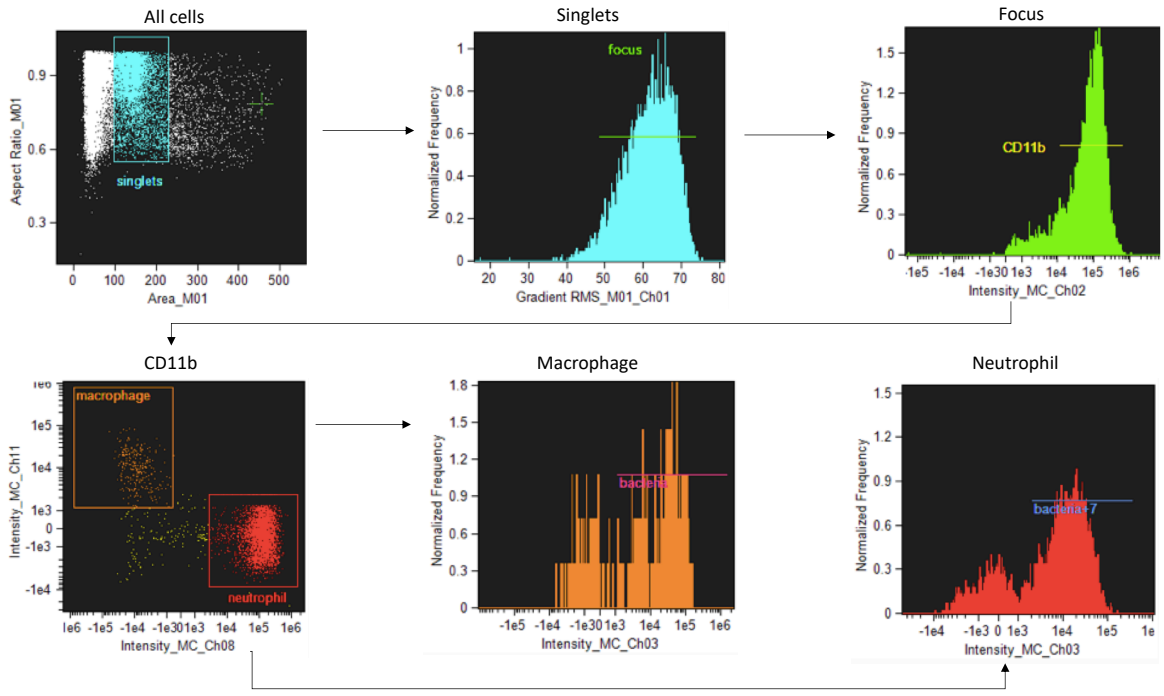

Figure 3.3 Imagestream gating strategy.

3.2.9 Western blots

Immunoblot analyses of cardiac tissue samples were carried out using a semi-quantitative western blotting analysis. The antibody used were: 1:1,000 rabbit anti-Ser$^{176/180}$-IKKα/β, 1:1,000 rabbit anti-total IKKα/β, mouse anti-Ser$^{32/36}$-IκBα, mouse anti-total IκBα, rabbit anti-Tyr^{223}-BTK, rabbit anti-total BTK, rabbit anti-Tyr^{1217} PLCγ, rabbit anti-total PLCγ (from Cell Signalling), 1:5,000 rabbit anti NLRP3 inflammasome (from Abcam), mouse anti-caspase 1 (p20) (from Adipogen). The apex of the heart was taken and homogenized. Proteins were then extracted as previously described (254) and concentrations were quantified by bicinchoninic acid (BCA) protein assay (Thermo Fisher Scientific Rockford, IL). Proteins were separated by 8% sodium dodecyl sulphate (SDS)-PAGE and transferred to polyvinylidene fluoride membranes. Membranes were blocked in 10% milk solution with TBS-Tween and then incubated with the primary antibody overnight at 4°C. The next day the secondary antibody was added for 30 min at room temperature and visualised using the ECL detection system. Tubulin was used as a loading control. The immunoreactive bands were analysed by the Bio-Rad Image Lab Software™ 6.0.1 and results were normalised to the sham bands.

3.2.10 Statistical Analysis

Statistical differences were determined using a one-way ANOVA, followed by Bonferroni post hoc test or unpaired Student's t-test as appropriate (GraphPad Prism 8.0; significant when $P < 0.05$). Results are expressed as mean ± SEM for n observations of at least three independent experiments.

3.3 Results

3.3.1 *Xid* mice have 100% predicated survival after sepsis

Both WT and *Xid* mice that underwent sham-operated surgery had a severity score at 24 h of 0, demonstrating that they experienced no symptoms of sepsis. When compared to sham-operated mice, WT mice subjected to CLP showed clinical signs of severe sepsis (80%; score >3). In contrast, all *Xid* mice subjected to CLP had a score of ≤3 indicating only moderate sepsis (Figure 3.4 A). All mice in the WT-CLP group which received ibrutinib had a score of ≤3 indicating moderate sepsis and all mice in the *Xid*-CLP + ibrutinib group had a score ≤3. No significant differences were observed the two genotypes receiving ibrutinib (Figure 3.4 A).

When compared to sham-operated mice, WT mice subjected to CLP showed a decrease in the mean heart rate, whereas the mean heart rates of *Xid*-CLP remained similar to that of sham-operated animals (Figure 3.4 B). When compared to WT-CLP mice, the administration of ibrutinib 1 h after CLP attenuated the decline in heart rate (in WT-mice). Mice in the *Xid*-CLP + ibrutinib group had a similar heart rate to mice in the *Xid*-CLP group. *Xid*-CLP mice that received ibrutinib had a higher heart rate than WT-CLP mice treated with ibrutinib.

When compared to sham-operated mice, WT mice subjected to CLP experienced hypothermia (rectal temperature of <30^{o}C) at 24 h after the onset of CLP, whereas the rectal temperature of *Xid*-CLP, WT-CLP + ibrutinib and *Xid*-CLP + ibrutinib remained at 37^{o}C (Figure 3.4 C). A reduction in temperature to <30^{o}C or a change of 5^{o}C over time in each animal has been reported to predict death in mice with CLP (221). As mortality of animals is not an acceptable routine endpoint in the UK, I used the reduction in rectal temperature <30^{o}C as a surrogate marker for mortality. Using this surrogate marker, I predicted the mortality of WT-CLP mice to be 90% (confirming that our model is a model of severe sepsis), while the predicted mortality of *Xid*-CLP mice would be 0% (e.g. 100% predicted survival; Figure 3.4 D). WT mice receiving ibrutinib had a predicted mortality of 15%, whereas *Xid*-CLP mice receiving ibrutinib had a predicted mortality of 0%.

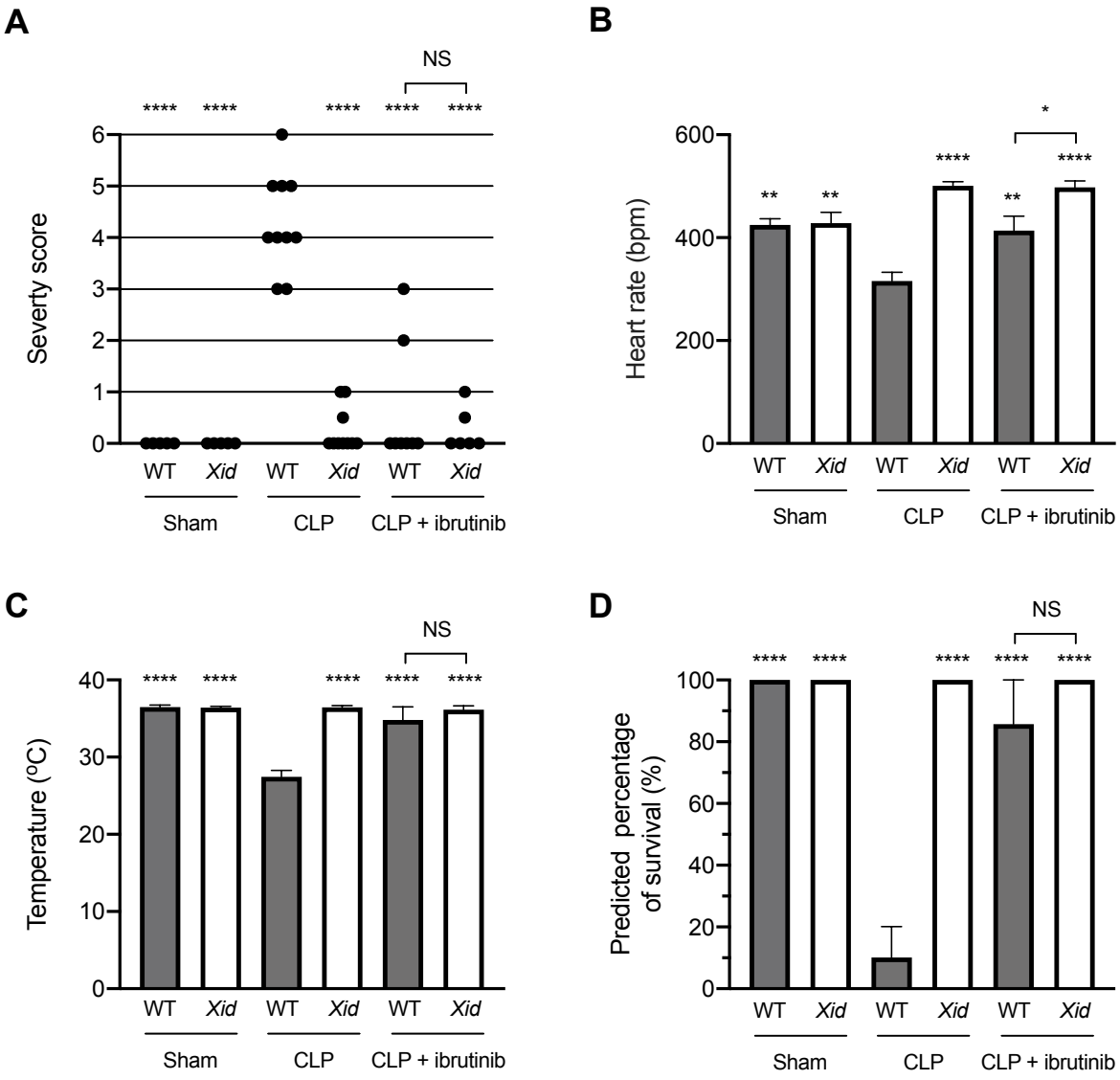

Figure 3.4 *Xid* mice have 100% predicated survival after sepsis. WT and *Xid* mice were randomly selected to undergo sham-operated or CLP surgery, 1 h later ibrutinib (30 mg/kg) was administered intravenously. At 24 h after CLP, physiological parameters of mice and their predicted survival were assessed. **(A)** Severity Score 24 h after CLP. **(B)** Temperature 24 h after CLP (ºC). **(C)** Predicted percentage of survival (%). **(D)** Heart rate 24 h after CLP (BPM). The following groups were studied WT sham ($n = 5$), *Xid* sham ($n = 5$), WT-CLP ($n = 10$), *Xid*-CLP ($n = 10$), WT-CLP + ibrutinib ($n = 8$) and *Xid*-CLP + ibrutinib ($n = 6$). Data are expressed as mean ± SEM and analysed by one-way ANOVA with a Bonferroni post hoc test. $^{**}P < 0.01$ and $^{****}P < 0.0001$ *versus* WT-CLP.

3.3.2 *Xid* mice are protected from sepsis-induced systolic cardiac dysfunction

Figure 3.5 A shows representative M-mode images in the short axis in sham-operated mice, CLP + vehicle mice and CLP + ibrutinib mice of WT and *Xid* genotypes. When compared to sham-operated mice, WT mice subjected to CLP showed a significant reduction in EF, FS, FAC, CO and SV, indicating severe global, systolic cardiac dysfunction. In contrast, *Xid*-mice subjected to CLP had only a very minor cardiac dysfunction and all indices of cardiac performance (EF, FS, FAC, CO and SV) were significantly higher from those measured in WT-CLP (Figure 3.5 B-F). Thus, the degree of cardiac dysfunction caused by CLP in *Xid* mice is significantly reduced when compared to that observed in WT-mice. When compared to WT-CLP mice (CBA background) treatment of WT-mice with ibrutinib 1 h after CLP attenuated the sepsis-induced cardiac dysfunction. In contrast, administration of ibrutinib to *Xid*-CLP mice did not affect cardiac function (Figure 3.5 B-F), indicating that the addition of ibrutinib in *Xid*-mice with CLP results in no beneficial or deleterious effects due to off-target actions of the drug.

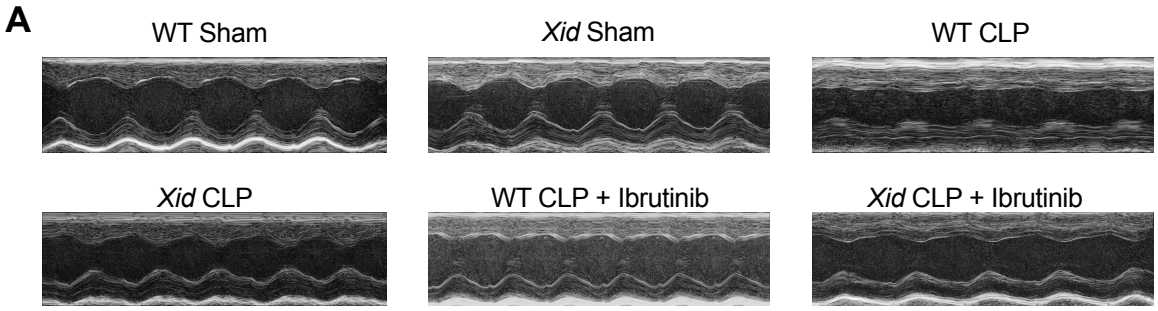
A
WT Sham
Xid Sham
WT CLP
Xid CLP
WT CLP + Ibrutinib
Xid CLP + Ibrutinib

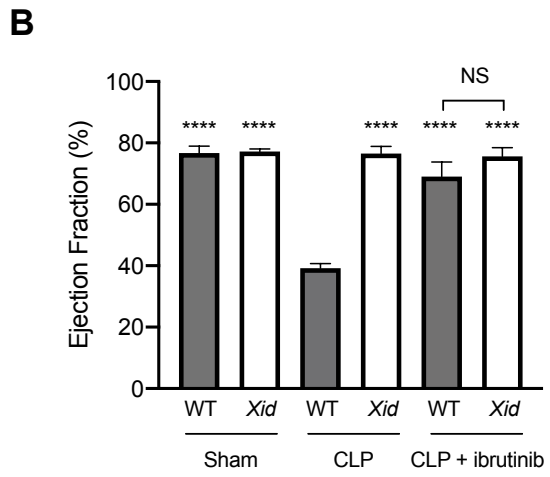
B
Ejection Fraction (%)
100
80
60
40
20
0
****
NS
WT
Xid
Sham
CLP
CLP + ibrutinib

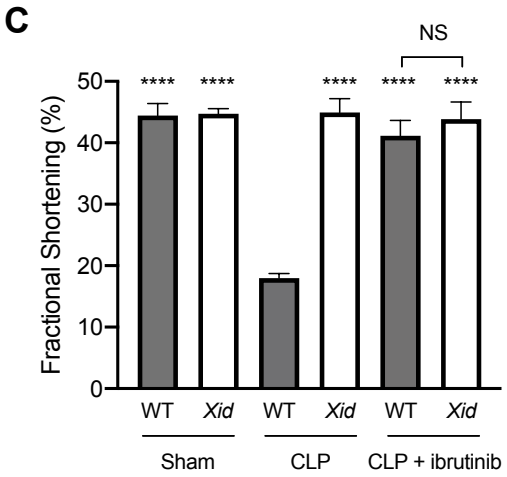
C
Fractional Shortening (%)
50
40
30
20
10
0
****
NS
WT
Xid
Sham
CLP
CLP + ibrutinib

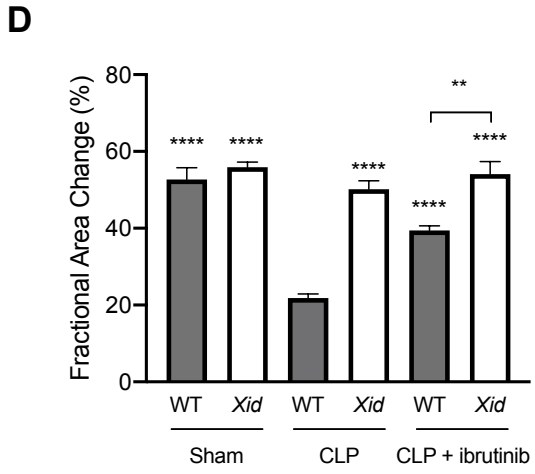
D
Fractional Area Change (%)
80
60
40
20
0
****
**
WT
Xid
Sham
CLP
CLP + ibrutinib

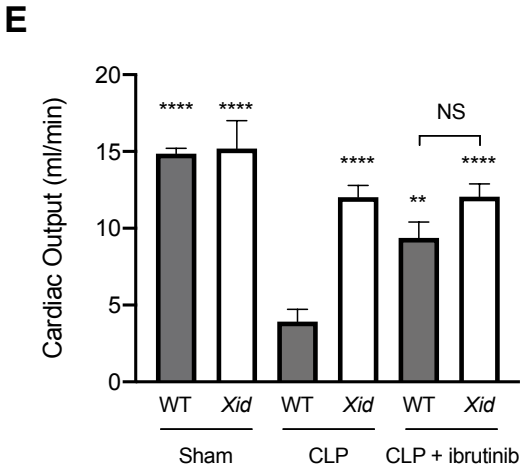
E
Cardiac Output (ml/min)
20
15
10
5
0
****
**
NS
WT
Xid
Sham
CLP
CLP + ibrutinib

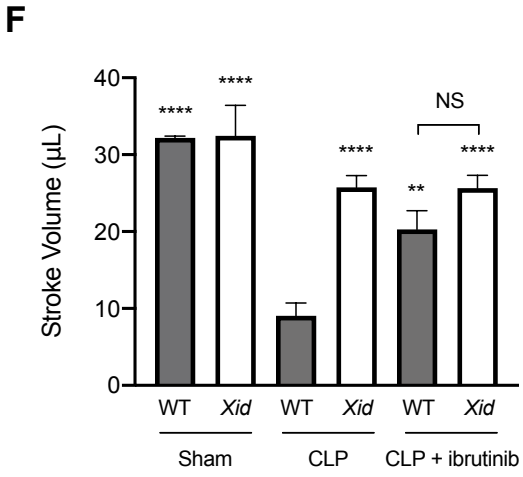
F
Stroke Volume (µL)
40
30
20
10
0
****
**
NS
WT
Xid
Sham
CLP
CLP + ibrutinib

Figure 3.5 *Xid* mice are protected from sepsis-induced systolic cardiac dysfunction. WT and *Xid* mice were randomly selected to undergo sham-operated or CLP surgery, 1 h later ibrutinib (30 mg/kg) was administered intravenously. At 24 h after CLP, cardiac function was assessed by echocardiography**. (A)** Representative M-mode echocardiograms. **(B)** Ejection fraction (%). **(C)** Fractional shortening (%). **(D)** Fractional area change (%). **(E)** Cardiac output (ml/min). **(F)** Stroke volume (μL). The following groups were studied WT sham (n = 5), *Xid* sham (n = 5), WT-CLP (n = 10), *Xid*-CLP (n = 10), WT-CLP + ibrutinib (n = 8) and *Xid*-CLP + ibrutinib (n = 6). Data are expressed as mean ± SEM and analysed by one-way ANOVA with a Bonferroni post hoc test. $^{**}P < 0.01$, $^{****}P < 0.0001$ *versus* WT-CLP.

3.3.3 *Xid* mice are protected from sepsis-induced diastolic dysfunction

There was no difference in diastolic function between WT and *Xid* sham-operated mice. When compared to sham-operated animals, WT mice subjected for 24 h to CLP demonstrated a significant increase in percentage MPI (Figure 3.6) indicating the development of diastolic, cardiac dysfunction. When compared to WT-CLP mice, *Xid* mice subjected to CLP were protected from developing diastolic dysfunction (Figure 3.6). No difference was observed with the administration of ibrutinib in WT-CLP and *Xid*-CLP they were both attenuated the development of diastolic dysfunction when compared to WT-CLP mice.

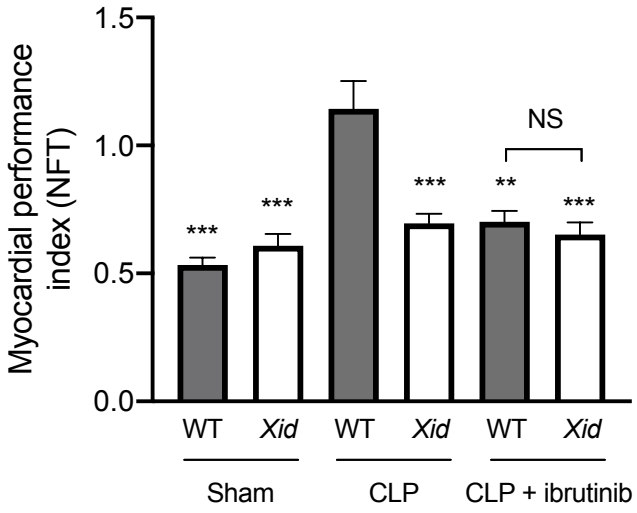

Figure 3.6 *Xid* mice are protected from sepsis-induced diastolic dysfunction. WT and *Xid* mice were randomly selected to undergo sham-operated or CLP surgery, 1 h later ibrutinib (30 mg/kg) was administered intravenously. At 24 h after CLP, cardiac function was assessed by echocardiography**. (A)** Myocardial performance index (NFT). The following groups were studied WT sham (n = 5), *Xid* sham (n = 5), WT-CLP (n = 10), *Xid*-CLP (n = 10), WT-CLP + ibrutinib (n = 8) and *Xid*-CLP + ibrutinib (n = 6). Data are expressed as mean ± SEM and analysed by one-way ANOVA with a Bonferroni post hoc test. $^{**}P < 0.01$, $^{***}P < 0.001$ *versus* WT-CLP.

3.3.4 *Xid* mice are protected from sepsis-induced global cardiac dysfunction

More recently myocardial strain analysis has been shown to be a more direct measurement of intrinsic myocardial contractility, as it measures the amount of deformation that occurs when force is applied. From the original length of the myocardium, a positive strain value describes elongation/thickening of the wall, whereas negative values describe shortening. During contraction, the myocardium shortens longitudinally and circumferential (negative strain) and thickens radially (positive strain). Figure 3.7 A&B depicts the speckle tracking movement of the endocardium, while Figure 3.7 C&D shows representative 3D images of longitudinal and circumferential strain in sham-operated and CLP mice of both genotypes. When compared to sham-operated mice, the myocardium of WT-CLP mice elongates and contracts in both the longitudinal and circumferential direction (contraction observed as blue peaks and elongation observed as red peaks), leading to a reduced negative percentage for global longitudinal strain and global circumferential strain. However, in *Xid*-CLP mice the myocardium only contracts longitudinally and circumferential leading to a global longitudinal strain and global circumferential strain values similar to that of sham-operated animals (Figure 3.7 E&F). Thus, CLP in WT mice leads to global cardiac dysfunction, while *Xid*-CLP mice are protected from developing cardiac dysfunction.

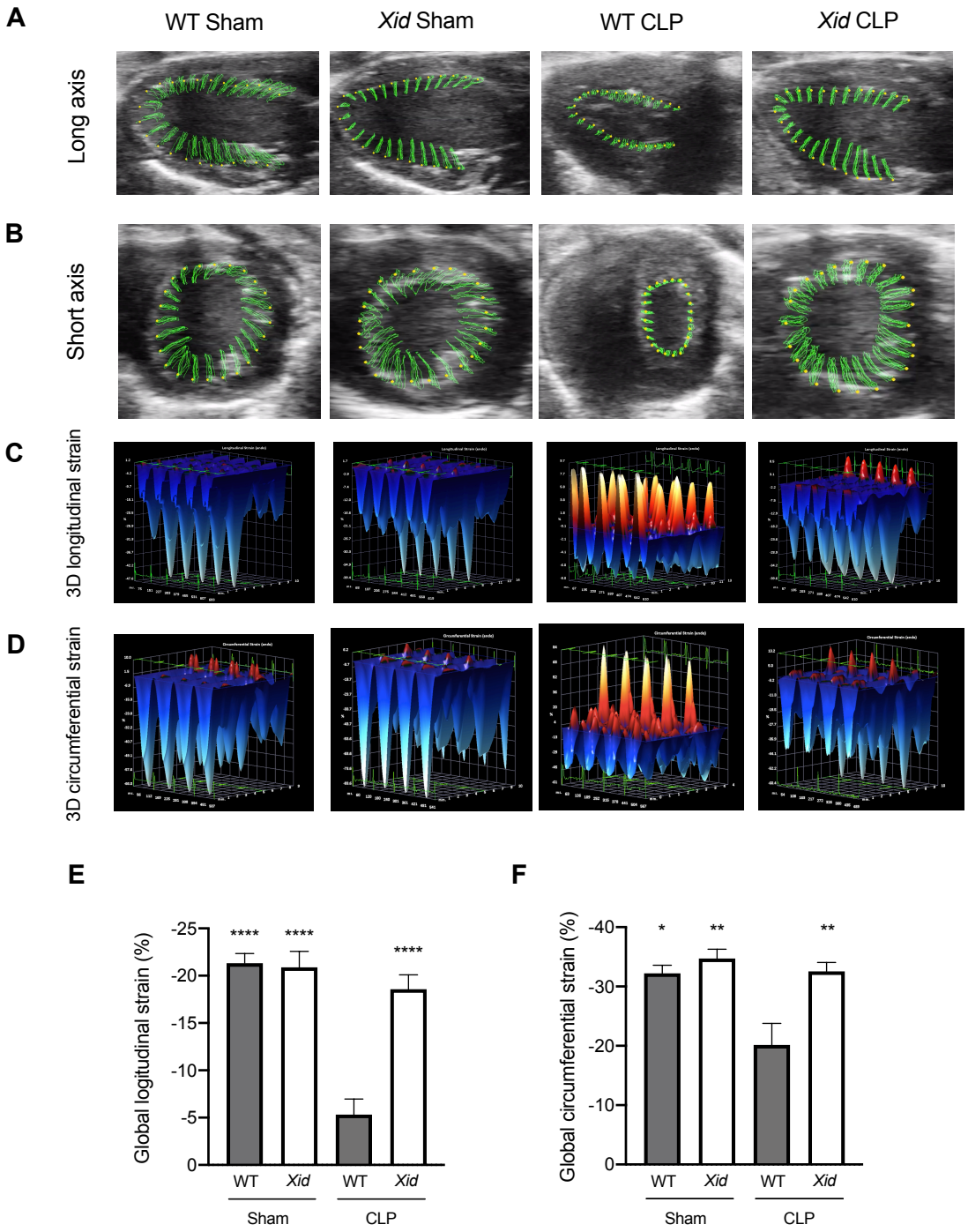

Figure 3.7 *Xid* mice are protected from sepsis-induced global cardiac dysfunction. WT and *Xid* mice were randomly selected to undergo sham-operated or CLP surgery, 24 h later cardiac function was assessed by echocardiography. **(A)** Representative long axis speckle tracking of the endocardium. **(B)** Representative short axis speckle tracking of the endocardium. **(C)** Representative 3D longitudinal strain. **(D)** Representative 3D circumferential strain. **(E)** Global longitudinal strain (%). **(F)** Global circumferential strain (%). The following groups were studied WT sham ($n = 5$), *Xid* sham ($n = 5$), WT-CLP ($n = 10$) and *Xid*-CLP ($n = 10$). Data are expressed as mean ± SEM and analysed by one-way ANOVA with a Bonferroni post hoc test. *$P < 0.05$, **$P < 0.01$ and ****$P < 0.0001$ versus WT-CLP.

3.3.5 *Xid* mice are protected from sepsis-induced renal dysfunction and hepatocellular injury

In sham-operated mice (WT and *Xid*), there was no difference/development of kidney dysfunction, hepatocellular injury or cell injury. When compared to sham-operated mice, WT mice subjected to CLP had significant renal dysfunction (rise in urea and creatinine), hepatocellular injury (rise in ALT and AST) and cell injury (rise in LDH). In contrast, in *Xid* mice subjected to CLP, the degree of kidney dysfunction, hepatocellular injury and cell injury was significantly reduced when compared to WT-CLP mice (Figure 3.8 A-E). When compared to WT-CLP, treatment of WT-CLP mice with ibrutinib (1 h after CLP) significantly attenuated the rise of plasma/serum urea, creatinine, ALT, AST and LDH. In contrast, administration of ibrutinib in *Xid*-CLP-mice had no significant effect on organ dysfunction (as this was prevented in *Xid*-mice). No significant difference was observed between WT-CLP + ibrutinib and *Xid*-CLP + ibrutinib for any of the parameters of organ dysfunction measured.

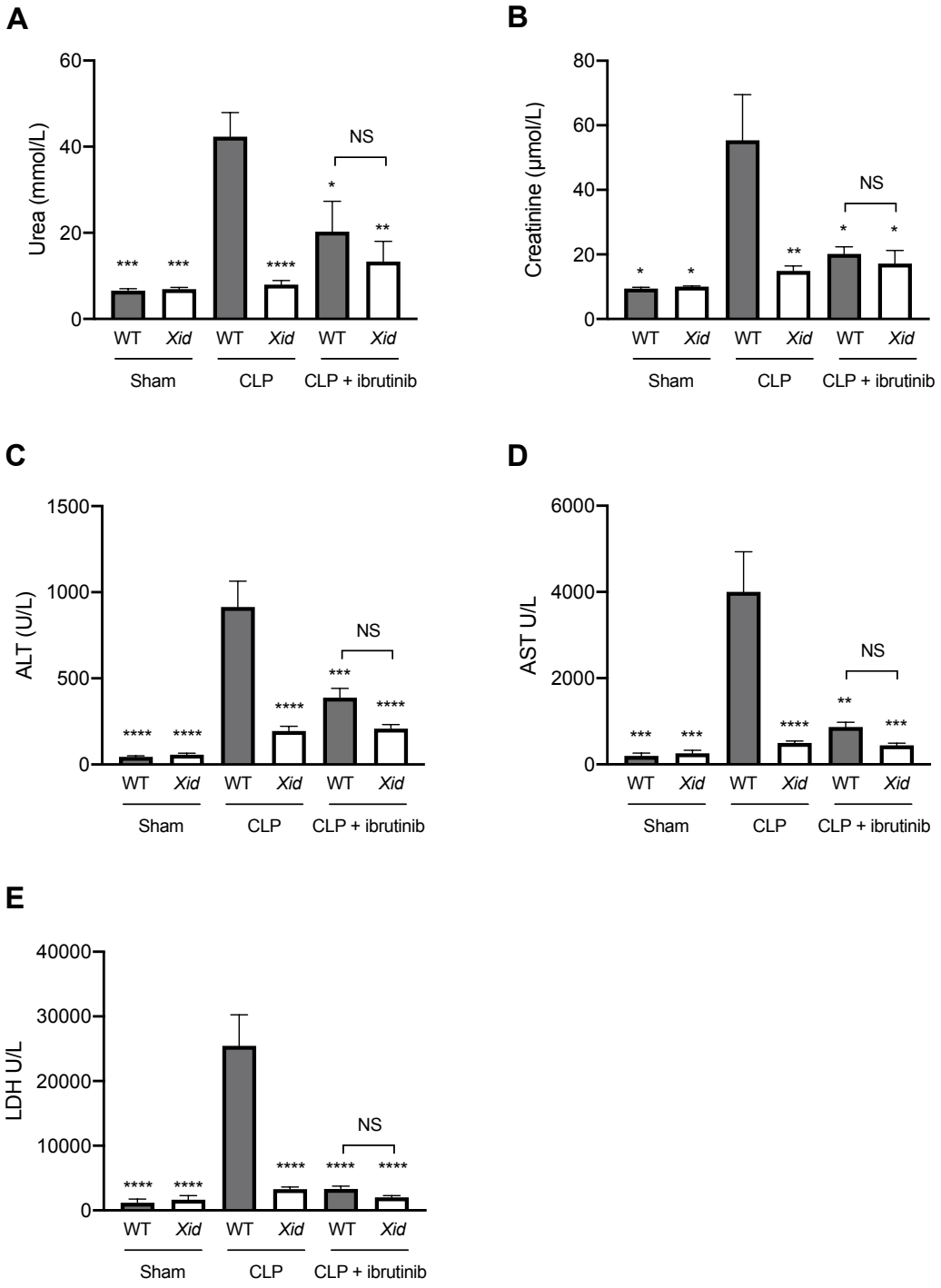

Figure 3.8 *Xid* mice are protected from sepsis induced kidney dysfunction and hepatocellular injury. WT and *Xid* mice were randomly assigned to undergo sham-operated or CLP surgery, 24 h later kidney and liver function parameters were assessed in serum. **(A)** Urea (mmol/L). **(B)** Creatinine (µmol/L). **(C)** ATL (U/L). **(D)** AST (U/L). **(E)** Lactate dehydrogenase (U/L). The following groups were studied WT sham (n = 5), *Xid* sham (n = 5), WT-CLP (n = 10), *Xid*-CLP (n = 10), WT-CLP + ibrutinib (n = 8) and *Xid*-CLP (n = 6). Data are expressed as mean ± SEM and analysed by one-way ANOVA with a Bonferroni post hoc test. *$P < 0.05$, **$P < 0.01$, ***$P < 0.001$ ****$P < 0.0001$ versus WT-CLP.

3.3.6 *Xid* mice do not present with systemic inflammation after polymicrobial sepsis

Using a multiplex array, I analysed 31 cytokines and chemokines in the serum of all animals. When compared to sham-operated mice, WT mice subjected to CLP sepsis showed a significant increase in the serum levels of pro-inflammatory cytokines TNF-α, IL-6 and IL-1β, the anti-inflammatory cytokine IL-10, neutrophils chemoattractant chemokines (KC & ENA-78), monocyte chemoattractant chemokines (MCP-1, MIP-1α and MIP-1β) and G-CSF. In contrast, the levels of these cytokines and chemokines in the serum of *Xid*-CLP, WT-CLP + ibrutinib and *Xid*-CLP + ibrutinib mice were significantly reduced when compared to WT-CLP mice (Figure 3.9 A-I). Interestingly, when compared to WT-CLP, *Xid*-CLP animals resulted in a significant increase in CCL27, IL-2 and CXCL12. The alterations of a further 19 cytokines and chemokines can be seen in Figure 3.9 M and absolute values in in appendix Table S2.

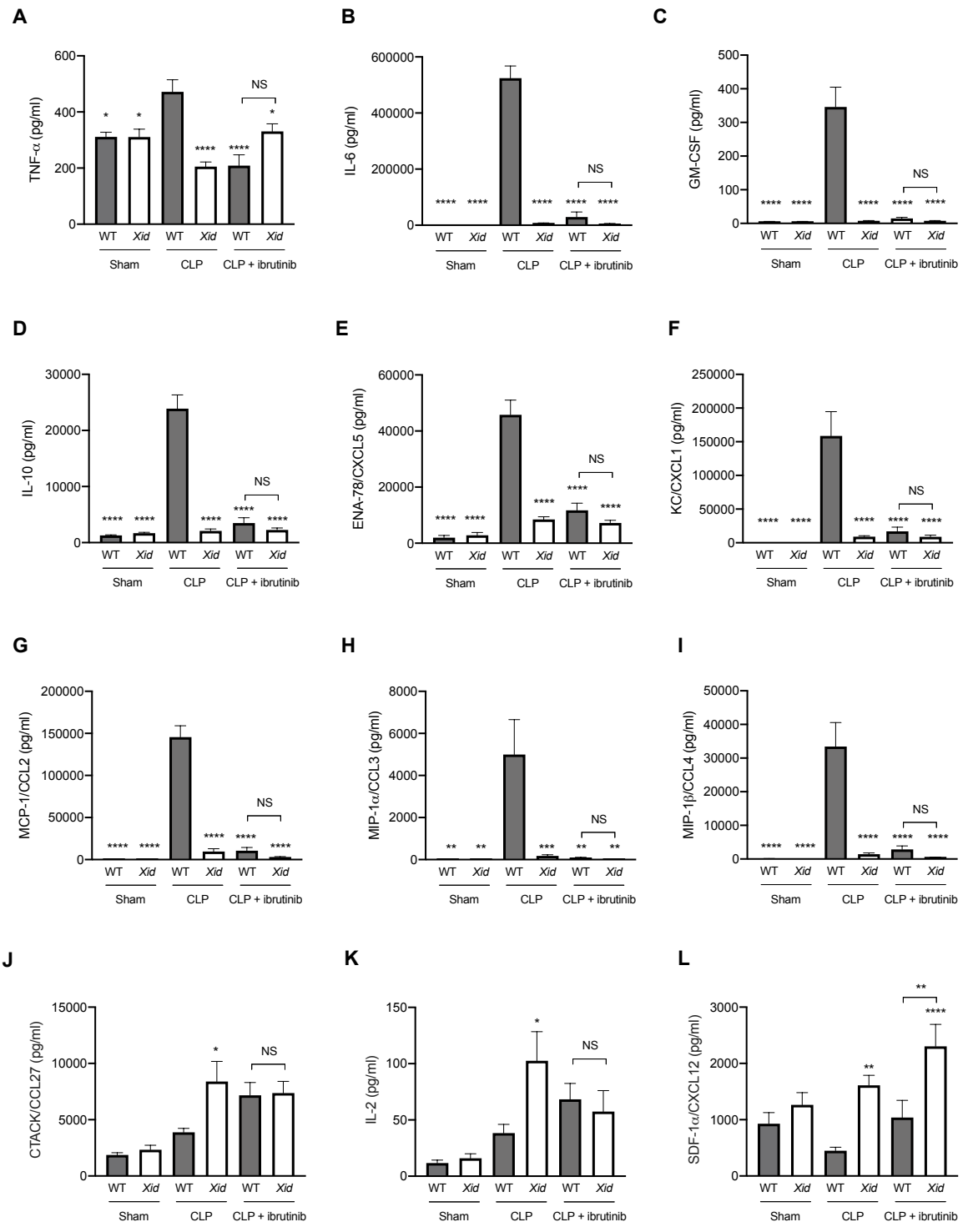
A
TNF-α (pg/ml)
600
400
200
0
NS
*
*
****
****
*
WT Xid WT Xid WT Xid
Sham
CLP
CLP + ibrutinib
B
IL-6 (pg/ml)
600000
400000
200000
0
NS
****
****
****
****
****
C
GM-CSF (pg/ml)
500
400
300
200
100
0
NS
****
****
****
****
****
D
IL-10 (pg/ml)
30000
20000
10000
0
NS
****
****
****
****
****
E
ENA-78/CXCL5 (pg/ml)
60000
40000
20000
0
NS
****
****
****
****
****
F
KC/CXCL1 (pg/ml)
250000
200000
150000
100000
50000
0
NS
****
****
****
****
****
G
MCP-1/CCL2 (pg/ml)
200000
150000
100000
50000
0
NS
****
****
****
****
****
H
MIP-1α/CCL3 (pg/ml)
8000
6000
4000
2000
0
NS
**
**
***
**
**
I
MIP-1β/CCL4 (pg/ml)
50000
40000
30000
20000
10000
0
NS
****
****
****
****
****
J
CTACK/CCL27 (pg/ml)
15000
10000
5000
0
*
NS
K
IL-2 (pg/ml)
150
100
50
0
*
NS
L
SDF-1α/CXCL12 (pg/ml)
3000
2000
1000
0
**
****
**

M

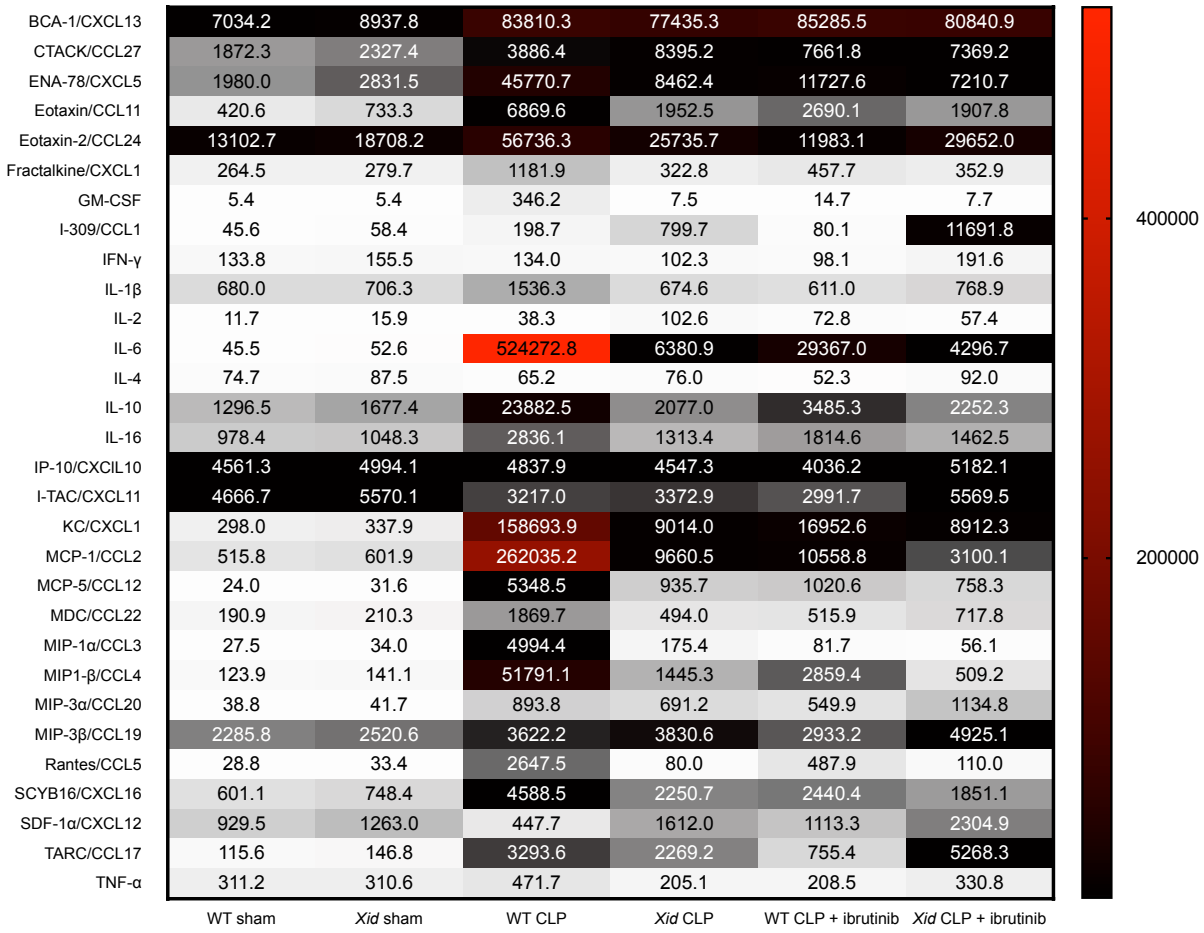

Figure 3.9 *Xid* mice do not present with systemic inflammation after polymicrobial sepsis. WT and *Xid* mice were randomly selected to undergo sham-operated or CLP surgery, 1 h later ibrutinib (30 mg/kg) was administered intravenously. 24 h later cytokines and chemokines were assessed in serum. **(A)** TNF-a serum concentration (pg/mol). **(B)** IL-6 serum concentration (pg/mol). **(C)** GM-CSF serum concentration (pg/mol). **(D)** IL-10 serum concentration (pg/mol). **(E)** ENA-78/CXCL5 serum concentration (pg/mol). **(F)** KC/CXCL1 serum concentration (pg/mol). **(G)** MCP-1/CCL2 serum concentration (pg/mol). **(H)** MIP-1α/CCL3 serum concentration (pg/mol). **(I)** MIP-1β/CCL4 serum concentration (pg/mol). **(J)** CTACK/CCL27 serum concentration (pg/mol). **(K)** IL-2 serum concentration (pg/mol). **(L)** SDF-1α/CXCL12 serum concentration (pg/mol) **(M)** Heatmap of 31 cytokines and chemokines**.** The following groups were studied WT sham (n = 5), *Xid* sham (n = 5), WT-CLP (n = 10), *Xid*-CLP (n = 10), WT-CLP + ibrutinib (n = 8) and *Xid*-CLP (n = 6). Data are expressed as mean ± SEM and analysed by one-way ANOVA with a Bonferroni post hoc test. *P < 0.05, **P < 0.01, ***P < 0.001 ****P < 0.0001 *versus* WT-CLP.

3.3.7 *Xid* mice have fewer infiltrating innate immune cells in the peritoneum and enhanced polarisation to M2 macrophages in sepsis.

I then evaluated the cell composition and phenotype in the peritoneal exudates of all animals by flow cytometry. When compared to sham-operated mice, WT mice subjected to CLP showed a significant increase in the number of neutrophils and macrophages in the peritoneum. In contrast, *Xid*-CLP mice exhibited a significant reduction in the number of infiltrating neutrophils and macrophages when compared to WT-CLP mice (Figure 3.10 A-C). Upon further analysis of the subsets of macrophages, I found that the macrophages obtained from WT-CLP mice are predominately of the pro-inflammatory M1 phenotype (60% M1 and 40% M2), while the macrophages of *Xid*-CLP are of the pro-resolving (anti-inflammatory) M2 phenotype (40% M1 and 60% M2) (Figure 3.10 D-E).

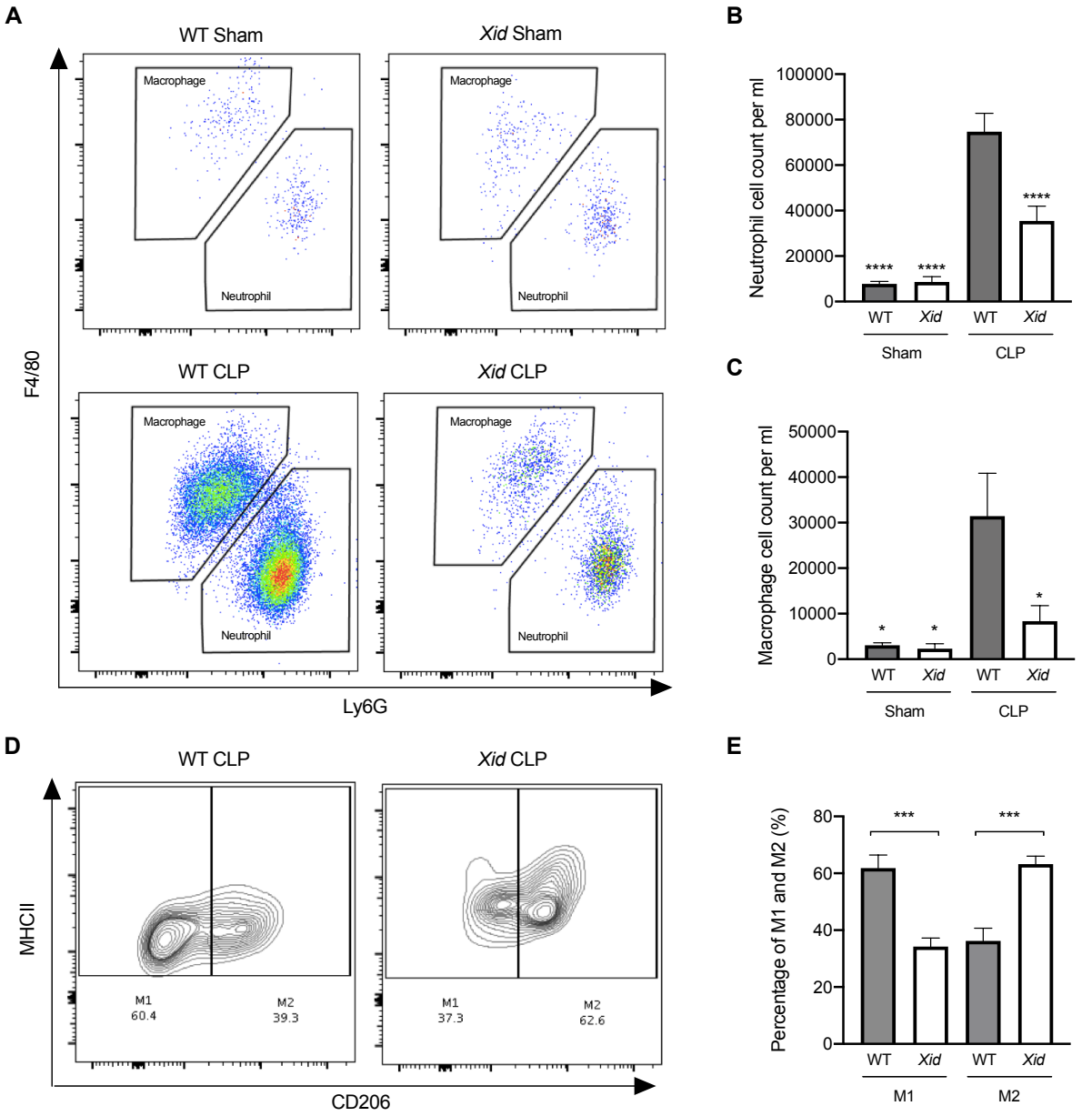

Figure 3.10 *Xid* mice have fewer infiltrating innate immune cells in the peritoneum and enhanced polarisation to M2 macrophages in sepsis. WT and *Xid* mice were randomly assigned to undergo sham-operated or CLP surgery, 24 h later peritoneal lavage fluid was analysed. **(A)** Scattergrams illustrating macrophage (identified as F4/80^{+}Ly6G^{-}) and neutrophils (identified as F4/80^{-}Ly6G^{+}). **(B)** Peritoneal neutrophil (F4/80^{-}Ly6G^{+}) cell count per ml. **(C)** Peritoneal macrophage (F4/80^{+}Ly6G^{-}) cell count per ml. **(D)** Contour plot illustrating percentage of M1 (identified as MHCII^{+}CD206^{-}) and M2 macrophages (identified as MHCII^{+}CD206^{+}). **(E)** Percentage of M1 and M2 macrophages in WT mice and *Xid* mice (%). The following groups were studied WT sham (n = 5), *Xid* sham (n = 5), WT-CLP (n = 10) and *Xid*-CLP (n = 10). Data are expressed as mean ± SEM and analysed by one-way ANOVA with a Bonferroni post hoc test. *P < 0.05, ***P < 0.001 ****P < 0.0001 *versus* WT-CLP.

3.3.8 *Xid* mice have fewer infiltrating adaptive immune cells in the peritoneum

When compared to sham-operated mice, WT mice subjected to CLP resulted in a significant increase in B cells and no significant difference was observed in infiltrating T cells. In contrast, *Xid*-CLP mice exhibited a significant reduction in the number of infiltrating B cells, but no significant difference in the number of infiltrating T cell levels was observed when compared to WT-CLP mice (Figure 3.11 A-C).

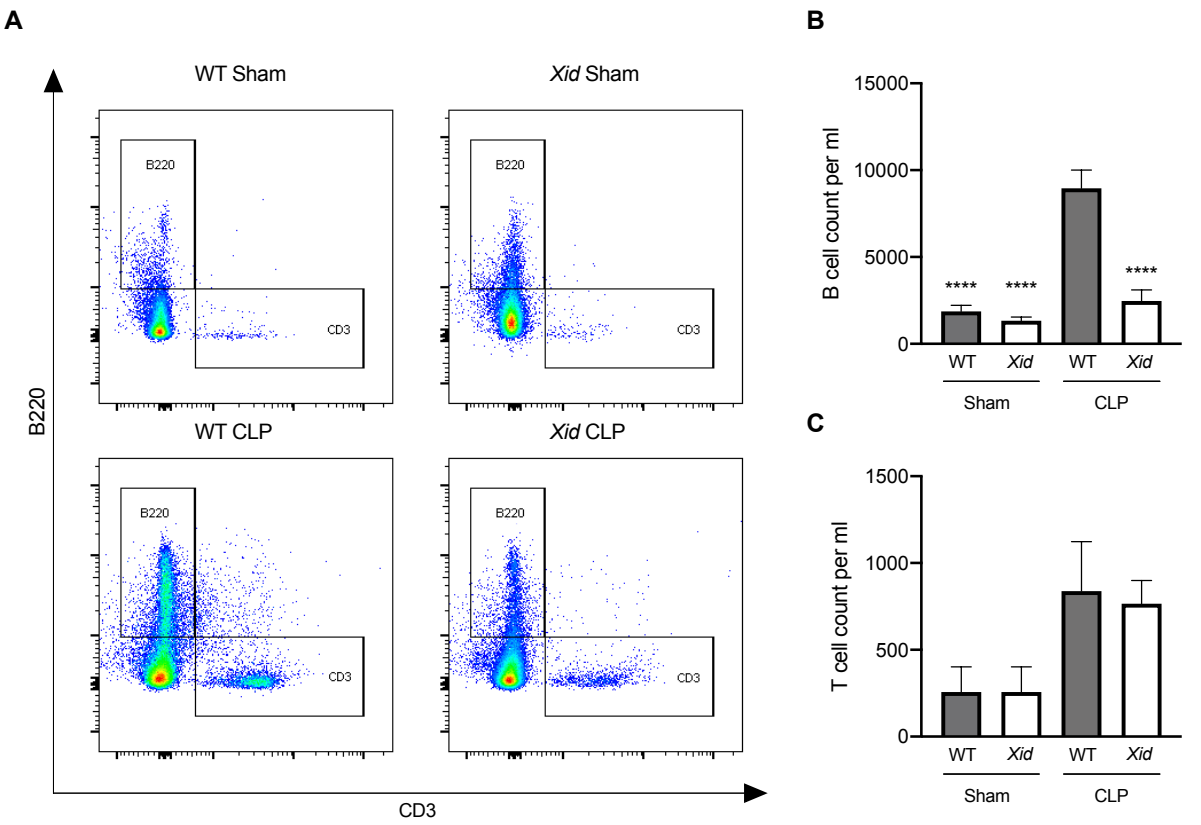

Figure 3.11 *Xid* mice have fewer infiltrating adaptive immune cells in the peritoneum. WT and *Xid* mice were randomly assigned to undergo sham-operated or CLP surgery, 24 h later peritoneal lavage fluid was analysed. **(A)** Scattergrams illustrating T cells (identified as $CD3^{+}B220^{-}$ and B cells (identified as $B220^{+}CD3^{-}$). **(B)** Peritoneal B cell count per ml. **(C)** Peritoneal T cell count per ml. The following groups were studied WT sham ($n = 5$), *Xid* sham ($n = 5$), WT-CLP ($n = 10$) and *Xid*-CLP ($n = 10$). Data are expressed as mean ± SEM and analysed by one-way ANOVA with a Bonferroni post hoc test. ****$P < 0.0001$ *versus* WT-CLP.

3.3.9 *Xid* mice have fewer bacteria in peritoneum and blood

The survival of sepsis relies on the body's ability to remove bacteria from the site of infection; thus, I analysed the levels of bacteria in the peritoneal cavity (site of infection) and whole blood by flow cytometry 24 h after CLP. WT and *Xid* mice subjected to sham operation demonstrated no difference in the levels of bacteria. When compared to sham-operated mice, WT mice subjected to CLP exhibited elevated peritoneal and blood bacteria counts (Figure 3.12 A-D). However, *Xid*-CLP mice had significantly fewer bacteria in the peritoneal cavity and blood than WT-CLP mice, showing that *Xid*-mice clear bacteria more efficiently than WT mice (Figure 3.12 A-D).

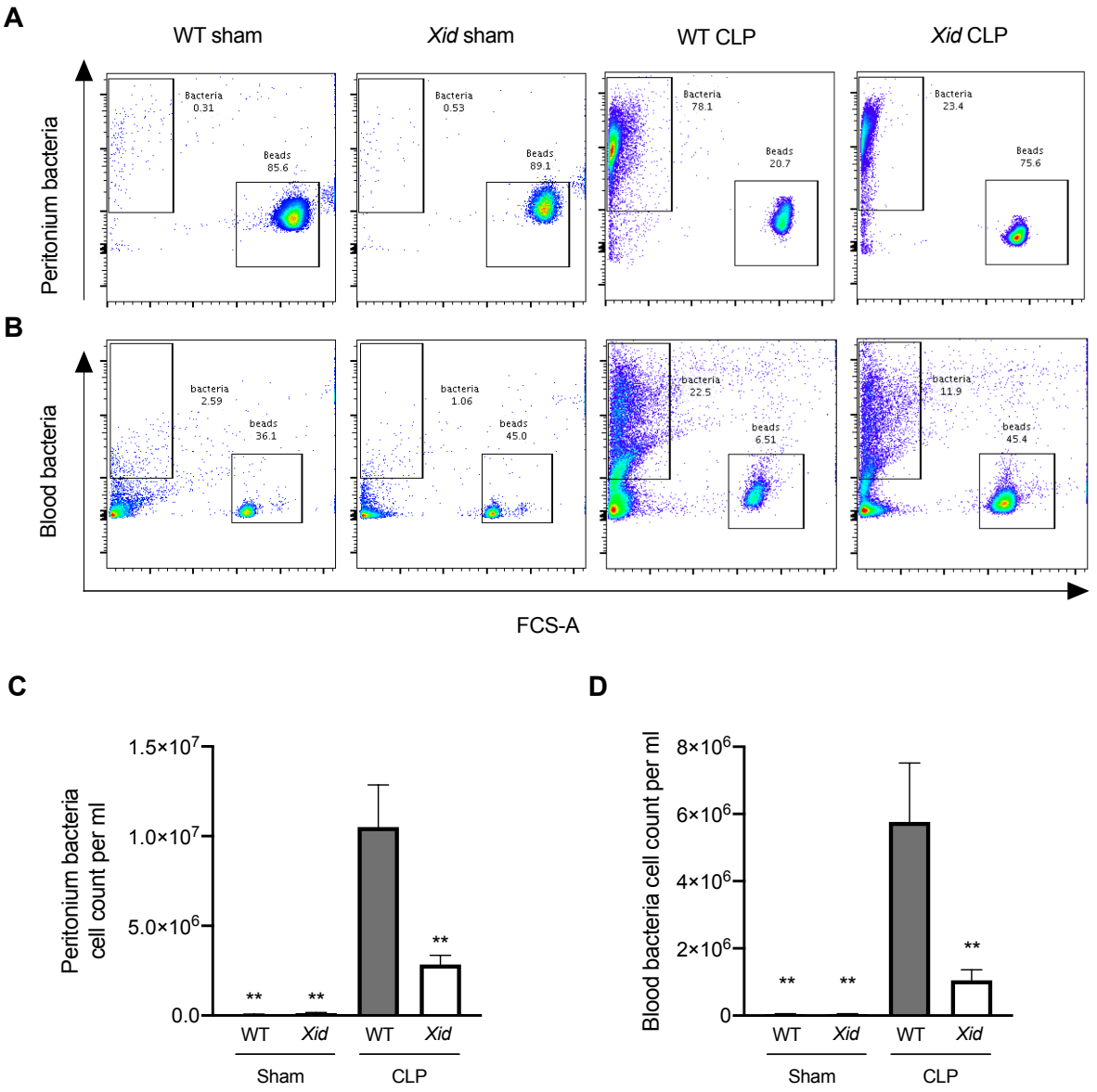

Figure 3.12 *Xid* mice have fewer bacteria in peritoneum and blood. WT and *Xid* mice were randomly assigned to undergo sham-operated or CLP surgery, 24 h later peritoneal lavage fluid and blood was analysed. **(A)** Representative images of bacteria in the peritoneal cavity. **(B)** Representative images of bacteria in whole blood. **(C)** Peritoneal bacteria cell count per ml. **(D)** Blood bacteria cell count per ml. The following groups were studied WT sham (n = 5), *Xid* sham (n = 5), WT-CLP (n = 10), *Xid*-CLP (n = 10), All data are expressed as mean ± SEM for n number of observations. A value of $^{**}P < 0.01$, was considered to be statistically significant when compared to WT-CLP by one-way ANOVA followed by a Bonferroni's post hoc test.

3.3.10 *Xid* macrophages and neutrophils have increased phagocytotic ability

Clearance of bacteria is secondary to phagocytosis of bacteria by neutrophils and macrophages. *Xid* mice subjected to CLP presented with a reduced number of infiltrating immune cells but also reduced bacterial cell counts at 24 h post CLP. This raises the question as to how fewer infiltrating immune cells are able to clear more bacteria? To address this question, I investigated whether *Xid* neutrophils and macrophages have increased phagocytic ability *in vivo*. I found that the percentage of neutrophils and macrophages, which are phagocytosing bacteria, are similar in WT-CLP and *Xid*-CLP mice. However, neutrophils and macrophages of *Xid*-CLP mice contain more bacteria per immune cell than WT-CLP mice, showing a 100% increase in the phagocytic ability of both macrophages (Figure 3.13 A-D) and neutrophils (Figure 3.14 A-D). Collectively, this data clearly demonstrates that *Xid* mice with a deficiency in BTK show enhanced phagocytosis *in vivo* resulting in improved clearance of bacteria during a septic episode.

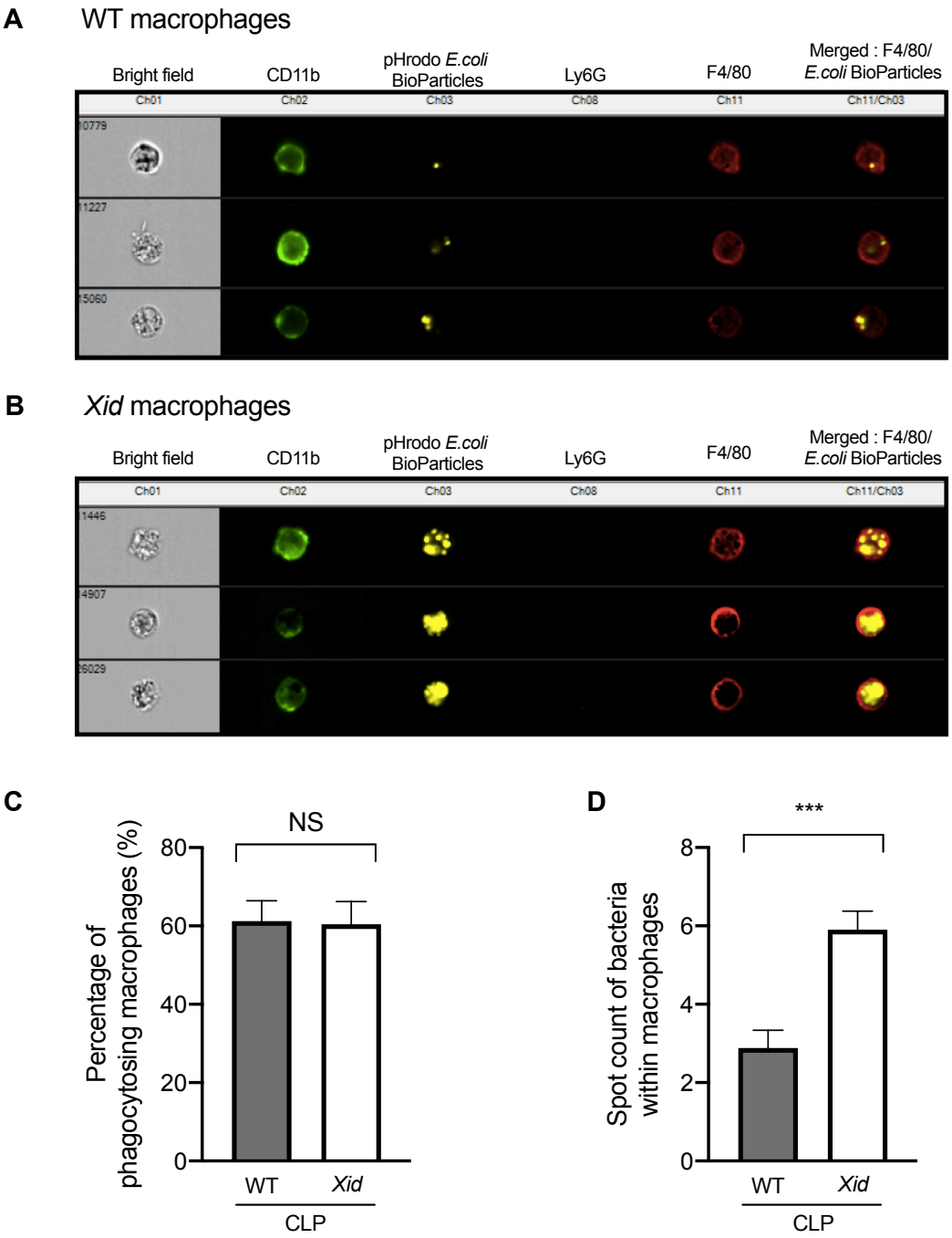

Figure 3.13 *Xid* macrophages have increased phagocytic ability. WT and *Xid* mice were randomly assigned to undergo sham-operated or CLP surgery, 24 h later peritoneal lavage fluid was analysed. **(A)** Representative images of WT-CLP macrophages phagocytosis on the imagestream. **(B)** Representative images of *Xid*-CLP macrophages phagocytosis on the imagestream. **(C)** Percentage of macrophages that phagocytose (%). **(D)** Average number of bacteria within macrophages. The following groups were studied WT-CLP (n = 8) and *Xid*-CLP (n = 8). Data are expressed as mean ± SEM and analysed by a students unpaired T-test. ***$P < 0.001$ versus WT-CLP.

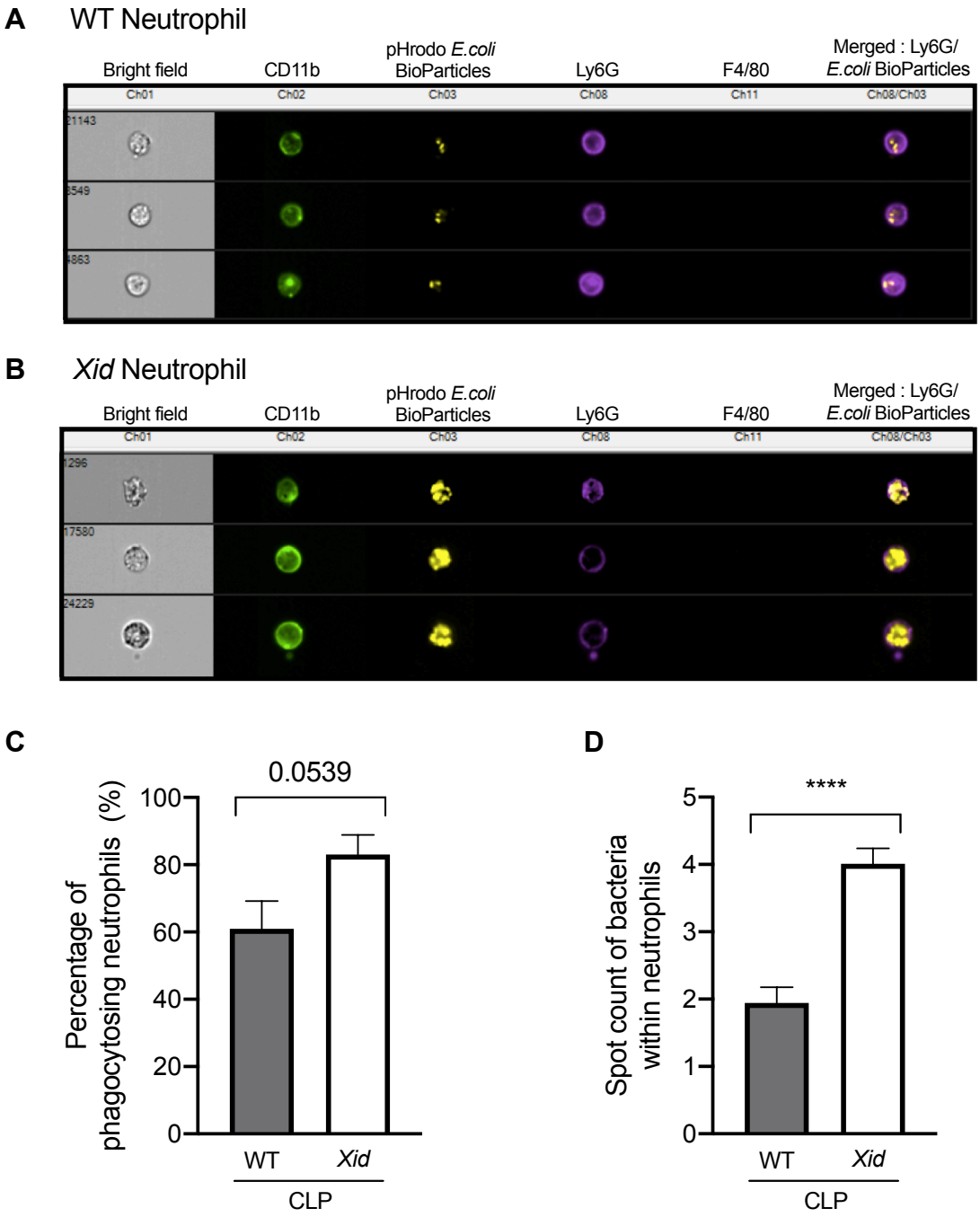

Figure 3.14 *Xid* neutrophils have increased phagocytic ability. WT and *Xid* mice were randomly assigned to undergo sham-operated or CLP surgery, 24 h later peritoneal lavage fluid was analysed. **(A)** Representative images of WT-CLP neutrophils phagocytosis on the imagestream. **(B)** Representative images of *Xid*-CLP neutrophils phagocytosis on the imagestream. **(C)** Percentage of macrophages that phagocytose (%). **(D)** Average number of bacteria within neutrophils. The following groups were studied WT-CLP (n = 8) and *Xid*-CLP (n = 8). Data are expressed as mean ± SEM and analysed by students unpaired T-test.. ****$P < 0.0001$ versus WT-CLP.

3.3.11 Cardiac BTK is not activated in *Xid* mice after polymicrobial sepsis

To understand the signalling mechanism(s) associated with the observed cardiac dysfunction in CLP-sepsis, I investigated the effect of BTK deficiency in *Xid* mice on the activation of key signalling pathways of inflammation: BTK, NF-κB and NLRP3 inflammasome activation. When compared to sham-operated mice, WT mice subjected to CLP showed an increase of BTK activation as demonstrated by significant increases in the phosphorylation of cardiac BTK at Tyr^{223} and the phosphorylation of PLCγ at Tyr^{1217}. No activation of BTK was detected in *Xid* mice subjected to CLP and the phosphorylation of cardiac BTK at Tyr^{223} and the phosphorylation of PLCγ at Tyr^{1217} in *Xid*-CLP mice were similar to that of sham-operated animals (Figure 3.15 A-B).

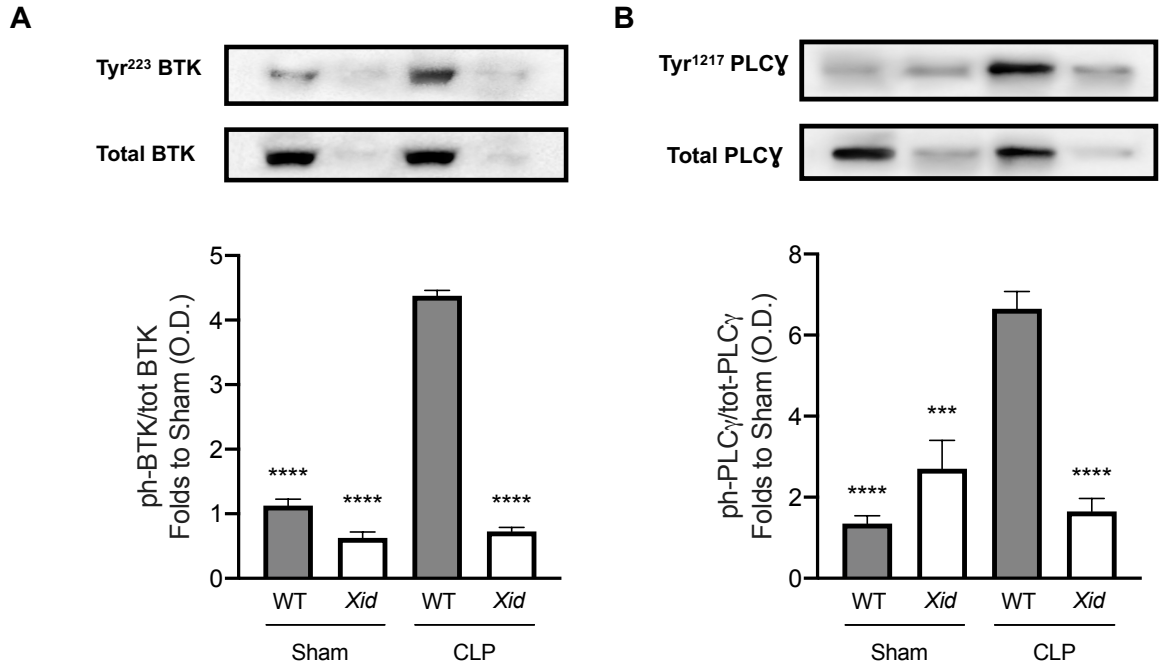

Figure 3.15 BTK is not activated in the heart of *Xid* mice after polymicrobial sepsis. WT and *Xid* mice were randomly assigned to undergo sham-operated or CLP surgery and 24 h later signalling events in the cardiac tissue were assessed. Densitometric analysis of the bands is expressed as relative optical density (O.D.) of **(A)** phosphorylation of BTK at Tyr^{223} corrected for the corresponding total BTK and normalized using the related sham bands. **(B)** Phosphorylation of PLCγ at Tyr^{1217} corrected for the corresponding total PLCγ and normalised using the related sham bands. The following groups were studied WT sham, *Xid* sham, WT-CLP and *Xid*-CLP, $n = 4$ per group. Data are expressed as mean ± SEM and analysed by one-way ANOVA with a Bonferroni post hoc test. $^{***}P < 0.001$ $^{****}P < 0.0001$ *versus* WT-CLP.

3.3.12 Cardiac NF-κB is not activated in *Xid* mice after polymicrobial sepsis

NF-κB activation plays a key role in the pathophysiology of sepsis. When compared to sham-operated mice, WT-CLP mice exhibit a significant increase in NF-κB activation as demonstrated by significant increases in the phosphorylation of IKKα/β at $Ser^{176/180}$ and the phosphorylation of IκBα at $Ser^{32/36}$. When compared to WT-CLP mice, *Xid*-CLP mice the phosphorylation of IKKα/β at $Ser^{176/180}$ and IκBα at $Ser^{32/36}$ was significantly reduced, indicating that the degree of activation of NF-κB caused by sepsis in the heart was significantly lower in *Xid*-mice than in WT-mice (Figure 3.16 C-D).

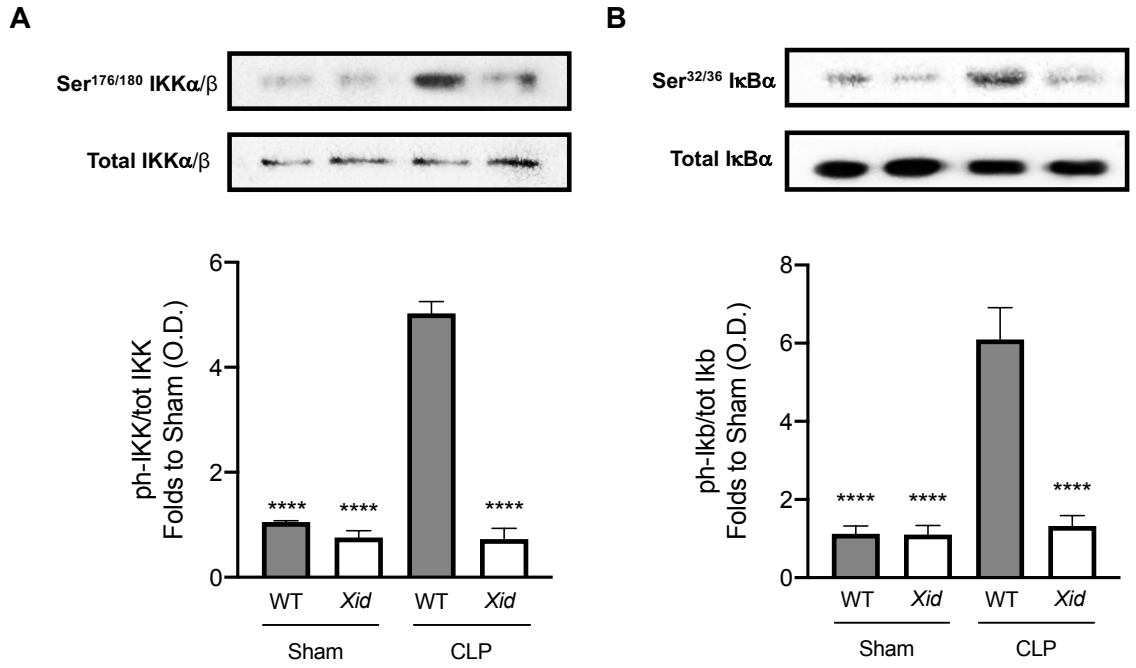

Figure 3.16 Cardiac NF-κB is not activated in *Xid* mice after polymicrobial sepsis. WT and *Xid* mice were randomly assigned to undergo sham-operated or CLP surgery and 24 h later signalling events in the cardiac tissue were assessed. Densitometric analysis of the bands is expressed as relative optical density (O.D.) of **(A)** Phosphorylation of IKKα/β at $Ser^{176/180}$ corrected for the corresponding total IKKα/β and normalised using the sham related bands. **(B)** Phosphorylation of IκBα at $Ser^{32/36}$ corrected for the corresponding total IκBα and normalised using the related sham band. The following groups were studied WT sham, *Xid* sham, WT-CLP and *Xid*-CLP, $n = 4$ per group. Data are expressed as mean ± SEM and analysed by one-way ANOVA with a Bonferroni post hoc test. ****$P < 0.0001$ *versus* WT-CLP.

3.3.13 The NLRP3 inflammasome is not activated in the heart of *Xid* mice after polymicrobial sepsis.

When compared to sham-operated mice, WT mice subjected to CLP showed an increase in the activation of the NLRP3 inflammasome, demonstrated by an increase in the expression of the NLRP3 inflammasome and cleavage of pro-caspase-1 to caspase-1 in the heart as well as an increase in the production of IL-1β in serum (Figure 3.17 A-C). In contrast, *Xid*-CLP mice showed reduced activation of NLRP3 inflammasome as demonstrated by a decrease in the expression of the NLRP3 inflammasome, cleavage of pro-caspase-1 to caspase-1 and IL-1β, when compared to WT-CLP mice (Figure 3.17 A-C).

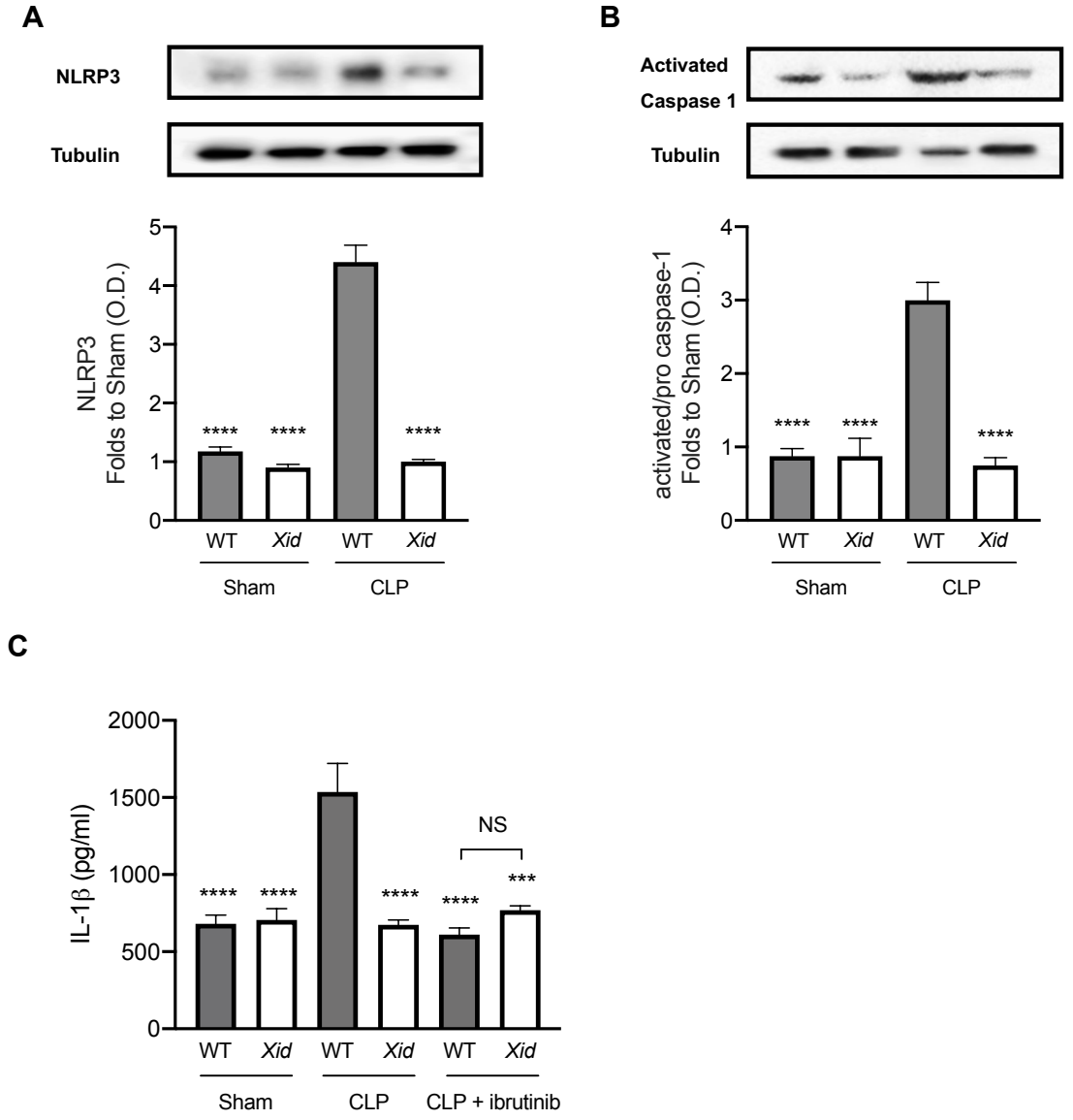

Figure 3.17 The NLRP3 inflammasome is not activated in the heart of *Xid* mice after polymicrobial sepsis. WT and *Xid* mice were randomly assigned to undergo sham-operated or CLP surgery and 24 h later signalling events in the cardiac tissue were assessed. Densitometric analysis of the bands is expressed as relative optical density (O.D.) of **(A)** NLRP3 activation, corrected against tubulin and normalized using the sham related bands. **(B)** Pro-caspase-1 against activated caspase-1 and normalized using the sham related bands. **(C)** Serum IL-1β (pg/ml). The following groups were studied WT sham, *Xid* sham, WT-CLP and *Xid*-CLP, $n = 4$ per group. Data are expressed as mean ± SEM and analysed by one-way ANOVA with a Bonferroni post hoc test. ***$P < 0.001$ ****$P < 0.0001$ *versus* WT-CLP.

3.4 Discussion

Sepsis is the overwhelming host response to infection (bacterial, fungal or viral) leading to shock and multiple organ dysfunction. I have previously reported that BTK inhibitors (ibrutinib, acalabrutinib) significantly attenuate sepsis-induced cardiac dysfunction, but BTK inhibitors have many off-target effects (255). In the present chapter, I investigated whether the beneficial effects are exclusively due to inhibition of BTK and whether a reduction in systemic inflammation due to BTK inhibition effects bacterial clearance. I addressed these questions by conducting a model of polymicrobial sepsis in *Xid* mice (which have a missense mutation in the BTK gene, resulting in BTK to be functionally impaired). I report here for the first time that *Xid* mice are protected from sepsis-induced multiple organ dysfunction (cardiac, renal and hepatocellular) due to increased bacterial clearance and suppression of systemic inflammation (cytokine storm).

It has been reported that a reduction in temperature <30^{o}C or a change of temperature of 5^{o}C over time predicts mortality in animals with sepsis (221). Using this more humane surrogate marker, I found that *Xid* mice with sepsis have a predicted mortality of 0% (100% survival), while WT-mice with sepsis would have a predicted mortality of 90% (10% survival). I found that ibrutinib does not affect predicted mortality in *Xid*-CLP mice resulting in a predicted mortality of 0% (100% survival) and that delayed administration of ibrutinib in WT-CLP mice led to a predicated mortality of 15% (85% survival). It would be useful to confirm the impact of impairment in BTK function in *Xid*-mice on outcome (mortality) in a more long-term sepsis model.

Sepsis results in multiple organ failure including cardiac dysfunction, renal dysfunction and hepatocellular injury. I report here for the first time that *Xid* mice subjected to sepsis are protected from developing cardiac dysfunction, hepatocellular injury and renal dysfunction. Most notably, ibrutinib significantly reduced sepsis-induced multiple organ failure in WT-mice but had no further beneficial effect in *Xid*-mice subjected to CLP-indicating that the observed beneficial effect of ibrutinib in WT-mice can solely be explained by inhibition of BTK-activity. I have reported in chapter 2 that inhibition of BTK by ibrutinib or acalabrutinib attenuated sepsis-induced cardiac and renal dysfunction in C57Bl/6 mice (255) and additionally I have now shown that delayed administration of ibrutinib in WT-CLP (CBA background) also

attenuates sepsis-induced cardiac dysfunction, renal dysfunction and hepatocellular injury, confirming that BTK inhibitors work in two different genetic backgrounds of mice. Furthermore, in this chapter, I report that administration of ibrutinib (which inhibits a significant number of kinases in addition to BTK, more than acalabrutinib) in *Xid*-CLP mice does neither result in further beneficial effects nor any adverse effects on cardiac, renal or liver (dys)function. Inhibition of BTK has been reported to protect against sepsis-induced lung injury (256,257), attenuates liver damage in a model of warm ischaemia and reperfusion (258) and also ameliorates kidney disease in spontaneous lupus nephritis (259). Thus, I here provide evidence that inhibition of BTK alone is sufficient to prevent sepsis-induced multiple organ injury.

Ejection fraction is commonly used as a marker for cardiac function and can be used to detect relatively large changes in cardiac function. Due to the advances in cardiac imaging (speckle tracking analysis) (260), one can now also detect much more subtle changes in cardiac function and are able to diagnose heart failure with preserved EF specifically by focusing on the global longitudinal strain (261). Hoffman *et al*. found that myocardial strain is a preferable measure for monitoring cardiovascular function in murine sepsis mouse models, as it detects cardiac dysfunction earlier and more reliably than EF (224). In WT (CBA background) mice subjected to CLP-sepsis, I observed (within 24 h of the onset of sepsis) a severe, global cardiac dysfunction with significant changes in EF and cardiac strain (longitudinal and circumferential). In contrast, when *Xid* mice were subjected to CLP-sepsis, I found no significant reduction in EF and also no change in the more sensitive and reliable strain analysis, showing conclusively that inactivation of BTK in *Xid*-mice prevents the development of sepsis-induced cardiac dysfunction.

I then investigated the mechanism(s) by which inactivation of BTK protects mice against sepsis-induced multiple organ failure. In septic patients, an essential treatment is early source control (removal of infection), which is associated with improved outcomes (44). I found that CLP in *Xid* mice results in a reduction of the number of bacteria in both peritoneum and blood (at 24 h after onset of CLP) when compared to WT-CLP mice. This may well be due to an increase in phagocytosis in *Xid* mice. Macrophages obtained from *Xid*-mice do, however, not show defects in phagocytosis (262,263) and I found that the percentage of phagocytosing cells are similar in both WT and *Xid* mice. I discovered, however, that macrophages obtained from

Xid-mice with sepsis had taken up a significantly larger number of bacteria. This was also true for neutrophils from *Xid*-mice. I believe that the increase in phagocytosis by macrophages and neutrophils from *Xid*-mice could explain the observed increase in the clearance of bacteria in peritoneum and blood. Beguem *et al*. found that monocytes from healthy volunteers stimulated with LPS and treated with evobrutinib resulted in an increased rate of phagocytosis *in vitro* due to a switch of macrophages from the pro-inflammatory M1 to the pro-resolving M2 phenotype and this was associated with reduced secretion of TNF-α (264). In addition, *Xid* mice infected with *F. tularensis* showed enhanced bacterial clearance from the lung and spleen, which correlated with a significant improvement of survival when compared to wild-type controls (265).

This raises the question of the underlying mechanisms that enables or drives increased phagocytosis in *Xid*-mice? Neither inhibition of BTK activity with ibrutinib nor inactivation of BTK in *Xid* mice affects monocyte FcγR-mediated phagocytosis, but it does suppress FcγR-mediated cytokine production. The decrease of calcium flux due to BTK inhibition also does not affect phagocytosis but does decrease cytokine production (262). BTK inhibition results in the polarisation to M2 macrophages (which have greater phagocytic ability (266)), demonstrated by increased expression of CD206. CD206 is involved in phagocytosis of a number of bacterial strains. For example, monocyte-derived macrophages that express high levels of CD206 phagocytosed 78% of *E.coli*, while monocyte-derived macrophages that express low levels of CD206 only phagocytosed 30% of *E.coli* (267). Excessive activation of neutrophils is known to decrease survival and enhance susceptibility to subsequent bacterial infections (268). One mechanism that may contribute to the pathology of sepsis is the release of neutrophil extracellular traps as they contain the beneficial antimicrobial nuclear proteins but also damaging citrullinated histones, elastase, myeloperoxidase and MMP-3 (269,270). The release of neutrophil extracellular traps results in ineffective phagocytosis (271). Florence *et al*. showed that BTK was increased in the lung neutrophils and inhibiting BTK protected mice against lethal influenza by reducing the release of neutrophil extracellular traps. The decrease of neutrophil extracellular traps was also observed in human peripheral blood neutrophils incubated with influenza and BTK inhibitor (257). However, the exact molecular mechanisms underlying this phenomenon are yet to be elucidated. Future studies are required to increase our understanding as to how *Xid* macrophages and neutrophils phagocytose more bacteria per immune cell.

BTK plays a fundamental role in signalling and function of B cells, but BTK is also highly expressed in myeloid cells such as macrophages and neutrophils (155) and inactivation of BTK results in reduced cell-mediated inflammatory responses (272,273). I report here that *Xid*-CLP mice have reduced infiltrating innate immune cells (macrophages and neutrophils) in the peritoneum (site of infection). I propose that this may lead to a reduction of the formation of cytokines/chemokines in the serum and, hence, will prevent the cytokines storm.

Macrophages play an important role in the two phases of sepsis (early pro-inflammatory phase and the later anti-inflammatory phase), as they can have either pro-inflammatory or anti-inflammatory properties. Initially, M1 macrophages (pro-inflammatory) activate inflammation by secreting TNF-α, IL-1β, IL-6 and IL-12 to promote the removal of the pathogen, then M2 macrophages repair tissue and resolve inflammation by secreting cytokines including IL-10 (274,275). If the M1 macrophage-driven pro-inflammatory response cannot be controlled, the resultant cytokine storm can be a key driver of the severity of sepsis leading to organ failure and death (276). Inhibition of BTK drives the switch from the pro-inflammatory M1 phenotype to pro-resolving M2 phenotype in response to LPS (243). Here I report that macrophages obtained from septic *Xid*-mice have a pro-resolving M2 phenotype, whereas macrophages obtained from septic WT-mice have the M1 phenotype. Most notably, macrophages of the M2 phenotype have a greater phagocytotic function resulting in increased clearance of apoptotic cells and acceleration of resolution (266). Indeed, M2 macrophages protect against sepsis-induced lung injury (277) and sepsis-induced acute kidney injury (278). Transplantation of M2 macrophages has been suggested as a potential therapeutic approach for sepsis-induced lung injury (277).

Xid mice have a reduced number of B cells and BTK is not expressed in T cells. I report here that *Xid*-CLP mice show a decrease in the number of B cells, but not in T cells when compared to WT-CLP mice. The potential contribution of B and T cells to the pathophysiology of early sepsis is controversial. Kelly-Scumpia *et al*. set out to report how suppression of the adaptive immune response affects the early innate immune responses. They reported that $Rag^{-/-}$ deficient mice (which have no mature B and T cells) have reduced survival in sepsis (CLP surgery). Additionally, they found that B-cell deficient mice, but not T-cell deficient mice had a reduced

survival in sepsis and that the 'treatment' of $RAG^{-/-}$ and B-cell deficient mice with B cells improved survival in sepsis, suggesting that B cells, but not T cells, play an important role in the pathophysiology of sepsis (279). Contradictory to these results, Bossman *et al*. found that the survival of $Rag^{-/-}$ subjected to CLP was similar to that of WT-mice (280). In addition, neonatal $Rag^{-/-}$ mice subjected to sepsis (caecal slurry) did not have higher mortality than WT mice (281). T cells have been shown to be protective (282), detrimental (283,284) or do not contribute to the severity of sepsis (285,286). Characteristic of sepsis-induced immunosuppression are reductions in CD4+ T cells and a shift from T_{H1} to T_{H2} phenotype (287), and it has been proposed that stopping this shift increases survival in septic patients (288).

BTK plays a pivotal role in the activation of TLRs and, hence, the signalling steps leading to the activation of NF-κB (239), which plays a key role in the pathophysiology of septic cardiomyopathy (289). Here I report that *Xid* mice subjected to polymicrobial sepsis have reduced activation of BTK and NF-κB (measured as phosphorylation of IKKα/β and IκBα) in the heart. I have previously reported that BTK inhibitors ibrutinib or acalabrutinib reduce the activation of cardiac BTK and NF-κB in mice subjected to sepsis (255). Furthermore, it has been shown that inhibition of NF-κB activation with an inhibitor of IKK also attenuates the cardiac dysfunction associated with polymicrobial sepsis (289). Purvis *et al*. showed that ibrutinib treatment attenuated the activation of NF-κB and gene expression of cytokines in the diabetic kidney and liver (273). Thus, I propose that an impairment in the activation of BTK in *Xid* mice leads to reduced activation of NF-κB in the heart, which contributes to or accounts for the observed reduction in organ injury and dysfunction observed in *Xid*-mice with sepsis.

Activation of NF-κB leads to an increase in the production of cytokines and chemokines such as the pro-inflammatory cytokines TNF-α, IL-6, IL-1β and the anti-inflammatory cytokine IL-10, neutrophils chemoattractant chemokines (KC & ENA-78), monocyte chemoattractant chemokines (MCP-1, MIP-1α and MIP-1β) and G-CSF, all of which contribute to the systemic inflammation and organ dysfunction associated with sepsis (244). Out of all these cytokines, the ones increased most in our model of murine sepsis were IL-6, KC and MCP-1. The levels of IL-8 and monocyte chemoattractant protein-1 (MCP-1) are associated with early 48-h and 28-day mortality in sepsis patients (290). Most notably, I report that in *Xid*-mice subjected to CLP-sepsis, all of these cytokines and chemokines are markedly reduced. WT-CLP treated with ibrutinib also reduces the production of sepsis-associated cytokines and chemokines and

no difference is observed with the addition of ibrutinib to *Xid*-CLP mice. Thus, an impairment of BTK activation in *Xid*-mice prevents NF-κB-dependent, systemic inflammation (cytokine storm) resulting in a reduction in organ injury/dysfunction.

BTK is also involved in the assembly/activation of the NLRP3 inflammasome in both mice and humans (166,167). The activation of the NLRP3 inflammasome also plays a role in the pathophysiology of sepsis and septic cardiomyopathy (291). Pharmacological inhibition of NLRP3 activation with MCC950 (NLRP3 inflammasome inhibitor) reduced the neurological and cognitive impairment in septic animals (250). It has also been reported that genetic deficiency of NLRP3 promotes resolution of inflammation in polymicrobial sepsis (105). I report here that the activation of the NLRP3 inflammasome (measured as NLRP3 activation, caspase-1 activation and production of IL-1β release) was largely reduced in *Xid*-mice subjected to CLP when compared to WT-mice with sepsis. I previously reported that BTK inhibitors (ibrutinib or acalabrutinib) inhibit the activation of the NLRP3 inflammasome in the heart and production of IL-1β in septic animals (255). Purvis *et al*. showed that ibrutinib treatment attenuated the activation NLRP3 inflammasome in the diabetic kidney and liver (273). Thus, I propose that prevention of the activation of the NLRP3 inflammasome secondary to reduced activation of BTK importantly contributes to the reduction in inflammation and organ dysfunction observed in septic *Xid*-mice.

I have shown that *Xid*-mice subjected to CLP have increased bacterial clearance and reduced systemic inflammation (secondary to reduced activation of the NLRP3 inflammasome and NF-κB) and cardiac (organ) dysfunction. There is good evidence that the mortality of patients with sepsis increases with an increase in the number of organs failing (SOFA scores).

3.4.1 Conclusion

I report here for the first time that inactivation of BTK is responsible for conferring protection against multiple organ failure in a clinically relevant model of sepsis. Most importantly I have shown that the inactivation of BTK in *Xid* mice results in an increase of phagocytosis in macrophages and neutrophils, thus, increasing bacterial clearance in both peritoneum and blood. Inactivation of BTK also results in a phenotypic switch of macrophages from M1 to the M2 phenotype, which aids in the resolution of sepsis. The suppression of the immune system

by inactivated BTK also leads to reduced activation of NF-κB and the NLRP3 inflammasome, therefore, preventing the induction of the cytokine storm. As the administration of ibrutinib to *Xid*-CLP mice did not result in any additional (beneficial) effects on the alterations in organ dysfunction and cytokine/chemokines formation caused by sepsis, our data strongly suggest that BTK inactivation is responsible for the observed effects of ibrutinib. Lastly, I have found that BTK expression in humans is increased in the blood of septic non-survivors. Thus, BTK inhibitors may be repurposed for the use in sepsis (or other conditions associated with excessive local or systemic inflammation including COVID-19) due to their ability to reduce systemic inflammation (cytokine storm), their ability to enhance the phagocytosis of neutrophils/macrophages and switch macrophages from the pro-inflammatory M1 to the anti-inflammatory M2 phenotype.

Chapter 4 Ribonuclease 1 attenuates sepsis-induced cardiac dysfunction

4.1 Introduction

Septic research has mainly focused on PAMPs interacting with PRRs, leading to the activation of NF-κB and thus the production of pro-inflammatory cytokines and chemokines. However, DAMPs also contribute to the pathogenesis of sepsis by activating PRRs and their subsequent inflammatory signalling pathways (292), for example the release of eRNA from dying cells binds to and activates the TLR3 signalling pathway leading to activation of NF-κB and production of pro-inflammatory cytokines and chemokines (Figure 4.1). Clinically the severity of sepsis has been shown to correlate with increased levels of DAMPs, such as high mobility group box-1 protein (HMGB1) (293), cold-inducible RNA-binding protein (CIRP) (294) and histone (295). DAMPs are host nuclear or cytoplasmic non-microbial molecules (296) and are released from tissue injury, specifically from cells through inflammasome activation or passively following cell death (297). However, little is known about the role of eRNA in sepsis-induced cardiac dysfunction. eRNA is a term used to describe several types of RNA (microRNA, transfer RNA, small interfering RNA and long non-coding RNA), which are diverse in function but share a common attribute of being found in the extracellular environment (298).

Cardiac apoptosis is a programmed cell death caused by intrinsic or extrinsic signalling pathway (as previously described in section 1.6.5) and contributes to the pathophysiology of cardiac dysfunction. It is unknown whether intrinsic factors such as eRNA play a role in the activation of septic cardiac apoptosis.

eRNA is modulated by endogenous RNase. RNase 1 is an antimicrobial peptide which is expressed in all tissues and bodily fluids and contributes to the immune system by degrading pathogenic RNA and eRNA (released from tissue injury and necrosis) (Figure 4.1) (193). RNase 1 is regulated by RNH1 (which is induced by oxidative stress (299)), thus increased levels of RNH1 negatively affects the antimicrobial ability of RNase. Here I hypothesis that administration of RNase may attenuate sepsis-induced organ dysfunction in a model of polymicrobial sepsis.

The roles of RNase, RNH1 and eRNA in the pathophysiology of sepsis still require further research. In this chapter I set out to investigate whether:

1) RNase 1 administration attenuates sepsis-induced multiple organ failure (cardiac, renal and liver dysfunction).
2) The effect of RNase 1 administration in septic mice on the production of sepsis associated cytokines and chemokines.
3) RNase 1 reduces the levels of bacteria in the peritoneal cavity of septic mice
4) Cardiac apoptosis is involved in the pathophysiology of septic mice and whether RNase 1 administration reduces the level of cardiac apoptosis.
5) RNase 1 levels in serum of septic mice over a 24 h time course.
6) At 24 h in septic mice measure the levels of RNase 1, eRNA and RNH1 in serum.

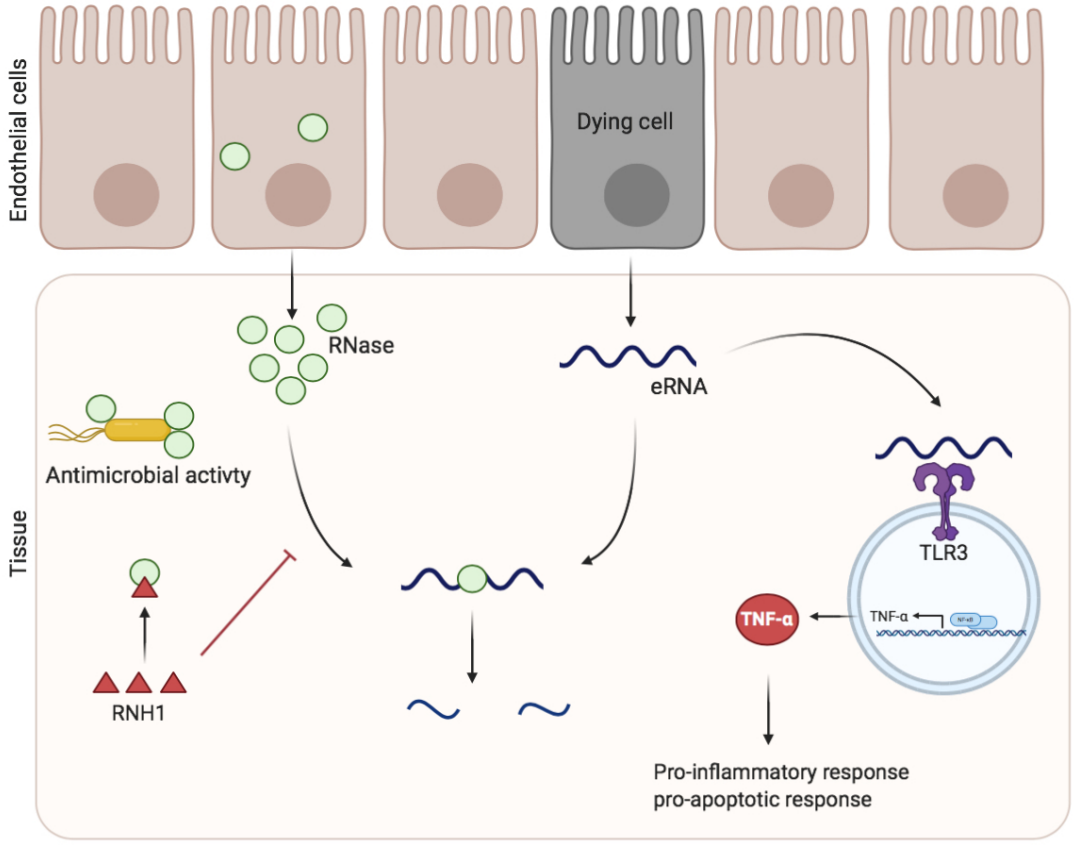

Figure 4.1 Schematic diagram of RNase activity. RNase is released from the endothelial cells and eRNA is released from dying/necrotic cells. eRNA binds to TLR3 resulting in the production of pro-inflammatory cytokines such as TNF-α, which activates the pro-apoptotic response. RNase degrades eRNA but is inhibited by RNH1. RNase also has antimicrobial activity.

4.2 Methods

4.2.1 Animals

This study was carried out on forty-one 10-week-old, male C57BL/6 mice (Charles River Laboratories UK Ltd., Kent, UK), weighing 25–30 g and kept under standard laboratory conditions. The animals were allowed to acclimatise to laboratory conditions for at least one week before undergoing experiments. Six mice were housed together (in each cage) with access to a chow diet and water *ad libitum*. They were subjected to a 12-h light and dark cycle with a temperature maintained at 19–23°C. The cages were cleaned regularly approximately every three days, with water being changed daily. Research staff inspected the animals each day for any signs of illness or abnormal behaviour.

4.2.2 Caecal ligation and puncture (CLP) surgery

Caecal ligation and puncture (CLP) surgery was performed in 10-week-old male C57Bl/6 mice (Table 4.1) as previously described in chapter 2. The mice were randomly assigned to under CLP or sham-operated surgery. Briefly, mice were anaesthetised with isoflurane (2% delivered in O_2) and the caecum was fully ligated below the ileocaecal valve. A double puncture was made with an 18-G needle into the caecum and a small amount of faeces was squeezed out after which the caecum was returned to its anatomical position, then the laparotomy was closed. All animals received fluids (5 ml/kg saline into the abdomen before closure and 10 ml/kg saline s.c., immediately after surgery). At 6 and 18 h after surgery all animals received antibiotics (Imipenem/Cilastatin; 20 mg/kg dissolved in 7.5 ml/kg of saline s.c.), and analgesics (buprenorphine; 0.05 mg/kg i.p.). Sham-operated mice underwent the same procedure, but without CLP. RNase 1 or its vehicle was administrated before sepsis induction (50 µg/kg RNase 1 or 0.9% NaCl, i.v.), directly after surgery (200 µg/100 µL RNase 1 or 100 µL 0.9% NaCl, s.c.), and again 4 h after surgery (500 µg/100 µL RNase 1 or 100 µL 0.9% NaCl, s.c.). The surgeon was blinded to which group received the treatment or the vehicle. At the end of the study, mice were sacrificed, peritoneal lavage fluid and organs were collected under sterile conditions, and blood was withdrawn by cardiac puncture.

A clinical score for monitoring the health of experimental mice was used to evaluate the symptoms consistent with murine sepsis. The maximum score of 6 comprised the presence of the following signs: lethargy, piloerection, tremors, periorbital exudates, respiratory distress, and diarrhoea. Mice with a clinical score >3 were defined as exhibiting severe sepsis, against a moderate sepsis score of ≤3. Animals were culled at 24 h after the onset of sepsis (CLP).

Table 4.1 Experimental groups used to investigate the treatment of RNase 1 in CLP-induced cardiac dysfunction.

Strain	Group	Total number
C57BL/6 10 weeks	Sham + vehicle	12
	Sham + RNase	5
	CLP + vehicle	12
	CLP + RNase	12

4.2.3 Assessment of cardiac function *in vivo*

At 24 h post CLP, mice were anaesthetised (0.5 - 2% isoflurane in O_2); body temperature was maintained at 37°C and heart rate was maintained at 450 bpm. Then, cardiac function was assessed by M-mode and B-mode echocardiography using the VisualSonics Vevo 3100 echocardiographic system and an MX550D transducer as previously described in section 2.2.9. The following parameters were measured: left ventricular EF, FS, FAC, CO, SV, ESV and EDV.

4.2.4 Quantification of renal dysfunction, hepatocellular injury and cell injury

After 24 h, mice were sacrificed by terminal cardiac puncture, where terminal blood samples were immediately decanted into 1.3 ml serum gel tubes (Sarstedt, Nürnbrecht, Germany). Blood was left to coagulate for at least 10 min at room temperature, then samples were centrifuged at 9000 rpm for 3 min to separate the serum. Then 100 µl of serum was snap-frozen in liquid nitrogen and sent to an independent veterinary testing laboratory (MRC Harwell Institute, Oxford, UK) to evaluate the following biomarkers in a blinded fashion: Urea and creatinine (as markers of renal dysfunction), alanine aminotransferase (ALT) and aspartate transaminase (AST) (markers of hepatocellular injury).

4.2.5 Cytokine analysis

Cytokines, chemokines and a growth factor were determined in serum by Bio-Plex Pro Mouse Chemokine 33-Plex panel assay (Bio-Rad, Kabelsketal, Germany) as previously described in chapter 2. The cytokines IL-1ß, –2, –4, –6, –10, –16, CCL1, –2, –3, –4, –5, –7, –11, –12, –17, –19, –20, –22, –24, –27, IFN-γ, TNF-α and the chemokines CX3CL1, CXCL1, –2, –5, –10, –11, –12, –13, –16 and the growth factor GM-CSF.

4.2.6 Peritoneal lavage

Mice were euthanised by an overdose of isoflurane inhalation. Once confirmed dead peritoneal cells were obtained by injecting 5 ml of 2mM EDTA + PBS -/- using a 25-G needle. Cells attached were dislodged by gentle massage of the peritoneum and collected by using an 18-G needle. Approximately 4 ml of the peritoneal fluid was obtained and decanted into 15 ml falcon tubes on ice.

4.2.7 Bacteria quantification

Accurate evaluation of the number of bacteria in peritoneal lavage fluid was performed by flow cytometry using the SYTO BC bacteria counting kit (Thermo Fischer Scientific) as previously described in chapter 2.

4.2.8 Western blots

Immunoblot analyses of cardiac tissue samples were carried out using a semi-quantitative western blotting analysis. The antibody used were caspase-9 (C9) mouse (catalog 9508), Bcl-2 (D17C4) rabbit (catalog 3498), caspase-3 rabbit (catalog 9662), and Bax (D3R2M) rabbit (catalog 14796) all from cell signalling. The apex of the heart was taken and homogenized in homogenisation buffer 20 mM HEPES, pH 7.9, 1 mM $MgCl_2$, 0.5 mM EDTA, 1% Nonidet P-40, 1 mM EGTA, 1 mM DTT, 0.5 mM PMSF, 1 µL/mL PIC). Proteins were then extracted as previously described above and concentrations were quantified by bicinchoninic acid (BCA) protein assay (Thermo Fisher Scientific Rockford, IL). Proteins were separated by 8% sodium dodecyl sulphate (SDS)-PAGE and transferred to polyvinylidene fluoride membranes.

Membranes were blocked for 1 h in blocking buffer (10% BSA in TBS containing 0.1% Tween) and then incubated with the primary antibody diluted in 5% BSA in TBS containing 0.1% Tween overnight at 4°C. The next day the membrane was washed 3 times and the membrane was incubated for 30 min with the HRP-conjugated secondary antibody at room temperature. Protein bands were detected with enhanced chemiluminescent (ECL) detection system. The immunoreactive bands were visualized by autoradiography and the densitometric analysis was performed using Gel Pro Analyzer 4.5, 2000 software (Media Cybernetics). Results were normalized by using Tubulin as an endogenous control.

4.2.9 TUNEL assay

Hearts were washed with saline and placed in formalin for 24 h after which they were transferred to 70% ethanol and embedded in paraffin. Tissue sections were cut at 5 µm. Paraffin was dewaxed by a series of alcohol: Xylene (2 x 5 min), 100% ethanol (5 min), 95% ethanol (5 min), 90% ethanol (5 min), 80% ethanol (5 min), 70% ethanol (5 min) and PBS (2 x 5 min). Slides were then incubated with 0.1 M citrate buffer (pH 6.0) for 5 min at 350W. Slides were allowed to cool for at least 1 h. Slides were washed twice with PBS and the area around the sample was dried. After which 50 µL of TUNEL reaction mixture was added to each sample (In Situ Cell Death Detection Kit TMR red (Roche)) and incubated for 1 h at 37°C in the dark. Slides were then rinsed three times with PBS and covered with ProLong Gold. An LSM 710 confocal microscope (Zeiss) and ImageJ software were used to detect and quantify apoptotic cells.

4.2.10 ELISA

The levels of the RNH1 and RNase 1 in mice serum were determined using a commercial ELISA kit (LifeSpan BioSciences). The ELISAs do not distinguish between bound RNase 1 and unbound RNase 1 with RNH1. Then 100 µL of standard, blank and sample were administered into the 96 plate well in duplicate and incubated for 1 h at 37°C. Excess liquid was aspirated and 100 µL of detection reagent A was added to each well and incubated for 1 h at 37°C. Excess liquid was aspirated and washed 3 times by adding 350 µL of 1 x wash buffer to each well. 100 µL of detection reagent B was added to each well and incubated for 30 min at 37°C. After 30 min excess liquid was aspirated off and washed 5 times. 90 µL of TMB

substrate was added to each well and incubated for 15 min at 37°C in the dark. 50 µL of stop solution was then added. Optical density was immediately evaluated by a microplate reader set at 450 nm.

4.2.11 Statistical analysis

Statistical differences were determined using a one-way ANOVA, followed by Bonferroni post hoc test or unpaired Student's t-test as appropriate (GraphPad Prism 8.0; significant when $P < 0.05$). Results are expressed as mean ± SEM where *n* represents the number of animals studied.

4.3 Results

4.3.1 Physiological measurements of mice 24 h after surgery

Mice that underwent sham-operated surgery and treated with either vehicle or RNase resulted in a severity score at 24 h of 0, demonstrating that they experienced no symptoms of sepsis. When compared to sham-operated mice, WT mice which underwent CLP demonstrated clinical signs of sepsis. When compared to CLP mice treated with vehicle, CLP mice that received RNase 1 all had a severity score of < 3 indicating moderate sepsis. (Figure 4.2 A). When compared to sham-operated mice, mice subjected to CLP and treated with vehicle showed a decrease in heart rate, whereas the heart rate of CLP mice which received RNase 1 remained similar to that of sham-operated animals (Figure 4.2 B). There was no difference in body temperature between sham-operated mice which received vehicle or RNase 1, as the temperature remained at the normal physiological range of 37°C. When compared to sham-operated animals, mice subjected for 24 h to CLP and treated with vehicle demonstrated a significant decrease in temperature < 30°C, indicating the development of sepsis-induced hypothermia. When compared to CLP mice treated with vehicle, CLP mice that received RNase 1 were protected from developing hypothermia (Figure 4.2 C). Using the mortality surrogate marker of a reduction in temperature <30°C or a change of 5°C over time I find that both sham-operated mice had a predicted mortality of 0%. In contrast, the predicted mortality of CLP mice is 67%, confirming that this is a severe model of sepsis. Mice subjected to CLP and treated with RNase have a predicted mortality of 17% (Figure 4.2 D).

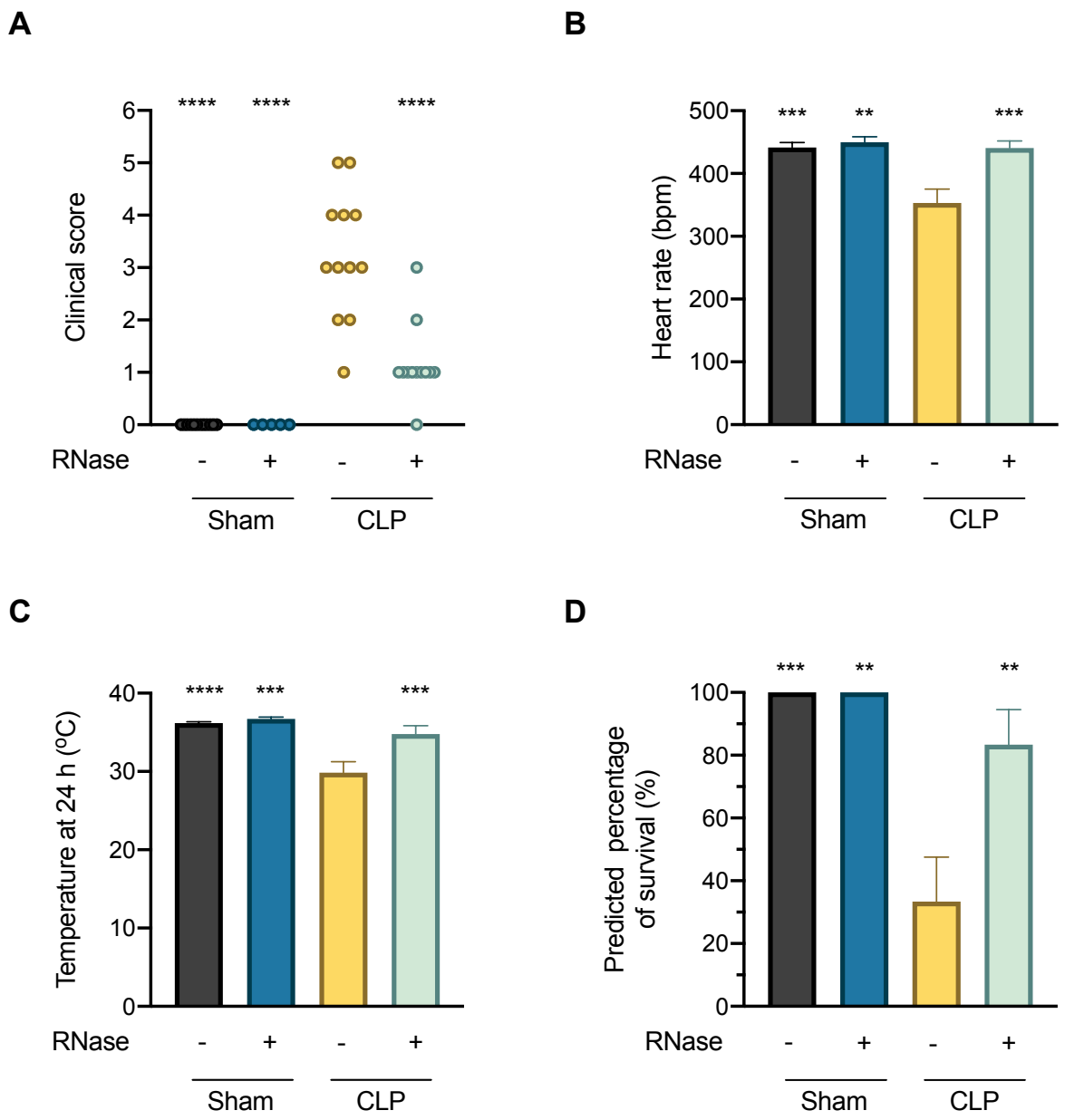

Figure 4.2 Physiological measurements of mice 24 h after surgery. Mice were randomly selected to undergo sham-operated or CLP surgery and received either RNase 1 or vehicle (saline). At 24 h after CLP, physiological measurements of the mice were assessed. **(A)** Severity Score 24 h after CLP. **(B)** Heart rate 24 h after CLP (bmp). **(C)** Temperature 24 h after CLP (°C). **(D)** Predicted percentage of survival (%). The following groups were studied sham + vehicle (n = 12), sham + RNase (n = 5), CLP + vehicle (n = 12), CLP + RNase (n = 12). All data are expressed as mean ± SEM for n number of observations. A value of ****P < 0.0001, *** P < 0.001 and **P < 0.01 was considered to be statistically significant when compared to CLP + vehicle by one-way ANOVA followed by a Bonferroni's post hoc test.

4.3.2 RNase 1 attenuates sepsis-induced cardiac dysfunction

When compared to sham-operated animals, mice subjected for 24 h to CLP and treated with vehicle demonstrated a significant reduction in percentage EF, FS, FAC, SV, CO (Figure 4.3 A-F) and an increase in ESV, indicating the development of systolic, cardiac dysfunction. When compared to CLP-mice treated with vehicle, administration of RNase 1 in CLP-mice significantly attenuated the decline in EF, FS, FAC, SV, CO and the increase in ESV caused by CLP (Figure 4.3 A-F). No significant differences in EDV were observed between all groups. There was no difference between sham-operated mice which received vehicle or RNase 1.

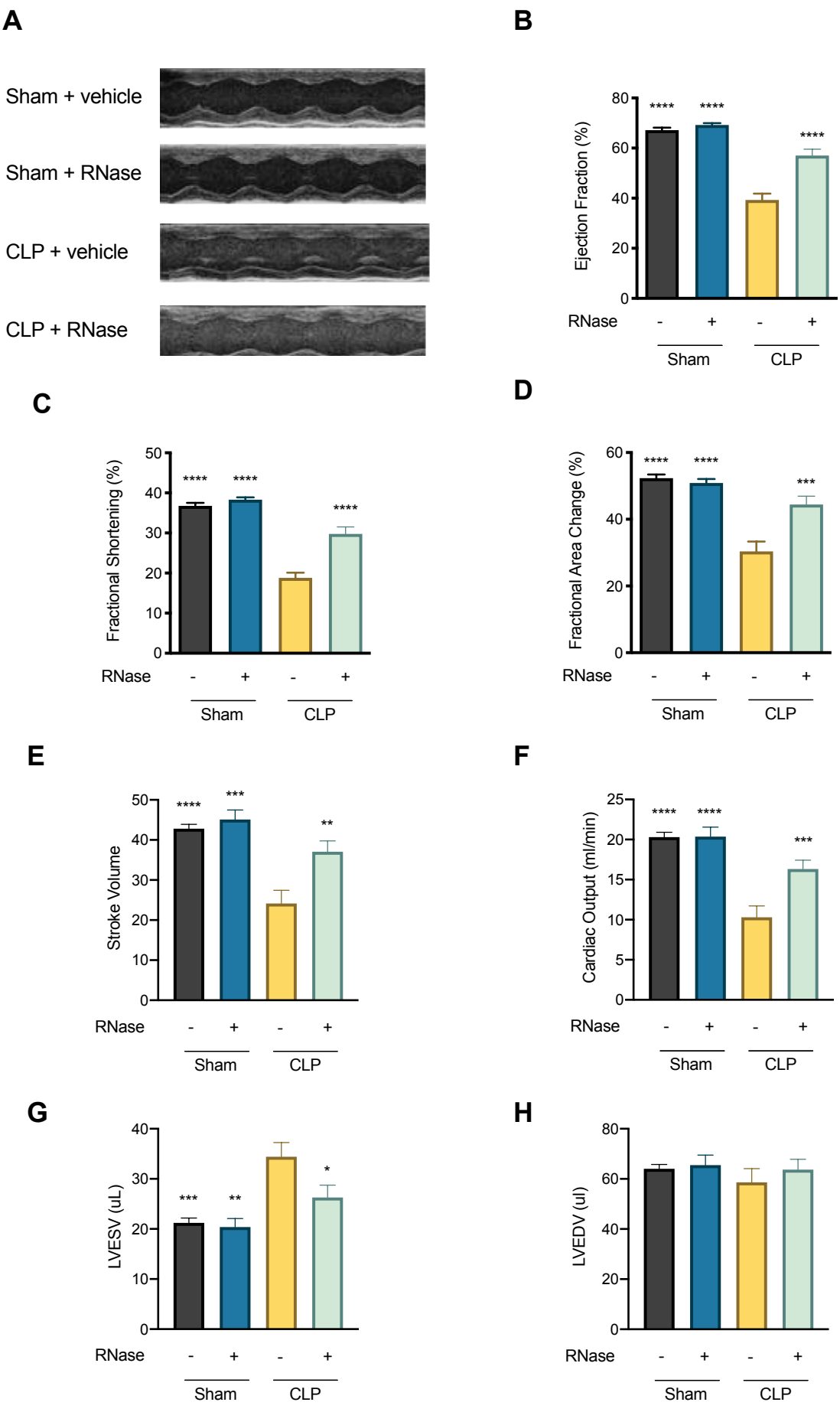
A
Sham + vehicle
Sham + RNase
CLP + vehicle
CLP + RNase
B
Ejection Fraction (%)
80
60
40
20
0
****
****
****
RNase
-
+
-
+
Sham
CLP
C
Fractional Shortening (%)
50
40
30
20
10
0
****
****
****
RNase
-
+
-
+
Sham
CLP
D
Fractional Area Change (%)
60
40
20
0
****
****
***
RNase
-
+
-
+
Sham
CLP
E
Stroke Volume
50
40
30
20
10
0
****
***
**
RNase
-
+
-
+
Sham
CLP
F
Cardiac Output (ml/min)
25
20
15
10
5
0
****
****
***
RNase
-
+
-
+
Sham
CLP
G
LVESV (uL)
40
30
20
10
0
***
**
*
RNase
-
+
-
+
Sham
CLP
H
LVEDV (ul)
80
60
40
20
0
RNase
-
+
-
+
Sham
CLP

Figure 4.3 RNase 1 attenuates sepsis-induced cardiac dysfunction. Mice were randomly selected to undergo sham-operated or CLP surgery and received either RNase 1 or vehicle (saline). At 24 h after CLP, cardiac function was assessed by echocardiography. **(A)** Representative M-mode echocardiograms. **(B)** Ejection fraction (%). **(C)** Fractional shortening (%). **(D)** Fractional area change (%). **(E)** Stroke volume (μL). **(F)** Cardiac output (ml/min). **(G)** End-systolic volume (μL). **(H)** End-diastolic volume (μL). The following groups were studied sham + vehicle ($n = 12$), sham + RNase ($n = 5$), CLP + vehicle ($n = 12$), CLP + RNase ($n = 12$). All data are expressed as mean ± SEM for n number of observations. A value of $^{****}P < 0.0001$, $^{***}P < 0.001$, $^{**}P < 0.01$, $^{*}P < 0.05$ was considered to be statistically significant when compared to CLP + vehicle by one-way ANOVA followed by a Bonferroni's post hoc test.

4.3.3 RNase reduces sepsis-induced kidney dysfunction

When compared to sham-operated mice, mice subjected to CLP for 24 h and treated with vehicle developed renal dysfunction (rise in urea and creatinine). When compared to CLP-mice treated with vehicle, CLP-mice treated with RNase 1 showed significant decreases in serum urea and creatinine, demonstrating that RNase 1 reduced the sepsis-induced renal dysfunction. There were no significant differences between sham-operated mice receiving vehicle or RNase 1 (Figure 4.4 A&B).

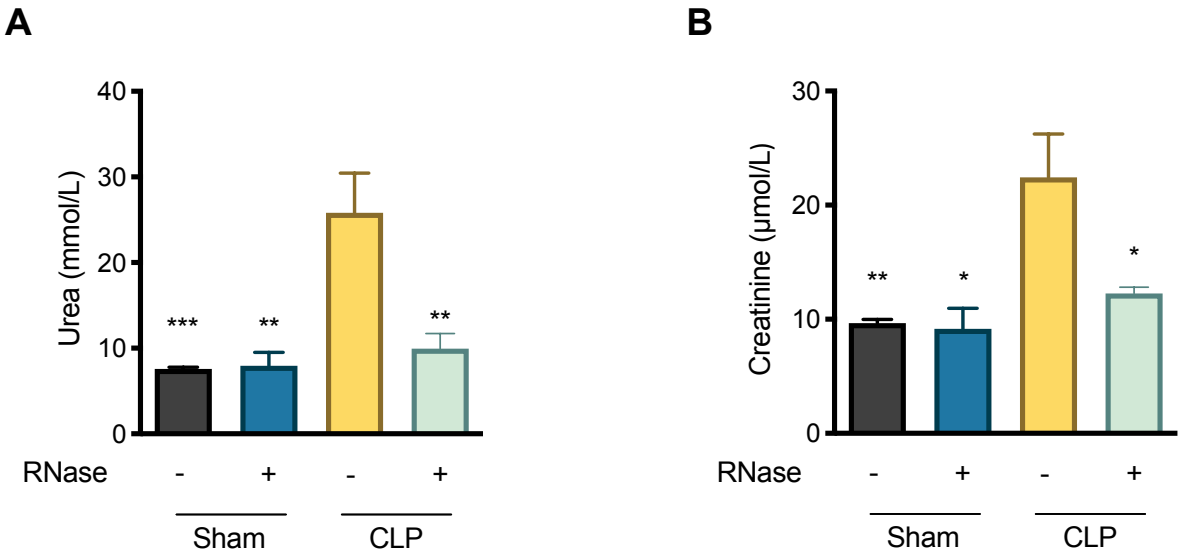

Figure 4.4 RNase 1 reduces sepsis-induced renal dysfunction. Mice were randomly selected to undergo sham-operated or CLP surgery and received either RNase 1 or vehicle (saline). At 24 h after CLP, renal function was assessed in serum. **(A)** Urea (mmol/L). **(B)** Creatinine (µmol/L). The following groups were studied sham + vehicle (n = 12), sham + RNase (n = 5), CLP + vehicle (n = 12), CLP + RNase (n = 12). All data are expressed as mean ± SEM for n number of observations. A value of *** $P < 0.001$, ** $P < 0.01$, * $P < 0.05$ was considered to be statistically significant when compared to CLP + vehicle by one-way ANOVA followed by a Bonferroni's post hoc test.

4.3.4 RNase 1 does not reduce sepsis-induced hepatocellular injury

When compared to sham-operated mice, mice subjected to CLP for 24 h and treated with vehicle developed hepatocellular injury (rise in ALT and AST). When compared to CLP-animals treated with vehicle, CLP-animals treated with RNase 1 resulted in no significant decreases in serum AST and ALT. There were no significant differences between sham-operated mice receiving vehicle or RNase 1 (Figure 4.5 A&B).

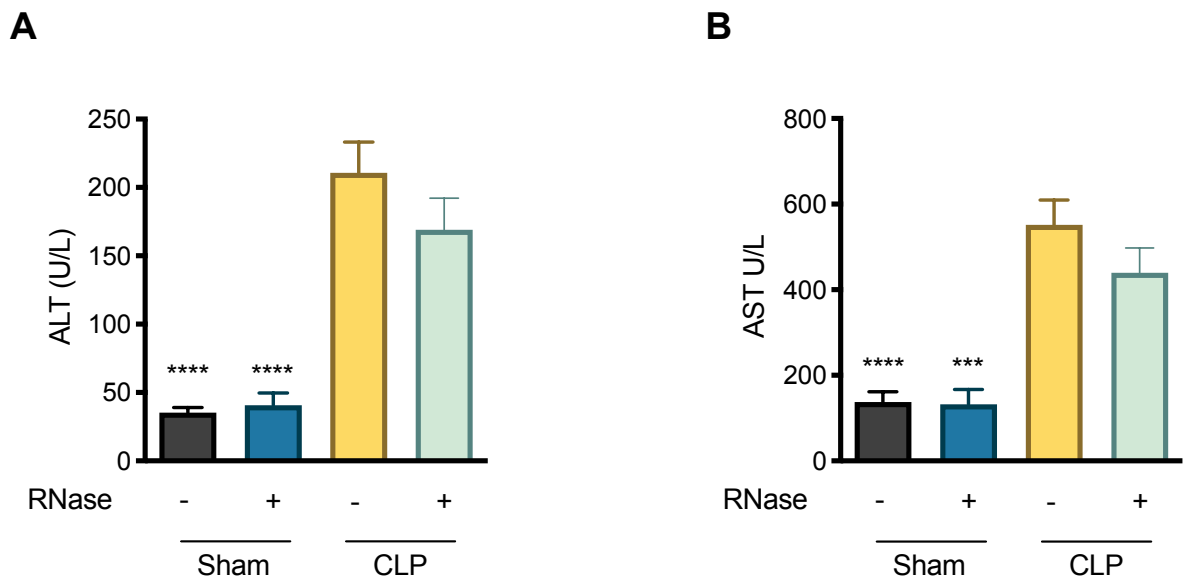

Figure 4.5 RNase 1 does not reduce sepsis-induced hepatocellular injury. Mice were randomly selected to undergo sham-operated or CLP surgery and received either RNase 1 or vehicle (saline). At 24 h after CLP, hepatocellular injury was assessed in serum. **(A)** ALT (U/L). **(B)** AST (U/L). The following groups were studied sham + vehicle ($n = 12$), sham + RNase ($n = 5$), CLP + vehicle ($n = 12$), CLP + RNase ($n = 12$). All data are expressed as mean ± SEM for n number of observations. A value of **** $P < 0.0001$ and ***$P < 0.001$ was considered to be statistically significant when compared to CLP + vehicle by one-way ANOVA followed by a Bonferroni's post hoc test.

4.3.5 Effect of RNase 1 on the number of bacteria in the peritoneum

When compared to sham-operated mice, mice subjected to CLP for 24 h and treated with vehicle developed a significant increase in peritoneal bacteria. When compared to CLP-animals treated with vehicle, CLP-animals treated with RNase 1 did not significantly decrease the number of bacteria in the peritoneum. There were no significant differences between sham-operated mice receiving vehicle or RNase 1 (Figure 4.6 A&B).

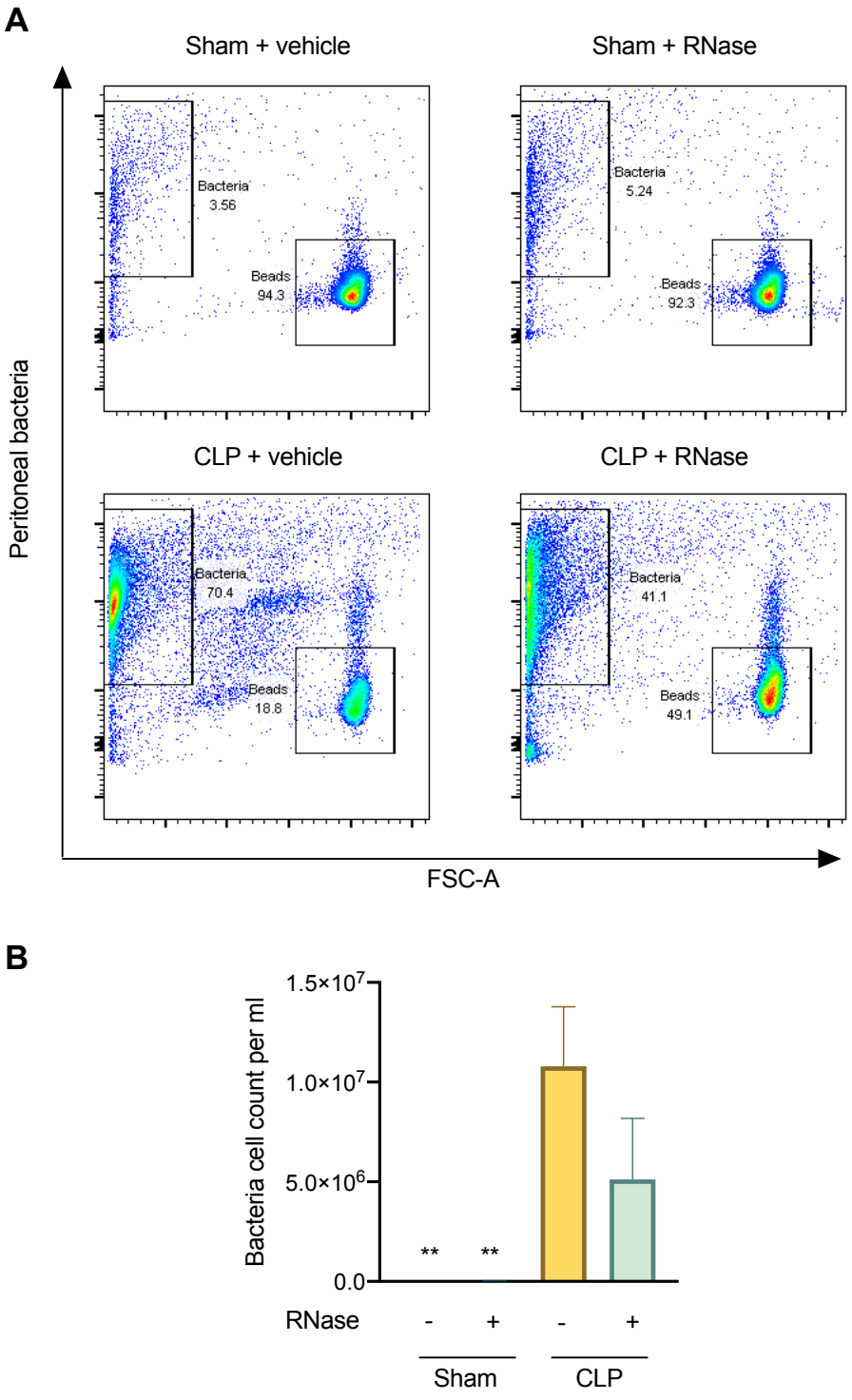

Figure 4.6 Effect of RNase 1 on the number of bacteria in the peritoneum. Mice were randomly selected to undergo sham-operated or CLP surgery and received either RNase 1 or vehicle (saline). At 24 h after CLP, bacteria were assessed in the peritoneal cavity. **(A)** Scattergraphs illustrating peritoneal bacteria **(B)** Bacteria cell count per ml. The following groups were studied, sham + vehicle, sham + RNase, CLP + vehicle and CLP + RNase. All data are expressed as mean ± SEM for $n = 5$ per group. A value of $^{**}P < 0.01$ was considered to be statistically significant when compared to CLP + vehicle by one-way ANOVA followed by a Bonferroni's post hoc test.

4.3.6 Effect of RNase on the systemic inflammation

When compared to sham-operated mice there were increases in 33 cytokines and chemokines in the serum of mice subjected to CLP for 24 h. When compared to CLP mice, mice which underwent CLP and were treated with RNase 1 resulted in a decrease of cytokines and chemokines, specifically TNF-α (Figure 4.7).

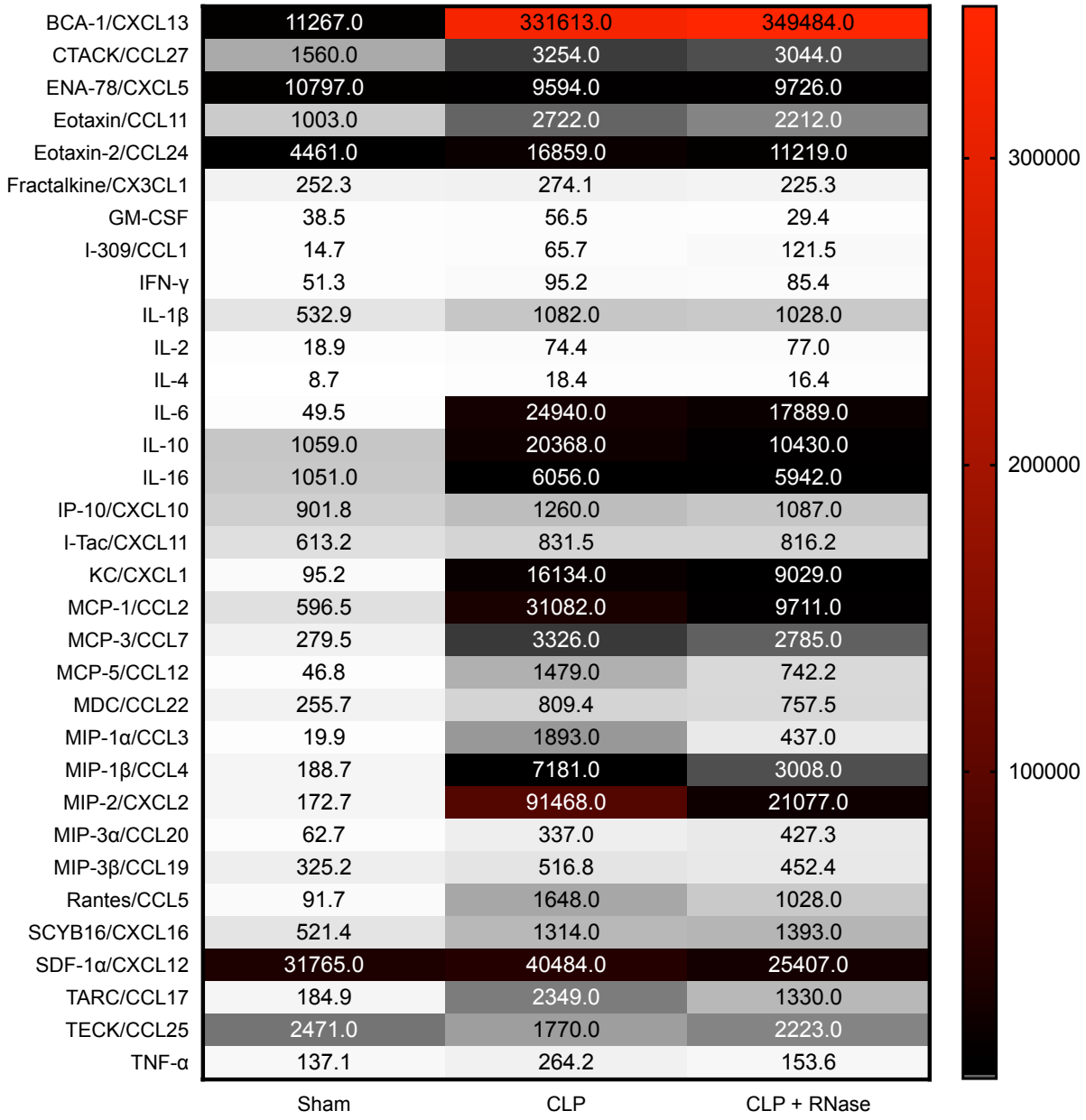

Figure 4.7 Effect of RNase on the systemic inflammation. Mice were randomly selected to undergo sham-operated or CLP surgery and received either RNase 1 or vehicle (saline). At 24 h after CLP, cytokines and chemokines were assessed in serum. **(A)** Heat map of cytokines and chemokines in serum. The following groups were studied sham + vehicle, CLP + vehicle and CLP + RNase. All data are expressed as mean for $n = 8$ per group.

4.3.7 RNase 1 decreases cardiac apoptosis in septic mice

To gain a better understanding of the underlying signalling events involved in the observed beneficial effects of RNase 1 on sepsis-associated cardiomyopathy, I investigated the relevant apoptosis pathways in cardiac tissue at 24 hours after onset of sepsis. When compared to sham-operated mice, mice subjected to CLP for 24 h and treated with vehicle developed a significant increase in the activation of the intrinsic apoptosis pathway as demonstrated by increases in the levels of Bax, cleavage of pro-caspase 9 to caspase 9 and cleavage of pro-caspase 3 to caspase 3 and decease in Bcl-2 in the cardiac tissue. When compared to CLP-animals treated with vehicle, CLP-animals treated with RNase 1 showed a significant decrease in the levels of Bax, caspase 9 and caspase 3 and an increase in Bcl-2 in the cardiac tissue (Figure 4.8 A&B), demonstrating that RNase 1 decreases the intrinsic apoptosis pathway in the heart.

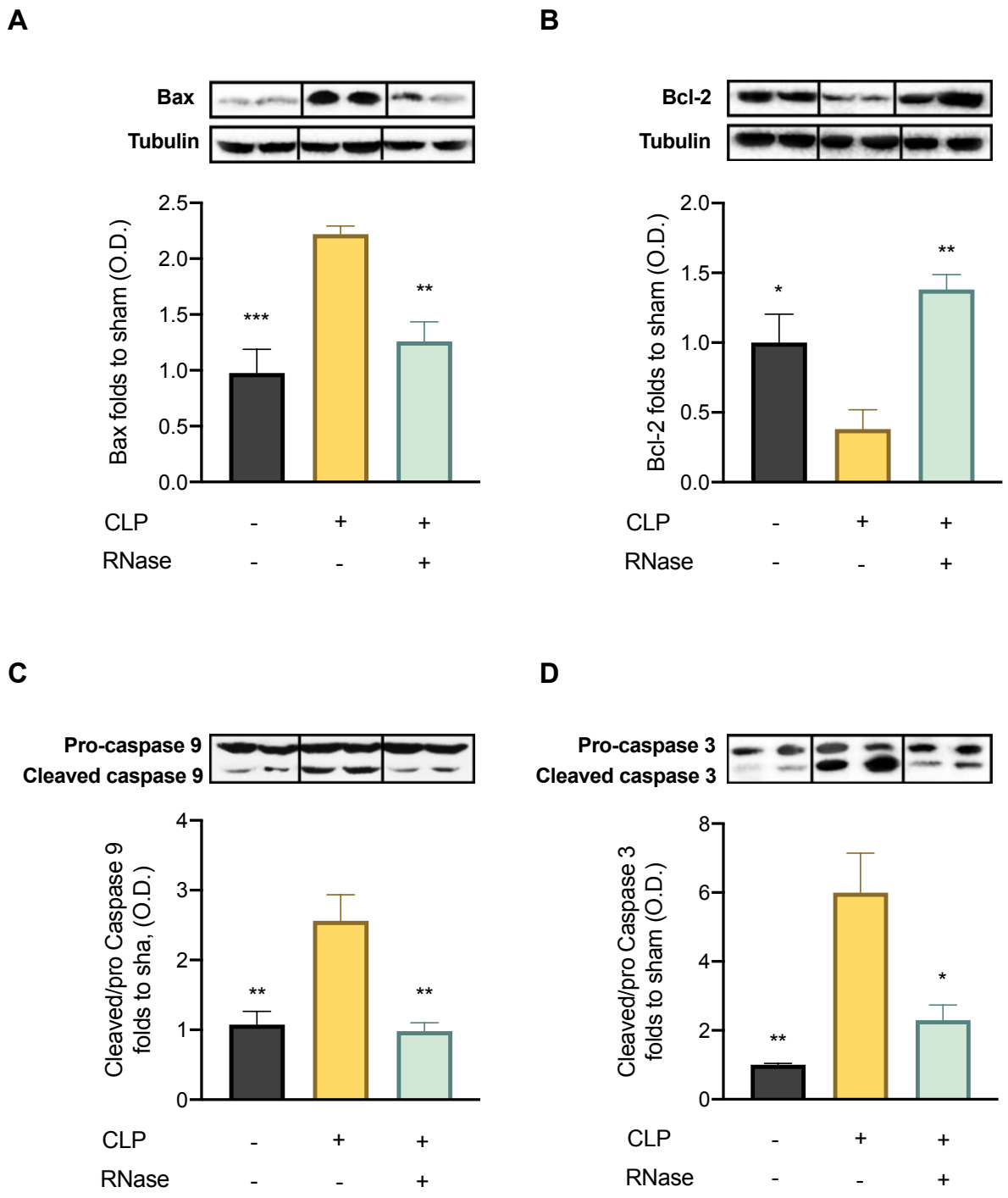

Figure 4.8 RNase 1 decreases cardiac apoptosis in septic mice. Mice were randomly selected to undergo sham-operated or CLP surgery and received either RNase 1 or vehicle (saline). At 24 h after CLP, hearts were analysed by Western blot to analysis the apoptosis signalling pathway. The activation of the following was investigated: **(A)** Bax **(B)** Bcl-2 **(C)** Caspase 9 **(D)** Caspase 3. The following groups were studied sham + vehicle ($n = 4$), sham + RNase ($n = 4$), CLP + vehicle ($n = 5$) and CLP + RNase ($n = 5$). All data are expressed as mean ± SEM for n number of observations. A value of *** $P < 0.001$, ** $P < 0.01$ and * $P < 0.05$ was considered to be statistically significant when compared to CLP + vehicle by one-way ANOVA followed by a Bonferroni's post hoc test.

4.3.8 Effect of RNase on cardiac TUNEL fluorescence in septic mice

When compared to sham-operated mice, mice subjected to CLP for 24 h and treated with vehicle resulted in no significant increase of cardiac TUNEL fluorescence. When compared to CLP-animals treated with vehicle, CLP-animals treated with RNase 1 showed no significant decrease in cardiac TUNEL fluorescence. There were no significant differences between sham-operated mice receiving vehicle or RNase 1 (Figure 4.9 A&B).

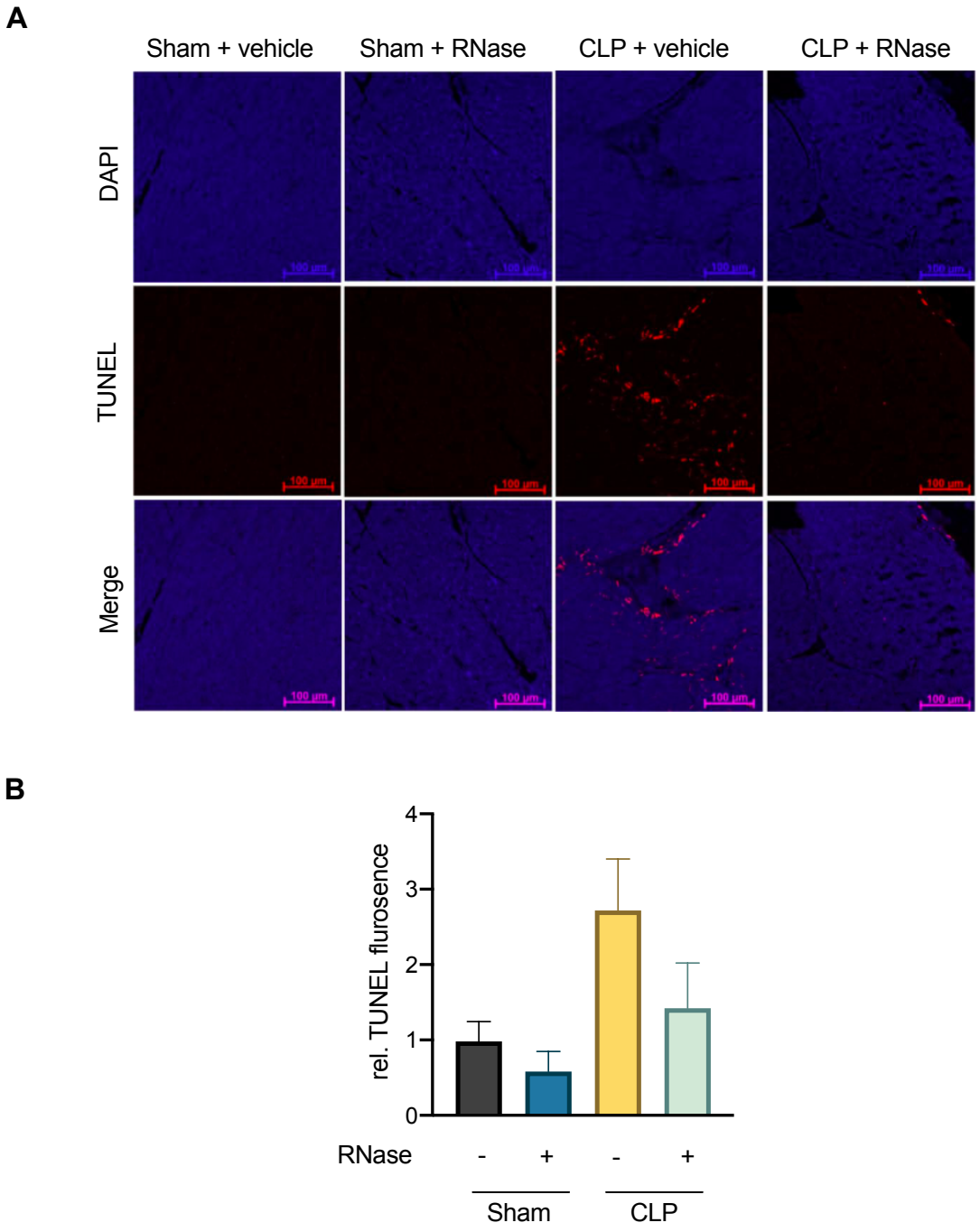

Figure 4.9 Effect of RNase on cardiac TUNEL fluorescence in septic mice. Mice were randomly selected to undergo sham-operated or CLP surgery and receive either RNase 1 or vehicle (saline). At 24 h after CLP, hearts were analysed by TUNEL assay to analysis cardiac apoptosis. **(A)** Apoptotic cells were labelled with TUNEL (red) and nuclei or cardiomyocytes were stained with DAPI (blue) scale bar 100 μm. **(B)** Quantification of TUNEL fluorescence. The following groups were studied, sham + vehicle, sham + RNase, CLP + vehicle and CLP + RNase. All data is expressed as mean ± SEM for $n = 5$ for all groups. A value of $^*P < 0.05$ was considered to be statistically significant when compared to CLP + vehicle by one-way ANOVA followed by a Bonferroni's post hoc test.

4.3.9 Time course of RNase levels in the serum of sham-operated and septic mice

At 1 h after CLP surgery RNase 1 levels were significantly reduced when compared to sham-operated mice. At 3 h after surgery both sham-operated and CLP mice resulted in a decrease in RNase levels. CLP RNase levels were significantly lower than sham-operated mice. At 6 h after surgery sham-operated mice experienced a slight increase in RNase 1 and CLP RNase levels remained similar to CLP RNase levels at 3 h. There was a significant difference between sham-operated and CLP RNase levels at 6 h. At 12 h sham-operated RNase levels increased from 6 h and CLP RNase levels remained similar to levels at 6 h. A significant difference is observed between sham-operated and CLP mice at 12 h. Finally, at 24 h after surgery sham-operated RNase levels dropped to levels that were similar at 3 h after sham-operated mice. CLP mice resulted in a slight increase in RNase levels from 12 h. A significant difference was observed between sham-operated and CLP mice in RNase levels at 24 h (Figure 4.10).

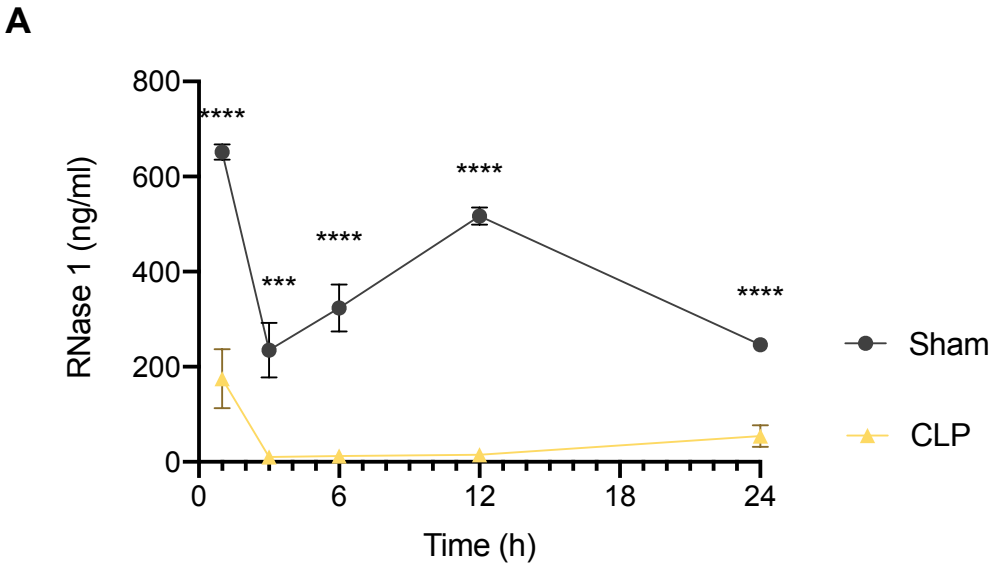

Figure 4.10 Time course of RNase levels in serum of sham-operated and septic mice. Mice were randomly selected to undergo sham-operated or CLP surgery. At 1, 3, 6, 12 and 24 h mice were sacrificed, and serum was collected for RNase 1 analysis. All data are expressed as mean ± SEM for sham (n = 3) and CLP (n = 4). A value of ****P < 0.0001 and *** P < 0.001 was considered to be statistically significant when compared to CLP by an unpaired t-test.

4.3.10 Concentration of RNase, RNH1 and eRNA in the serum of septic mice at 24 h

When compared to sham-operated mice, mice subjected to CLP exhibited a decrease in RNase 1 levels at 24 h after CLP surgery and this was associated with an increase in ribonuclease 1 inhibitor. No difference was observed in eRNA levels in serum between sham-operated and CLP-operated mice. When compared to CLP mice treated with vehicle, mice which underwent CLP and were treated with RNase 1 showed an increase in RNase 1 levels and a small, but not significant, decrease in ribonuclease 1 inhibitor in serum. No difference in eRNA levels was observed between CLP + vehicle and CLP + RNase mice (Figure 4.11).

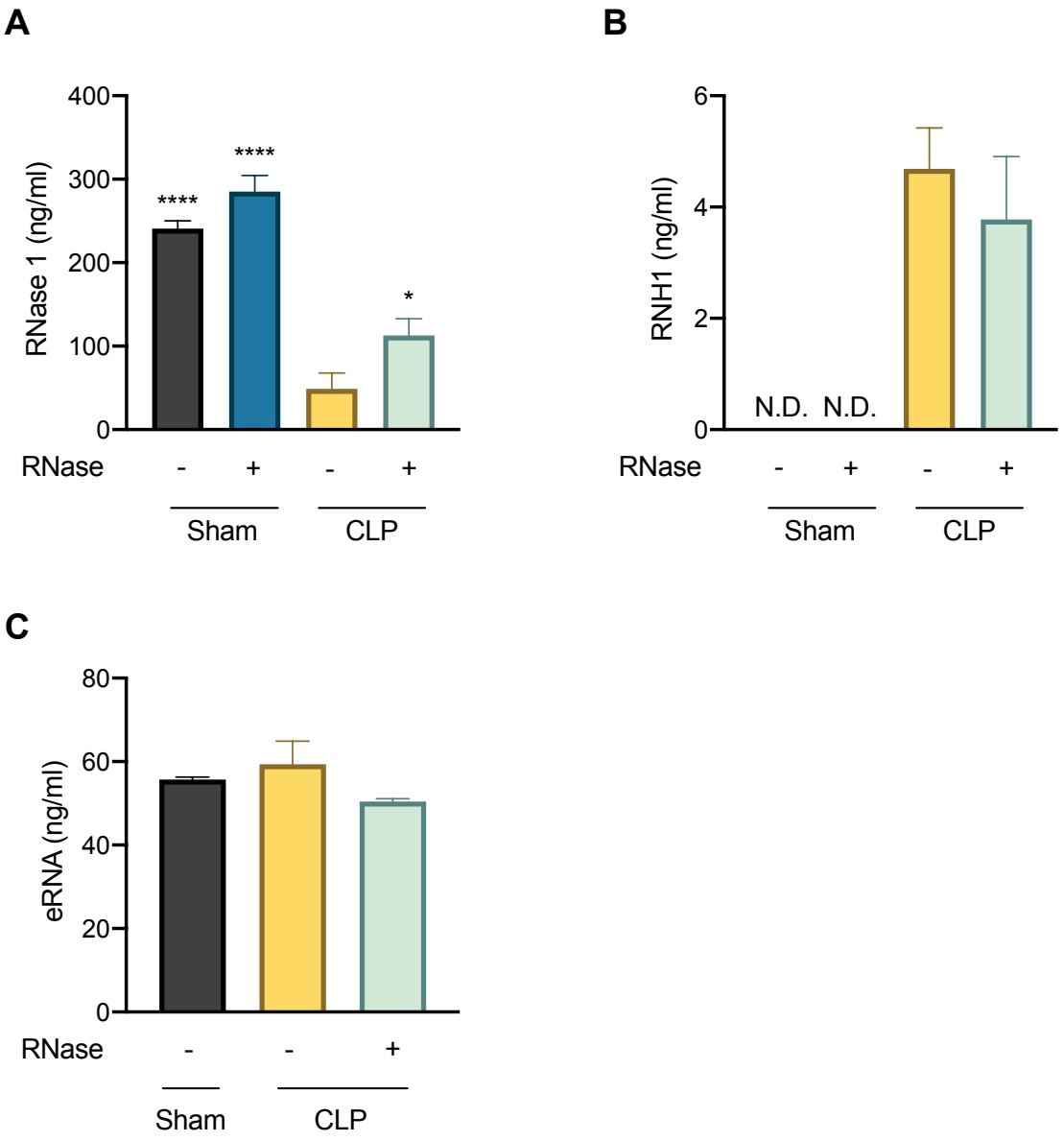

Figure 4.11 Concentration of RNase, RNH1 and eRNA in the serum of septic mice at 24 h. Mice were randomly selected to undergo sham-operated or CLP surgery and receive either RNase 1 or vehicle (saline). At 24 h after CLP, mice were sacrificed, and serum was collected for further analysis by ELISA. **(A)** Concentration of RNase 1 (ng/ml). **(B)** Concentration of ribonuclease 1 inhibitor (ng/ml). **(C)** Extracellular RNA (ng/ml). The following groups were studied sham + vehicle (n = 5), sham + RNase (n = 5), CLP + vehicle (n = 8) and CLP + RNase (n = 9). All data are expressed as mean ± SEM for n number of observations. A value of **** $P < 0.0001$ and *$P < 0.05$ was considered to be statistically significant when compared to CLP + vehicle by one-way ANOVA followed by a Bonferroni's post hoc test.

4.4 Discussion

Sepsis leads to cell damage and tissue injury which results in the release of eRNA promoting systemic inflammation. RNase A counteracts the inflammatory properties of eRNA and has been found to be elevated in septic patients. The aim of this study was to investigate whether administration of RNase 1 would attenuate sepsis-induced cardiac dysfunction and the potential role of RNase 1 in cardiac apoptosis.

The administration of RNase in the polymicrobial murine sepsis model resulted in attenuation of sepsis-induced cardiac dysfunction. Additionally, Stieger *et al*. found that administration of RNase 1 in their mouse model of myocardial infarction resulted in persevered left ventricular function 24 h after myocardial infarction, as demonstrated by an increase of FS when compared to the controls (300). Also, in a rat model of heart transplantation, rats treated with RNase 1 had a longer graft survival and flow cytometry analysis of the heart revealed reduced leukocyte infiltration, oedema, and thrombus formation when compared to controls (301). All these studies confirm that RNase has a protective role in the heart.

The administration of RNase to CLP mice resulted in a reduction of kidney dysfunction (measured as urea and creatinine) when compared to the CLP + vehicle, demonstrating that RNase 1 protects the kidney from sepsis-induced kidney dysfunction. RNase 4 and 7 are expressed by epithelial cells in the urinary tract, with the collecting duct being the main site of production (302,303). It has previously been shown that RNase 7 in urine is 1.5-fold lower in females who have UTI than those who are healthy, and RNase 7 humanized mice are protected against infections with uropathogenic *E.coli*. These findings show that RNase 7 plays a role in the host defence of kidney and bladder against uropathogenic *E.coli* (304).

An increase in cytokine production results in the decrease of circulating RNase 1 via epigenetic modifications, which increases eRNA induced inflammation and contributes to the disruption of the vascular homeostasis (198). I report in this chapter that administration of RNase 1 attenuates the increase in cytokines and chemokines caused by CLP-sepsis. There is evidence that the clearance of eRNA by RNase 1 might be responsible for the observed decrease of inflammation (200,213). Ma *et al*. found that administration of RNase 1 attenuates hepatic ischaemia reperfusion injury in aged mice through the inhibition of cytokine production (212).

RNases are antimicrobial peptides and have characteristics that allow them to interact with pathogens e.g. having a net positive charge allowing for RNases to bind to microbial membranes and forming amphipathic structures in hydrophobic environments allowing for them to penetrate the bacterial phospholipid bilayer. However, RNase 1 is not recognised as a robust antimicrobial but is considered to be an anti-viral (305). In this chapter I found that administration of RNase 1 did not result in a significant decrease in the number of bacteria in the peritoneal cavity. Lu *et al*. screened the 7 human RNases *in vitro* for their antimicrobial potency. They found that only RNase 3, 6 and 7 could completely inhibit the growth of *M. aurum* cultures, whereas the other RNases did not reduce the mycobacteria concentration. Longer exposure times to RNase 3, 6 and 7 lead to increased mycobacteria clearance (306). My results contradict Lu study, but they only focused on the clearance of one type of bacteria whereas my *in vivo* model is polymicrobial. Administration of RNase 1 has been shown to have antiviral activity against HIV-1 (307) and also leads to the activation of dendritic cells (201). Administration of Ear1 (similar to human RNase 1) in the rat lead to reduced growth of *E.coli* showing the potential role of RNase 1 in animal models (308).

It has been shown *ex vivo* that inhibition of caspase activation in the apoptosis pathway reduces depression of cardiac function (309). However, post-mortem examination of patients with sepsis and healthy controls revealed that < 0.2% of the cells had undergone apoptosis and there were no differences between the two groups (126). Here I report that CLP results in an increase of cardiac apoptosis (demonstrated as a rise of Bax levels, activation of caspase 9 and 3 and a decrease of Bcl-2) as well as an increase in TUNEL staining. Administration of RNase 1 to mice subjected to sepsis results in a significant decrease in the activation of the apoptosis signalling pathway and a decrease in TUNEL staining. Additionally, other studies have investigated reducing apoptosis as a therapeutic intervention by caspase inhibition in cardiomyopathy induced ischemia-reperfusion and rapid ventricular pacing (310,311). In a model of myocardial ischemia-reperfusion administration of RNase 1 reduced the infarct size and reduced necrotic cell death in ischemic hearts (213). As mentioned previously Stieger *et al*. not only found RNase 1 preserved left ventricular function but also resulted in a reduction of apoptosis 24 hours after ligation of the left anterior descending artery (LAD) in mice (300).

In serum of septic patients, the levels of RNase 1, eRNA and RNH1 are elevated when compared to healthy participants (206,298). However, in my mouse model of polymicrobial sepsis, I found that that levels of RNase 1 decrease to low levels in septic mice even 1 h after CLP surgery. RNH1 level was significantly increased in CLP mice but, no significant difference was observed in eRNA levels between sham-operated and CLP mice. The discrepancies between human septic serum and mouse septic serum could be due to the time of the measurement. The levels of eRNA in septic patients were measured 3 days after diagnosis, whereas the concentration of eRNA was measured only at 24 h after CLP surgery. Stieger *et al*. showed that eRNA levels were elevated within 30 min after ligation of LAD and at 2 h hour reaching a maximum eRNA concentration in serum. However, at 4 h after LAD eRNA levels returned to baseline (300).

4.4.1 Limitations of RNase experiments

A limitation of these experiments is that administration of RNase 1 was given as a pre-treatment just before CLP surgery, and I have yet to investigate whether the delayed administration of RNase 1 would affect cardiac, renal and hepatocellular function after CLP surgery. I have seen in chapter 2 that cardiac function is affected 1 h after CLP as demonstrated by a decrease in cardiac output and stroke volume. It would be useful to confirm my hypothesis that eRNA is elevated in earlier time points after CLP surgery, by measuring eRNA levels in mice 2 h after CLP surgery like Stieger *et al*. in the LAD model. I only measured eRNA 24 h after CLP surgery, where I expect eRNA had returned to baseline levels.

4.4.2 Conclusion

In conclusion administration of RNase 1 attenuates sepsis-induced cardiac dysfunction due to reduced cardiac apoptosis by the intrinsic pathway and a reduction in sepsis-associated cytokines/chemokines. Whether it can be translated as a therapeutic treatment for septic patients still remains to be answered, but it is clear that RNase 1 plays a role in the pathophysiology of sepsis, specifically the cardiac dysfunction associated with sepsis.

Chapter 5 General Discussion

Research into sepsis has increased our understanding of the pathophysiology and resulted in changes to the guidelines for managing sepsis. But despite these efforts, sepsis is still a common life-threatening, heterogenic condition, globally affecting 50 million people and resulting in the death of 11 million every year. Sepsis represents 20% of all deaths worldwide (13) and is a major public health problem. Despite intensive, supportive care and current treatments (antibiotic therapy and fluid resuscitation), no targeted therapies have proven effective at reducing mortality (312,313). Therefore, research into new therapeutics for sepsis-induced organ dysfunction is of great importance (220).

5.1 The differences between murine sepsis models and human responses

Laws and regulatory agencies worldwide require new drugs to first be tested on animals before entering clinical trials in humans. However, finding a model that reflects the complexity of sepsis (both hyper and hypoinflammatory phases) is challenging. Murine models are most commonly used as they have multiple advantages (Table 5.1).

Table 5.1 Advantages of murine models

Advantages of murine models	Description
High fecundity	✓ Reach sexual maturity at 6-8 weeks ✓ 8 pups per litter
Accelerated life cycle	✓ Accelerated life cycle (life expectancy is 24 months)
Low maintenance and cheap	✓ Docile ✓ Minimal husbandry routine
Necessity for preclinical animal model	✓ Regulatory agencies require preclinical animal models, before moving to clinical studies
Inbred, outbred and transgenic strain	✓ Inbred animals allow for little variability ✓ Using genetically modified mice helps to understand the importance of a particular gene in the pathophysiology of sepsis.
Widespread availability of mice and reagents	✓ Often availability of immunological reagents for mice exceeds that of humans
Evolving humanized mice	✓ Humanized mice via method dictated by leads to a complement of mature human T and B cells that are not rejected by the mouse

Murine sepsis models are classified into three categories based on their mechanism: administration of an exogenous toxin, administration of a viable pathogen and disruption of the animal protective barrier resulting in bacterial invasion (Table 5.2).

Table 5.2 Murine models of sepsis

Type of murine model	Example	Advantages	Disadvantages
Exogenous administration of toxin	**Endotoxemia model:**	✓ Simple and reproducible ✓ Acute response	× LPS only activates TLR4 signalling pathway
	systemic administration of LPS/PepG	✓ Highly controlled and standardised model	× Does not reflect all complex physiological human responses × High, rapid and transient increase in cytokines, which differ from human sepsis × Variability in dose, toxin and route of administration × Each bottle of LPS maybe stronger or weaker than the previous, concentrations change
Exogenous administration of a viable pathogen	**Inoculation of live bacteria**	✓ Presence of a bacterium allows insights into mechanisms of host response to pathogens	× Growth and quantification of bacteria is needed before administration × Single bacterium model does not reflect the diversity of bacterium in human sepsis × Humans do not normally have a large quantity of bacteria introduced, but more of a focus that persistently challenges the body with bacteria × High doses of bacteria will result in an endotoxemia response due to the lysis of bacteria giving off LPS × Variability in bacterial load, route of administration and bacterial strain
	Intraperitoneal implantation of fibrin clot impregnated with viable bacteria	✓ Fibrin delays systemic absorption of trapped bacteria, promoting development of a local septic focus ✓ Reduces early mortality	× Involves single bacteria strain, whereas human intra-abdominal sepsis if often polymicrobial
	Cecal slurry	✓ Induces polymicrobial sepsis ✓ Favours innate immune response ✓ Preferable in neonatal mice given their small size and technical ease to perform	× No component of tissue necrosis × Inflammation does not persist as long as CLP or CASP
Disruption of the endogenous protective barrier	**Cecal ligation and puncture (CLP)**	✓ Simple procedure ✓ Infectious focus ✓ Polymicrobial sepsis model ✓ Using the complete spectrum of host enteric bacteria ✓ Recreates human sepsis progression with similar hemodynamic and metabolic phases and the presence of both hyper and hypoinflammaotry phases ✓ Prolonged and lower elevation of cytokine release similar to humans	× Variable disruption of the endogenous protective barrier ability in severity due to difference in experimental procedure, e.g. the size of the needle × Age and strain variability
	Colon ascends stent peritonitis (CASP)	✓ Produces polymicrobial sepsis and diffuse peritonitis ✓ Causes resulting bacteraemia ✓ Operator able to alter sepsis severity	× No component of tissue necrosis × Technically more challenging than CLP × Less characterised hemodynamic response

In chapter 2, I have established an endotoxaemia model (LPS/PepG administration) and a clinically relevant model of sepsis (CLP surgery), which is classed as the "gold standard model" (314). Administration of bacterial wall fragments such as LPS and PepG leads to systemic inflammation and organ dysfunction in the absence of infection (see below), while CLP is a disruption of the endogenous protective barrier leading to microbial flora from the animal itself being leaked into the peritoneum causing infection, which then triggers systemic inflammation and organ dysfunction.

The endotoxaemia model results in an acute hyperinflammatory response, caused by the activation of the TLR4 (found e.g. on the surface of macrophages and monocytes) and TLR2 signalling pathways. Excessive activation of these pathways and the associated excessive systemic inflammatory response leads to impaired myocardial contractility, lactic acidosis, arterial hypotension, an early transient increase in TNF, prolonged elevation of IL-6 and a delayed increase in HMGB-1. All of these aspects of experimental 'sepsis' are also found in human sepsis, but the magnitude of the changes is significantly different between rodents and man. Firstly, humans are more 1000 times more sensitive to LPS than mice, with mice having an LD_{50} of LPS between 5-15 mg/kg (315). Injection of LPS (in mice) does not result in the hyperdynamic cardiovascular state observed in human sepsis (316). Another shortcoming of the LPS/PepG model is that humans are rarely exposed to a single large bolus of an endotoxin. The 'source' of the sepsis response in man is often polymicrobial resulting in a slow release of bacteria and their wall-fragments (and/or toxins) from a septic insult. As a result of this, humans experience a more delayed increase in cytokines and chemokines, which may eventually culminate in a cytokine storm, whereas LPS/PepG injection results in an earlier and shorter duration of proinflammatory cytokine/chemokine release than that triggered by sepsis in humans, reaching a maximum concentration 2 h after LPS/PepG injection and begin to decline after 8 h (224,317). Overall, LPS/PepG is useful for studying hyperinflammation, but not of general sepsis, as it fails to replicate infection with live bacteria as the driver of systemic inflammation and organ failure (318). Thus, interventions which kill bacteria (e.g. antibiotics) would, for example, not be effective in models of toxaemia.

The majority of infections (which ultimately lead to the development of sepsis) start in either the lung or the peritoneal cavity (319) and, hence, most investigators use either a model of peritonitis (CLP) or pneumonia as models of sepsis. Indeed, the CLP model is currently

considered to be the "gold standard" as it reproduces a number of factors/responses found in human sepsis including polymicrobial infection, systemic inflammation and multiple organ injury/dysfunction (314,320), although one may argue that the pneumonia model is a better model of sepsis caused by community-acquired pneumonia and/or COVID-19. CLP is associated with three different insults: trauma to the abdominal tissue secondary to laparotomy, caecum ligation resulting in necrosis and the puncture of the caecum resulting in faecal peritonitis, which ultimately leads to translocation of bacteria into the bloodstream leading (when uncontrolled) to septic shock (321). CLP mice experience a more delayed release of cytokines and chemokines similar to that seen in humans (224,317). Even though the use of the CLP model of sepsis has helped to gain a better insight into the pathophysiology of human sepsis, even this experimental animal model does not recapitulate the entire spectrum of the events occurring in human sepsis. Furthermore, the variation in the CLP model results in different rates of mortality potentially contributing to conflicting datasets (322). The severity of CLP is affected by the following factors: length of the caecum that is ligated (323), number of punctures, size of the needle used for punctures and whether antibiotics are administered (321). The intestinal flora is not uniform between animals or species and it has been reported that the type of bacteria in the caecum can influence the severity of CLP and mortality. Wilmore *et al*. showed that phylum proteobacteria in the caecum resulted in protection against CLP-induced sepsis (324).

During a septic insult mice and humans respond differently (Table 5.3). During sepsis, mice develop bradypnea and bradycardia in comparison to septic humans who develop tachypnoea and tachycardia (325,326). At room temperature a septic mouse will become hypothermic with their temperature decreasing accordingly to the severity of the disease, whereas a septic human will develop a fever (327). The "leakiness" of the gut is often considered the key regulator in the development of multiple organ failure, but the surface area between different species varies, for example the mouse's surface area ratio of the small intestine to colon is 22-fold lower than humans (328).

There are also known differences between the innate and adaptive immunity of mouse and humans (Table 5.3). In the human innate immunity the neutrophil is the most predominant leukocyte in the blood (50-70%) whereas, in the mouse lymphocytes are most common (70-90%) (329). Human neutrophils are a source of defensins (a type of antimicrobial peptide,

involved in the host defence against an infection), but neutrophils in mice do not express defensins (330). The number of platelets is ten times higher in mice than humans. Stimulation of macrophages with LPS and IFN-γ result in mouse macrophages to express iNOS, whereas human macrophages do not express iNOS upon stimulation with LPS and IFN-gamma (331). Regarding the adaptive immunity, humans and mice present with differences in antibody class switching and B cell development (332), as well as the developments and regulation of T cells (333). Even within strains of mice there is a difference in expression of T_{H1}, T_{H2} and TH_{17}.

Table 5.3 Example of some of the differences between mice and men that may affect the development of sepsis. Table adapted from (313).

	Mice	**Humans**
Physiology		
Circadian rhythm	*Nocturnal*	*Diurnal*
Nutrition	*Standardised chow diet*	*Varied*
Glucose levels	*Decreases after sepsis*	*Increases after sepsis*
Temperature	*Decreases after sepsis*	*Increases after sepsis*
Metabolic rate	*Decreases after sepsis*	*Increases after sepsis*
Immune system		
Predominant white blood cells	*Lymphocyte*	*Neutrophil*
Enzymatic content in neutrophils	*Low*	*High*
a-defensin production by neutrophils	*No*	*Yes*
Expression of CXCR1 on neutrophils	*No*	*Yes*
NETosis after sepsis	*Increased*	*Decreased*
Missing genes	*IL-8, IL-32, IL37, LFA-3*	*MCP-5*
	TLR10, caspase 10	*TLR11, TLR12*
Main inflammasome player in LPS sensing	*Caspase 11*	*Caspase 4 and 5*

5.2 Why does translational research sometimes fail?

For over 30 years researchers have shown effective treatments, antibodies or genetically engineered mice having beneficial improvements to a septic insult. However, despite the advances in research made through murine models the translation of a drug from animal models to humans often fail in sepsis, due to a multitude of disadvantages that murine models pose (Table 5.4).

Table 5.4 Disadvantages of murine models

Disadvantages of murine models	Description
Interspecies differences	× Human genome is larger than the mouse by 14% (315,334). × Differences in the innate and adaptive immune system of mice and humans. × Predominant leukocyte in humans is the neutrophil accounting for 50-70% of the total leukocyte population. However, in mice the lymphocyte accounts for 75-90% of the total leukocyte population.
Differences between strains	× Each strain of mice has a different genetic makeup. × Inbreed strains are well known whereas outbred are not and not used for sepsis studies. × Adaptive immunity varies within strains e.g. C57BL/6 mice TH1 predominant response favouring macrophages and cell mediated immunity where as BALB/c A/J and DBA/2 exhibit a TH2 predominant response = antibody production and eosinophil activation (335).
Effect of the environment	× Mice are kept in pathogen free facilities and as a result have an immature immune system (336).
Age	× Mice are often 10 weeks old when used which is the equivalent to young adults, however sepsis is a disease of the extreme ages as well. × Age mice cost more and have a limited availability.
Gender	× Males represent majority of the studies. × Hormonal differences affect the survival in sepsis.
Mouse homogeneity	× Sepsis is a heterogenic condition using inbred mice does not represent the vast differences within the human population.
Comorbid disease	× In the elderly community there is a prevalence of comorbid diseases, which is often not reflected in animal models.
Ability to provide supportive care	× Unable to administer mechanical ventilation, vasopressors, renal replacement therapy and delivery of nutrition.
Variability within murine models	× The inflammatory response varies between the different models of sepsis.

Most sepsis models use young and healthy animals (usually of male gender), while most patients with sepsis are older and have significant co-morbidities including diabetes and chronic kidney disease. These co-morbidities amplify the cytokine storm associated with sepsis and increase organ dysfunction and mortality. For most interventions shown to be effective in sepsis, it is unknown whether they would also be effective in older animals with co-morbidities.

Furthermore, numerous studies have been conducted in the endotoxin model (337–340), which is known to poorly mimic septic cardiomyopathy. However, even in more clinically relevant models few studies incorporate adequate fluid resuscitation, the use of antibiotics and most studies administer the treatment very early < 4 h after septic insult or as a pre-treatment. These factors favour a beneficial outcome and can lead to false positives and suggest limited predictive value of preclinical models (341). In contrast patients are diagnosed and receive treatment much later on where often organ dysfunction has already developed, this delay in receiving treatment severely effects a patient's outcome and contributes to the shortcomings of translating new treatments from mice to men.

Seok *et al.* researched gene expression in human and murine leukocytes following burn/trauma/endotoxaemia, from their data they stated "genomic responses in mouse models poorly mimic human inflammatory diseases" thus concluding that mouse models are unsuitable for studying human inflammatory conditions (342). This paper was picked up by the lay press calling to eliminate animal studies altogether, due to the multiple flaws and lack of translatability into human and ethical issues. A classic example of the failings of transability from mouse to man is the use of TNF-α antibodies. Mice treated with anti-TNF were protected from a lethal dose of LPS (343). Yet the use of anti-TNF in septic patients failed to reduce mortality (344,345). When conducted in a clinically relevant mouse model (CLP) treatment with anti-TNF also failed to show any protective benefits in CLP mice (346,347) showing that inappropriate mouse models are to blame for the failings of the septic human anti-TNF trials.

Even though murine models have disadvantages, there is also variability between different laboratories in the models of sepsis, making it difficult to compare results. For example, the length of the ligation, number of punctures, size of needle and whether antibiotics or fluid resuscitation is used effect the severity of the CLP model. Ideally, investigators need to standardise murine models to make data comparable. Overall, there is no perfect animal model of sepsis, but they are the only option to examine a fully intact biological system which is essential in furthering our understanding of the pathophysiology of the disease (348).

5.3 Bruton's tyrosine kinase

I have shown in both models (endotoxaemia and CLP) that the BTK inhibitors ibrutinib or acalabrutinib attenuate LPS and CLP-induced cardiac dysfunction. Interestingly, the degree of

cardiac dysfunction correlates with the degree of BTK activation. BTK is involved in the activation of TLR's which recognise bacteria and stimulate the immune response by leading to the activation of NF-κB and NLRP3 inflammasome and subsequently the production of cytokines and chemokines in serum. The BTK inhibitors ibrutinib or acalabrutinib inhibit the activation of BTK and, hence, reduce the activation of NF-κB and NLRP3 inflammasome and subsequently a decrease in the production of cytokines/chemokines in serum (Chapter 2).

The discovery that BTK inhibitors attenuate sepsis-induced cardiac dysfunction, raised the question whether the observed effects of these compounds were solely due to BTK inhibition or due to (at least in part) an off-target effect? Ibrutinib inhibits a lot of other kinases, whereas acalabrutinib is more selective and both BTK inhibitors strongly inhibit 5 kinases BTK, RIPK2, Tec, Bmx and Erbb4 (see kinome array, chapter 3.1). To confirm whether BTK inhibition is responsible for the observed effects, I replicated the model of polymicrobial sepsis in *Xid* mice, which have a missense mutation within the BTK gene (arginine to cysteine at position 28 (R28C)) in the N-terminally located pleckstrin homology domain, resulting in expression of a BTK protein that is functionally inactive (183,184).

In chapter 3, I report that genetic deficiency of the BTK gene alone in *Xid* mice confers protection against cardiac, renal and liver injury in polymicrobial sepsis and reduces hyperimmune stimulation ('cytokine storm') induced by an overwhelming bacterial infection. These beneficial effects are (at least in part) due to enhanced bacterial phagocytosis *in vivo* and decreased activation of NF-κB and the NLRP3 inflammasome. The inactivation of BTK leads to reduced innate immune cell recruitment and a phenotypic switch from M1 to M2 macrophages, aiding the resolution of sepsis. By reanalysing the microarray dataset generated by Parnell *et al*. from the blood of patients with sepsis, I have shown (in chapter 3) that BTK expression is increased in the blood of septic non-survivors, while lower expression is associated with survival from sepsis, indicating that the activation of BTK plays a role in sepsis. Importantly, no further reduction in organ damage is seen in *Xid* mice treated with the BTK inhibitor ibrutinib, demonstrating that the protective effects of BTK inhibitors in polymicrobial sepsis are mediated solely by inhibition of BTK and not by off-target effects of this class of drugs.

The FDA has approved the use of the irreversible BTK inhibitors ibrutinib (first generation) in chronic lymphatic leukaemia, mantle cell lymphoma, Waldenstrom macroglobulinemia, and graft vs. host disease (169) and acalabrutinib (more selective, second-generation) in mantle cell lymphoma (170). Ibrutinib is also approved by the EMA for the treatment of chronic lymphatic leukaemia, mantle cell lymphoma, and Waldenstrom macroglobulinemia (171), whereas acalabrutinib has received an orphan designation for chronic lymphatic leukaemia, mantle cell lymphoma, and lymphoplasmacytic lymphoma (172–174). I have proposed in this thesis the potential for repurposing BTK inhibitors for the use in sepsis or other acute inflammatory conditions. Currently, BTK inhibitors are in clinical trials for multiple sclerosis (349), rheumatoid arthritis (350) and COVID-19 (351). The recent COVID-19 pandemic has driven the search for drugs that can be repurposed to either reduce virus load and/or the cytokine storm in patients with severe COVID-19 infections. COVID-19 has resulted in the development of cardiovascular complications such as heart failure, arrhythmia, myocarditis, cardiogenic shock and thromboembolic events in patients without any history of cardiovascular disease (352). It has been found that myocardial injury (measured by elevated TnT levels) due to COVID-19 is associated with high mortality rates. COVID-19 patients which did not have any pre-existing cardiovascular disease, but presented with myocardial injury, resulted in a mortality of 37.5%. The percentage of mortality increased to 69.44% in patients who had pre-existing cardiovascular disease and also presented with myocardial injury. If there was no myocardial injury from COVID-19, the mortality was 7.62% (without pre-existing cardiovascular disease) and 13.33% (with pre-existing cardiovascular disease) (353). AstraZeneca is currently in clinical trials testing acalabrutinib in patients with severe COVID-19 (Acalabrutinib: NCT04346199) and have found that BTK activation and IL-6 production is increased in the blood of COVID-19 patients (351). Roschewski *et al*. showed that severe COVID-19 patients receiving acalabrutinib had improved oxygenation and reduced CRP and plasma IL-6, suggesting that BTK inhibitors may be useful in the treatment of COVID-19. BTK inhibitor zanubrutinib is also in clinical trials for COVID-19 at BeiGene (Zanubrutinib: NCT04382586). Zanubrutinib is a second generation irreversible BTK inhibitor, which in November 2019 was granted accelerated approval for mantle cell lymphoma by the FDA (354). Interestingly, ibrutinib protects mice from lethal influenza-induced lung injury (257). Infection with seasonal influenza A virus (IAV) leads to lung inflammation and respiratory failure, similar symptoms to that of COVID-19. Re-purposing BTK inhibitors for non-chronic diseases e.g. in acute excessive inflammation maybe an attractive avenue for BTK inhibitors, as the long-term use

of ibrutinib in cancer therapy has resulted in adverse effects such as bleeding complications (355) and increased rates of atrial fibrillations (356). Further studies would need to be carried out in an acute setting to determine both efficacy and potential any adverse effects of BTK inhibitors in disease associated with acute inflammation.

5.4 RNase

In chapter 4, I report that administration of the antimicrobial peptide RNase 1 also results in attenuation of sepsis-induced cardiac dysfunction. I discovered that RNase 1 levels are decreased in the serum of septic mice and there is no significant difference between eRNA and RNH1 levels in serum of septic and treated mice, even though eRNA and RNH1 are elevated in humans with sepsis (298). The discrepancies between human septic serum and mouse septic serum could be due to the time of the measurement. eRNA levels were shown to be elevated between 30 min to 2 h, but at 4 h eRNA levels and returned to baseline in mice (300). In septic humans eRNA was measured 3 days after diagnosis, indicating a potential later increase in the release of eRNA (298). The cardiac dysfunction of septic mice was associated with an increase in cardiac apoptosis as demonstrated by TUNEL staining and the apoptosis intrinsic signalling pathways via western blots measured by increased activation of Bax, caspase-3, caspase-9 and a decrease in the activation of Bcl-2. Most notably, the administration of RNase 1 resulted in a decrease in both cardiac apoptosis and cardiac dysfunction.

In the context of SARS-CoV-2, the role of RNase A has yet to be evaluated. However, in SARS-CoV (which is genetically similar to SARS-CoV-2 (357)) the crystallographic study of coronavirus revealed that the active site of endoribonuclease is structurally similar to that of RNase A (358). The effects of RNase A inhibitors on coronavirus resulted in a decrease of coronavirus replication in cell culture (359), indicating that they have the potential to modulate viral replication. Further studies are required to understand the role of RNase in SARS-Cov-2.

5.5 Limitations of the studies

One of the major limitations of all of the studies that I have done in this thesis is the inability to perform survival studies. There are strict regulations governing such experiments due to the inevitable pain and suffering these animals would have to endure. The lack of survival

(mortality data) is a major shortcoming of the preclinical efficacy studies reported here and may cast doubt when over my conclusion that e.g. BTK-inhibitors may be useful for the treatment of patients with sepsis. I have shown that delayed administration of ibrutinib or acalabrutinib protects mice against the consequences of sepsis for 24 h, but it is not clear whether these early beneficial effects can be sustained in a prolonged sepsis model. I have used the reduction in body temperature < 30°C as a surrogate marker to predict survival, but ideally survival studies may need to be conducted. Even in clinical trials, long term studies are not carried out, as normally a 28-day or 30-day mortality study is conducted and many patients have significant morbidity and even mortality after day 28/30 (360). Within the hospital setting, we have seen an improvement in 28-day mortality, however, there is an increase with associated-sepsis mortality that escalates yearly. Historically early deaths are associated with inadequate resuscitation and cardiac failure between 0 – 10 days, with a spike in late deaths occurring between 20 - 30 days due to persistent organ injury/failure (361,362). Nowadays this has been evaluated and is determined that two early peaks occur between 0 – 30 days with mortality being much lower than the past. However, late deaths occur after 60 days and continue to rise over time (362) (Figure 5.1).

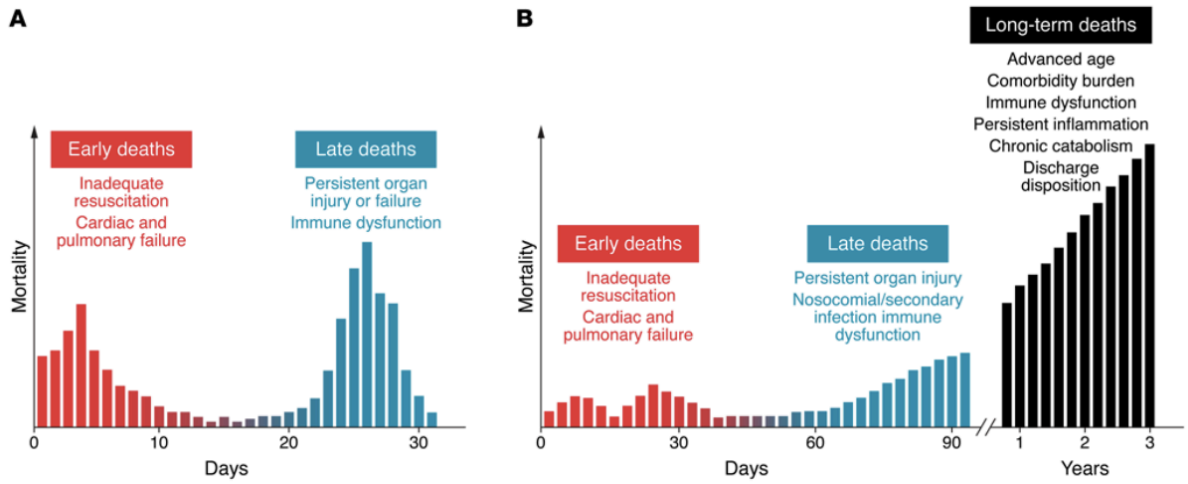

Figure 5.1 Historical and current sepsis mortality distribution. (A) Historic mortality. **(B)** Modern mortality over time. The figure is taken from (362).

I have performed all these experiments on young healthy male mice. However, sepsis is not exclusive in healthy males, as it is a disease effecting everyone from neonatal to the elderly (where sepsis is most prominent) and of course both sexes. The majority of our ageing population present with co-morbidities, which impact on the septic response: for instance, type

1 and 2 diabetes have been shown to exacerbate sepsis and result in a higher mortality (242). In humans, comorbidities like type 1 and 2 diabetes are common among the population along with hypertension, cancer, atherosclerosis and renal disease. In CLP-sepsis, the degree of organ injury/dysfunction caused by CLP is age-dependent, with older mice experiencing more severe organ failure (363–366). I choose to perform these experiments exclusively in young healthy males for a number of reasons. Firstly, the three Rs. It has been shown that females have a natural protection against sepsis due to higher levels of circulating oestrogen or their precursors (367,368). High levels of oestrogen and/or oestradiol results in an increase in the activation of Akt, eNOS and a decrease in the activation of NF-κB and production of pro-inflammatory cytokines, resulting in protection of cardiac dysfunction caused by sepsis, endotoxaemia (368), ischemia-reperfusion injury (369), or trauma-haemorrhage (370). Thus, if I included males and females into the study, I would have to increase the numbers of my mice. To my knowledge, there is no evidence that interventions work in males, but not in females. By trying to reduce the number of mice used I choose to exclusively perform these experiments on male mice. Secondly, the cost of aged mice or mice with co-morbidities increases drastically, making it unfeasible to routinely perform experiments in these animals. As *Xid* mice are X-linked dependent, it is also more difficult to obtain *Xid* females than *Xid* male mice.

5.6 Future investigations

I choose to administer BTK inhibitors 1 h after CLP surgery due to measurable septic parameters being visible within 1 h (decrease in CO and SV). However, in a clinical setting no patient receives a treatment within 1 h of an infection. It would be interesting to determine how late after onset of septic insult can BTK inhibitors be administered and still observe a positive effect. My time course data in chapter 2 suggests that the mouse is able to control the infection up to 12 h, indicating that there is a 12 h therapeutic window. Future studies could test out my hypothesis of administering BTK inhibitors at 3, 6 and 12 h after CLP surgery. Ideally if survival studies could be carried out this would also improve the model and translatability of the findings.

I found that *Xid* mice subjected to CLP have the same percentage of macrophages and neutrophils phagocytosing bacteria, but *Xid*-mice with CLP phagocytose more bacteria per immune cell when compared to WT-mice. This raises the question of the underlying mechanisms that enables or drives increased phagocytosis in *Xid*-mice? However, the exact

molecular mechanisms underlying this phenomenon are yet to be elucidated. Future studies are required to increase our understanding as to how *Xid* macrophages and neutrophils phagocytose more bacteria per immune cell.

By reanalysing Parnell *et al*. dataset I revealed that BTK expression was significantly increased in septic non-survivors and that BTK expression was similar in septic survivors and healthy patients. This indicates that increased BTK expression in septic patients correlates with mortality. This is an interesting finding, but it was conducted on a small cohort. It would be beneficial to confirm Parnell *et al*. findings of increased expression of BTK in septic non-survivors by analysing BTK activation and pro-inflammatory cytokines in the blood of septic patients in a larger cohort.

Considering sepsis results in multiple organ failure and one of the main causes of infection is pneumonia, I have not looked at lung inflammation in my model of sepsis. It would have been useful to measure bacteria and infiltrating immune cells in bronchoalveolar lavage fluid. De Porto *et al*. showed that treatment with ibrutinib 3 h before and 9 h after intranasal LTA instillation (a model of pneumonia) reduced the infiltration and activation of macrophages and neutrophils, resulting in decreased release of cytokines and plasma leakage into the lungs (272). However, research has shown that in severe CLP (mice predicted to die) CLP-septic mice do not result in significant levels of lung injury as demonstrated by normal levels of arterial oxygen saturation, no increase in pro- or anti- inflammatory cytokines in bronchoalveolar fluid, no increase in recruitment of neutrophils in the lung and no histological evidence of damage to the lung (325).

The number of sepsis cases is rising and globally it is the number one cause of death. However, for those who do recover from sepsis face a future battle, cognitive impairment and functional disability (371). Unfortunately, there is little research on the long-term effects of sepsis on cognitive and functional limitations, despite the fact these issues put a major financial burden on the healthcare system as well as families/caregivers of the affected (372). It is suspected that many patients are discharged with cognitive and functional impairments (373) and the onset of disability is associated with increased mortality (374). Future research is required to look into these issues which maybe partially preventable. It would be interesting to investigate the effect of BTK inhibitors on cognitive function in septic mice.

5.7 Conclusion

In conclusion in this thesis, I have shown that BTK-inhibitors ibrutinib or acalabrutinib attenuate sepsis-induced cardiac dysfunction by reducing the production of cytokines/chemokines in serum and reducing the activation of cardiac BTK, NF-κB and the NLRP3 inflammasome. I have also shown that these effects are exclusively due to BTK inhibition by showing that *Xid* mice (which have a deficiency in the activation of BTK) are protected from developing sepsis-induced multiple organ failure (cardiac, renal and hepatocellular injury) and excessive systemic inflammation (cytokine storm). I find that the administration of ibrutinib (a non-specific BTK inhibitor) results in no further benefit or adverse effect on septic *Xid* mice. In the *Xid* mice, they present with a reduced number of infiltrating macrophages and neutrophils, which show enhanced phagocytosis ability resulting in fewer bacteria in the peritoneal cavity. The *Xid* macrophages polarise to an M2 anti-inflammatory state aiding in the resolution of sepsis. I propose that BTK inhibitors could be repurposed for sepsis. Finally, I have shown that the administration of the antimicrobial peptide RNase 1 attenuates sepsis-induced cardiac dysfunction and cardiac apoptosis.

References

1. Geroulanos S, Douka ET. Historical perspective of the word "sepsis." *Intensive Care Med* (2006) **32**:2077. doi:10.1007/s00134-006-0392-2
2. Loudon I. Ignaz Phillip Semmelweis' studies of death in childbirth. *J R Soc Med* (2013) **106**:461–3. doi:10.1177/0141076813507844
3. Pitt D, Aubin J-M. Joseph Lister: father of modern surgery. *Can J Surg* (2012) **55**:E8-9. doi:10.1503/cjs.007112
4. Bone AC, Balk RA, Cerra FB, Dellinger RP, Fein AM, Knaus WA, Schein RM, Sibbaid WJ. American College of Chest Physicians/Society of Critical Care Medicine Consensus Conference: definitions for sepsis and organ failure and guidelines for the use of innovative therapies in sepsis. *Crit Care Med* (1992) **20**:864–874.
5. Levy MM, Fink MP, Marshall JC, Abraham E, Angus D, Cook D, Cohen J, Opal SM, Vincent JL, Ramsay G. 2001 SCCM/ESICM/ACCP/ATS/SIS International Sepsis Definitions Conference. *Intensive Care Med* (2003) **29**:530–538. doi:10.1007/s00134-003-1662-x
6. Rathour S, Kumar S, Hadda V, Bhalla A, Sharma N, Varma S. PIRO concept: staging of sepsis. *J Postgr Med* (2015) **61**:235–242. doi:10.4103/0022-3859.166511
7. Vincent JL, Opal SM, Marshall JC, Tracey KJ. Sepsis definitions: time for change. *Lancet* (2013) **381**:774–775. doi:10.1016/s0140-6736(12)61815-7
8. Singer M, Deutschman CS, Seymour CW, Shankar-Hari M, Annane D, Bauer M, Bellomo R, Bernard GR, Chiche J-DD, Coopersmith CM, et al. The Third International Consensus Definitions for Sepsis and Septic Shock (Sepsis-3). *JAMA* (2016) **315**:801–810. doi:10.1001/jama.2016.0287
9. Churpek MM, Zadravecz FJ, Winslow C, Howell MD, Edelson DP. Incidence and Prognostic Value of the Systemic Inflammatory Response Syndrome and Organ Dysfunctions in Ward Patients. *Am J Respir Crit Care Med* (2015) **192**:958–964. doi:10.1164/rccm.201502-0275OC
10. Hotchkiss RS, Monneret G, Payen D. Sepsis-induced immunosuppression: from cellular dysfunctions to immunotherapy. *Nat Rev Immunol* (2013) **13**:862–874. doi:10.1038/nri3552
11. Vincent JL, de Mendonca A, Cantraine F, Moreno R, Takala J, Suter PM, Sprung CL, Colardyn F, Blecher S. Use of the SOFA score to assess the incidence of organ

dysfunction/failure in intensive care units: results of a multicenter, prospective study. Working group on “sepsis-related problems” of the European Society of Intensive Care Medicine. *Crit Care Med* (1998) **26**:1793–1800.

12. Finkelsztein EJ, Jones DS, Ma KC, Pabón MA, Delgado T, Nakahira K, Arbo JE, Berlin DA, Schenck EJ, Choi AMK, et al. Comparison of qSOFA and SIRS for predicting adverse outcomes of patients with suspicion of sepsis outside the intensive care unit. *Crit Care* (2017) **21**:73. doi:10.1186/s13054-017-1658-5
13. Rudd KE, Johnson SC, Agesa KM, Shackelford KA, Tsoi D, Kievlan DR, Colombara D V, Ikuta KS, Kissoon N, Finfer S, et al. Global, regional, and national sepsis incidence and mortality, 1990-2017: analysis for the Global Burden of Disease Study. *Lancet (London, England)* (2020) **395**:200–211. doi:10.1016/S0140-6736(19)32989-7
14. Bennett S. Sepsis in the intensive care unit - ScienceDirect. *ScienceDirect* (2012) **30**:673–678.
15. Tsertsvadze A, Royle P, McCarthy N. Community-onset sepsis and its public health burden: protocol of a systematic review. *Syst Rev* (2015) **4**:119. doi:10.1186/s13643-015-0103-6
16. Padkin A, Goldfrad C, Brady AR, Young D, Black N, Rowan K. Epidemiology of severe sepsis occurring in the first 24 hrs in intensive care units in England, Wales, and Northern Ireland. *Crit Care Med* (2003) **31**:2332–2338. doi:10.1097/01.ccm.0000085141.75513.2b
17. Martin GS, Mannino DM, Eaton S, Moss M. The epidemiology of sepsis in the United States from 1979 through 2000. *N Engl J Med* (2003) **348**:1546–54. doi:10.1056/NEJMoa022139
18. Dombrovskiy VY, Martin AA, Sunderram J, Paz HL. Rapid increase in hospitalization and mortality rates for severe sepsis in the United States: a trend analysis from 1993 to 2003. *Crit Care Med* (2007) **35**:1244–50. doi:10.1097/01.CCM.0000261890.41311.E9
19. Kumar G, Kumar N, Taneja A, Kaleekal T, Tarima S, McGinley E, Jimenez E, Mohan A, Khan RA, Whittle J, et al. Nationwide trends of severe sepsis in the 21st century (2000-2007). *Chest* (2011) **140**:1223–1231. doi:10.1378/chest.11-0352
20. Rubens M, Saxena A, Ramamoorthy V, Das S, Khera R, Hong J, Armaignac D, Veledar E, Nasir K, Gidel L. Increasing Sepsis Rates in the United States: Results From National Inpatient Sample, 2005 to 2014. *J Intensive Care Med* (2020) **35**:858–868. doi:10.1177/0885066618794136

21. Rhee C, Klompas M. Sepsis trends: increasing incidence and decreasing mortality, or changing denominator? *J Thorac Dis* (2020) **12**:S89–S100. doi:10.21037/jtd.2019.12.51
22. Martin GS. Sepsis, severe sepsis and septic shock: changes in incidence, pathogens and outcomes. *Expert Rev Anti Infect Ther* (2012) **10**:701–706. doi:10.1586/eri.12.50
23. Hall MJ, Williams SN, DeFrances CJ, Golosinskiy A. Inpatient care for septicemia or sepsis: a challenge for patients and hospitals. *NCHS Data Brief* (2011)1–8.
24. Harrison DA, Welch CA, Eddleston JM. The epidemiology of severe sepsis in England, Wales and Northern Ireland, 1996 to 2004: secondary analysis of a high quality clinical database, the ICNARC Case Mix Programme Database. *Crit Care* (2006) **10**:R42. doi:10.1186/cc4854
25. Cohen J, Vincent JL, Adhikari NK, Machado FR, Angus DC, Calandra T, Jaton K, Giulieri S, Delaloye J, Opal S, et al. Sepsis: a roadmap for future research. *Lancet Infect Dis* (2015) **15**:581–614. doi:10.1016/s1473-3099(15)70112-x
26. Rhee C, Gohil S, Klompas M. Regulatory mandates for sepsis care--reasons for caution. *N Engl J Med* (2014) **370**:1673–1676. doi:10.1056/NEJMp1400276
27. Levy MM, Dellinger RP, Townsend SR, Linde-Zwirble WT, Marshall JC, Bion J, Schorr C, Artigas A, Ramsay G, Beale R, et al. The Surviving Sepsis Campaign: results of an international guideline-based performance improvement program targeting severe sepsis. *Crit Care Med* (2010) **38**:367–74. doi:10.1097/CCM.0b013e3181cb0cdc
28. Cannon CM, Holthaus C V, Zubrow MT, Posa P, Gunaga S, Kella V, Elkin R, Davis S, Turman B, Weingarten J, et al. The GENESIS project (GENeralized Early Sepsis Intervention Strategies): a multicenter quality improvement collaborative. *J Intensive Care Med* (2013) **28**:355–68. doi:10.1177/0885066612453025
29. Miller RR, Dong L, Nelson NC, Brown SM, Kuttler KG, Probst DR, Allen TL, Clemmer TP, Intermountain Healthcare Intensive Medicine Clinical Program. Multicenter implementation of a severe sepsis and septic shock treatment bundle. *Am J Respir Crit Care Med* (2013) **188**:77–82. doi:10.1164/rccm.201212-2199OC
30. Gaieski DF, Edwards JM, Kallan MJ, Carr BG. Benchmarking the incidence and mortality of severe sepsis in the United States. *Crit Care Med* (2013) **41**:1167–1174. doi:10.1097/CCM.0b013e31827c09f8
31. Angus DC, Linde-Zwirble WT, Lidicker J, Clermont G, Carcillo J, Pinsky MR.

Epidemiology of severe sepsis in the United States: analysis of incidence, outcome, and associated costs of care. *Crit Care Med* (2001) **29**:1303–1310.

32. Finfer S, Bellomo R, Lipman J, French C, Dobb G, Myburgh J. Adult-population incidence of severe sepsis in Australian and New Zealand intensive care units. *Intensive Care Med* (2004) **30**:589–596. doi:10.1007/s00134-004-2157-0
33. Alberti C, Brun-Buisson C, Burchardi H, Martin C, Goodman S, Artigas A, Sicignano A, Palazzo M, Moreno R, Boulme R, et al. Epidemiology of sepsis and infection in ICU patients from an international multicentre cohort study. *Intensive Care Med* (2002) **28**:108–121. doi:10.1007/s00134-001-1143-z
34. McPherson D, Griffiths C, Williams M, Baker A, Klodawski E, Jacobson B, Donaldson L. Sepsis-associated mortality in England: an analysis of multiple cause of death data from 2001 to 2010. *BMJ Open* (2013) **3**: doi:10.1136/bmjopen-2013-002586
35. Murray CJ, Lopez AD. Measuring the global burden of disease. *N Engl J Med* (2013) **369**:448–457. doi:10.1056/NEJMra1201534
36. Vincent JL, Rello J, Marshall J, Silva E, Anzueto A, Martin CD, Moreno R, Lipman J, Gomersall C, Sakr Y, et al. International study of the prevalence and outcomes of infection in intensive care units. *Jama* (2009) **302**:2323–2329. doi:10.1001/jama.2009.1754
37. Fleischmann C, Scherag A, Adhikari NKJ, Hartog CS, Tsaganos T, Schlattmann P, Angus DC, Reinhart K. Assessment of Global Incidence and Mortality of Hospital-treated Sepsis. Current Estimates and Limitations. *Am J Respir Crit Care Med* (2016) **193**:259–272. doi:10.1164/rccm.201504-0781OC
38. Dellinger RP, Carlet JM, Masur H, Gerlach H, Calandra T, Cohen J, Gea-Banacloche J, Keh D, Marshall JC, Parker MM, et al. Surviving Sepsis Campaign guidelines for management of severe sepsis and septic shock. *Crit Care Med* (2004) **32**:858–873.
39. Dellinger RP, Levy MM, Carlet JM, Bion J, Parker MM, Jaeschke R, Reinhart K, Angus DC, Brun-Buisson C, Beale R, et al. Surviving Sepsis Campaign: International guidelines for management of severe sepsis and septic shock: 2008. *Intensive Care Med* (2008) **34**:17–60. doi:10.1007/s00134-007-0934-2
40. Dellinger RP, Levy MM, Rhodes A, Annane D, Gerlach H, Opal SM, Sevransky JE, Sprung CL, Douglas IS, Jaeschke R, et al. Surviving sepsis campaign: international guidelines for management of severe sepsis and septic shock: 2012. *Crit Care Med*

(2013) **41**:580–637. doi:10.1097/CCM.0b013e31827e83af

41. Weiss SL, Peters MJ, Alhazzani W, Agus MSD, Flori HR, Inwald DP, Nadel S, Schlapbach LJ, Tasker RC, Argent AC, et al. Surviving Sepsis Campaign International Guidelines for the Management of Septic Shock and Sepsis-Associated Organ Dysfunction in Children. *Pediatr Crit Care Med* (2020) **21**:e52–e106. doi:10.1097/PCC.0000000000002198
42. Barochia A V, Cui X, Eichacker PQ. The Surviving Sepsis Campaign's Revised Sepsis Bundles. *Curr Infect Dis Rep* (2013) **15**: doi:10.1007/s11908-013-0351-3
43. Rhodes A, Phillips G, Beale R, Cecconi M, Chiche JD, De Backer D, Divatia J, Du B, Evans L, Ferrer R, et al. The Surviving Sepsis Campaign bundles and outcome: results from the International Multicentre Prevalence Study on Sepsis (the IMPreSS study). *Intensive Care Med* (2015) **41**:1620–1628. doi:10.1007/s00134-015-3906-y
44. Rhodes A, Evans LE, Alhazzani W, Levy MM, Antonelli M, Ferrer R, Kumar A, Sevransky JE, Sprung CL, Nunnally ME, et al. Surviving Sepsis Campaign: International Guidelines for Management of Sepsis and Septic Shock: 2016. *Intensive Care Med* (2017) **43**:304–377. doi:10.1007/s00134-017-4683-6
45. Levy MM, Evans LE, Rhodes A. The Surviving Sepsis Campaign Bundle: 2018 update. *Intensive Care Med* (2018) **44**:925–928. doi:10.1007/s00134-018-5085-0
46. Kumar A, Roberts D, Wood KE, Light B, Parrillo JE, Sharma S, Suppes R, Feinstein D, Zanotti S, Taiberg L, et al. Duration of hypotension before initiation of effective antimicrobial therapy is the critical determinant of survival in human septic shock. *Crit Care Med* (2006) **34**:1589–1596. doi:10.1097/01.ccm.0000217961.75225.e9
47. De Backer D, Biston P, Devriendt J, Madl C, Chochrad D, Aldecoa C, Brasseur A, Defrance P, Gottignies P, Vincent J-L, et al. Comparison of dopamine and norepinephrine in the treatment of shock. *N Engl J Med* (2010) **362**:779–89. doi:10.1056/NEJMoa0907118
48. De Backer D, Aldecoa C, Njimi H, Vincent J-L. Dopamine versus norepinephrine in the treatment of septic shock: a meta-analysis*. *Crit Care Med* (2012) **40**:725–30. doi:10.1097/CCM.0b013e31823778ee
49. Asfar P, Meziani F, Hamel J-F, Grelon F, Megarbane B, Anguel N, Mira J-P, Dequin P-F, Gergaud S, Weiss N, et al. High versus low blood-pressure target in patients with septic shock. *N Engl J Med* (2014) **370**:1583–93. doi:10.1056/NEJMoa1312173
50. Lamontagne F, Meade MO, Hébert PC, Asfar P, Lauzier F, Seely AJE, Day AG,

Mehta S, Muscedere J, Bagshaw SM, et al. Higher versus lower blood pressure targets for vasopressor therapy in shock: a multicentre pilot randomized controlled trial. *Intensive Care Med* (2016) **42**:542–550. doi:10.1007/s00134-016-4237-3

51. Mikkelsen ME, Miltiades AN, Gaieski DF, Goyal M, Fuchs BD, Shah C V, Bellamy SL, Christie JD. Serum lactate is associated with mortality in severe sepsis independent of organ failure and shock. *Crit Care Med* (2009) **37**:1670–7. doi:10.1097/CCM.0b013e31819fcf68
52. Trzeciak S, Dellinger RP, Chansky ME, Arnold RC, Schorr C, Milcarek B, Hollenberg SM, Parrillo JE. Serum lactate as a predictor of mortality in patients with infection. *Intensive Care Med* (2007) **33**:970–7. doi:10.1007/s00134-007-0563-9
53. Shapiro NI, Howell MD, Talmor D, Nathanson LA, Lisbon A, Wolfe RE, Weiss JW. Serum Lactate as a Predictor of Mortality in Emergency Department Patients with Infection. *Ann Emerg Med* (2005) **45**:524–528. doi:10.1016/j.annemergmed.2004.12.006
54. Nguyen HB, Rivers EP, Knoblich BP, Jacobsen G, Muzzin A, Ressler JA, Tomlanovich MC. Early lactate clearance is associated with improved outcome in severe sepsis and septic shock. *Crit Care Med* (2004) **32**:1637–42. doi:10.1097/01.ccm.0000132904.35713.a7
55. Marik P, Bellomo R. Lactate clearance as a target of therapy in sepsis: A flawed paradigm. *OA Crit Care* (2013) **1**: doi:10.13172/2052-9309-1-1-431
56. Cao C, Yu M, Chai Y. Pathological alteration and therapeutic implications of sepsis-induced immune cell apoptosis. *Cell Death Dis* (2019) **10**:782. doi:10.1038/s41419-019-2015-1
57. Dolin HH, Papadimos TJ, Chen X, Pan ZK. Characterization of Pathogenic Sepsis Etiologies and Patient Profiles: A Novel Approach to Triage and Treatment. *Microbiol insights* (2019) **12**:1178636118825081. doi:10.1177/1178636118825081
58. Leibovici L, Shraga I, Drucker M, Konigsberger H, Samra Z, Pitlik SD. The benefit of appropriate empirical antibiotic treatment in patients with bloodstream infection. *J Intern Med* (1998) **244**:379–86. doi:10.1046/j.1365-2796.1998.00379.x
59. Taylor PR, Roy S, Leal SM, Sun Y, Howell SJ, Cobb BA, Li X, Pearlman E. Activation of neutrophils by autocrine IL-17A-IL-17RC interactions during fungal infection is regulated by IL-6, IL-23, RORγt and dectin-2. *Nat Immunol* (2014) **15**:143–51. doi:10.1038/ni.2797

60. Page DB, Donnelly JP, Wang HE. Community-, Healthcare-, and Hospital-Acquired Severe Sepsis Hospitalizations in the University HealthSystem Consortium. *Crit Care Med* (2015) **43**:1945–51. doi:10.1097/CCM.0000000000001164
61. Pittet D, Wenzel RP. Nosocomial bloodstream infections. Secular trends in rates, mortality, and contribution to total hospital deaths. *Arch Intern Med* (1995) **155**:1177–1184.
62. Trick WE, Jarvis WR. Epidemiology of nosocomial fungal infection in the 1990s. *Rev Iberoam Micol* (1998) **15**:2–6.
63. Burchard KW, Minor LB, Slotman GJ, Gann DS. Fungal sepsis in surgical patients. *Arch Surg* (1983) **118**:217–21. doi:10.1001/archsurg.1983.01390020065011
64. Zahar J-R, Timsit J-F, Garrouste-Orgeas M, Français A, Vesin A, Vesim A, Descorps-Declere A, Dubois Y, Souweine B, Haouache H, et al. Outcomes in severe sepsis and patients with septic shock: pathogen species and infection sites are not associated with mortality. *Crit Care Med* (2011) **39**:1886–95. doi:10.1097/CCM.0b013e31821b827c
65. Lin G-L, McGinley JP, Drysdale SB, Pollard AJ. Epidemiology and Immune Pathogenesis of Viral Sepsis. *Front Immunol* (2018) **9**:2147. doi:10.3389/fimmu.2018.02147
66. Southeast Asia Infectious Disease Clinical Research Network D. Causes and outcomes of sepsis in southeast Asia: a multinational multicentre cross-sectional study. *Lancet Glob Heal* (2017) **5**:e157–e167. doi:10.1016/S2214-109X(17)30007-4
67. Chowell G, Bertozzi SM, Colchero MA, Lopez-Gatell H, Alpuche-Aranda C, Hernandez M, Miller MA. Severe respiratory disease concurrent with the circulation of H1N1 influenza. *N Engl J Med* (2009) **361**:674–9. doi:10.1056/NEJMoa0904023
68. Shane AL, Sánchez PJ, Stoll BJ. Neonatal sepsis. *Lancet (London, England)* (2017) **390**:1770–1780. doi:10.1016/S0140-6736(17)31002-4
69. Lin G-L, McGinley JP, Drysdale SB, Pollard AJ. Epidemiology and Immune Pathogenesis of Viral Sepsis. *Front Immunol* (2018) **9**: doi:10.3389/FIMMU.2018.02147
70. Li H, Liu L, Zhang D, Xu J, Dai H, Tang N, Su X, Cao B. SARS-CoV-2 and viral sepsis: observations and hypotheses. *Lancet (London, England)* (2020) **395**:1517–1520. doi:10.1016/S0140-6736(20)30920-X
71. Guo Y-R, Cao Q-D, Hong Z-S, Tan Y-Y, Chen S-D, Jin H-J, Tan K-S, Wang D-Y, Yan Y. The origin, transmission and clinical therapies on coronavirus disease 2019

(COVID-19) outbreak – an update on the status. *Mil Med Res* (2020) **7**:11. doi:10.1186/s40779-020-00240-0

72. Huang C, Wang Y, Li X, Ren L, Zhao J, Hu Y, Zhang L, Fan G, Xu J, Gu X, et al. Clinical features of patients infected with 2019 novel coronavirus in Wuhan, China. *Lancet (London, England)* (2020) **395**:497–506. doi:10.1016/S0140-6736(20)30183-5
73. Zhou F, Yu T, Du R, Fan G, Liu Y, Liu Z, Xiang J, Wang Y, Song B, Gu X, et al. Clinical course and risk factors for mortality of adult inpatients with COVID-19 in Wuhan, China: a retrospective cohort study. *Lancet* (2020) **395**:1054–1062. doi:10.1016/S0140-6736(20)30566-3
74. Ruan Q, Yang K, Wang W, Jiang L, Song J. Clinical predictors of mortality due to COVID-19 based on an analysis of data of 150 patients from Wuhan, China. *Intensive Care Med* (2020) **46**:846–848. doi:10.1007/s00134-020-05991-x
75. Newton K, Dixit VM. Signaling in Innate Immunity and Inflammation. *Cold Spring Harb Perspect Biol* (2012) **4**:a006049. doi:10.1101/cshperspect.a006049
76. Takeuchi O, Akira S. Pattern recognition receptors and inflammation. *Cell* (2010) **140**:805–820. doi:10.1016/j.cell.2010.01.022
77. Mogensen TH. Pathogen Recognition and Inflammatory Signaling in Innate Immune Defenses. *Clin Microbiol Rev* (2009) **22**:240–273. doi:10.1128/cmr.00046-08
78. Abraham E. Nuclear factor-kappaB and its role in sepsis-associated organ failure. *J Infect Dis* (2003) **187 Suppl**:S364-9. doi:10.1086/374750
79. Akira S, Uematsu S, Takeuchi O. Pathogen recognition and innate immunity. *Cell* (2006) **124**:783–801. doi:10.1016/j.cell.2006.02.015
80. Oliveira-Nascimento L, Massari P, Wetzler LM. The Role of TLR2 in Infection and Immunity. *Front Immunol* (2012) **3**:1–17. doi:10.3389/fimmu.2012.00079
81. Ramachandran G. Gram-positive and gram-negative bacterial toxins in sepsis: A brief review. *Virulence* (2014) **5**:213–218. doi:10.4161/viru.27024
82. Qiao S, Luo Q, Zhao Y, Zhang XC, Huang Y. Structural basis for lipopolysaccharide insertion in the bacterial outer membrane. *Nature* (2014) **511**:108–111. doi:doi:10.1038/nature13484
83. Morath S, Geyer A, Hartung T. Structure–Function Relationship of Cytokine Induction by Lipoteichoic Acid fromStaphylococcus aureus. *J Exp Med* (2001) **193**:393–398.
84. Beeby M, Gumbart JC, Roux B, Jensen GJ. Architecture and assembly of the Gram-positive cell wall. *Mol Microbiol* (2013) **88**:664–672. doi:10.1111/mmi.12203

85. Annane D, Bellissant E, Cavaillon JM. Septic shock. *Lancet* (2005) **365**:63–78. doi:10.1016/s0140-6736(04)17667-8

86. Hailman E, Henri S. Lichenstein David S. Miller, David A. Johnson, Michael Kelley, LeighA. Busse,MarkM. Zukowski, and SamuelD. Wright MMW. Lipopolysaccharide (LPS)-binding protein accelerates the binding of LPS to CD14. *J Exp Med* (1994) **179**:269–277.

87. Park BS, Lee JO. Recognition of lipopolysaccharide pattern by TLR4 complexes. *Exp Mol Med* (2013) **45**:e66-. doi:10.1038/emm.2013.97

88. O'Neill LAJ, Bowie AG. The family of five: TIR-domain-containing adaptors in Toll-like receptor signalling. *Nat Rev Immunol* (2007) **7**:353–364. doi:doi:10.1038/nri2079

89. Ye H, Arron JR, Lamothe B, Cirilli M, Kobayashi T, Shevde NK, Segal D, Dzivenu OK, Vologodskaia M, Yim M, et al. Distinct molecular mechanism for initiating TRAF6 signalling. *Nature* (2002) **418**:443–447. doi:10.1038/nature00888

90. Xia ZP, Sun L, Chen X, Pineda G, Jiang X, Adhikari A, Zeng W, Chen ZJ. Direct activation of protein kinases by unanchored polyubiquitin chains. *Nature* (2009) **461**:114–119. doi:10.1038/nature08247

91. Herman SE, Mustafa RZ, Gyamfi JA, Pittaluga S, Chang S, Chang B, Farooqui M, Wiestner A. Ibrutinib inhibits BCR and NF-kappaB signaling and reduces tumor proliferation in tissue-resident cells of patients with CLL. *Blood* (2014) **123**:3286–3295. doi:10.1182/blood-2014-02-548610

92. Jacobs MD, Harrison SC. Structure of an IkappaBalpha/NF-kappaB complex. *Cell* (1998) **95**:749–758.

93. Israël A. The IKK Complex, a Central Regulator of NF-κB Activation. *Cold Spring Harb Perspect Biol* (2010) **2**:a000158. doi:10.1101/cshperspect.a000158

94. Johnson GL, Nakamura K. The c-Jun Kinase/Stress-activated Pathway: Regulation, Function and Role in Human Disease. *Biochim Biophys Acta* (2007) **1773**:1341–1348. doi:10.1016/j.bbamcr.2006.12.009

95. Kagan JC, Su T, Horng T, Chow A, Akira S, Medzhitov R. TRAM couples endocytosis of Toll-like receptor 4 to the induction of interferon-beta. *Nat Immunol* (2008) **9**:361–368. doi:10.1038/ni1569

96. Yamamoto M, Sato S, Hemmi H, Uematsu S, Hoshino K, Kaisho T, Takeuchi O, Takeda K, Akira S. TRAM is specifically involved in the Toll-like receptor 4-mediated MyD88-independent signaling pathway. *Nat Immunol* (2003) **4**:1144–1150.

doi:10.1038/ni986

97. Taniguchi T, Ogasawara K, Takaoka A, Tanaka N. IRF family of transcription factors as regulators of host defense. *Annu Rev Immunol* (2001) **19**:623–655. doi:10.1146/annurev.immunol.19.1.623

98. Hacker H, Redecke V, Blagoev B, Kratchmarova I, Hsu LC, Wang GG, Kamps MP, Raz E, Wagner H, Hacker G, et al. Specificity in Toll-like receptor signalling through distinct effector functions of TRAF3 and TRAF6. *Nature* (2006) **439**:204–207. doi:10.1038/nature04369

99. Sato M, Suemori H, Hata N, Asagiri M, Ogasawara K, Nakao K, Nakaya T, Katsuki M, Noguchi S, Tanaka N, et al. Distinct and essential roles of transcription factors IRF-3 and IRF-7 in response to viruses for IFN-alpha/beta gene induction. *Immunity* (2000) **13**:539–548.

100. Cunnion RE, Schaer GL, Parker MM, Natanson C, Parrillo JE. The coronary circulation in human septic shock. *Circulation* (1986) **73**:637–644.

101. Rabuel C, Mebazaa A. Septic shock: a heart story since the 1960s. *Intensive Care Med* (2006) **32**:799–807. doi:10.1007/s00134-006-0142-5

102. Martinon F, Burns K, Tschopp J. The inflammasome: a molecular platform triggering activation of inflammatory caspases and processing of proIL-beta. *Mol Cell* (2002) **10**:417–426.

103. Hotchkiss RS, Karl IE. Reevaluation of the role of cellular hypoxia and bioenergetic failure in sepsis. *Jama* (1992) **267**:1503–1510.

104. Zhang W, Tao A, Lan T, Cepinskas G, Kao R, Martin CM, Rui T. Carbon monoxide releasing molecule-3 improves myocardial function in mice with sepsis by inhibiting NLRP3 inflammasome activation in cardiac fibroblasts. *Basic Res Cardiol* (2017) **112**:16. doi:10.1007/s00395-017-0603-8

105. Lee S, Nakahira K, Dalli J, Siempos II, Norris PC, Colas RA, Moon J-S, Shinohara M, Hisata S, Howrylak JA, et al. NLRP3 Inflammasome Deficiency Protects against Microbial Sepsis via Increased Lipoxin B $_4$ Synthesis. *Am J Respir Crit Care Med* (2017) **196**:713–726. doi:10.1164/rccm.201604-0892OC

106. Hunter JDD, Doddi M. Sepsis and the heart. *Br J Anaesth* (2010) **104**:3–11. doi:10.1093/bja/aep339

107. Parrillo JE, Parker MM, Natanson C, Suffredini AF, Danner RL, Cunnion RE, Ognibene FP. Septic shock in humans. Advances in the understanding of pathogenesis,

cardiovascular dysfunction, and therapy. *Ann Intern Med* (1990) **113**:227–242.

108. Kumar A, Thota V, Dee L, Olson J, Uretz E, Parrillo JE. Tumor necrosis factor alpha and interleukin 1beta are responsible for in vitro myocardial cell depression induced by human septic shock serum. *J Exp Med* (1996) **183**:949–58.
109. Schulz R, Panas DL, Catena R, Moncada S, Olley PM, Lopaschuk GD. The role of nitric oxide in cardiac depression induced by interleukin-1 beta and tumour necrosis factor-alpha. *Br J Pharmacol* (1995) **114**:27–34.
110. Zhong J, Hwang TC, Adams HR, Rubin LJ. Reduced L-type calcium current in ventricular myocytes from endotoxemic guinea pigs. *Am J Physiol* (1997) **273**:H2312-24.
111. Hinshaw LB. Sepsis/septic shock: participation of the microcirculation: an abbreviated review. *Crit Care Med* (1996) **24**:1072–1078.
112. Wiggers CJ. Myocardial depression in shock; a survey of cardiodynamic studies. *Am Hear J* (1947) **33**:633–650.
113. Parrillo JE, Burch C, Shelhamer JH, Parker MM, Natanson C, Schuette W. A circulating myocardial depressant substance in humans with septic shock. Septic shock patients with a reduced ejection fraction have a circulating factor that depresses in vitro myocardial cell performance. *J Clin Invest* (1985) **76**:1539–1553. doi:10.1172/jci112135
114. Finkel MS, Oddis C V, Jacob TD, Watkins SC, Hattler BG, Simmons RL. Negative inotropic effects of cytokines on the heart mediated by nitric oxide. *Science (80-)* (1992) **257**:387–389.
115. Zhang H, Park Y, Wu J, Chen X, Lee S, Yang J, Dellsperger K, Zhang C. Role of TNF-α in vascular dysfunction. *Clin Sci* (2009) **116**:219–230. doi:10.1042/cs20080196
116. Semeraro N, Ammollo CT, Semeraro F, Colucci M. Sepsis-Associated Disseminated Intravascular Coagulation and Thromboembolic Disease. *Mediterr J Hematol Infect Dis* (2010) **2**:e2010024. doi:10.4084/mjhid.2010.024
117. Wellmer A, Gerber J, Ragheb J, Zysk G, Kunst T, Smirnov A, Brück W, Nau R. Effect of Deficiency of Tumor Necrosis Factor Alpha or Both of Its Receptors on Streptococcus pneumoniae Central Nervous System Infection and Peritonitis. *Infect Immun* (2001) **69**:6881–6886. doi:10.1128/iai.69.11.6881-6886.2001
118. Parameswaran N, Patial S. Tumor necrosis factor-alpha signaling in macrophages. *Crit*

Rev Eukaryot Gene Expr (2010) **20**:87–103.

119. Panacek EA, Kaul M. IL-6 as a Marker of Excessive TNF-α Activity in Sepsis. *Sepsis* (1999) **3**:65–73. doi:10.1023/A:1009878726176
120. Moncada S, Higgs A. The L-arginine-nitric oxide pathway. *N Engl J Med* (1993) **329**:2002–2012. doi:10.1056/nejm199312303292706
121. Förstermann U, Sessa WC. Nitric oxide synthases: regulation and function. *Eur Hear J* (2012) **33**:829–837. doi:10.1093/eurheartj/ehr304
122. Khadour FH, Panas D, Ferdinandy P, Schulze C, Csont T, Lalu MM, Wildhirt SM, Schulz R. Enhanced NO and superoxide generation in dysfunctional hearts from endotoxemic rats. *Am J Physiol Hear Circ Physiol* (2002) **283**:H1108-15. doi:10.1152/ajpheart.00549.2001
123. Thiemermann C. Nitric oxide and septic shock. *Gen Pharmacol* (1997) **29**:159–166.
124. Szabo C, Southan GJ, Thiemermann C. Beneficial effects and improved survival in rodent models of septic shock with S-methylisothiourea sulfate, a potent and selective inhibitor of inducible nitric oxide synthase. *Proc Natl Acad Sci U S A* (1994) **91**:12472–12476.
125. Herbertson MJ, Werner HA, Walley KR. Nitric oxide synthase inhibition partially prevents decreased LV contractility during endotoxemia. *Am J Physiol* (1996) **270**:H1979-84. doi:10.1152/ajpheart.1996.270.6.H1979
126. Takasu O, Gaut JP, Watanabe E, To K, Fagley RE, Sato B, Jarman S, Efimov IR, Janks DL, Srivastava A, et al. Mechanisms of cardiac and renal dysfunction in patients dying of sepsis. *Am J Respir Crit Care Med* (2013) **187**:509–517. doi:10.1164/rccm.201211-1983OC
127. Crouser ED. Mitochondrial dysfunction in septic shock and multiple organ dysfunction syndrome. *Mitochondrion* (2004) **4**:729–741. doi:10.1016/j.mito.2004.07.023
128. Brealey D, Singer M. Mitochondrial Dysfunction in Sepsis. *Curr Infect Dis Rep* (2003) **5**:365–371.
129. Rudiger A, Singer M. Mechanisms of sepsis-induced cardiac dysfunction. *Crit Care Med* (2007) **35**:1599–1608. doi:10.1097/01.ccm.0000266683.64081.02
130. Abi-Gerges N Mebazaa A, et al. TB. Sequential changes in autonomic regula- tion of cardiac myocytes after in vivo endo- toxin injection in rat. *Am J Respir Crit Care Med* (1999) **160**:1196 –1204. doi:10.1186/s40779-016-0099-9
131. Buckley JF, Singer M, Clapp LH. Role of KATP channels in sepsis. *Cardiovasc Res*

(2006) **72**:220–230. doi:10.1016/j.cardiores.2006.07.011

132. Wu LL, Liu MS. Altered ryanodine receptor of canine cardiac sarcoplasmic reticulum and its underlying mechanism in endotoxin shock. *J Surg Res* (1992) **53**:82–90.

133. Ballard-Croft C, Maass DL, Sikes PJ, Horton JW. Sepsis and burn complicated by sepsis alter cardiac transporter expression. *Burns* (2007) **33**:72–80. doi:10.1016/j.burns.2006.06.009

134. Balija TM, Lowry SF. Lipopolysaccharide and sepsis-associated myocardial dysfunction. *Curr Opin Infect Dis* (2011) **24**:248–253. doi:10.1097/QCO.0b013e32834536ce

135. Hotchkiss R, Swanson. PE, Freeman B, Tinsley K, Cobb J, Matuschak G, Buchman T, Karl I. Apoptotic cell death in patients with sepsis, shock, and multiple organ dysfunction. *Crit Care Med* (1999) **27**: doi:10.1097/00003246-199907000-00002

136. Elmore S. Apoptosis: A Review of Programmed Cell Death. *Toxicol Pathol* (2007) **35**:495. doi:10.1080/01926230701320337

137. Li P, Nijhawan D, Budihardjo I, Srinivasula S, Ahmad M, Alnemri E, Wang X. Cytochrome c and dATP-dependent formation of Apaf-1/caspase-9 complex initiates an apoptotic protease cascade. *Cell* (1997) **91**: doi:10.1016/S0092-8674(00)80434-1

138. Englert JA, Bobba C, Baron RM. Integrating molecular pathogenesis and clinical translation in sepsis-induced acute respiratory distress syndrome. *JCI Insight* (2019) **4**: doi:10.1172/JCI.INSIGHT.124061

139. Chaudhry N, Duggal AK. Sepsis Associated Encephalopathy. *Adv Med* (2014) **2014**:762320. doi:10.1155/2014/762320

140. Sternbach GL. The Glasgow coma scale. *J Emerg Med* (2000) **19**:67–71. doi:10.1016/s0736-4679(00)00182-7

141. Rangel-Frausto MS, Pittet D, Costigan M, Hwang T, Davis CS, Wenzel RP. The natural history of the systemic inflammatory response syndrome (SIRS). A prospective study. *JAMA* (1995) **273**:117–23.

142. Neveu H, Kleinknecht D, Brivet F, Loirat P, Landais P. Prognostic factors in acute renal failure due to sepsis. Results of a prospective multicentre study. *Nephrol Dial Transplant* (1996) **11**:293–299. doi:10.1093/ndt/11.2.293

143. Zarbock A, Gomez H, Kellum JA. Sepsis-induced acute kidney injury revisited: pathophysiology, prevention and future therapies. *Curr Opin Crit Care* (2014) **20**:588–95. doi:10.1097/MCC.0000000000000153

144. Recknagel P, Gonnert FA, Westermann M, Lambeck S, Lupp A, Rudiger A, Dyson A, Carré JE, Kortgen A, Krafft C, et al. Liver dysfunction and phosphatidylinositol-3-kinase signalling in early sepsis: experimental studies in rodent models of peritonitis. *PLoS Med* (2012) **9**:e1001338. doi:10.1371/journal.pmed.1001338
145. Canabal JM, Kramer DJ. Management of sepsis in patients with liver failure. *Curr Opin Crit Care* (2008) **14**:189–197. doi:10.1097/MCC.0b013e3282f6a435
146. Gonnert FA, Kunisch E, Gajda M, Lambeck S, Weber M, Claus RA, Bauer M, Kinne RW. Hepatic Fibrosis in a Long-term Murine Model of Sepsis. *Shock* (2012) **37**:399–407. doi:10.1097/SHK.0b013e31824a670b
147. Protzer U, Maini MK, Knolle PA. Living in the liver: hepatic infections. *Nat Rev Immunol* (2012) **12**:201–213. doi:10.1038/nri3169
148. Bilzer M, Roggel F, Gerbes AL. Role of Kupffer cells in host defense and liver disease. *Liver Int* (2006) **26**:1175–1186. doi:10.1111/j.1478-3231.2006.01342.x
149. Deng M, Scott MJ, Loughran P, Gibson G, Sodhi C, Watkins S, Hackam D, Billiar TR. Lipopolysaccharide clearance, bacterial clearance, and systemic inflammatory responses are regulated by cell type-specific functions of TLR4 during sepsis. *J Immunol* (2013) **190**:5152–60. doi:10.4049/jimmunol.1300496
150. Wong CHY, Jenne CN, Petri B, Chrobok NL, Kubes P. Nucleation of platelets with bloodborne pathogens on Kupffer cell precedes other innate immunity and contributes to bacterial clearance. *Nat Immunol* (2013) **14**:785. doi:10.1038/NI.2631
151. Koo DJ, Chaudry IH, Wang P. Kupffer Cells Are Responsible for Producing Inflammatory Cytokines and Hepatocellular Dysfunction during Early Sepsis. *J Surg Res* (1999) **83**:151–157. doi:10.1006/jsre.1999.5584
152. Gustot T, Durand F, Lebrec D, Vincent J-L, Moreau R. Severe sepsis in cirrhosis. *Hepatology* (2009) **50**:2022–2033. doi:10.1002/hep.23264
153. Vetrie D, Vořechovský I, Sideras P, Holland J, Davies A, Flinter F, Hammarström L, Kinnon C, Levinsky R, Bobrow M, et al. The gene involved in X-linked agammaglobulinaemia is a member of the src family of protein-tyrosine kinases. *Nature* (1993) **361**:226–233. doi:10.1038/361226a0
154. Tsukada S, Saffran DC, Rawlings DJ, Parolini O, Allen RC, Klisak I, Sparkes RS, Kubagawa H, Mohandas T, Quan S. Deficient expression of a B cell cytoplasmic tyrosine kinase in human X-linked agammaglobulinemia. *Cell* (1993) **72**:279–90.
155. Weber ANR, Bittner Z, Liu X, Dang T-M, Radsak MP, Brunner C. Bruton's Tyrosine

Kinase: An Emerging Key Player in Innate Immunity. *Front Immunol* (2017) **8**:1454. doi:10.3389/fimmu.2017.01454

156. Mohamed AJ, Yu L, Backesjo CM, Vargas L, Faryal R, Aints A, Christensson B, Berglof A, Vihinen M, Nore BF, et al. Bruton's tyrosine kinase (Btk): function, regulation, and transformation with special emphasis on the PH domain. *Immunol Rev* (2009) **228**:58–73. doi:10.1111/j.1600-065X.2008.00741.x
157. Varnai P, Rother KI, Balla T. Phosphatidylinositol 3-kinase-dependent membrane association of the Bruton's tyrosine kinase pleckstrin homology domain visualized in single living cells. *J Biol Chem* (1999) **274**:10983–10989.
158. Yang W DS. BAP-135, a target for Bruton's tyrosine kinase in response to B cell receptor engagement. *Proc Natl Acad Sci U S A* (1997) **94**:604–609.
159. Park H, Wahl MI, Afar DE, Turck CW, Rawlings DJ, Tam C, Scharenberg AM, Kinet JP, Witte ON. Regulation of Btk function by a major autophosphorylation site within the SH3 domain. *Immunity* (1996) **4**:515–525.
160. Rodriguez R Perisic O, Bravo J, Paul A, Jones NP, Light Y,Swann K, Williams RL, Katan M M atsuda M. Tyrosine Residues in Phospholipase Cgamma 2 Essential for the Enzyme Function in B-Cell Signaling. *JBiolChem* (2017) **276**:47982–47992.
161. Petro JB, Rahman SM, Ballard DW, Khan WN. Bruton's tyrosine kinase is required for activation of IkappaB kinase and nuclear factor kappaB in response to B cell receptor engagement. *J Exp Med* (2000) **191**:1745–54. doi:10.1084/jem.191.10.1745
162. Berridge MJ. Inositol trisphosphate and calcium signalling. *Nature* (1993) **361**:315–325. doi:10.1038/361315a0
163. Li ZW, Chu W, Hu Y, Delhase M, Deerinck T, Ellisman M, Johnson R, Karin M. The IKKbeta subunit of IkappaB kinase (IKK) is essential for nuclear factor kappaB activation and prevention of apoptosis. *J Exp Med* (1999) **189**:1839–1845.
164. Jefferies CA, O'Neill LA. Bruton's tyrosine kinase (Btk)-the critical tyrosine kinase in LPS signalling? *Immunol Lett* (2004) **92**:15–22. doi:10.1016/j.imlet.2003.11.017
165. Horwood NJ, Page TH, McDaid JP, Palmer CD, Campbell J, Mahon T, Brennan FM, Webster D, Foxwell BM. Bruton's tyrosine kinase is required for TLR2 and TLR4-induced TNF, but not IL-6, production. *J Immunol* (2006) **176**:3635–3641.
166. Liu X, Pichulik T, Wolz O-O, Dang T-M, Stutz A, Dillen C, Delmiro Garcia M, Kraus H, Dickhöfer S, Daiber E, et al. Human NACHT, LRR, and PYD domain–containing protein 3 (NLRP3) inflammasome activity is regulated by and potentially targetable

through Bruton tyrosine kinase. *J Allergy Clin Immunol* (2017) **140**:1054-1067.e10. doi:10.1016/J.JACI.2017.01.017

167. Ito M, Shichita T, Okada M, Komine R, Noguchi Y, Yoshimura A, Morita R. Bruton's tyrosine kinase is essential for NLRP3 inflammasome activation and contributes to ischaemic brain injury. *Nat Commun* (2015) **6**:7360. doi:10.1038/ncomms8360
168. Wu H, Huang Q, Qi Z, Chen Y, Wang A, Chen C, Liang Q, Wang J, Chen W, Dong J, et al. Irreversible inhibition of BTK kinase by a novel highly selective inhibitor CHMFL-BTK-11 suppresses inflammatory response in rheumatoid arthritis model. *Sci Rep* (2017) **7**:466. doi:10.1038/s41598-017-00482-4
169. Sanford DS, Wierda WG, Burger JA, Keating MJ, O'Brien SM. Three Newly Approved Drugs for Chronic Lymphocytic Leukemia: Incorporating Ibrutinib, Idelalisib, and Obinutuzumab into Clinical Practice. *Clin Lymphoma Myeloma Leuk* (2015) **15**:385–391. doi:10.1016/j.clml.2015.02.019
170. Markham A, Dhillon S. Acalabrutinib: First Global Approval. *Drugs* (2018) **78**:139–145. doi:10.1007/s40265-017-0852-8
171. European Medicines Agency. Imbruvica. (2019) Available at: https://www.ema.europa.eu/en/medicines/human/EPAR/imbruvica
172. European Medicines Agency. Orphan designation: Acalabrutinib for: Treatment of lymphoplasmacytic lymphoma. (2016) Available at: https://www.ema.europa.eu/en/medicines/human/orphan-designations/eu3161626
173. European Medicines Agency. Orphan designation: Acalabrutinib for: Treatment of mantle cell lymphoma. (2016) Available at: https://www.ema.europa.eu/en/medicines/human/orphan-designations/eu3161625
174. European Medicines Agency. Orphan designation: Acalabrutinib for: Treatment of chronic lymphocytic leukaemia / small lymphocytic lymphoma. (2016) Available at: https://www.ema.europa.eu/en/medicines/human/orphan-designations/eu3161626
175. Aalipour A, Advani RH. Bruton's tyrosine kinase inhibitors and their clinical potential in the treatment of B-cell malignancies: focus on ibrutinib. *Ther Adv Hematol* (2014) **5**:121–133. doi:10.1177/2040620714539906
176. Liu SF, Malik AB. NF-κB activation as a pathological mechanism of septic shock and inflammation. *Am J Physiol - Lung Cell Mol Physiol* (2006) **290**:622–645. doi:10.1152/ajplung.00477.2005
177. Coldewey SM, Rogazzo M, Collino M, Patel NSA, Thiemermann C. Inhibition of IκB

kinase reduces the multiple organ dysfunction caused by sepsis in the mouse. *Dis Model Mech* (2013) **6**:1031–1042. doi:10.1242/dmm.012435

178. Jacobson Nadja Kopp, Jacob V. Layer, Robert A. Redd, Sebastian Tschuri, Sarah Haebe, Diederik van Bodegom, C. HSP90 Inhibition Overcomes Ibrutinib Resistance in Mantle Cell Lymphoma. *Blood* (2016) **128**:2517–2526.
179. Chen J, Kieswich JE, Chiazza F, Moyes AJ, Gobbetti T, Purvis GSD, Salvatori DCF, Patel NSA, Perretti M, Hobbs AJ, et al. IκB Kinase Inhibitor Attenuates Sepsis-Induced Cardiac Dysfunction in CKD. *J Am Soc Nephrol* (2017) **28**:94–105. doi:10.1681/ASN.2015060670
180. Patel V, Balakrishnan K, Bibikova E, Ayres M, Keating MJ, Wierda WG, Gandhi V. Comparison of Acalabrutinib, A Selective Bruton Tyrosine Kinase Inhibitor, with Ibrutinib in Chronic Lymphocytic Leukemia Cells. *Clin Cancer Res* (2017) **23**:3734–3743. doi:10.1158/1078-0432.ccr-16-1446
181. Herman SEM, Montraveta A, Niemann CU, Mora-Jensen H, Gulrajani M, Krantz F, Mantel R, Smith LL, McClanahan F, Harrington BK, et al. The Bruton Tyrosine Kinase (BTK) Inhibitor Acalabrutinib Demonstrates Potent On-Target Effects and Efficacy in Two Mouse Models of Chronic Lymphocytic Leukemia. *Clin Cancer Res* (2017) **23**:2831–2841. doi:10.1158/1078-0432.ccr-16-0463
182. Byrd JC, Harrington B, O'Brien S, Jones JA, Schuh A, Devereux S, Chaves J, Wierda WG, Awan FT, Brown JR, et al. Acalabrutinib (ACP-196) in Relapsed Chronic Lymphocytic Leukemia. *N Engl J Med* (2016) **374**:323–332. doi:10.1056/NEJMoa1509981
183. Rawlings DJ, Saffran DC, Tsukada S, Largaespada DA, Grimaldi JC, Cohen L, Mohr RN, Bazan JF, Howard M, Copeland NG. Mutation of unique region of Bruton's tyrosine kinase in immunodeficient XID mice. *Science* (1993) **261**:358–61. doi:10.1126/science.8332901
184. Thomas J, Sideras P, Smith C, Vorechovsky I, Chapman V, Paul W. Colocalization of X-linked agammaglobulinemia and X-linked immunodeficiency genes. *Science (80-)* (1993) **261**:355–358. doi:10.1126/SCIENCE.8332900
185. Scher I. The CBA/N mouse strain: an experimental model illustrating the influence of the X-chromosome on immunity. *Adv Immunol* (1982) **33**: doi:10.1016/S0065-2776(08)60834-2
186. Khan WN, Frederick Alt tll W, Gerstein RM, Malynn BA, Larsson I, Rathbun G,

Davidson L, Miiller S, Kantor AB, Herzenberg LA, et al. Defective B Cell Development and Function in Bfk-Deficient Mice. (1995).

187. Perlmutter RM, Nahm M, Stein KE, Slack J, Zitron I, Paul WE, Davie JM. Immunoglobulin subclass-specific immunodeficiency in mice with an X-linked B-lymphocyte defect. *J Exp Med* (1979) **149**:993–998. doi:10.1084/jem.149.4.993

188. Ackerman SJ, Loegering DA, Venge P, Olsson I, Harley JB, Fauci AS, Gleich GJ. Distinctive cationic proteins of the human eosinophil granule: major basic protein, eosinophil cationic protein, and eosinophil-derived neurotoxin. *J Immunol* (1983) **131**:2977–82.

189. Sur S, Glitz DG, Kita H, Kujawa SM, Peterson EA, Weiler DA, Kephart GM, Wagner JM, George TJ, Gleich GJ, et al. Localization of eosinophil-derived neurotoxin and eosinophil cationic protein in neutrophilic leukocytes. *J Leukoc Biol* (1998) **63**:715–722. doi:10.1002/jlb.63.6.715

190. Cormier SA, Yuan S, Crosby JR, Protheroe CA, Dimina DM, Hines EM, Lee NA, Lee JJ. T(H)2-mediated pulmonary inflammation leads to the differential expression of ribonuclease genes by alveolar macrophages. *Am J Respir Cell Mol Biol* (2002) **27**:678–87. doi:10.1165/rcmb.4882

191. Egesten A, Dyer K, Batten D, Domachowske J, Rosenberg H. Ribonucleases and host defense: identification, localization and gene expression in adherent monocytes in vitro. *Biochim Biophys Acta* (1997) **1358**: doi:10.1016/S0167-4889(97)00081-5

192. Rosenberg HF. RNase A ribonucleases and host defense: an evolving story. *J Leukoc Biol* (2008) **83**:1079–1087. doi:10.1189/jlb.1107725

193. Koczera P, Martin L, Marx G, Schuerholz T. The Ribonuclease A Superfamily in Humans: Canonical RNases as the Buttress of Innate Immunity. *Int J Mol Sci* (2016) **17**: doi:10.3390/IJMS17081278

194. Sorrentino S. The eight human "canonical" ribonucleases: molecular diversity, catalytic properties, and special biological actions of the enzyme proteins. *FEBS Lett* (2010) **584**:2194–200. doi:10.1016/j.febslet.2010.04.018

195. Findlay D, Herries DG, Mathias AP, Rabin BR, Ross CA. The active site and mechanism of action of bovine pancreatic ribonuclease. 7. The catalytic mechanism. *Biochem J* (1962) **85**:152. doi:10.1042/BJ0850152

196. M T, D P, J V, MV N, D A, E B. Ribonucleases as a host-defence family: evidence of evolutionarily conserved antimicrobial activity at the N-terminus. *Biochem J* (2013)

456: doi:10.1042/BJ20130123

197. Futami J, Tsushima Y, Murato Y, Tada H, Sasaki J, Seno M, Yamada H. Tissue-specific expression of pancreatic-type RNases and RNase inhibitor in humans. *DNA Cell Biol* (1997) **16**: doi:10.1089/DNA.1997.16.413
198. Fischer S, Nishio M, Dadkhahi S, Gansler J, Saffarzadeh M, Shibamiyama A, Kral N, Baal N, Koyama T, Deindl E, et al. Expression and localisation of vascular ribonucleases in endothelial cells. *Thromb Haemost* (2011) **105**: doi:10.1160/TH10-06-0345
199. Landré JBP, Hewett PW, Olivot J-M, Friedl P, Ko Y, Sachinidis A, Moenner M. Human endothelial cells selectively express large amounts of pancreatic-type ribonuclease (RNase 1). *J Cell Biochem* (2002) **86**:540–552. doi:10.1002/jcb.10234
200. Zernecke A, Preissner KT. Extracellular Ribonucleic Acids (RNA) Enter the Stage in Cardiovascular Disease. *Circ Res* (2016) **118**:469–479. doi:10.1161/CIRCRESAHA.115.307961
201. Yang D, Chen Q, Rosenberg HF, Rybak SM, Newton DL, Wang ZY, Fu Q, Tchernev VT, Wang M, Schweitzer B, et al. Human ribonuclease A superfamily members, eosinophil-derived neurotoxin and pancreatic ribonuclease, induce dendritic cell maturation and activation. *J Immunol* (2004) **173**:6134–42. doi:10.4049/jimmunol.173.10.6134
202. Wu D, Yu W, Kishikawa H, Folkerth RD, Iafrate AJ, Shen Y, Xin W, Sims K, Hu G. Angiogenin loss-of-function mutations in amyotrophic lateral sclerosis. *Ann Neurol* (2007) **62**:609–617. doi:10.1002/ana.21221
203. Thiyagarajan N, Ferguson R, Subramanian V, Acharya KR. Structural and molecular insights into the mechanism of action of human angiogenin-ALS variants in neurons. *Nat Commun* (2012) **3**:1121. doi:10.1038/ncomms2126
204. Henneke M, Diekmann S, Ohlenbusch A, Kaiser J, Engelbrecht V, Kohlschütter A, Krätzner R, Madruga-Garrido M, Mayer M, Opitz L, et al. RNASET2-deficient cystic leukoencephalopathy resembles congenital cytomegalovirus brain infection. *Nat Genet* (2009) **41**:773–775. doi:10.1038/ng.398
205. Thorn A, Steinfeld R, Ziegenbein M, Grapp M, Hsiao H-H, Urlaub H, Sheldrick GM, Gärtner J, Krätzner R. Structure and activity of the only human RNase T2. *Nucleic Acids Res* (2012) **40**:8733–8742. doi:10.1093/nar/gks614
206. Martin L, Koczera P, Simons N, Zechendorf E, Hoeger J, Marx G, Schuerholz T. The

Human Host Defense Ribonucleases 1, 3 and 7 Are Elevated in Patients with Sepsis after Major Surgery—A Pilot Study. *Int J Mol Sci* (2016) **17**:294. doi:10.3390/ijms17030294

207. Lu L, Li J, Moussaoui M, Boix E. Immune Modulation by Human Secreted RNases at the Extracellular Space. *Front Immunol* (2018) **9**:1012. doi:10.3389/fimmu.2018.01012
208. Rucksaken R, Pairojkul C, Pinlaor P, Khuntikeo N, Roytrakul S, Selmi C, Pinlaor S. Plasma Autoantibodies against Heat Shock Protein 70, Enolase 1 and Ribonuclease/Angiogenin Inhibitor 1 as Potential Biomarkers for Cholangiocarcinoma. *PLoS One* (2014) **9**:e103259. doi:10.1371/journal.pone.0103259
209. Venge, Bystrom, Carlson, Hakansson, Karawacjzyk, Peterson, Seveus, Trulson. Eosinophil cationic protein (ECP): molecular and biological properties and the use of ECP as a marker of eosinophil activation in disease. *Clin <html_ent glyph="@amp;" ascii="&"/> Exp Allergy* (1999) **29**:1172–1186. doi:10.1046/j.1365-2222.1999.00542.x
210. Shamri R, Xenakis JJ, Spencer LA. Eosinophils in innate immunity: an evolving story. *Cell Tissue Res* (2011) **343**:57–83. doi:10.1007/s00441-010-1049-6
211. Larson KA, Olson E V, Madden BJ, Gleich GJ, Lee NA, Lee JJ. Two highly homologous ribonuclease genes expressed in mouse eosinophils identify a larger subgroup of the mammalian ribonuclease superfamily. *Proc Natl Acad Sci* (1996) **93**:12370–12375. doi:10.1073/PNAS.93.22.12370
212. Ma G, Chen C, Jiang H, Qiu Y, Li Y, Li X, Zhang X, Liu J, Zhu T. Ribonuclease attenuates hepatic ischemia reperfusion induced cognitive impairment through the inhibition of inflammatory cytokines in aged mice. *Biomed Pharmacother* (2017) **90**:62–68. doi:10.1016/J.BIOPHA.2017.02.094
213. Cabrera-Fuentes H, Ruiz-Meana M, Simsekyilmaz S, Kostin S, Inserte J, Saffarzadeh M, Galuska S, Vijayan V, Barba I, Barreto G, et al. RNase1 prevents the damaging interplay between extracellular RNA and tumour necrosis factor-α in cardiac ischaemia/reperfusion injury. *Thromb Haemost* (2014) **112**:1110–1119. doi:10.1160/th14-08-0703
214. Simsekyilmaz S, Cabrera-Fuentes HA, Meiler S, Kostin S, Baumer Y, Liehn EA, Weber C, Boisvert WA, Preissner KT, Zernecke A. Role of Extracellular RNA in Atherosclerotic Plaque Formation in Mice. *Circulation* (2014) **129**:598–606.

doi:10.1161/CIRCULATIONAHA.113.002562

215. Dickson KA, Haigis MC, Raines RT. Ribonuclease Inhibitor: Structure and Function. *Prog Nucleic Acid Res Mol Biol* (2005) **80**:349. doi:10.1016/S0079-6603(05)80009-1

216. Lomax JE, Bianchetti CM, Chang A, Phillips GN, Jr., Fox BG, Raines RT. Functional Evolution of Ribonuclease Inhibitor: Insights from Birds and Reptiles. *J Mol Biol* (2014) **426**:3041. doi:10.1016/J.JMB.2014.06.007

217. Daniels R. Surviving the first hours in sepsis: getting the basics right (an intensivist's perspective). *J Antimicrob Chemother* (2011) **66**:ii11–ii23. doi:10.1093/jac/dkq515

218. Richards M. Sepsis management as an NHS clinical priority. UK sepsis group. (2014) Available at: http://www.england.nhs.uk/wp-content/uploads/2013/12/sepsis-brief.pdf [Accessed March 1, 2019]

219. Parrillo JE, Parker MM, Natanson C, Suffredini AF, Danner RL, Cunnion RE, Ognibene FP. Septic Shock in Humans. *Ann Intern Med* (1990) **113**:227. doi:10.7326/0003-4819-113-3-227

220. Martin L, Derwall M, Al Zoubi S, Zechendorf E, Reuter DA, Thiemermann C, Schuerholz T. The Septic Heart: Current Understanding of Molecular Mechanisms and Clinical Implications. *Chest* (2019) **155**:427–437. doi:10.1016/J.CHEST.2018.08.1037

221. Mai SHC, Sharma N, Kwong AC, Dwivedi DJ, Khan M, Grin PM, Fox-Robichaud AE, Liaw PC. Body temperature and mouse scoring systems as surrogate markers of death in cecal ligation and puncture sepsis. *Intensive Care Med Exp* (2018) **6**:20. doi:10.1186/s40635-018-0184-3

222. Morgan E, Varro R, Sepulveda H, Ember JA, Apgar J, Wilson J, Lowe L, Chen R, Shivraj L, Agadir A, et al. Cytometric bead array: a multiplexed assay platform with applications in various areas of biology. *Clin Immunol* (2004) **110**:252–266. doi:10.1016/j.clim.2003.11.017

223. Varro R, Chen R, Sepulveda H, Apgar J. "Bead-Based Multianalyte Flow Immunoassays," in *Methods in molecular biology (Clifton, N.J.)*, 125–152. doi:10.1007/978-1-59745-323-3_9

224. Hoffman M, Kyriazis ID, Lucchese AM, de Lucia C, Piedepalumbo M, Bauer M, Schulze PC, Bonios MJ, Koch WJ, Drosatos K. Myocardial Strain and Cardiac Output are Preferable Measurements for Cardiac Dysfunction and Can Predict Mortality in Septic Mice. *J Am Heart Assoc* (2019) **8**: doi:10.1161/JAHA.119.012260

225. Laitano O, Van Steenbergen D, Mattingly AJ, Garcia CK, Robinson GP, Murray KO,

Clanton TL, Nunamaker EA. Xiphoid Surface Temperature Predicts Mortality in a Murine Model of Septic Shock. *Shock* (2018) **50**:226–232. doi:10.1097/SHK.0000000000001007

226. Mei J, Riedel N, Grittner U, Endres M, Banneke S, Emmrich JV. Body temperature measurement in mice during acute illness: implantable temperature transponder versus surface infrared thermometry. *Sci Rep* (2018) **8**:3526. doi:10.1038/s41598-018-22020-6
227. Trammell RA, Toth LA. Markers for predicting death as an outcome for mice used in infectious disease research. *Comp Med* (2011) **61**:492–8.
228. Warn PA, Brampton MW, Sharp A, Morrissey G, Steel N, Denning DW, Priest T. Infrared body temperature measurement of mice as an early predictor of death in experimental fungal infections. *Lab Anim* (2003) **37**:126–31. doi:10.1258/00236770360563769
229. Hunter JE, Butterworth J, Perkins ND, Bateson M, Richardson CA. Using body temperature, food and water consumption as biomarkers of disease progression in mice with Eμ-myc lymphoma. *Br J Cancer* (2014) **110**:928–34. doi:10.1038/bjc.2013.818
230. Carrara M, Baselli G, Ferrario M. Mortality Prediction Model of Septic Shock Patients Based on Routinely Recorded Data. *Comput Math Methods Med* (2015) **2015**:761435. doi:10.1155/2015/761435
231. Dietrichs ES, Håheim B, Kondratiev T, Traasdahl E, Tveita T. Effects of hypothermia and rewarming on cardiovascular autonomic control in vivo. *J Appl Physiol* (2018) **124**:850–859. doi:10.1152/japplphysiol.00317.2017.-Rewarm
232. Deveci D, Egginton S, Egginton S, Deveci D, Egginton S. Differing mechanisms of cold-induced changes in capillary supply in m. tibialis anterior of rats and hamsters. *J Exp Biol* (2002) **205**:829–40. doi:10.1242/jeb.00972
233. Wilson TE, Crandall CG. Effect of thermal stress on cardiac function. *Exerc Sport Sci Rev* (2011) **39**:12–7. doi:10.1097/JES.0b013e318201eed6
234. Xiao H, Remick DG. Correction of perioperative hypothermia decreases experimental sepsis mortality by modulating the inflammatory response. *Crit Care Med* (2005) **33**:161–7. doi:10.1097/01.ccm.0000151049.19253.54
235. Altara R, Mallat Z, Booz GW, Zouein FA. The CXCL10/CXCR3 Axis and Cardiac Inflammation: Implications for Immunotherapy to Treat Infectious and Noninfectious Diseases of the Heart. *J Immunol Res* (2016) **2016**:4396368.

doi:10.1155/2016/4396368

236. Altara R, Manca M, Hessel MH, Gu Y, van Vark LC, Akkerhuis KM, Staessen JA, Struijker-Boudier HAJ, Booz GW, Blankesteijn WM. CXCL10 Is a Circulating Inflammatory Marker in Patients with Advanced Heart Failure: a Pilot Study. *J Cardiovasc Transl Res* (2016) **9**:302–314. doi:10.1007/s12265-016-9703-3
237. Altara R, Gu Y-M, Struijker-Boudier HAJ, Thijs L, Staessen JA, Blankesteijn WM. Left Ventricular Dysfunction and CXCR3 Ligands in Hypertension: From Animal Experiments to a Population-Based Pilot Study. *PLoS One* (2015) **10**:e0141394. doi:10.1371/journal.pone.0141394
238. Kurosaki T, Maeda A, Ishiai M, Hashimoto A, Inabe K, Takata M. Regulation of the phospholipase C-gamma2 pathway in B cells. *Immunol Rev* (2000) **176**:19–29.
239. Jefferies CA, Doyle S, Brunner C, Dunne A, Brint E, Wietek C, Walch E, Wirth T, O'Neill LAJ. Bruton's tyrosine kinase is a Toll/interleukin-1 receptor domain-binding protein that participates in nuclear factor kappaB activation by Toll-like receptor 4. *J Biol Chem* (2003) **278**:26258–64. doi:10.1074/jbc.M301484200
240. Pritts TA, Moon MR, Wang Q, Hungness ES, Salzman AL, Fischer JE, Hasselgren PO. Activation of NF-kappaB varies in different regions of the gastrointestinal tract during endotoxemia. *Shock* (2000) **14**:118–22.
241. Liu SF, Ye X, Malik AB. Pyrrolidine dithiocarbamate prevents I-kappaB degradation and reduces microvascular injury induced by lipopolysaccharide in multiple organs. *Mol Pharmacol* (1999) **55**:658–67.
242. Al Zoubi S, Chen J, Murphy C, Martin L, Chiazza F, Collotta D, Yaqoob MM, Collino M, Thiemermann C. Linagliptin Attenuates the Cardiac Dysfunction Associated With Experimental Sepsis in Mice With Pre-existing Type 2 Diabetes by Inhibiting NF-κB. *Front Immunol* (2018) **9**:2996. doi:10.3389/fimmu.2018.02996
243. Ní Gabhann J, Hams E, Smith S, Wynne C, Byrne JC, Brennan K, Spence S, Kissenpfennig A, Johnston JA, Fallon PG, et al. Btk Regulates Macrophage Polarization in Response to Lipopolysaccharide. *PLoS One* (2014) **9**:e85834. doi:10.1371/journal.pone.0085834
244. Chaudhry H, Zhou J, Zhong Y, Ali MM, McGuire F, Nagarkatti PS, Nagarkatti M. Role of cytokines as a double-edged sword in sepsis. *In Vivo* (2013) **27**:669–84.
245. Fong Y, Tracey KJ, Moldawer LL, Hesse DG, Manogue KB, Kenney JS, Lee AT, Kuo GC, Allison AC, Lowry SF. Antibodies to cachectin/tumor necrosis factor reduce

interleukin 1 beta and interleukin 6 appearance during lethal bacteremia. *J Exp Med* (1989) **170**:1627–33. doi:10.1084/JEM.170.5.1627

246. Cohen J. The immunopathogenesis of sepsis. *Nature* (2002) **420**:885–891. doi:10.1038/nature01326

247. Zhang W, Xu X, Kao R, Mele T, Kvietys P, Martin CM, Rui T. Cardiac Fibroblasts Contribute to Myocardial Dysfunction in Mice with Sepsis: The Role of NLRP3 Inflammasome Activation. *PLoS One* (2014) **9**:e107639. doi:10.1371/journal.pone.0107639

248. Berghe T Vanden, Demon D, Bogaert P, Vandendriessche B, Goethals A, Depuydt B, Vuylsteke M, Roelandt R, Van Wonterghem E, Vandenbroecke J, et al. Simultaneous Targeting of IL-1 and IL-18 Is Required for Protection against Inflammatory and Septic Shock. *Am J Respir Crit Care Med* (2014) **189**:282–291. doi:10.1164/rccm.201308-1535OC

249. Pomerantz BJ, Reznikov LL, Harken AH, Dinarello CA. Inhibition of caspase 1 reduces human myocardial ischemic dysfunction via inhibition of IL-18 and IL-1beta. *Proc Natl Acad Sci U S A* (2001) **98**:2871–6. doi:10.1073/pnas.041611398

250. Fu Q, Wu J, Zhou X-Y, Ji M-H, Mao Q-H, Li Q, Zong M-M, Zhou Z-Q, Yang J-J. NLRP3/Caspase-1 Pathway-Induced Pyroptosis Mediated Cognitive Deficits in a Mouse Model of Sepsis-Associated Encephalopathy. *Inflammation* (2019) **42**:306–318. doi:10.1007/s10753-018-0894-4

251. An R, Feng J, Xi C, Xu J, Sun L. miR-146a Attenuates Sepsis-Induced Myocardial Dysfunction by Suppressing IRAK1 and TRAF6 via Targeting ErbB4 Expression. *Oxid Med Cell Longev* (2018) **2018**:1–9. doi:10.1155/2018/7163057

252. Sônego F, Castanheira FVS, Czaikoski PG, Kanashiro A, Souto FO, França RO, Nascimento DC, Freitas A, Spiller F, Cunha LD, et al. MyD88-, but not Nod1- and/or Nod2-deficient mice, show increased susceptibility to polymicrobial sepsis due to impaired local inflammatory response. *PLoS One* (2014) **9**:e103734. doi:10.1371/journal.pone.0103734

253. Pal Singh S, Dammeijer F, Hendriks RW. Role of Bruton's tyrosine kinase in B cells and malignancies. *Mol Cancer* (2018) **17**:57. doi:10.1186/s12943-018-0779-z

254. Collino M, Pini A, Mugelli N, Mastroianni R, Bani D, Fantozzi R, Papucci L, Fazi M, Masini E. Beneficial effect of prolonged heme oxygenase 1 activation in a rat model of chronic heart failure. *Dis Model Mech* (2013) **6**:1012–20. doi:10.1242/dmm.011528

255. O'Riordan CE, Purvis GSD, Collotta D, Chiazza F, Wissuwa B, Al Zoubi S, Stiehler L, Martin L, Coldewey SM, Collino M, et al. Bruton's Tyrosine Kinase Inhibition Attenuates the Cardiac Dysfunction Caused by Cecal Ligation and Puncture in Mice. *Front Immunol* (2019) **10**:2129. doi:10.3389/fimmu.2019.02129

256. Zhou P, Ma B, Xu S, Zhang S, Tang H, Zhu S, Xiao S, Ben D, Xia Z. Knockdown of Burton's tyrosine kinase confers potent protection against sepsis-induced acute lung injury. *Cell Biochem Biophys* (2014) **70**:1265–1275. doi:10.1007/s12013-014-0050-1

257. Florence JM, Krupa A, Booshehri LM, Davis SA, Matthay MA, Kurdowska AK. Inhibiting Bruton's tyrosine kinase rescues mice from lethal influenza-induced acute lung injury. *Am J Physiol - Lung Cell Mol Physiol* (2018) **315**:L52. doi:10.1152/AJPLUNG.00047.2018

258. Palumbo T, Nakamura K, Lassman C, Kidani Y, Bensinger SJ, Busuttil R, Kupiec-Weglinski J, Zarrinpar A. Bruton Tyrosine Kinase Inhibition Attenuates Liver Damage in a Mouse Warm Ischemia and Reperfusion Model. *Transplantation* (2017) **101**:322–331. doi:10.1097/TP.0000000000001552

259. Chalmers SA, Glynn E, Garcia SJ, Panzenbeck M, Pelletier J, Dimock J, Seccareccia E, Bosanac T, Khalil S, Harcken C, et al. BTK inhibition ameliorates kidney disease in spontaneous lupus nephritis. *Clin Immunol* (2018) **197**:205–218. doi:10.1016/J.CLIM.2018.10.008

260. Blessberger H, Binder T. Two dimensional speckle tracking echocardiography: basic principles. *Heart* (2010) **96**:716–722. doi:10.1136/HRT.2007.141002

261. Potter E, Marwick TH. Assessment of Left Ventricular Function by Echocardiography. *JACC Cardiovasc Imaging* (2018) **11**:260–274. doi:10.1016/j.jcmg.2017.11.017

262. Ren L, Campbell A, Fang H, Gautam S, Elavazhagan S, Fatehchand K, Mehta P, Stiff A, Reader BF, Mo X, et al. Analysis of the Effects of the Bruton's tyrosine kinase (Btk) Inhibitor Ibrutinib on Monocyte Fcγ Receptor (FcγR) Function. *J Biol Chem* (2016) **291**:3043–52. doi:10.1074/jbc.M115.687251

263. Mangla A, Khare A, Vineeth V, Panday NN, Mukhopadhyay A, Ravindran B, Bal V, George A, Rath S. Pleiotropic consequences of Bruton tyrosine kinase deficiency in myeloid lineages lead to poor inflammatory responses. *Blood* (2004) **104**:1191–1197. doi:10.1182/blood-2004-01-0207

264. Yasemin Beguem Alankus, Roland Grenningloh, Philipp Haselmayer AB and JB. Inhibition of Bruton's Tyrosine Kinase (BTK) Prevents Inflammatory Macrophage

Differentiation: A Potential Role in RA and SLE - ACR Meeting Abstracts. in *American College of Rheumatology*, 70 (suppl 10).

265. Crane DD, Griffin AJ, Wehrly TD, Bosio CM. B1a cells enhance susceptibility to infection with virulent Francisella tularensis via modulation of NK/NKT cell responses. *J Immunol* (2013) **190**:2756–66. doi:10.4049/jimmunol.1202697
266. Rőszer T. Understanding the Mysterious M2 Macrophage through Activation Markers and Effector Mechanisms. *Mediators Inflamm* (2015) **2015**:1–16. doi:10.1155/2015/816460
267. Schulz D, Severin Y, Zanotelli VRT, Bodenmiller B. In-Depth Characterization of Monocyte-Derived Macrophages using a Mass Cytometry-Based Phagocytosis Assay. *Sci Rep* (2019) **9**:1925. doi:10.1038/s41598-018-38127-9
268. Liu F-C, Chuang Y-H, Tsai Y-F, Yu H-P. Role of Neutrophil Extracellular Traps Following Injury. *Shock* (2014) **41**:491–498. doi:10.1097/SHK.0000000000000146
269. Czaikoski PG, Mota JMSC, Nascimento DC, Sônego F, Castanheira FV e S, Melo PH, Scortegagna GT, Silva RL, Barroso-Sousa R, Souto FO, et al. Neutrophil Extracellular Traps Induce Organ Damage during Experimental and Clinical Sepsis. *PLoS One* (2016) **11**:e0148142. doi:10.1371/journal.pone.0148142
270. Colón DF, Wanderley CW, Franchin M, Silva CM, Hiroki CH, Castanheira FVS, Donate PB, Lopes AH, Volpon LC, Kavaguti SK, et al. Neutrophil extracellular traps (NETs) exacerbate severity of infant sepsis. *Crit Care* (2019) **23**:113. doi:10.1186/s13054-019-2407-8
271. Manfredi AA, Ramirez GA, Rovere-Querini P, Maugeri N. The Neutrophil's Choice: Phagocytose vs Make Neutrophil Extracellular Traps. *Front Immunol* (2018) **9**:288. doi:10.3389/fimmu.2018.00288
272. de Porto AP, Liu Z, de Beer R, Florquin S, de Boer OJ, Hendriks RW, van der Poll T, de Vos AF. Btk inhibitor ibrutinib reduces inflammatory myeloid cell responses in the lung during murine pneumococcal pneumonia. *Mol Med* (2019) **25**:3. doi:10.1186/s10020-018-0069-7
273. Purvis GSD, Collino M, Aranda-Tavio H, Chiazza F, O'Riordan CE, Zeboudj L, Mohammad S, Collotta D, Verta R, Guisot NES, et al. Inhibition of Bruton's tyrosine kinase regulates macrophage NF-κB and NLRP3 inflammasome activation in metabolic inflammation. *Br J Pharmacol* (2020)bph.15182. doi:10.1111/bph.15182
274. Liu Y-C, Zou X-B, Chai Y-F, Yao Y-M. Macrophage Polarization in Inflammatory

Diseases. *Int J Biol Sci* (2014) **10**:520–529. doi:10.7150/ijbs.8879

275. Atri C, Guerfali FZ, Laouini D. Role of Human Macrophage Polarization in Inflammation during Infectious Diseases. *Int J Mol Sci* (2018) **19**: doi:10.3390/ijms19061801
276. Stearns-Kurosawa DJ, Osuchowski MF, Valentine C, Kurosawa S, Remick DG. The Pathogenesis of Sepsis. *Annu Rev Pathol* (2011) **6**:19. doi:10.1146/ANNUREV-PATHOL-011110-130327
277. Shen Y, Song J, Wang Y, Chen Z, Zhang L, Yu J, Zhu D, Zhong M. M2 macrophages promote pulmonary endothelial cells regeneration in sepsis-induced acute lung injury. *Ann Transl Med* (2019) **7**: doi:10.21037/ATM.2019.02.47
278. Li X, Mu G, Song C, Zhou L, He L, Jin Q, Lu Z. Role of M2 Macrophages in Sepsis-Induced Acute Kidney Injury. *SHOCK* (2018) **50**:233–239. doi:10.1097/SHK.0000000000001006
279. Kelly-Scumpia KM, Scumpia PO, Weinstein JS, Delano MJ, Cuenca AG, Nacionales DC, Wynn JL, Lee PY, Kumagai Y, Efron PA, et al. B cells enhance early innate immune responses during bacterial sepsis. *J Exp Med* (2011) **208**:1673–1682. doi:10.1084/jem.20101715
280. Bosmann M, Russkamp NF, Patel VR, Zetoune FS, Sarma J V, Ward PA. The Outcome of Polymicrobial Sepsis is Independent of T and B Cells. *Shock* (2011) **36**:396–401. doi:10.1097/SHK.0b013e3182295f5f
281. Wynn JL, Scumpia PO, Winfield RD, Delano MJ, Kelly-Scumpia K, Barker T, Ungaro R, Levy O, Moldawer LL. Defective innate immunity predisposes murine neonates to poor sepsis outcome but is reversed by TLR agonists. *Blood* (2008) **112**:1750–1758. doi:10.1182/blood-2008-01-130500
282. Stromberg PE, Woolsey CA, Clark AT, Clark JA, Turnbull IR, McConnell KW, Chang KC, Chung C-S, Ayala A, Buchman TG, et al. CD4+ lymphocytes control gut epithelial apoptosis and mediate survival in sepsis. *FASEB J* (2009) **23**:1817. doi:10.1096/FJ.08-119024
283. Enoh V, Lin S, Lin C, Toliver-Kinsky T, Murphey E, Varma T, Sherwood E. Mice depleted of alphabeta but not gammadelta T cells are resistant to mortality caused by cecal ligation and puncture. *Shock* (2007) **27**: doi:10.1097/SHK.0B013E31802B5D9F
284. Busse M, Traeger T, Pötschke C, Billing A, Dummer A, Friebe E, Kiank C, Grunwald U, Jack RS, Schütt C, et al. Detrimental role for CD4+ T lymphocytes in murine

diffuse peritonitis due to inhibition of local bacterial elimination. *Gut* (2008) **57**:188–195. doi:10.1136/GUT.2007.121616

285. Enoh V, Lin S, Etogo A, Lin C, Sherwood E. CD4+ T-cell depletion is not associated with alterations in survival, bacterial clearance, and inflammation after cecal ligation and puncture. *Shock* (2008) **29**: doi:10.1097/SHK.0B013E318070C8B9
286. Scumpia P, Delano M, Kelly K, O'Malley K, Efron P, McAuliffe P, Brusko T, Ungaro R, Barker T, Wynn J, et al. Increased natural CD4+CD25+ regulatory T cells and their suppressor activity do not contribute to mortality in murine polymicrobial sepsis. *J Immunol* (2006) **177**: doi:10.4049/JIMMUNOL.177.11.7943
287. Ferguson NR, Galley HF, Webster NR. T helper cell subset ratios in patients with severe sepsis. *Intensive Care Med* (1999) **25**:106–109. doi:10.1007/s001340050795
288. Wu H-P, Chung K, Lin C-Y, Jiang B-Y, Chuang D-Y, Liu Y-C. Associations of T helper 1, 2, 17 and regulatory T lymphocytes with mortality in severe sepsis. *Inflamm Res* (2013) **62**:751. doi:10.1007/S00011-013-0630-3
289. Chen J, Kieswich JE, Chiazza F, Moyes AJ, Gobbetti T, Purvis GSD, Salvatori DCF, Patel NSA, Perretti M, Hobbs AJ, et al. IκB Kinase Inhibitor Attenuates Sepsis-Induced Cardiac Dysfunction in CKD. *J Am Soc Nephrol* (2017) **28**:94–105. doi:10.1681/ASN.2015060670
290. Bozza FA, Salluh JI, Japiassu AM, Soares M, Assis EF, Gomes RN, Bozza MT, Castro-Faria-Neto HC, Bozza PT. Cytokine profiles as markers of disease severity in sepsis: a multiplex analysis. *Crit Care* (2007) **11**:R49. doi:10.1186/CC5783
291. Kumar V. Inflammasomes: Pandora's box for sepsis. *J Inflamm Res* (2018) **11**:477–502. doi:10.2147/JIR.S178084
292. McCarthy CG, Goulopoulou S, Wenceslau CF, Spitler K, Matsumoto T, Webb RC. Toll-like receptors and damage-associated molecular patterns: novel links between inflammation and hypertension. *Am J Physiol Heart Circ Physiol* (2014) **306**:H184-96. doi:10.1152/ajpheart.00328.2013
293. Sundén-Cullberg J, Norrby-Teglund A, Rouhiainen A, Rauvala H, Herman G, Tracey KJ, Lee ML, Andersson J, Tokics L, Treutiger CJ. Persistent elevation of high mobility group box-1 protein (HMGB1) in patients with severe sepsis and septic shock. *Crit Care Med* (2005) **33**:564–73. doi:10.1097/01.ccm.0000155991.88802.4d
294. Zhou Y, Dong H, Zhong Y, Huang J, Lv J, Li J. The Cold-Inducible RNA-Binding Protein (CIRP) Level in Peripheral Blood Predicts Sepsis Outcome. *PLoS One* (2015)

10:e0137721. doi:10.1371/journal.pone.0137721

295. Ekaney ML, Otto GP, Sossdorf M, Sponholz C, Boehringer M, Loesche W, Rittirsch D, Wilharm A, Kurzai O, Bauer M, et al. Impact of plasma histones in human sepsis and their contribution to cellular injury and inflammation. *Crit Care* (2014) **18**:543. doi:10.1186/s13054-014-0543-8
296. Roh JS, Sohn DH. Damage-Associated Molecular Patterns in Inflammatory Diseases. *Immune Netw* (2018) **18**:e27. doi:10.4110/in.2018.18.e27
297. Denning N-L, Aziz M, Gurien SD, Wang P. DAMPs and NETs in Sepsis. *Front Immunol* (2019) **10**:2536. doi:10.3389/fimmu.2019.02536
298. Zechendorf E, O'Riordan CE, Stiehler L, Wischmeyer N, Chiazza F, Collotta D, Denecke B, Ernst S, Müller-Newen G, Coldewey SM, et al. Ribonuclease 1 attenuates septic cardiomyopathy and cardiac apoptosis in a murine model of polymicrobial sepsis. *JCI insight* (2020) **5**: doi:10.1172/jci.insight.131571
299. Lomax JE, Bianchetti CM, Chang A, Phillips GN, Fox BG, Raines RT. Functional evolution of ribonuclease inhibitor: insights from birds and reptiles. *J Mol Biol* (2014) **426**:3041–56. doi:10.1016/j.jmb.2014.06.007
300. Stieger P, Daniel J-M, Thölen C, Dutzmann J, Knöpp K, Gündüz D, Aslam M, Kampschulte M, Langheinrich A, Fischer S, et al. Targeting of Extracellular RNA Reduces Edema Formation and Infarct Size and Improves Survival After Myocardial Infarction in Mice. *J Am Heart Assoc* (2017) **6**: doi:10.1161/JAHA.116.004541
301. Kleinert E, Langenmayer MC, Reichart B, Kindermann J, Griemert B, Blutke A, Troidl K, Mayr T, Grantzow T, Noyan F, et al. Ribonuclease (RNase) Prolongs Survival of Grafts in Experimental Heart Transplantation. *J Am Heart Assoc* (2016) **5**: doi:10.1161/JAHA.116.003429
302. Spencer JD, Schwaderer AL, Dirosario JD, McHugh KM, McGillivary G, Justice SS, Carpenter AR, Baker PB, Harder J, Hains DS. Ribonuclease 7 is a potent antimicrobial peptide within the human urinary tract. *Kidney Int* (2011) **80**:174–80. doi:10.1038/ki.2011.109
303. Murtha MJ, Eichler T, Bender K, Metheny J, Li B, Schwaderer AL, Mosquera C, James C, Schwartz L, Becknell B, et al. Insulin receptor signaling regulates renal collecting duct and intercalated cell antibacterial defenses. *J Clin Invest* (2018) **128**:5634–5646. doi:10.1172/JCI98595
304. Eichler T, Bender K, Murtha MJ, Schwartz L, Metheny J, Solden L, Jaggers RM,

Bailey MT, Gupta S, Mosquera C, et al. Ribonuclease 7 Shields the Kidney and Bladder from Invasive Uropathogenic Escherichia coli Infection. *J Am Soc Nephrol* (2019) **30**:1385–1397. doi:10.1681/ASN.2018090929

305. Schwartz L, Cohen A, Thomas J, Spencer JD. The Immunomodulatory and Antimicrobial Properties of the Vertebrate Ribonuclease A Superfamily. *Vaccines* (2018) **6**: doi:10.3390/vaccines6040076
306. Lu L, Arranz-Trullén J, Prats-Ejarque G, Pulido D, Bhakta S, Boix E. Human Antimicrobial RNases Inhibit Intracellular Bacterial Growth and Induce Autophagy in Mycobacteria-Infected Macrophages. *Front Immunol* (2019) **10**:1500. doi:10.3389/fimmu.2019.01500
307. Bedoya VI, Boasso A, Hardy AW, Rybak S, Shearer GM, Rugeles MT. Ribonucleases in HIV Type 1 Inhibition: Effect of Recombinant RNases on Infection of Primary T Cells and Immune Activation-Induced RNase Gene and Protein Expression. *AIDS Res Hum Retroviruses* (2006) **22**:897–907. doi:10.1089/aid.2006.22.897
308. Ishihara K, Asai K, Nakajima M, Mue S, Ohuchi K. Preparation of recombinant rat eosinophil-associated ribonuclease-1 and -2 and analysis of their biological activities. *Biochim Biophys Acta* (2003) **1638**:164–72. doi:10.1016/s0925-4439(03)00077-2
309. Lancel S, Joulin O, Favory R, Goossens JF, Kluza J, Chopin C, Formstecher P, Marchetti P, Neviere R. Ventricular myocyte caspases are directly responsible for endotoxin-induced cardiac dysfunction. *Circulation* (2005) **111**:2596–604. doi:10.1161/CIRCULATIONAHA.104.490979
310. Yaoita H, Ogawa K, Maehara K, Maruyama Y. Attenuation of ischemia/reperfusion injury in rats by a caspase inhibitor. *Circulation* (1998) **97**:276–81. doi:10.1161/01.cir.97.3.276
311. Laugwitz KL, Moretti A, Weig HJ, Gillitzer A, Pinkernell K, Ott T, Pragst I, Städele C, Seyfarth M, Schömig A, et al. Blocking caspase-activated apoptosis improves contractility in failing myocardium. *Hum Gene Ther* (2001) **12**:2051–63. doi:10.1089/10430340152677403
312. Marshall JC. Why have clinical trials in sepsis failed? *Trends Mol Med* (2014) **20**:195–203. doi:10.1016/j.molmed.2014.01.007
313. Cavaillon J, Singer M, Skirecki T. Sepsis therapies: learning from 30 years of failure of translational research to propose new leads. *EMBO Mol Med* (2020) **12**: doi:10.15252/emmm.201810128

314. Dejager L, Pinheiro I, Dejonckheere E, Libert C. Cecal ligation and puncture: the gold standard model for polymicrobial sepsis? *Trends Microbiol* (2011) **19**:198–208. doi:10.1016/j.tim.2011.01.001

315. Stortz JA, Raymond SL, Mira JC, Moldawer LL, Mohr AM, Efron PA. Murine Models of Sepsis and Trauma: Can We Bridge the Gap? *ILAR J* (2017) **58**:90–105. doi:10.1093/ilar/ilx007

316. Fink MP, Heard SO. Laboratory models of sepsis and septic shock. *J Surg Res* (1990) **49**:186–96. doi:10.1016/0022-4804(90)90260-9

317. Remick DG, Newcomb DE, Bolgos GL, Call DR. Comparison of the mortality and inflammatory response of two models of sepsis: lipopolysaccharide vs. cecal ligation and puncture. *Shock* (2000) **13**:110–6. doi:10.1097/00024382-200013020-00004

318. Deitch EA. Animal models of sepsis and shock: a review and lessons learned. *Shock* (1998) **9**:1–11. doi:10.1097/00024382-199801000-00001

319. van der Poll T. Preclinical sepsis models. *Surg Infect* (2012) **13**:287–292. doi:10.1089/sur.2012.105

320. Seemann S, Zohles F, Lupp A. Comprehensive comparison of three different animal models for systemic inflammation. *J Biomed Sci* (2017) **24**:60. doi:10.1186/s12929-017-0370-8

321. Toscano MG, Ganea D, Gamero AM. Cecal Ligation Puncture Procedure. *J Vis Exp* (2011)2860. doi:10.3791/2860

322. Remick DG, Ayala A, Chaudry IH, Coopersmith CM, Deutschman C, Hellman J, Moldawer L, Osuchowski MF. Premise for Standardized Sepsis Models. *SHOCK* (2019) **51**:4–9. doi:10.1097/SHK.0000000000001164

323. Ruiz S, Vardon-Bounes F, Merlet-Dupuy V, Conil J-M, Buléon M, Fourcade O, Tack I, Minville V. Sepsis modeling in mice: ligation length is a major severity factor in cecal ligation and puncture. *Intensive care Med Exp* (2016) **4**:22. doi:10.1186/s40635-016-0096-z

324. Wilmore JR, Gaudette BT, Gomez Atria D, Hashemi T, Jones DD, Gardner CA, Cole SD, Misic AM, Beiting DP, Allman D. Commensal Microbes Induce Serum IgA Responses that Protect against Polymicrobial Sepsis. *Cell Host Microbe* (2018) **23**:302-311.e3. doi:10.1016/j.chom.2018.01.005

325. Iskander KN, Craciun FL, Stepien DM, Duffy ER, Kim J, Moitra R, Vaickus LJ, Osuchowski MF, Remick DG. Cecal ligation and puncture-induced murine sepsis does

not cause lung injury. *Crit Care Med* (2013) **41**:159–70. doi:10.1097/CCM.0b013e3182676322

326. Hoover DB, Ozment TR, Wondergem R, Li C, Williams DL. Impaired heart rate regulation and depression of cardiac chronotropic and dromotropic function in polymicrobial sepsis. *Shock* (2015) **43**:185–91. doi:10.1097/SHK.0000000000000272
327. Zolfaghari PS, Pinto BB, Dyson A, Singer M. The metabolic phenotype of rodent sepsis: cause for concern? *Intensive care Med Exp* (2013) **1**:25. doi:10.1186/2197-425X-1-6
328. Nguyen TLA, Vieira-Silva S, Liston A, Raes J. How informative is the mouse for human gut microbiota research? *Dis Model Mech* (2015) **8**:1–16. doi:10.1242/dmm.017400
329. Doeing DC, Borowicz JL, Crockett ET. Gender dimorphism in differential peripheral blood leukocyte counts in mice using cardiac, tail, foot, and saphenous vein puncture methods. *BMC Clin Pathol* (2003) **3**:3. doi:10.1186/1472-6890-3-3
330. Risso A. Leukocyte antimicrobial peptides: multifunctional effector molecules of innate immunity. *J Leukoc Biol* (2000) **68**:785–792. doi:10.1189/JLB.68.6.785
331. Bogdan C. Nitric oxide and the immune response. *Nat Immunol* (2001) **2**:907–16. doi:10.1038/ni1001-907
332. Gordon J, Grafton G, Wood PM, Larché M, Armitage RJ. Modelling the human immune response: can mice be trusted? Commentary. *Curr Opin Pharmacol* (2001) **1**:431–5. doi:10.1016/s1471-4892(01)00074-1
333. Mestas J, Hughes CCW. Of mice and not men: differences between mouse and human immunology. *J Immunol* (2004) **172**:2731–8. doi:10.4049/jimmunol.172.5.2731
334. Waterston RH, Lindblad-Toh K, Birney E, Rogers J, Abril JF, Agarwal P, Agarwala R, Ainscough R, Alexandersson M, An P, et al. Initial sequencing and comparative analysis of the mouse genome. *Nature* (2002) **420**:520–562. doi:10.1038/nature01262
335. Mills CD, Kincaid K, Alt JM, Heilman MJ, Hill AM. M-1/M-2 macrophages and the Th1/Th2 paradigm. *J Immunol* (2000) **164**:6166–6173.
336. Beura LK, Hamilton SE, Bi K, Schenkel JM, Odumade OA, Casey KA, Thompson EA, Fraser KA, Rosato PC, Filali-Mouhim A, et al. Normalizing the environment recapitulates adult human immune traits in laboratory mice. *Nature* (2016) **532**:512–516. doi:10.1038/nature17655
337. Wei X, Meng X, Yuan Y, Shen F, Li C, Yang J. Quercetin exerts cardiovascular

protective effects in LPS-induced dysfunction in vivo by regulating inflammatory cytokine expression, NF-κB phosphorylation, and caspase activity. *Mol Cell Biochem* (2018) **446**:43–52. doi:10.1007/s11010-018-3271-6

338. Zhang N, Feng H, Liao H-H, Chen S, Yang Z, Deng W, Tang Q-Z. Myricetin attenuated LPS induced cardiac injury in vivo and in vitro. *Phytother Res* (2018) **32**:459–470. doi:10.1002/ptr.5989
339. Chagnon F, Coquerel D, Salvail D, Marsault E, Dumaine R, Auger-Messier M, Sarret P, Lesur O. Apelin Compared With Dobutamine Exerts Cardioprotection and Extends Survival in a Rat Model of Endotoxin-Induced Myocardial Dysfunction. *Crit Care Med* (2017) **45**:e391–e398. doi:10.1097/CCM.0000000000002097
340. Cunha-Goncalves D, Perez-de-Sa V, Larsson A, Thörne J, Blomquist S. Inotropic support during experimental endotoxemic shock: part II. A comparison of levosimendan with dobutamine. *Anesth Analg* (2009) **109**:1576–83. doi:10.1213/ane.0b013e3181af40e0
341. Guillon A, Preau S, Aboab J, Azabou E, Jung B, Silva S, Textoris J, Uhel F, Vodovar D, Zafrani L, et al. Preclinical septic shock research: why we need an animal ICU. *Ann Intensive Care* (2019) **9**:66. doi:10.1186/s13613-019-0543-6
342. Seok J, Warren HS, Cuenca AG, Mindrinos MN, Baker H V, Xu W, Richards DR, McDonald-Smith GP, Gao H, Hennessy L, et al. Genomic responses in mouse models poorly mimic human inflammatory diseases. *Proc Natl Acad Sci U S A* (2013) **110**:3507–3512. doi:10.1073/pnas.1222878110
343. Beutler B, Milsark IW, Cerami AC. Passive immunization against cachectin/tumor necrosis factor protects mice from lethal effect of endotoxin. *Science* (1985) **229**:869–71. doi:10.1126/science.3895437
344. Dhainaut JF, Vincent JL, Richard C, Lejeune P, Martin C, Fierobe L, Stephens S, Ney UM, Sopwith M. CDP571, a humanized antibody to human tumor necrosis factor-alpha: safety, pharmacokinetics, immune response, and influence of the antibody on cytokine concentrations in patients with septic shock. CPD571 Sepsis Study Group. *Crit Care Med* (1995) **23**:1461–9. doi:10.1097/00003246-199509000-00004
345. Reinhart K, Wiegand-Löhnert C, Grimminger F, Kaul M, Withington S, Treacher D, Eckart J, Willatts S, Bouza C, Krausch D, et al. Assessment of the safety and efficacy of the monoclonal anti-tumor necrosis factor antibody-fragment, MAK 195F, in patients with sepsis and septic shock: a multicenter, randomized, placebo-controlled,

dose-ranging study. *Crit Care Med* (1996) **24**:733–42. doi:10.1097/00003246-199605000-00003

346. Remick D, Manohar P, Bolgos G, Rodriguez J, Moldawer L, Wollenberg G. Blockade of tumor necrosis factor reduces lipopolysaccharide lethality, but not the lethality of cecal ligation and puncture. *Shock* (1995) **4**:89–95. doi:10.1097/00024382-199508000-00002
347. Eskandari MK, Bolgos G, Miller C, Nguyen DT, DeForge LE, Remick DG. Anti-tumor necrosis factor antibody therapy fails to prevent lethality after cecal ligation and puncture or endotoxemia. *J Immunol* (1992) **148**:2724–30.
348. Osuchowski MF, Remick DG, Lederer JA, Lang CH, Aasen AO, Aibiki M, Azevedo LC, Bahrami S, Boros M, Cooney R, et al. Abandon the mouse research ship? Not just yet! *Shock* (2014) **41**:463–475. doi:10.1097/shk.0000000000000153
349. Montalban X, Arnold DL, Weber MS, Staikov I, Piasecka-Stryczynska K, Willmer J, Martin EC, Dangond F, Syed S, Wolinsky JS. Placebo-Controlled Trial of an Oral BTK Inhibitor in Multiple Sclerosis. *N Engl J Med* (2019) **380**:2406–2417. doi:10.1056/NEJMoa1901981
350. Chan P, Yu J, Chinn L, Prohn M, Huisman J, Matzuka B, Hanley W, Tuckwell K, Quartino A. Population Pharmacokinetics, Efficacy Exposure-response Analysis, and Model-based Meta-analysis of Fenebrutinib in Subjects with Rheumatoid Arthritis. *Pharm Res* (2020) **37**:25. doi:10.1007/s11095-019-2752-y
351. Roschewski M, Lionakis MS, Sharman JP, Roswarski J, Goy A, Monticelli MA, Roshon M, Wrzesinski SH, Desai J V, Zarakas MA, et al. Inhibition of Bruton tyrosine kinase in patients with severe COVID-19. *Sci Immunol* (2020) **5**: doi:10.1126/sciimmunol.abd0110
352. Driggin E, Madhavan M V, Bikdeli B, Chuich T, Laracy J, Biondi-Zoccai G, Brown TS, Der Nigoghossian C, Zidar DA, Haythe J, et al. Cardiovascular Considerations for Patients, Health Care Workers, and Health Systems During the COVID-19 Pandemic. *J Am Coll Cardiol* (2020) **75**:2352–2371. doi:10.1016/j.jacc.2020.03.031
353. Guo T, Fan Y, Chen M, Wu X, Zhang L, He T, Wang H, Wan J, Wang X, Lu Z. Cardiovascular Implications of Fatal Outcomes of Patients With Coronavirus Disease 2019 (COVID-19). *JAMA Cardiol* (2020) **5**:1. doi:10.1001/jamacardio.2020.1017
354. FDA grants accelerated approval to zanubrutinib for mantle cell lymphoma | FDA. Available at: https://www.fda.gov/drugs/resources-information-approved-drugs/fda-

grants-accelerated-approval-zanubrutinib-mantle-cell-lymphoma [Accessed August 25, 2020]

355. Kamel S, Horton L, Ysebaert L, Levade M, Burbury K, Tan S, Cole-Sinclair M, Reynolds J, Filshie R, Schischka S, et al. Ibrutinib inhibits collagen-mediated but not ADP-mediated platelet aggregation. *Leukemia* (2015) **29**:783–787. doi:10.1038/leu.2014.247

356. Wiczer TE, Levine LB, Brumbaugh J, Coggins J, Zhao Q, Ruppert AS, Rogers K, McCoy A, Mousa L, Guha A, et al. Cumulative incidence, risk factors, and management of atrial fibrillation in patients receiving ibrutinib. *Blood Adv* (2017) **1**:1739–1748. doi:10.1182/bloodadvances.2017009720

357. Petersen E, Koopmans M, Go U, Hamer DH, Petrosillo N, Castelli F, Storgaard M, Al Khalili S, Simonsen L. Comparing SARS-CoV-2 with SARS-CoV and influenza pandemics. *Lancet Infect Dis* (2020) **0**: doi:10.1016/S1473-3099(20)30484-9

358. Deng X, Baker SC. An "Old" protein with a new story: Coronavirus endoribonuclease is important for evading host antiviral defenses. *Virology* (2018) **517**:157–163. doi:10.1016/j.virol.2017.12.024

359. Ortiz-Alcantara J, Bhardwaj K, Frieman M, Baric rs, Kao cc. Virus Adaptation and Treatment Dovepress small molecule inhibitors of the sArs-coV nsp15 endoribonuclease. *Virus Adapt Treat* (2010) **2**:125–133. doi:10.2147/VAAT.S12733

360. Vincent J-L, Jones G, David S, Olariu E, Cadwell KK. Frequency and mortality of septic shock in Europe and North America: a systematic review and meta-analysis. *Crit Care* (2019) **23**:196. doi:10.1186/s13054-019-2478-6

361. Moore FA, Moore EE. Evolving concepts in the pathogenesis of postinjury multiple organ failure. *Surg Clin North Am* (1995) **75**:257–77. doi:10.1016/s0039-6109(16)46587-4

362. Delano MJ, Ward PA. Sepsis-induced immune dysfunction: can immune therapies reduce mortality? *J Clin Invest* (2016) **126**:23–31. doi:10.1172/JCI82224

363. Saito H, Sherwood ER, Varma TK, Evers BM. Effects of aging on mortality, hypothermia, and cytokine induction in mice with endotoxemia or sepsis. *Mech Ageing Dev* (2003) **124**:1047–58. doi:10.1016/j.mad.2003.08.002

364. Doi K, Leelahavanichkul A, Yuen PS, Star RA. Animal models of sepsis and sepsis-induced kidney injury. *J Clin Invest* (2009) **119**:2868–2878. doi:10.1172/jci39421

365. Turnbull IR, Wlzorek JJ, Osborne D, Hotchkiss RS, Coopersmith CM, Buchman TG.

Effects of age on mortality and antibiotic efficacy in cecal ligation and puncture. *Shock* (2003) **19**:310–3. doi:10.1097/00024382-200304000-00003

366. Miyaji T, Hu X, Yuen PS, Muramatsu Y, Iyer S, Hewitt SM, Star RA. Ethyl pyruvate decreases sepsis-induced acute renal failure and multiple organ damage in aged mice. *Kidney Int* (2003) **64**:1620–1631. doi:10.1046/j.1523-1755.2003.00268.x
367. Bösch F, Angele MK, Chaudry IH. Gender differences in trauma, shock and sepsis. *Mil Med Res* (2018) **5**:35. doi:10.1186/s40779-018-0182-5
368. Chen J, Chiazza F, Collino M, Patel NSA, Coldewey SM, Thiemermann C. Gender Dimorphism of the Cardiac Dysfunction in Murine Sepsis: Signalling Mechanisms and Age-Dependency. *PLoS One* (2014) **9**:e100631. doi:10.1371/journal.pone.0100631
369. Bae S, Zhang L. Gender differences in cardioprotection against ischemia/reperfusion injury in adult rat hearts: focus on Akt and protein kinase C signaling. *J Pharmacol Exp Ther* (2005) **315**: doi:10.1124/JPET.105.090803
370. Hsu J, Kan W, Hsieh C, Choudhry M, Bland K, Chaudry I. Mechanism of salutary effects of estrogen on cardiac function following trauma-hemorrhage: Akt-dependent HO-1 up-regulation. *Crit Care Med* (2009) **37**:2338–2344. doi:10.1097/CCM.0B013E3181A030CE
371. Iwashyna TJ, Ely EW, Smith DM, Langa KM. Long-term cognitive impairment and functional disability among survivors of severe sepsis. *JAMA* (2010) **304**:1787–94. doi:10.1001/jama.2010.1553
372. Fried TR, Bradley EH, Williams CS, Tinetti ME. Functional disability and health care expenditures for older persons. *Arch Intern Med* (2001) **161**:2602–7. doi:10.1001/archinte.161.21.2602
373. Yende S, Angus DC. Long-term outcomes from sepsis. *Curr Infect Dis Rep* (2007) **9**:382–6. doi:10.1007/s11908-007-0059-3
374. Rozzini R, Sabatini T, Cassinadri A, Boffelli S, Ferri M, Barbisoni P, Frisoni GB, Trabucchi M. Relationship between functional loss before hospital admission and mortality in elderly persons with medical illness. *J Gerontol A Biol Sci Med Sci* (2005) **60**:1180–3. doi:10.1093/gerona/60.9.1180

APPENDIX

A. INITIAL RESUSCITATION

1. Sepsis and septic shock are medical emergencies, and we recommend that treatment and resuscitation begin immediately (BPS).
2. We recommend that, in the resuscitation from sepsis-induced hypoperfusion, at least 30 mL/kg of IV crystalloid fluid be given within the first 3 hours (strong recommendation, low quality of evidence).
3. We recommend that, following initial fluid resuscitation, additional fluids be guided by frequent reassessment of hemodynamic status (BPS).
   Remarks: Reassessment should include a thorough clinical examination and evaluation of available physiologic variables (heart rate, blood pressure, arterial oxygen saturation, respiratory rate, temperature, urine output, and others, as available) as well as other noninvasive or invasive monitoring, as available.
4. We recommend further hemodynamic assessment (such as assessing cardiac function) to determine the type of shock if the clinical examination does not lead to a clear diagnosis (BPS).
5. We suggest that dynamic over static variables be used to predict fluid responsiveness, where available (weak recommendation, low quality of evidence).
6. We recommend an initial target mean arterial pressure of 65 mm Hg in patients with septic shock requiring vasopressors (strong recommendation, moderate quality of evidence).
7. We suggest guiding resuscitation to normalize lactate in patients with elevated lactate levels as a marker of tissue hypoperfusion (weak recommendation, low quality of evidence).

B. SCREENING FOR SEPSIS AND PERFORMANCE IMPROVEMENT

1. We recommend that hospitals and hospital systems have a performance improvement program for sepsis, including sepsis screening for acutely ill, high risk patients (BPS).

C. DIAGNOSIS

1. We recommend that appropriate routine microbiologic cultures (including blood) be obtained before starting antimicrobial therapy in patients with suspected sepsis or septic shock if doing so results in no substantial delay in the start of antimicrobials (BPS).
   Remarks: Appropriate routine microbiologic cultures always include at least two sets of blood cultures (aerobic and anaerobic).

D. ANTIMICROBIAL THERAPY

1. We recommend that administration of IV antimicrobials should be initiated as soon as possible after recognition and within one hour for both sepsis and septic shock (strong recommendation, moderate quality of evidence).
2. We recommend empiric broad-spectrum therapy with one or more antimicrobials for patients presenting with sepsis or septic shock to cover all likely pathogens (including bacterial and potentially fungal or viral coverage) (strong recommendation, moderate quality of evidence).
3. We recommend that empiric antimicrobial therapy be narrowed once pathogen identification and sensitivities are established and/or adequate clinical improvement is noted (BPS).
4. We recommend against sustained systemic antimicrobial prophylaxis in patients with severe inflammatory states of noninfectious origin (e.g., severe pancreatitis, burn injury) (BPS).
5. We recommend that dosing strategies of antimicrobials be optimized based on accepted pharmacokinetic/pharmacodynamic principles and specific drug properties in patients with sepsis or septic shock

(BPS).

6. We suggest empiric combination therapy (using at least two antibiotics of different antimicrobial classes) aimed at the most likely bacterial pathogen(s) for the initial management of septic shock (weak recommendation, low quality of evidence).
   Remarks: Readers should review Table 6 for definitions of empiric, targeted/definitive, broad-spectrum, combination, and multidrug therapy before reading this section.
7. We suggest that combination therapy not be routinely used for ongoing treatment of most other serious infections, including bacteremia and sepsis without shock (weak recommendation, low quality of evidence).
   Remarks: This does not preclude the use of multidrug therapy to broaden antimicrobial activity.
8. We recommend against combination therapy for the routine treatment of neutropenic sepsis/bacteremia (strong recommendation, moderate quality of evidence).
   Remarks: This does not preclude the use of multidrug therapy to broaden antimicrobial activity.
9. If combination therapy is used for septic shock, we recommend de-escalation with discontinuation of combination therapy within the first few days in response to clinical improvement and/or evidence of infection resolution. This applies to both targeted (for culture-positive infections) and empiric (for culture-negative infections) combination therapy (BPS).
10. We suggest that an antimicrobial treatment duration of 7 to 10 days is adequate for most serious infections associated with sepsis and septic shock (weak recommendation, low quality of evidence).
11. We suggest that longer courses are appropriate in patients who have a slow clinical response, undrainable foci of infection, bacteremia with *Staphylococcus aureus*, some fungal and viral infections, or immunologic deficiencies, including neutropenia (weak recommendation, low quality of evidence).
12. We suggest that shorter courses are appropriate in some patients, particularly those with rapid clinical resolution following effective source control of intra-abdominal or urinary sepsis and those with anatomically uncomplicated pyelonephritis (weak recommendation, low quality of evidence).
13. We recommend daily assessment for de-escalation of antimicrobial therapy in patients with sepsis and septic shock (BPS).
14. We suggest that measurement of procalcitonin levels can be used to support shortening the duration of antimicrobial therapy in sepsis patients (weak recommendation, low quality of evidence).
15. We suggest that procalcitonin levels can be used to support the discontinuation of empiric antibiotics in patients who initially appeared to have sepsis, but subsequently have limited clinical evidence of infection (weak recommendation, low quality of evidence).

E. SOURCE CONTROL

1. We recommend that a specific anatomic diagnosis of infection requiring emergent source control should be identified or excluded as rapidly as possible in patients with sepsis or septic shock, and that any required source control intervention should be implemented as soon as medically and logistically practical after the diagnosis is made (BPS).
2. We recommend prompt removal of intravascular access devices that are a possible source of sepsis or septic shock after other vascular access has been established (BPS).

F. FLUID THERAPY

1. We recommend that a fluid challenge technique be applied where fluid administration is continued as long as hemodynamic factors continue to improve (BPS).
2. We recommend crystalloids as the fluid of choice for initial resuscitation and subsequent intravascular volume replacement in patients with sepsis and septic shock (strong recommendation, moderate quality of evidence).

3. We suggest using either balanced crystalloids or saline for fluid resuscitation of patients with sepsis or septic shock (weak recommendation, low quality of evidence).
4. We suggest using albumin in addition to crystalloids for initial resuscitation and subsequent intravascular volume replacement in patients with sepsis and septic shock, when patients require substantial amounts of crystalloids (weak recommendation, low quality of evidence).
5. We recommend against using hydroxyethyl starches for intravascular volume replacement in patients with sepsis or septic shock (strong recommendation, high quality of evidence).
6. We suggest using crystalloids over gelatins when resuscitating patients with sepsis or septic shock (weak recommendation, low quality of evidence).

G. VASOACTIVE MEDICATIONS

1. We recommend norepinephrine as the first-choice vasopressor (strong recommendation, moderate quality of evidence).
2. We suggest adding either vasopressin (up to 0.03 U/min) (weak recommendation, moderate quality of evidence) or epinephrine (weak recommendation, low quality of evidence) to norepinephrine with the intent of raising mean arterial pressure to target, or adding vasopressin (up to 0.03 U/min) (weak recommendation, moderate quality of evidence) to decrease norepinephrine dosage.
3. We suggest using dopamine as an alternative vasopressor agent to norepinephrine only in highly selected patients (e.g., patients with low risk of tachyarrhythmias and absolute or relative bradycardia) (weak recommendation, low quality of evidence).
4. We recommend against using low-dose dopamine for renal protection (strong recommendation, high quality of evidence).
5. We suggest using dobutamine in patients who show evidence of persistent hypoperfusion despite adequate fluid loading and the use of vasopressor agents (weak recommendation, low quality of evidence).
   Remarks: If initiated, dosing should be titrated to an end point reflecting perfusion, and the agent reduced or discontinued in the face of worsening hypotension or arrhythmias.
6. We suggest that all patients requiring vasopressors have an arterial catheter placed as soon as practical if resources are available (weak recommendation, very low quality of evidence).

H. CORTICOSTEROIDS

1. We suggest against using IV hydrocortisone to treat septic shock patients if adequate fluid resuscitation and vasopressor therapy are able to restore hemodynamic stability. If this is not achievable, we suggest IV hydrocortisone at a dose of 200 mg per day (weak recommendation, low quality of evidence).

I. BLOOD PRODUCTS

1. We recommend that RBC transfusion occur only when hemoglobin concentration decreases to < 7.0 g/dL in adults in the absence of extenuating circumstances, such as myocardial ischemia, severe hypoxemia, or acute hemorrhage (strong recommendation, high quality of evidence).
2. We recommend against the use of erythropoietin for treatment of anemia associated with sepsis (strong recommendation, moderate quality of evidence).
3. We suggest against the use of fresh frozen plasma to correct clotting abnormalities in the absence of bleeding or planned invasive procedures (weak recommendation, very low quality of evidence).
4. We suggest prophylactic platelet transfusion when counts are < 10,000/mm^3 (10×10^9/L) in the absence of apparent

bleeding and when counts are < 20,000/mm^3 (20 × 10^9/L) if the patient has a significant risk of bleeding. Higher platelet counts (≥ 50,000/mm^3 [50 x 10^9/L]) are advised for active bleeding, surgery, or invasive procedures (weak recommendation, very low quality of evidence).

J. IMMUNOGLOBULINS

1. We suggest against the use of IV immunoglobulins in patients with sepsis or septic shock (weak recommendation, low quality of evidence).

K. BLOOD PURIFICATION

1. We make no recommendation regarding the use of blood purification techniques.

L. ANTICOAGULANTS

1. We recommend against the use of antithrombin for the treatment of sepsis and septic shock (strong recommendation, moderate quality of evidence).
2. We make no recommendation regarding the use of thrombomodulin or heparin for the treatment of sepsis or septic shock.

M. MECHANICAL VENTILATION

1. We recommend using a target tidal volume of 6 mL/kg predicted body weight compared with 12 mL/kg in adult patients with sepsis-induced acute respiratory distress syndrome (ARDS) (strong recommendation, high quality of evidence).
2. We recommend using an upper limit goal for plateau pressures of 30 cm H_2O over higher plateau pressures in adult patients with sepsis-induced severe ARDS (strong recommendation, moderate quality of evidence).
3. We suggest using higher positive end-expiratory pressure (PEEP) over lower PEEP in adult patients with sepsis-induced moderate to severe ARDS (weak recommendation, moderate quality of evidence).
4. We suggest using recruitment maneuvers in adult patients with sepsis-induced, severe ARDS (weak recommendation, moderate quality of evidence).
5. We recommend using prone over supine position in adult patients with sepsis-induced ARDS and a PaO_2/FIO_2 ratio < 150 (strong recommendation, moderate quality of evidence).
6. We recommend against using high-frequency oscillatory ventilation in adult patients with sepsis-induced ARDS (strong recommendation, moderate quality of evidence).
7. We make no recommendation regarding the use of noninvasive ventilation for patients with sepsis-induced ARDS.
8. We suggest using neuromuscular blocking agents for ≤ 48 hours in adult patients with sepsis-induced ARDS and a PaO_2/FIO_2 ratio < 150 mm Hg (weak recommendation, moderate quality of evidence).
9. We recommend a conservative fluid strategy for patients with established sepsis-induced ARDS who do not have evidence of tissue hypoperfusion (strong recommendation, moderate quality of evidence).
10. We recommend against the use of ß-2 agonists for the treatment of patients with sepsis-induced ARDS without bronchospasm (strong recommendation, moderate quality of evidence).
11. We recommend against the routine use of the pulmonary artery catheter for patients with sepsis-induced ARDS (strong recommendation, high quality of evidence).

12. We suggest using lower tidal volumes over higher tidal volumes in adult patients with sepsis-induced respiratory failure without ARDS (weak recommendation, low quality of evidence).
13. We recommend that mechanically ventilated sepsis patients be maintained with the head of the bed elevated between 30 and 45 degrees to limit aspiration risk and to prevent the development of ventilator-associated pneumonia (strong recommendation, low quality of evidence).
14. We recommend using spontaneous breathing trials in mechanically ventilated patients with sepsis who are ready for weaning (strong recommendation, high quality of evidence).
15. We recommend using a weaning protocol in mechanically ventilated patients with sepsis-induced respiratory failure who can tolerate weaning (strong recommendation, moderate quality of evidence).

N. SEDATION AND ANALGESIA

1. We recommend that continuous or intermittent sedation be minimized in mechanically ventilated sepsis patients, targeting specific titration end points (BPS).

O. GLUCOSE CONTROL

1. We recommend a protocolized approach to blood glucose management in ICU patients with sepsis, commencing insulin dosing when two consecutive blood glucose levels are > 180 mg/dL. This approach should target an upper blood glucose level ≤ 180 mg/dL rather than an upper target blood glucose level ≤ 110 mg/dL (strong recommendation, high quality of evidence).
2. We recommend that blood glucose values be monitored every 1 to 2 hours until glucose values and insulin infusion rates are stable, then every 4 hours thereafter in patients receiving insulin infusions (BPS).
3. We recommend that glucose levels obtained with point-of-care testing of capillary blood be interpreted with caution because such measurements may not accurately estimate arterial blood or plasma glucose values (BPS).
4. We suggest the use of arterial blood rather than capillary blood for point-of-care testing using glucose meters if patients have arterial catheters (weak recommendation, low quality of evidence).

P. RENAL REPLACEMENT THERAPY

1. We suggest that either continuous or intermittent renal replacement therapy (RRT) be used in patients with sepsis and acute kidney injury (weak recommendation, moderate quality of evidence).

2. We suggest using continuous therapies to facilitate management of fluid balance in hemodynamically unstable septic patients (weak recommendation, very low quality of evidence).

3. We suggest against the use of RRT in patients with sepsis and acute kidney injury for increase in creatinine or oliguria without other definitive indications for dialysis (weak recommendation, low quality of evidence).

Q. BICARBONATE THERAPY

1. We suggest against the use of sodium bicarbonate therapy to improve hemodynamics or to reduce vasopressor requirements in patients with hypoperfusion-induced lactic acidemia with pH ≥ 7.15 (weak recommendation, moderate quality of evidence).

R. VENOUS THROMBOEMBOLISM PROPHYLAXIS

1. We recommend pharmacologic prophylaxis (unfractionated heparin [UFH] or low-molecular-weight heparin [LMWH])

against venous thromboembolism (VTE) in the absence of contraindications to the use of these agents (strong recommendation, moderate quality of evidence).

2. We recommend LMWH rather than UFH for VTE prophylaxis in the absence of contraindications to the use of LMWH (strong recommendation, moderate quality of evidence).
3. We suggest combination pharmacologic VTE prophylaxis and mechanical prophylaxis, whenever possible (weak recommendation, low quality of evidence).
4. We suggest mechanical VTE prophylaxis when pharmacologic VTE is contraindicated (weak recommendation, low quality of evidence).

S. STRESS ULCER PROPHYLAXIS

1. We recommend that stress ulcer prophylaxis be given to patients with sepsis or septic shock who have risk factors for gastrointestinal (GI) bleeding (strong recommendation, low quality of evidence).
2. We suggest using either proton pump inhibitors or histamine-2 receptor antagonists when stress ulcer prophylaxis is indicated (weak recommendation, low quality of evidence).
3. We recommend against stress ulcer prophylaxis in patients without risk factors for GI bleeding (BPS).

T. NUTRITION

1. We recommend against the administration of early parenteral nutrition alone or parenteral nutrition in combination with enteral feedings (but rather initiate early enteral nutrition) in critically ill patients with sepsis or septic shock who can be fed enterally (strong recommendation, moderate quality of evidence).
2. We recommend against the administration of parenteral nutrition alone or in combination with enteral feeds (but rather to initiate IV glucose and advance enteral feeds as tolerated) over the first 7 days in critically ill patients with sepsis or septic shock for whom early enteral feeding is not feasible (strong recommendation, moderate quality of evidence).
3. We suggest the early initiation of enteral feeding rather than a complete fast or only IV glucose in critically ill patients with sepsis or septic shock who can be fed enterally (weak recommendation, low quality of evidence).
4. We suggest either early trophic/hypocaloric or early full enteral feeding in critically ill patients with sepsis or septic shock; if trophic/hypocaloric feeding is the initial strategy, then feeds should be advanced according to patient tolerance (weak recommendation, moderate quality of evidence).
5. We recommend against the use of omega-3 fatty acids as an immune supplement in critically ill patients with sepsis or septic shock (strong recommendation, low quality of evidence).
6. We suggest against routinely monitoring gastric residual volumes in critically ill patients with sepsis or septic shock (weak recommendation, low quality of evidence). However, we suggest measurement of gastric residuals in patients with feeding intolerance or who are considered to be at high risk of aspiration (weak recommendation, very low quality of evidence).
   Remarks: This recommendation refers to nonsurgical critically ill patients with sepsis or septic shock.
7. We suggest the use of prokinetic agents in critically ill patients with sepsis or septic shock and feeding intolerance (weak recommendation, low quality of evidence).
8. We suggest placement of post-pyloric feeding tubes in critically ill patients with sepsis or septic shock with feeding intolerance or who are considered to be at high risk of aspiration (weak recommendation, low quality of evidence).
9. We recommend against the use of IV selenium to treat sepsis and septic shock (strong recommendation, moderate quality of evidence).
10. We suggest against the use of arginine to treat sepsis and septic shock (weak recommendation, low quality of evidence).

11. We recommend against the use of glutamine to treat sepsis and septic shock (strong recommendation, moderate quality of evidence). 12. We make no recommendation about the use of carnitine for sepsis and septic shock.
U. SETTING GOALS OF CARE 1. We recommend that goals of care and prognosis be discussed with patients and families (BPS). 2. We recommend that goals of care be incorporated into treatment and end-of-life care planning, utilizing palliative care principles where appropriate (strong recommendation, moderate quality of evidence). 3. We suggest that goals of care be addressed as early as feasible, but no later than within 72 hours of ICU admission (weak recommendation, low quality of evidence).

Appendix 1: Surviving sepsis campaign international guidelines for management of sepsis and septic shock. The Grading of Recommendations Assessment Development and Evaluation (GRADE) system was used to assess the quality of evidence from high to low and determine the strength of the recommendation as strong, weak or best practice. 93 statements are provided with 32 strong recommendations, 39 weak recommendations, 18 best practice and no recommendations for four. Table taken from Rhodes *et al*. 2017.

Table S2. Average concentration of cytokines in serum. Mice underwent sham or CLP surgery, 24 h later 31 cytokines and chemokines were assessed in serum. Data are expressed as mean ± SEM (pg/ml). The following groups were studied WT sham (n = 5), *Xid* sham (n = 5), WT-CLP (n = 10), *Xid*-CLP (n = 10), WT-CLP + ibrutinib (n = 8), *Xid*-CLP + ibrutinib (n = 6).

	WT Sham		***Xid* Sham**		**WT CLP**		***Xid* CLP**		**WT CLP + ibrutinib**		***Xid* CLP + ibrutinib**	
	Mean	SEM +/-	Mean	SEM +/-	Mean	SEM +/-	Mean	SEM +/-	Mean	SEM +/-	Mean	SEM +/-
BCA-1/CXCL13	7034.2	3097.9	8937.8	2330.0	83810.3	4310.6	77435.3	2269.3	85285.5	3220.6	80840.9	1375.5
CTACK/CCL27	1872.3	202.1	2327.4	398.1	3886.4	339.4	8395.2	1781.0	7661.8	1191.3	7369.2	1032.9
ENA-78/CXCL5	1980.0	772.6	2831.5	987.5	45770.7	5248.7	8462.4	969.7	11727.6	2524.8	7210.7	982.8
Eotaxin/CCL11	420.6	151.2	733.3	171.2	6869.6	356.5	1952.5	224.5	2690.1	465.2	1907.8	179.3
Eotaxin-2/CCL24	13102.7	4999.2	18708.2	3000.5	56736.3	5714.4	25735.7	2079.7	11983.1	1876.6	29652.0	3562.5
Fractalkine/CXCL1	264.5	9.1	279.7	17.5	1181.9	109.7	322.8	12.2	457.7	47.5	352.9	20.4
GM-CSF	5.4	0.8	5.4	0.7	346.2	58.6	7.5	1.1	14.7	3.2	7.7	0.7
I-309/CCL1	45.6	4.9	58.4	14.0	198.7	66.5	799.7	190.5	80.1	15.6	11691.8	9593.7
IFN-γ	133.8	11.1	155.5	17.5	134.0	16.2	102.3	15.1	98.1	28.8	191.6	14.4
IL-1β	680.0	57.0	706.3	72.6	1536.3	184.7	674.6	31.4	611.0	43.8	768.9	28.0
IL-2	11.7	2.6	15.9	4.0	38.3	7.8	102.6	25.8	72.8	15.4	57.4	18.7
IL-6	45.5	4.8	52.6	6.7	524272.8	43243.2	6380.9	1557.2	29367.0	18095.0	4296.7	1827.7
IL-4	74.7	3.6	87.5	8.0	65.2	3.9	76.0	8.0	52.3	9.2	92.0	3.5
IL-10	1296.5	84.4	1677.4	159.6	23882.5	2465.0	2077.0	370.9	3485.3	947.8	2252.3	362.6
IL-16	978.4	68.9	1048.3	87.4	2836.1	207.4	1313.4	86.9	1814.6	200.3	1462.5	95.6
IP-10/CXClL10	4561.3	205.3	4994.1	536.0	4837.9	327.2	4547.3	583.3	4036.2	420.8	5182.1	157.5
I-TAC/CXCL11	4666.7	272.0	5570.1	490.2	3217.0	291.5	3372.9	340.1	2991.7	826.7	5569.5	376.0
KC/CXCL1	298.0	24.0	337.9	24.5	158693.9	35967.2	9014.0	1570.5	16952.6	6344.1	8912.3	2432.5
MCP-1/CCL2	515.8	36.3	601.9	59.7	262035.2	117148.0	9660.5	3217.7	10558.8	3887.3	3100.1	531.8
MCP-5/CCL12	24.0	4.9	31.6	4.5	5348.5	785.1	935.7	129.2	1020.6	157.1	758.3	70.1
MDC/CCL22	190.9	41.0	210.3	35.3	1869.7	235.7	494.0	48.3	515.9	36.1	717.8	69.6
MIP-1α/CCL3	27.5	2.1	34.0	3.7	4994.4	1664.0	175.4	56.9	81.7	24.5	56.1	2.2
MIP1-β/CCL4	123.9	6.9	141.1	12.9	51791.1	19413.9	1445.3	372.8	2859.4	1022.9	509.2	68.5
MIP-3α/CCL20	38.8	3.4	41.7	4.4	893.8	117.3	691.2	157.2	549.9	176.4	1134.8	163.6
MIP-3β/CCL19	2285.8	104.5	2520.6	204.6	3622.2	350.3	3830.6	351.0	2933.2	242.3	4925.1	465.9
Rantes/CCL5	28.8	5.4	33.4	5.9	2647.5	421.4	80.0	10.3	487.9	148.7	110.0	24.3
SCYB16/CXCL16	601.1	133.4	748.4	91.0	4588.5	467.1	2250.7	317.4	2440.4	447.1	1851.1	266.6
SDF-1α/CXCL12	929.5	197.3	1263.0	218.9	447.7	63.0	1612.0	177.7	1113.3	341.6	2304.9	389.7
TARC/CCL17	115.6	16.7	146.8	21.6	3293.6	376.2	2269.2	441.2	755.4	114.8	5268.3	1862.4
TNF-α	311.2	16.7	310.6	28.0	471.7	42.9	205.1	16.5	208.5	38.7	330.8	27.1